THE EFFECTS OF NOTCH PARAMETERS AND CRACK TIP PLASTICITY ON AC POTENTIAL DROP USED IN HIGH FREQUENCY CRACK MONITORING

by

ANTHONY EDWARD WALKER BSc(Hons)

A thesis submitted to the COUNCIL FOR NATIONAL ACADEMIC AWARDS in partial fulfilment for the degree of DOCTOR of PHILOSOPHY

Sponsoring Establishment :

Department of Mechanical and Production Engineering
Sheffield City Polytechnic
Sheffield S1 1WB

Collaborating Establishment :

Testwell Limited
12 High March
Long March Industrial Estate
Daventry
Northamptonshire NN11 4HB

May 1987

ACKNOWLEDGEMENTS

The author wishes to express his gratitude to Mr D E Eaton, Principal Lecturer in the Department of Mechanical and Production Engineering, and to Mr B S Plumb, Head of Electrical and Electronic Engineering Department, for their encouragement and helpful supervision during the course of this project. Thanks are also expressed to Dr N Trigwell, Technical Director of Testwell Ltd, and Dr F Sherratt for their helpful advice and constructive comments.

The technical assistance offered by Mr R Teasdale and his staff was much appreciated and especially to Mr K Wright for his valued assistance at various stages of this work.

Thanks also to the many other people who I have not mentioned but whose help and advice has been invaluable and greatly appreciated throughout the project.

Finally to Miss I Benevicius, Mrs B Lougher, Miss J Senior and Mrs J Simpson for typing the thesis.

DECLARATION

The author declares that no part of this work has been submitted in support of another degree or qualification to this or any other establishment. The author further declares that he has not been a registered candidate or enrolled student for another award of the CNAA or other academic or professional institution during the course of the research programme.

A E WALKER

ABSTRACT

THE EFFECT OF NOTCH PARAMETERS AND CRACK TIP PLASTICITY ON AC POTENTIAL DROP USED IN HIGH FREQUENCY CRACK MONITORING

A E Walker

The ACPD method is probably the most versatile of all the commercially available NDE techniques. However as applications of such systems increase so does the awareness of serious limitations in present ACPD knowledge. In particular high local crack and notch tip strains can have a marked effect on ACPD response leading to substantial errors in estimates of crackdepth and growth rates.

In the present study an investigation has been undertaken into the influence of elastic/plastic notch tip strain on the response of ACPD crack monitoring systems.

Experimental work has been undertaken to produce data on the ACPD response observed in two magnetically contrasting materials (EN1A mild steel, NE8 aluminium alloy) using a series of V and U notched bend specimens. An extensive elastic/plastic finite element analysis was conducted to accurately determine the different notch tip strain fields for both materials. A fundamental study was also undertaken into the influence of strain on the electrical resistivity and relative magnetic permeability, the two material parameters governing the ACPD response.

The information obtained from the investigations together with results from the FE analysis has made it possible to understand and quantify the influence of elastic/plastic deformation on ACPD response.

An electric field model has been successfully developed to explain and predict the effect of increasing strain on the ACPD response in materials where the skin effect is strong. Results have also shown the inapplicability of the compensation method of crack monitoring when levels of plasticity are appreciable and an alternative method has been proposed.

CONTENTS Page

Contents (Continued) Page

Contents (Continued) Page

Contents (Continued) Page

INDEX TO FIGURES

Index to Figures (Continued) Page

CHAPTER 5

CHAPTER 7

CHAPTER 8

INDEX TO PLATES PAGE NUMBER

INDEX TO TABLES PAGE NUMBER

NOMENCLATURE

PD : potential drop

NDE : non-destructive evaluation

DC : direct current

AC : alternating current

DCPD : direct current/potential drop

ACPD : alternating current/potential drop

ACFM : alternating current field measurements

FE : finite element

I_t : alternating current level

E(r) : electric field vector

ρ : electrical resistivity

J(r) : current density

f : frequency of AC supply

μ : magnetic permeability

μ_o : permeability of free space ($4\pi \times 10^{-7}$ Hm^{-1})

μ_r : relative magnetic permeability

B_o, B_1 : Bessel functions

r_o : radius of circular conductor

r : radial distance from centre of conductor

δ : skin depth

V_1, V_2 : probe voltages

Δ : distance apart of probe contacts

k : constant of proportionality in one-dimensional field solution.

a : crackdepth

V_c : voltage across plain material

V_n : voltage across notch

V_i : induced voltage signal

G : system gain

V_n : voltage signal across notch

V_c : compensating voltage signal

[V] : voltage output

ρ_{ms}, ρ_{al} : notch root radii of V notches

R_{ms}, R_{al} : notch radii of U notches

E : Young's modulus

K_t : elastic stress concentration factor

σ_{eq} : equivalent stress

σ_{xx}, σ_{xy} etc : local elastic/plastic stress components

$E_{eq\ el}$: equivalent elastic strain

$\delta E_{eq\ el}$: increment of equivalent plastic strain

δE_{xxpl}, δ_{xypl} Etc : increments of individual components of plastic strain

σ_1, σ_2 : principal stresses

d, d^1, d^{11} : depth of beam used in simple bending theory approximation

σ, σ^1, σ^{11} : stress in outer fibres of beam

M : bending moment

I : second moment of area

y : distance from neutral axis of beam

b : width of beam

$R\alpha$: radius of curvature of beam

α : vertical deflection of beam

L/2 : difference in X coordinates of noted 35 and 44

R : DC resistance

V : voltage

I : current level

V_o : zero load voltage offset

V_a : active voltage

V_d : dummy voltage

V_a' : adjusted value of active voltage

V_{ref} : average of recorded dummy voltages

l : span of voltage pick-ups

l_o : initial span of voltage pick-ups

A : cross-sectional area of tensile specimen

A_o : initial cross-sectional area of tensile specimens

E_{long} : longitudinal strain

E_{lat} : lateral strain

ν : Poisson's ratio

Z : AC impedance

K : constant of proportionality relating the product $l\mu_r^{\frac{1}{2}}$ to a potential drop

l_i : surface length of element i

μ_{ri} : value of μ_r in element i

C : integrating capacitor

R_1, R_2 : circuit resistors

B : magnetic flux density

H : magnetizing force

$i_m I_m$: current in energising coil

v_m, V_m : voltage across resistor R_1

N_1 : number of energising coils

N_2 : number of search coils

s : mean circumference of EN1A ring

E_s : RMS value of EMF induced in search coil

E_ϕ : RMS value of potential drop created across integrating capacitor, C

V_ϕ : voltage measured across integrating capacitor, C

CHAPTER 1 - INTRODUCTION

1.1 THE ELECTRICAL POTENTIAL METHOD IN NON-DESTRUCTIVE EVALUATION

The presence of cracklike flaws and stress concentrators cannot be avoided in any real engineering structure. However increasing demands for material and energy conservation have meant that components are being designed and manufactured with correspondingly smaller margins of safety. The modern engineering concept of damage tolerance has also emerged, where the presence of a flaw or crack does not necessarily mean that the component is at or near the end of its useful service life.

There have been several important developments that have allowed engineers to follow such a design philosophy safely. Recent progress in the theories of fracture and fatigue have given scientists and engineers a greater understanding of the mechanics behind these physical processes. Alongside these developments, and equally important, recent advancements in the field of non-destructive evaluation (NDE) have provided the necessary tools for the successful detection of flaws and cracks that would previously have gone unnoticed.

Of the NDE techniques currently available to the engineer the Alternating Current/Potential Drop (ACPD) or Alternating Current Field Measurement (ACFM) has received much attention. This method has proven itself to be one of the most versatile and easily applied of all the commercially available NDE techniques. In particular it can be readily automated to provide on-line monitoring capabilities and its effectiveness has been successfully demonstrated even in hostile environments (sea water, elevated temperature etc). ACPD

systems have now received general acceptance in the nuclear, aerospace and automotive industries where they provide a powerful and versatile crack dectection and monitoring capability.

As the possible applications of ACPD systems increase so does the awareness of certain serious limitations in current ACPD technology. In particular local crack and notch tip elastic/plastic deformation can have a marked effect on ACPD response. Such effects can lead to substantial errors in estimates of crackdepth and growth rates. Introduction of non-linear fracture mechanics concepts and the increasing use of ductile (J_{IC}) fracture toughness test methods has compounded this present lack of understanding. Without such knowledge accurate crack depth estimates in cases of ductile fracture and crack propagation would be almost impossible and present a severe restriction to the valuable on-line monitoring capabilities of ACPD systems.

The topicality and relevance of the ACPD method in modern NDE prompted the beginning of the present programme of work. Current understanding of the response of ACPD systems to strain and deformation ahead of a propagating fatigue crack or at the root of a notch is very restricted. Certainly present knowledge allows for little or no quantification of the magnitude or nature of their influence. Against a background of growing interest in ductile fracture test methods together with the increasing usage of ACPD monitoring techniques an understanding of the effects of strain on ACPD response is of great importance and relevance to the test engineer.

The aim of the current research programme is to study and quantify the influence of elastic and plastic deformation on the ACPD respose.

Fulfilment of this objective would thereby provide the necessary knowledge and understanding of such effects for more accurate and reliable ACPD crack monitoring methods. This would allow the ACPD method to be used in a reliable manner for a greatly increased range of ductile engineering metals and alloys, hence increasing the accuracy and applicability of this already versatile and useful NDE technique.

1.2 OPERATIONAL PRINCIPLES OF THE ELECTRICAL POTENTIAL METHOD

The successful dectection and monitoring of crack propagation and material damage has always been of great importance to the engineer. There are now a wide variety of techniques available, [1], (acoustic emission, eddy current etc) of which the electrical potential method has proven to be very successful.

The electrical potential or potential drop method actually has two distinct forms that are currently in widespread usage, employing either a direct (DCPD) or alternating current (ACPD) to create the electric field and potential gradient. However both methods work on similar physical principles and exhibit distinct advantages and disadvantages, [2].

When either a direct or alternating current is passed through a conductor the drop in potential between two points on the conductor will depend on a number of factors:

1	Test Conditions	current strength, temperature, environment etc..
2	Material Properties	electrical resistivity, magnetic permeability which are in turn influenced by the degree of plastic deformation and level of strain.

3	Measurement Geometry	dimensions and shape of testpiece or component, presence of notches or cracks, position of current inputs, position of voltage pickups etc..

It can be seen that one of the parameters governing the potential drop is the size and position of any defect present between the potential measuring points. Hence if all other parameters are known to be constant then the measured potential will be a function solely of crack geometry and so the size and shape of the crack may be inferred directly. Such direct correspondence between potential drop and crack geometry is the basic operating principle of all ACPD systems.

Before any predictions of crack profile can be accurately made the assumption that all other parameters remain constant must be considered. Clearly in most engineering situations the test parameters and overall specimen geometry may be assumed invariant. However since the material parameters of electrical resistivity and magnetic permeability are dependent on amount of plastic deformation and level of strain, careful consideration must be given to the material under examination and the strain levels likely to be experienced. [6, 8]

For instance in a brittle elastic material, eg HY100 structural steel, fracture will be preceded by only limited plasticity, so the assumption that PD is a function of only cracklength is valid. In more ductile materials, eg EN1A low carbon steel, appreciable localised plastic deformation around the cracktip is likely to occur leading to inhomogeneous material properties. Under these conditions

the ACPD response will also be affected by the variable material parameters of electrical resistivity and magnetic permeability and is no longer directly proportional to crack geometry.

This interaction of strain with the electrical and magnetic properties can have a marked effect on ACPD measurements, but at present is little understood.

1.2.1 Comparison of ACPD and DCPD Techniques

Although both of the electrical potential methods operate on the same physical principles, they exhibit quite different operational characteristics. Initial work in this field was largely concerned with the development of DCPD systems, perhaps due in part to the apparent simplicity of this method. Consequently at present DCPD is by far the most widespread of the two methods.

However there are several limiting factors to the operational accuracy of DCPD systems as listed below:

1 High Input Current	Because of the very low resistance of most alloys and metals, typically a few micro-ohms, a high input current (30-50A) is required to produce a measurable potential drop.
2 Voltage Drift of DC Amplifier	With high quality instrumentation the voltage drift of the DC operational amplifier is approximately $1\mu VK^{-1}$. This means for a temperature variation of 5K in the surroundings during operation could produce a variation in cracklength estimate of 0.5mm.

3	Thermoelectric EMF	At the point where the voltage pick-up leads are attached to the specimen a thermoelectric EMF is produced, typically 11 μVK^{-1} for an Fe-Cu junction. Hence a rogue potential drop is introduced into the system. For a pick-up temperature difference of 1K an error in the crack-length estimate of up to 1mm may occur.

It was largely due to the awareness of these inherent limitations with DCPD systems that provided the initial impetus for the production of a practical, alternative ACPD system. ACPD systems display several advantageous operating characteristics and these are listed below:

1	Low Input Current	Current is concentrated toward the surface of the specimen through the AC skin effect. Hence a measurable potential drop can be produced with a relatively low input current (2-10A).
2	High Noise Rejection	Use of high quality lock-in AC amplifiers ensures that good noise rejection capabilities and high signal gain are available.
3	No Thermoelectric Effect	With AC there are no thermally induced EMF's and the pick-ups do not have to be kept at constant temperature.
4	Absence of Drift	DC offsets and drift currents become unimportant in AC measurements

A more detailed comparison of the relative operating characteristics can be seen in Table 1.1. This clearly demonstrates the increased accuracy and sensitivity of the ACPD technique. There is however one major drawback with the use of AC and that is the increased sensitivity to variations in magnetic and electrical properties of the material under examination. These properties in their turn are influenced by degree of plastic deformation and levels of strain and such interactions are complex and their effect on ACPD response are at present not yet fully understood.

1.3 CHARACTERISTICS OF THE AC ELECTRIC FIELD DISTRIBUTION

1.3.1 The AC Electric Field and Skin Effect

One of the most striking features of the AC electric field distribution is the AC "skin effect", where the current becomes concentrated toward the surface of the conducting medium. A theoretical explanation of this phenomenon can be given by considering the AC electric field distribution in a circular conductor.

Consider an infinitely long cylindrical conductor having constant radius r_o and carrying an AC signal, It, where,

$$It = I\sqrt{2}\, e^{jwt} \qquad 1.1$$

It can be shown that the current distribution across any section of the conductor is governed by the following equations,

$$E(r) = \rho J(r) \qquad 1.2$$

$$r^2 \frac{\partial^2 E}{\partial r^2} + r \frac{\partial E}{\partial r} + k^2 r^2 E = 0 \qquad 1.3$$

$$\text{where, } k = (1 - j)\left(\frac{\pi f \mu}{\rho}\right)^{\frac{1}{2}} \qquad 1.4$$

Solution of 1.2 gives an expression of the current density, J(r),

in terms of the Bessel functions J_0 and J_1.

$$J(r) = \frac{Ik}{2\pi r_0} \frac{J_0(kr)}{J_1(kr_o)} \qquad 1.5$$

(J_0 and J_1 are Bessel functions of the first kind with complex arguments of zeroth and first order respectively)

In many practical situations the arguments will be large and both J_0 and J_1 can be approximated by an exponential function.

The absolute value of the current density can then be written as:

$$|J(r)| = \frac{1}{\sqrt{2\pi r_0}} \left(\frac{\pi f\mu}{\rho}\right)^{\frac{1}{2}} \left(\frac{r}{r_o}\right)^{\frac{1}{2}} \exp\left[\left(\frac{\pi f\mu}{\rho}\right)^{\frac{1}{2}}\right] \qquad 1.6$$

It can be seen that the term $\left(\frac{\pi f\mu}{\rho}\right)^{\frac{1}{2}}$ dominates the expression and determines the AC field distribution within the conductor.

The "skin depth" or "depth of penetration" of the AC signal is normally represented by the Greek symbol δ, and can be written as:

$$\delta = \left(\frac{\rho}{\pi f\mu}\right)^{\frac{1}{2}} = \left(\frac{\rho}{\pi f\mu_r\mu_o}\right)^{\frac{1}{2}} \qquad 1.7$$

Implicit in equation 1.6 is the concentration of the current toward the outer surface of the conductor and an exponential decrease in current strength moving inward toward the centre. (see figure 1.1)

In addition it can be shown that if $\delta << r$ then,

$$|J(\delta)| = \frac{1}{e} J(r_0) \qquad 1.8$$

Therefore δ represents the depth at which the current density has been attenuated to 37% of its value at the surface of the conductor.

The physical cause of the effect is associated with the time varying magnetic field produced by the AC itself. Eddy currents set up within the conductor act in accordance with Lenz's law to oppose the change of magnetic flux. Flux linkage increases toward the centre of the conductor with a corresponding increase in effective AC impedance. The overall effect is to concentrate the current toward the outer layers of the conductor where the impedance is at a minimum.

Due to the nature of the AC field distribution there is a marked increase in sensitivity over its DC equivalent to surface features such as cracks. For example in a strongly ferromagnetic material such as mild steel an AC signal at an operating frequency of 100Hz will give a PD of 1-2mV whereas the DC equivalent would be in the micro-volt range.

From consideration of equation 1.7 it can be seen that the "skin depth" will depend on the frequency of the supply and the electrical and magnetic properties of the material.

Comparative "skin depth" values are given in Table 1.2.

Energising frequencies of ACPD systems are typically of the order 2-10kHz which will produce a pronounced skin effect. As a general rule the high permeability of ferromagnetic alloys ($\mu_r >> 1$) produces a strong skin effect in such materials. In non-ferrous alloys the skin effect is less marked since $\mu_r = 1$ and the skin is largely governed by the electrical resistivity, ρ.

1.3.2 Geometrical Aspects

Correct interpretation of the electrical potential measurements is essential for the effective use of any ACPD system. As a straightforward example consider the case of a semi-infinite uniformly deep crack in a homogeneous conducting medium, see figure 1.2. In reality this situation approximates well to the case of a crack whose depth is very small compared to its length, but is large in comparison to the "skin depth". Current inputs are located at positions A and B such that a region DEFG, of uniform electric field with streamlines perpendicular and equipotentials parallel to the crack faces is created. Within this region the effective impedance will vary linearly with distance along any one streamline. The presence of a crack increases the effective current pathlength with a corresponding increase in potential measured across the faces of the crack.

Consider a "voltage probe" with pick-ups fixed distance Δ apart. Away from the crack the measured voltage will be V_1, but spanning the crack it will increase to V_2, (see figures 1.3 and 1.4).

Now since distance α voltage drop:

$$V_1 \alpha \Delta \qquad 1.9$$

$$V_2 \alpha(\Delta + 2a) \qquad 1.10$$

Therefore,

$$V_1 = k\Delta \qquad 1.11$$

$$V_2 = k(\Delta + 2a) \qquad 1.12$$

Rearranging,

$$a = \frac{\Delta}{2}\left\{\frac{V_2}{V_1} - 1\right\} \qquad 1.13$$

This provides a very simple estimate of crackdepth and is commonly known as the One-Dimensional Solution. Such a model is very idealised but forms a good first approximation in many practical situations.

In the case of part through cracks having a semi-elliptical or semi-circular geometry serious errors may occur when using equation 1.3 to produce estimates of crackdepth. To account for the non-uniformity of the electric field surrounding such defects a variety of empirical and theoretical approaches have been adopted.

Aboutarabi and Cowling [3] adopted a semi-empirical approach to the problem and produced a series of modification factors for the one-dimensional solution to size semi-elliptical fatigue cracks in structural steels. Dover et al [4, 5] chose a more rigorous mathematical approach. By considering the analogous hydrodynamic problem of irrotational flow over a plane containing a part circular crack an exact solution for the AC field distribution was produced. However, at present, there exists no exact solution for the case of a semi-elliptical surface crack.

It should be noted that throughout these geometric solutions material homogeneity and isotropy have been assumed. Rigorous application of the geometric theories must therefore be confined to situations of limited deformation where significant variations in material properties would not be a major consideration.

1.3.3 Material Considerations

Previous discussions on the influence of geometry on ACPD response were limited to isotropic, homogeneous materials whose properties were not affected during crack propagation. The tip of a propagating fatigue crack represents a region of very high strain, often producing extensive localised plastic deformation. Under such circumstances the material condition is no longer uniform and material parameters will have significantly altered. The degree of plasticity depends

on the level of stress and the ductility of the material, with many engineering components experiencing appreciable plastic deformation during their service lives.

The correlation between elastic/plastic deformation and associated changes in magnetic and electrical properties has been well known for some considerable time, (Bozorth [6]). The resistivity of all electrically conducting metals and alloys is determined by the ease with which the conducting electrons can pass through the ionic metal lattice. Disruption of the lattice structure via elastic and plastic deformation will therefore interfere with electron flow and alter the resistivity of the material. Rossiter [7] has used electrical resistivity measurements to study microstructural changes in several different metals and alloys. Similarly magnetic properties are affected via restrictions placed on the free movement and orientation of magnetic domains. Unlike resistivity, however, only ferromagnetic materials are susceptible to such changes since non-ferrous materials are considered to have a relative magnetic permeability close to unity. Collectively these two properties interact to affect the ACPD response via alteration of "skin depth", and in their turn are determined by strain and deformation. Esin and Jones [8] capitalised on this effect and used AC impedance measurements to study the onset of microplasticity in specimens of MBRY13L steel, aluminium and copper under uniaxial tensile loading conditions.

In the majority of ACPD measurement situations these influences are not only undesirable but also unavoidable leading to serious errors in estimates of crackdepth. Various authors have noted and commented upon these effects, most notably Okumura et al [9] and Ryman [10] during rising load fracture mechanics tests, where the PD was observed

to vary substantially both increasing and then decreasing with a monotonically increasing load. Truchon [11] also remarked on a curious "hysteresis" like response during low cycle fatigue experiments on smooth specimens. In all cases the phenomena was attributed to the high strain levels causing variation in electrical and magnetic properties but no further investigation was undertaken. Previous authors have proposed several different mechanisms to explain the interaction of elastic and plastic strain and deformation with electrical and magnetic properties. However in every case there was little or no experimental justification to support any of the proposed theories.

At present such effects are not clearly understood or quantified and until such time as they are, they present a continuing hindrance to the operational accuracy of ACPD crack monitoring systems.

1.4 HISTORICAL PERSPECTIVE

The principle of using electrical potential measurements to assess material damage in structures has been known for many years. Gallanderin investigated the application of PD measurements to NDE as early as 1912. However not until more recently did the idea receive further serious attention. Barnett and Traiano experimented in 1955 with the use of DC for the continuous on-line monitoring of several fatigue specimens under laboratory conditions. Using a series of round-notched specimens in rotating bending they produced a series of calibration curves for cracklength in terms of measured PD.

During the 1960's and 1970's the general acceptance of Linear Elastic Fracture Mechanics (LEFM) and growing interest in the fatigue of materials provided a great boost to electrical potential methods. They

were easily automated and could provide a continuous record of crackgrowth as accurately as most other methods available at the time. Initial work in this field concentrated on the use of direct current (DC). (See Knott [12] for a detailed account of the technique).

DCPD systems have been developed and used to monitor crackgrowth by a number of research workers. In 1971 Ritchie [13] developed a method of optimizing the location of the current inputs using graphitised electrical analogue paper to map the electric field distribution. Clark and Knott [14] managed to theoretically calculate the electric field by use of conformal mapping techniques for a variety of testpiece geometries (1975). Klintworth and Webster (1980)[15] also provided a theoretical field solution using both finite element methods and boundary integral techniques.

During this period there was a growing awareness of several inherent limitations in the operational accuracy of DC systems. Particularly the difficulty in maintaining steady high DC signals and the susceptibility to thermal EMF's. This stimulated renewed interest in the possibility of using AC as the energising signal. ACPD systems can capitalise on the AC "skin effect" and work at much lower current requirements and do not suffer from any thermal effects.

Over the past ten years there have been many workers in this field and much research work has taken place concurrently.

Carlsson [16] undertook a series of experimental measurements using AC in the MHz range to study the velocity of cleavage crack propagation in steels. Betz demonstrated the successful detection of cracks only 0.5mm long via a differential measuring technique using AC at 625Hz.

Marandet (1977)[17] used quite high currents (50A) at mains frequency during an investigation of J_{IC} test methods in a limited number of quenched and tempered steels. Tomlinson clearly demonstrated the advantage of the AC method over existing DC techniques. Employing an AC energising signal he was able to observe a 320mm long fatigue crack in a large turbine component at 540 °C. Merely the size of the component would have precluded the use of the more conventional DC because of the enormous current requirements. However an AC signal of 0.5A at 525Hz produced a sufficient PD to successfully detect the crack. Early work used relatively low supply frequencies and was restricted in application to notched and precracked specimens.

Later work by Marandet [18] used much higher energising frequencies (2A at 10kHz) to detect cracks under static and dynamic loading conditions. Marandet also remarked upon the curious backward PD slope prior to crack initiation or propagation. Verpoest (1981) [19] investigated AC at a range of frequencies. Choosing 40kHz to exploit the strong "skin effect" it was possible to detect the initiation of surface microcracks in unnotched fatigue specimens.

With increasing interest in ACPD methods the first of several commercial systems were marketed. Ryman (1979) [10,20] developed the "CPD1 AC Crack Detector" at Testwell Ltd of Daventry. Using a fixed energising frequency of 8kHz the instrument was successfully employed in crack propagation experiments on T-Butt welded and notched specimens. A very simple electric field model was also proposed and used to make crack depth estimates, the One-Dimensional Field Solution, see section 1.2.2. During COD/load tests the backward slope phenomenon was again observed. Ryman subsequently commented upon the increased sensitivity of AC systems to variation in electrical and magnetic properties

through material deformation and high strain. Another system, the "Crack Microgauge", also became available at this time. Produced by the Unit Inspection Co [4] following research work at the University College of London by Dover this system was also fixed frequency (6kHz). Dover and Michael [4,5] also proposed several electric field theories to account for non-linearities in the AC field distribution around short deep cracks. Aboutarabi and Cowling [3] took the complex field solutions of Michael and Dover and produced a series of simple modification factors for the one-dimensional solution. These were used in sizing semi-elliptical fatigue cracks in BS4340 Grade D steel. Further evidence of the variation in magnetic and electrical properties caused by strain and deformation was highlighted by Truchon [11]. During low cycle fatigue tests on notched specimens the PD was observed to vary considerably during a single strain cycle the amplitude being dependent upon the choice of material.

Recent (1986) advances in ACPD technology have seen the production of the first commercially available variable frequency systems. Testwell Ltd have introduced the CPD4 with a continuous frequency range of 0-100kHz. Matelect Ltd [21] have also marketed a similar system with multi-frequency operation at preselected discrete values of 300Hz, 10kHz, 30kHz and 100kHz.

1.5 AIMS OF THE PRESENT PROJECT

An investigation is undertaken to study and quantify the material parameters of strain and plastic deformation on ACPD response. Previous works reported in references 9, 10, 11 have commented on the influence of strain and conjectured upon the nature of the observed ACPD response. However none have furthered their initial studies and examined the observed phenomena in a rigorous experimental and

theoretical manner. Quantification and understanding of the nature of these effects would be useful in a number of ways in solving the problems associated with correct sizing of cracks where appreciable localised plasticity is present. This would allow the ACPD technique to be used with increased accuracy and reliability in a far wider range of ductile engineering metals and alloys where previously interpretation of the ACPD response has been complicated by the unknown effects of strain.

Exploratory experimental work has been carried out to investigate the influence of strain at the root of a notch on ACPD response using a series of mild steel (EN1A) bend specimens. Monitoring of the PD response across the notch as the bending load is increased and localised notch tip deformation occurs revealing several interesting characteristics:

(i) In the case of mild steel (EN1A) appreciable changes in the ACPD response across the notch are observed where no crack is present initially or initiates during test.

(ii) There exists no obvious one-to-one correspondence between any simple parameter of either strain or plasticity and ACPD response. Strain and plasticity levels are monotonically increasing functions of load whereas the ACPD response observed across the notch displayed several turning points and changes of gradient. The complex nature of the response is thought to be due to the influence of strain with the electrical and magnetic properties of the material. The net ACPD response observed resulting from the interaction of both parameters.

(iii) From initial observations with a single notch profile and material the reproducibility of the results is good.

Following the initial programme of research extensive experimental and theoretical work has been undertaken to investigate further and in greater depth the influence of strain and deformation on ACPD response.

The objectives of the present work are:

(a) To produce experimental data of the ACPD response across a series of different notch profiles in both a strongly ferromagnetic material (mild steel; EN1A) and a non-ferrous material (aluminium alloy; NE8) to localised elastic and plastic strain around the notch root.

(b) To correctly model the specimen geometry and loading conditions using finite element (FE) methods and obtain a detailed description of the local notch tip stress/strain field under both elastic and post-yield conditions.

(c) To investigate the influence of strain and deformation on the electrical and magnetic properties governing ACPD response in both materials.

(d) To examine the correlation between related aspects of (b) and (c) to obtain a greater understanding of the nature of the response observed in (a).

(e) To improve the accuracy and reliability with which ACPD systems may be used to size cracks and increase the applicability of the ACPD technique to a wider class of ductile engineering materials.

	DIRECT CURRENT	ALTERNATING CURRENT
Base Potential	400 μV	400 μV
Required Current	10A	3A
Noise Level at Output	0.1 μV	0.02 μV
Signal to Noise Ratio on Absolute Potential	4000 : 1	20000 : 1
Operating Sensitivity		
Amplifier Gain	10^4	5×10^4
Potential	100 μV/V	20 μV/V
Cracklength	14 mm/V	3 mm/V
Operating Resolution		
Potential	0.1 μV	0.02 μV
Cracklength	0.013 mm	0.003 mm
Sensitivity to Thermal EMF	High	None
Sensitivity to Leadwire Movement	None	Moderate

Table 1.1 Comparison of the Operating Characteristics of Typical ACPD and DCPD Systems

	μ_r (–)	ρ ($\mu\Omega$mm)	δ (mm)	Skin Depth δ(mm) at frequency f				
				10Hz	100Hz	1kHz	8kHz	1MHz
MILD STEEL	119.37(*)	210	$\frac{21.1}{\sqrt{f}}$	6.677	2.111	0.668	0.236	0.021
ALUMINIUM	1.0(**)	27	$\frac{82.7}{\sqrt{f}}$	26.165	8.274	2.616	0.925	0.083
SILVER	1.0(**)	16	$\frac{63.9}{\sqrt{f}}$	20.213	6.392	2.021	0.715	0.064

* This is taken as a typical value in the annealed condition

** For nonferrous materials $\mu_r = 1$ and is a constant.

Table 1.2 Skin Depth of Conducting Materials.

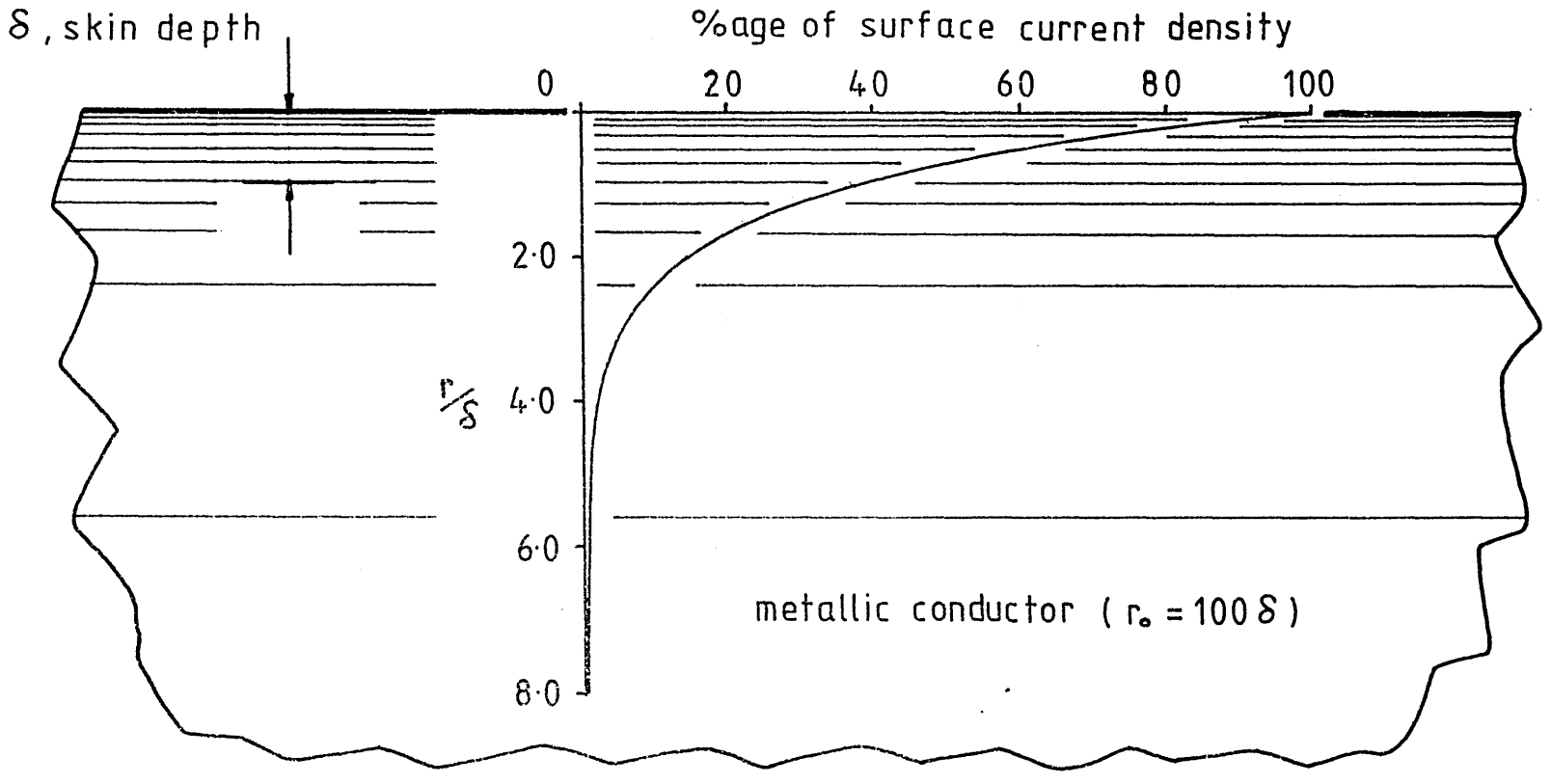

FIG 1.1 AC FIELD DISTRIBUTION IN SECTION OF ROUND METALLIC CONDUCTOR RADIUS $r_0 = 100\delta$

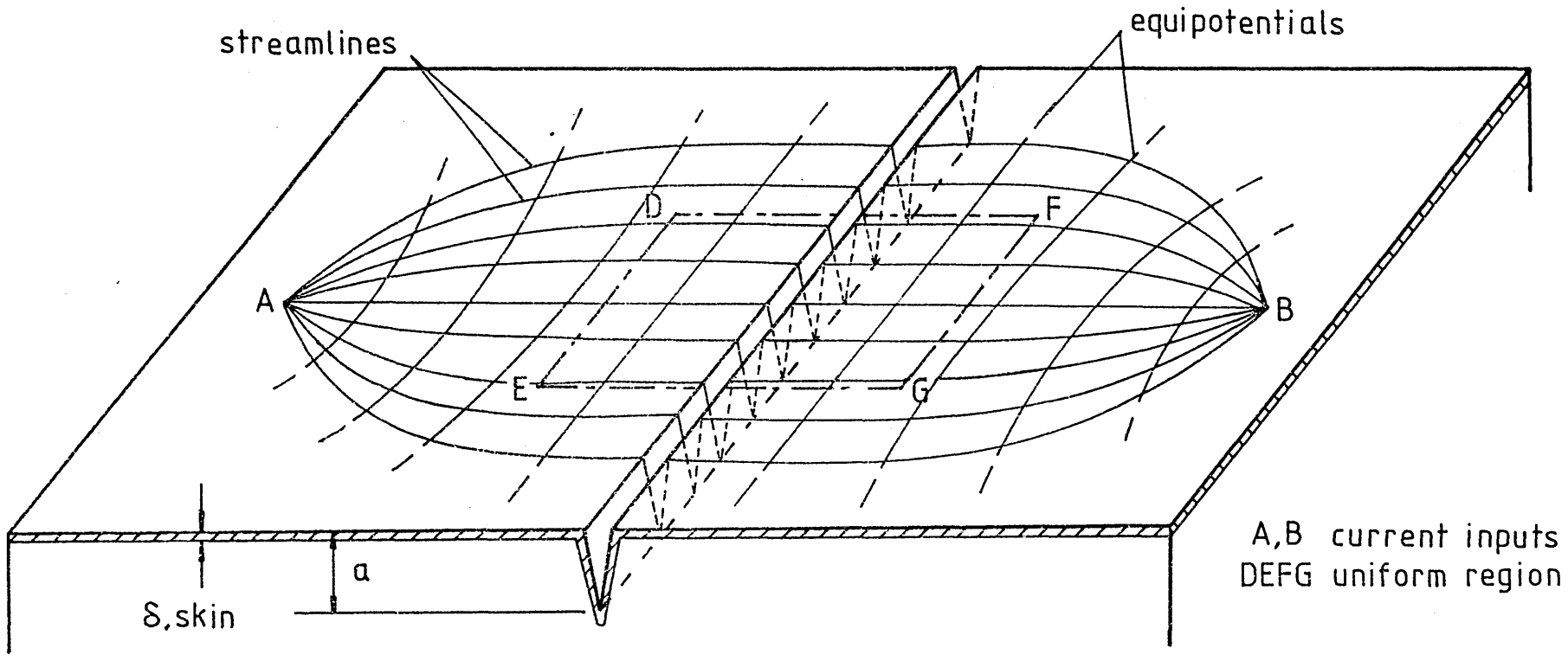

FIG 1.2 AC FIELD DISTRIBUTION AROUND A SEMI INFINITE SURFACE CRACK IN A CONDUCTING METAL PLATE

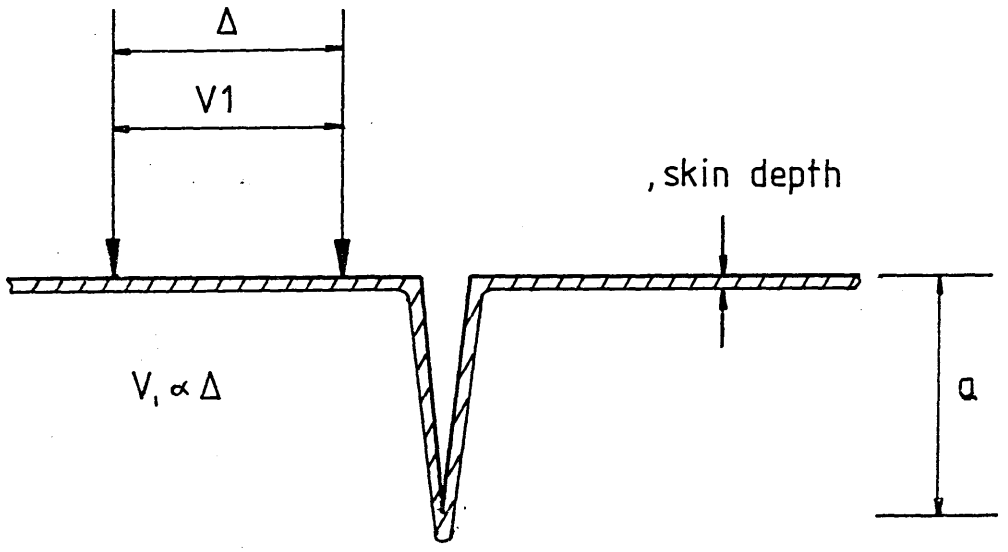

PROBE AWAY FROM CRACK

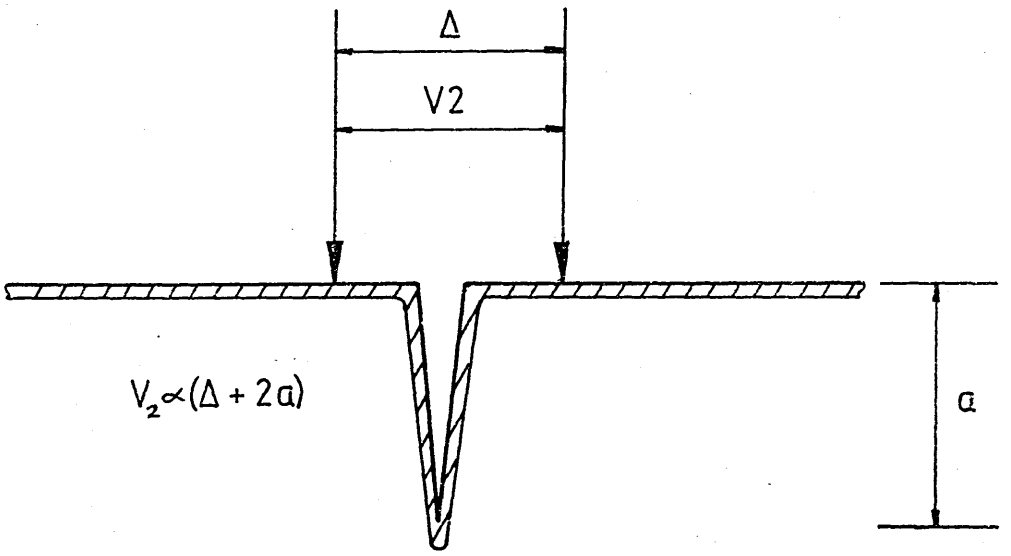

PROBE OVER CRACK

FIGS 1.3/1.4 PROBE POSITIONS FOR ACPD MEASUREMENTS ALONG STREAMLINE IN UNIFORM ELECTRIC FIELD

2.1 TESTPIECE SPECIFICATIONS

2.1.1 Testpiece Geometry

During the design of the specimen there were several important features that had to be considered and incorporated into the specimen geometry. The specimens were designed to have a fairly simple overall geometry, easing manufacture, and also to be sufficiently small and compact to be easily loaded above yield in the Mayes servo-hydraulic testing machine.

Another consideration was the depth and size of the notches which had to be small compared with the overall specimen dimensions to prevent premature net section yield, but large enough to have a distinctive localised stress field associated with a particular profile.

The overall testpiece dimensions can be seen in figure 2.1. These were the same for both the aluminium alloy NE8 and mild steel EN1A specimens. A large shallow radius was machined onto the underside of the specimen to give the minimum section at the notch and to ensure yield initiation at the notch root. Such a large, gentle radius would however not encourage premature yielding on the radiused side itself.

Both notch profiles were introduced into all the specimens using milling cutters of the required profiles prior to annealing. The V notches were machined using a standard 60° Charpy V cutter and the U notches by a specially ground semi-circular cutter. After machining the notch dimensions were checked by viewing on a shadowgraph machine. The dimensions of the U notches for aluminium alloy NE8 and the mild

steel EN1A can be seen in figures 2.5 and 2.3 respectively. Examination of the shadowgraph results for the V notches revealed that although the same milling cutter had been used the resultant notch profiles were slightly different with the V notch aluminium alloy specimens having overall slightly smaller dimensions than the mild steel, see figures 2.4 and 2.2. However the differences between the V notch profiles of each material were small but not inconsequential with each material having consistent profiles. Since the problem was unavoidable, it was considered necessary to investigate what effect, if any, the variation in notch geometry may have on the localised notch tip stress field. An elastic finite element analysis (FE) on both notch profiles in either of the two materials showed there was a slight discrepancy in the predicted values of peak notch stress and stress concentration factor for each of the two materials.

These results strongly suggested that however small the geometric differences were they could appreciably affect the localised stress/strain field at the notch tip although the effect on the overall global stress distribution would be negligible. From these conclusions that the V notch profiles were not equivalent in terms of stress distribution it was necessary to consider each separately during the stress analysis, hence each of the two V profiles were modelled separately during the FE analysis.

2.1.2 Material Condition

From the beginning of the experimental programme it was thought desirable to compare and contrast the ACPD responses observed in two magnetically different materials and so observe the effect of strain on the magnetic permeability ($\mu = \mu_r \mu_o$) and the electrical resistivity (ρ) separately. EN1A low alloy mild steel was chosen as

a material exhibiting strongly magnetic characteristics, hence giving an ACPD response dependent on both μ and ρ. The non-ferrous aluminium alloy NE8 was selected for its typically weak magnetic behaviour, where the effect of strain on ρ could be observed in isolation.

Both alloys were also considered representative of materials used in many real engineering components and would therefore give more relevant and applicable results than with materials chosen solely for their desirable electrical or magnetic characteristics. However there were several basic criteria that each of the materials were required to meet. A first, major, consideration was the desirability of good ductile properties. The nature of the project necessitated a choice of materials that would readily deform plastically and produce large notch root strains but would not fracture or tear at the notch root even at high load levels. The onset of fracture and crack extension at the notch root would only make interpretation of the results and isolation of the strain/PD response considerably more difficult.

Another very important consideration was the uniformity and consistency of the material properties. To achieve material homogeneity and isotropy both sets of specimens in both materials were annealed after machining and any light surface oxide layer removed using fine emery paper. The material condition and annealing conditions for both materials are given below.

EN1A MILD STEEL

Chemical composition (%)

C	Si	Mn	S	P
0.07-0.15	0.10 max	0.80-1.20	0.20-0.30	0.07 max

Heat Treatment

Process Annealed, 16 hours at 650 °C, Furnace Cool.

NE8 ALUMINIUM ALLOY

Chemical composition (%)

Mg	Cr	Mn
4.19	0.14	0.74

Heat Treatment

Annealed, 6 hours at 300 °C, Furnace Cool.

2.2 CPD3 CRACK MONITORING SYSTEM

2.2.1 Instrument Specification

The CPD3 crack monitoring system is a commercially available, portable, ACPD crack detection and minitoring instrument. The system is manufactured by Testwell Ltd of Daventry and was developed in association with the MOD and UKAEA. (Testwell Ltd are also the collaborating body in the SERC CASE award which supports this work). The instrument is capable of detecting changes in AC impedance due to crack propagation and/or material deformation in most electrically conducting materials. It is a compact and versatile system employing a constant AC generator and a high sensitivity detector/ demodulator with facilities for hard copy data recording and also signal analysis.

The complete CPD3 crack detection system can be seen schematically in figure 2.6. The instrument operates at a fixed energising frequency of 8 kHz, producing a marked AC skin effect in most

electrically conducting materials. The input current may be varied to suit the test and material requirements within a range of 0-10A but prolonged operation above a level of 7A is not recommended. The basic system gain of the instrument can also be varied within the range 2 000 to 70 000 by means of a ten-turn potentiometer and selection of the appropriate gain pushbuttons on the front panel of the CPD3. To assist data collection there is also provision for the supply of a negative DC signal to the modulated and amplifed output from the specimen. To reduce signal interference to a minimum, a bandpass filter has been included into the system prior to signal rectification.

2.2.2 Description of Controls

A full view of the CPD3 front panel can be seen in plate 2.1. This shows the pushbuttons and dials governing CPD3 operation (current level, gain etc). A brief description of the panel details and control functions is given below:

(1) Digital Voltmeter DVM: displays signal at the DC out terminals or the output current to specimen.

(2) On: 240V 50 Hz Mains Supply - "push" on.

(3) DC OUT: produces an amplified analogue equivalent signal of the PD detected across the specimen.

(4) V: displays signal available at DC out terminals onto DVM.

V (CAL): selection with CAL displays basic system gain in thousands on DVM.

(5) A: displays current output to specimen on DVM.

(6) EXT: selects external signal conditioning via D socket on Back Panel, removes internal level and offset controls.

(7) CAL (V): selection with V displays basic system gain in thousands on DVM.

(8) GAIN: adjusts the basic system gain over the range 2 000-10 000 and may be further multiplied by 1, 2, 3, 4, 5, 6 or 7 by selection of appropriate combinations of x1, x2, x4 pushbuttons.

(9) ZERO: removes the input signal and ground references the detector, overriding all signal conditioning apart from RANGE pushbuttons.

(10) LEVEL: adjusts output current to specimen (0-10A).

(11) OFFSET: applies a negative DC signal to the demodulated and amplified PD measured across the specimen. The offset range is 0-10 V operating over 0-30 V depending on selection of range buttons.

(11) RANGE: selects operating level for offset dial either 0-10 V, 10-20 V or 20-30 V.

(All buttons "push" to make, "push" to break.)

2.2.3 Material Compensation

There are several PD monitoring techniques available which may be employed with the CPD3 crack monitoring system. The method adopted throughout the current experimental work to monitor material damage via the CPD3 crack detector was that of material compensation. This method can allow for any variations in temperature or parasitic voltages produced on the surface of the specimen during instrument operation. This is achieved using two pairs of pick-ups, one across the notch and one across an adjacent plain section of material; any generally induced signals will theoretically be the same in each and are cancelled out by subsequent differential amplification.

As an example consider the schematic representation as shown in figures 2.7 and 2.8. Voltage pick-up leads are positioned both across the notch, AB, and across a plain section of material, BC, immediately adjacent to the notch. Let the signal induced by the presence of a defect be Vn and the signal measured across the plain section of specimen, the compensating signal, be Vc. Since both pick-ups are in close proximity to each other any induced signals due to temperature variations, static etc will be detected equally by both. Let Vi represent any induced signal then the signals measured in AB and BC at system gain of G, say, will be:

$$Vab = G [Vn + Vi] \qquad 2.1$$

$$Vbc = G [Vc + Vi] \qquad 2.2$$

Subtracting the signals,

$$Vab - Vbc = G [Vn - Vc] = [V] \qquad 2.3$$

Equation 2.3 represents a straightforward algebraic operation easily performed electrically using modern amplifier technology. Use of the compensation method can therefore eliminate any extraneous signals induced on the surface of the specimen. Moreover the amplified output voltage, [V], will now have a direct correspondence to the severity of any defect spanned by the pick-ups AB.

2.3 LOADING EQUIPMENT

2.3.1 The Mayes Servo-Hydraulic Testing Machine

Throughout the mechanical testing a Mayes servo-hyraulic testing machine was used to apply the bending load to the specimen via a purpose designed loading rig detailed in section 2.3.2.

The machine is servo-hydraulically powered with both tensile and compressive loading capabilities at several different load ranges with a maximum load range of 0-100 kN. An indication of the magnitude

of the applied load is given by the voltage output from the Mayes. For each of the available load ranges the Mayes gives 0-10 V output with the maximum voltage corresponding to the maximum applied load.

Load application may be controlled in a number of different ways depending upon the module selection on the front panel of the machine console. During testing only two of the modules were used, the POSITION and LOAD modules. The POSITION module controls the displacement of the lower ram of the Mayes and the LOAD module controls the force applied to the specimen via feedback from the load cell.

Generally speaking the POSITION control module was used for coarse adjustment of the Mayes ram and alignment of the specimen prior to loading. Once aligned correctly, load application was controlled with the LOAD module with either "automatic" or "manual" control options.

"Automatic" selection meant the load was applied at a preselected constant rate up to the final maximum load. The "Manual" option gives the operator full control over load application and was used most widely during the testing when it was found desirable to apply the load in incremental steps holding a constant load level during each.

The electrical output signal (10 V max) from the Mayes corresponding to the applied load or displacement was monitored via a digital voltmeter (DVM) but may also be used to drive a plotter or other similar data recording instrument.

2.3.2 Design of Bending Rig

From the beginning of the test programme it was decided to subject

the specimens to a pure, four-point, bending load with the tensile stresses on the notched side of the specimen. Pure bending was favoured in preference to three-point bending since the notch region would be subject to a uniform bending moment and with no shear. To achieve pure bending it was necessary to design a special four-point bending rig to fit the Mayes machine and transmit the load correctly to the specimen.

The upper part of the rig was manufactured to be fixed rigidly to the upper section of the Mayes machine via a large screw thread, see figure 2.9.

To allow for ease of alignment and give some adjustment to the system the lower part of the rig was designed to locate freely in the Mayes ram by means of a 75 mm diameter circular boss, see figure 2.10.

The upper and lower roller spacings are 80 mm and 120 mm respectively. The load was transmitted via four cylindrical metal rollers which were produced from 12 mm diameter hardened steel bar.

Since electrical potential methods were being used throughout the investigation the effect of insulating the rollers on the ACPD response was investigated. Trial tests using electically insulated rollers revealed no detectable difference in ACPD response from the uninsulated case. It was therefore concluded unnecessary to introduce the added experimental complication of insulating the rollers with either Tuffnell or other suitable material.

The lower pair of rollers are located on two elevated pillars with chamfered and cutback roller seatings to allow easier access for electrical contacts and reduce the risk of mechanical contact between specimen and loading rig. The loading pillars themselves were

attached to a solid steel base plate 25 mm thick via two large Allen bolts. This feature allowed the pillars, if necessary, to be shimmed up allowing some adjustment to achieve even roller/specimen contact. The upper part of the testrig was also drilled and tapped to allow for the attachment of earthing straps via two small Allen screws and was used as the earthing point for the mild steel specimens during testing. (see plate 3.2, chapter 3)

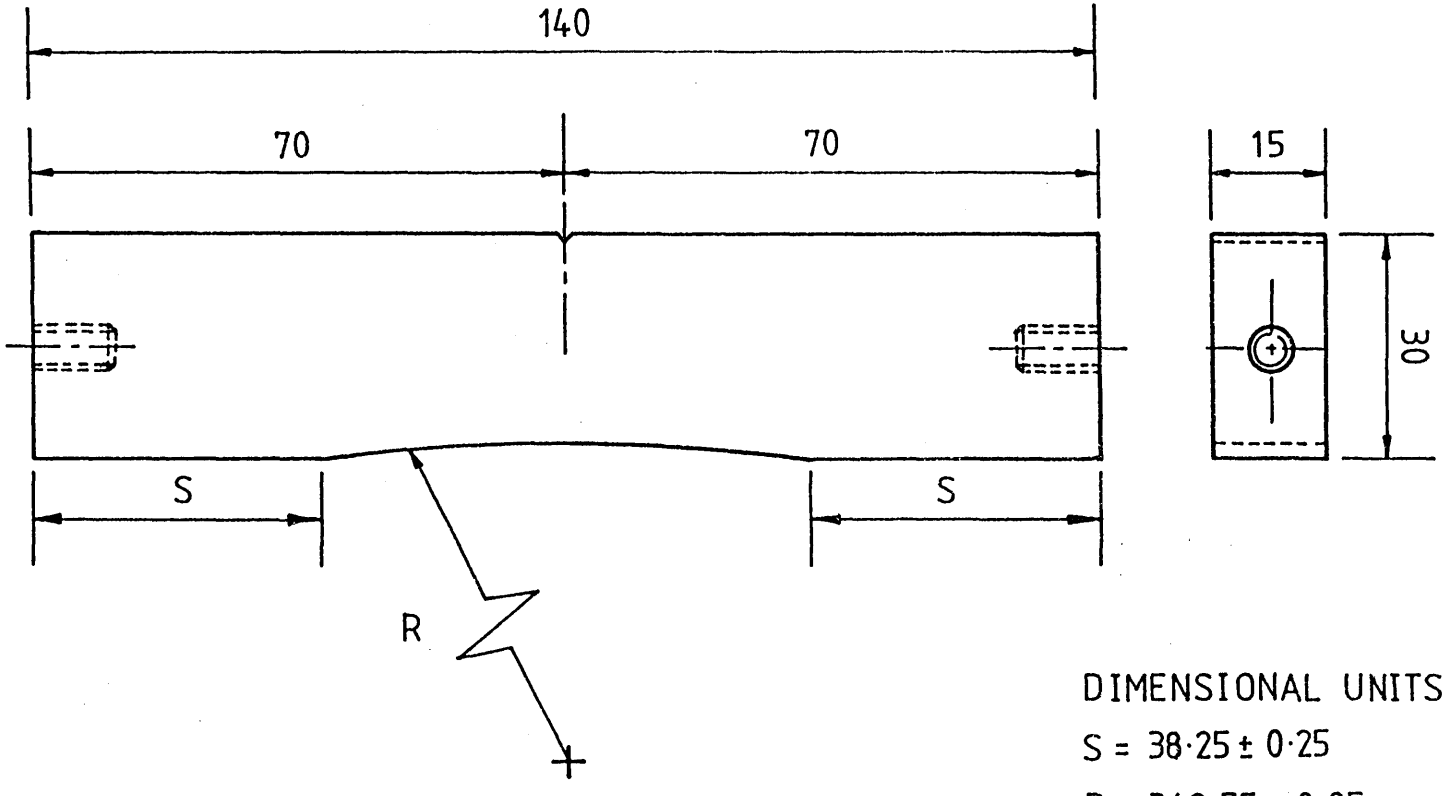

Fig 2.1 Overall Specimen Dimensions

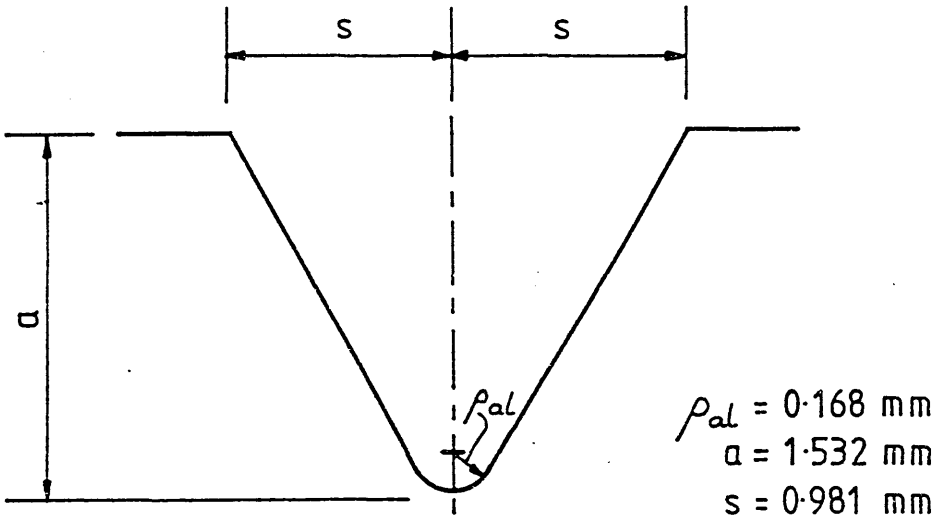

Fig 2.2 V Notch Profile EN1A

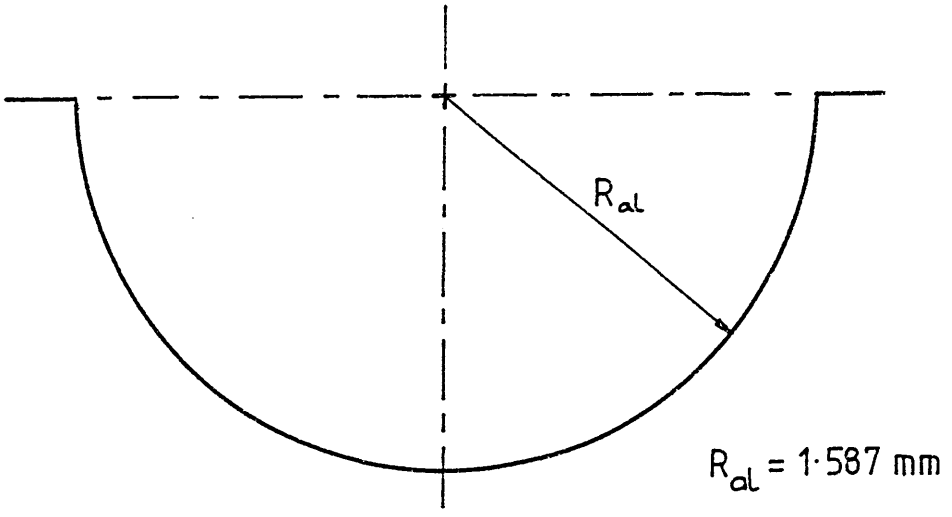

Fig 2.3 U Notch Profile EN1A

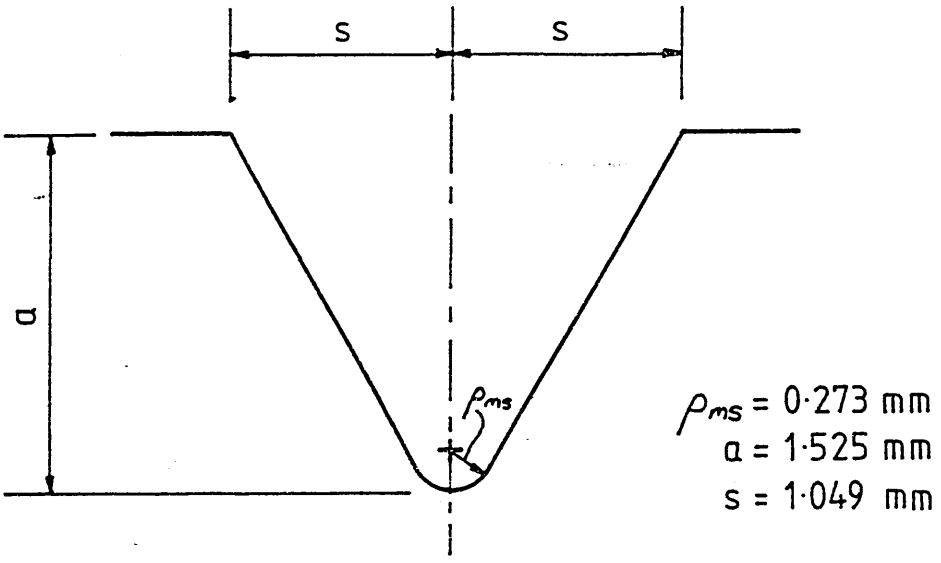

Fig 2.4 V Notch Profile NE8

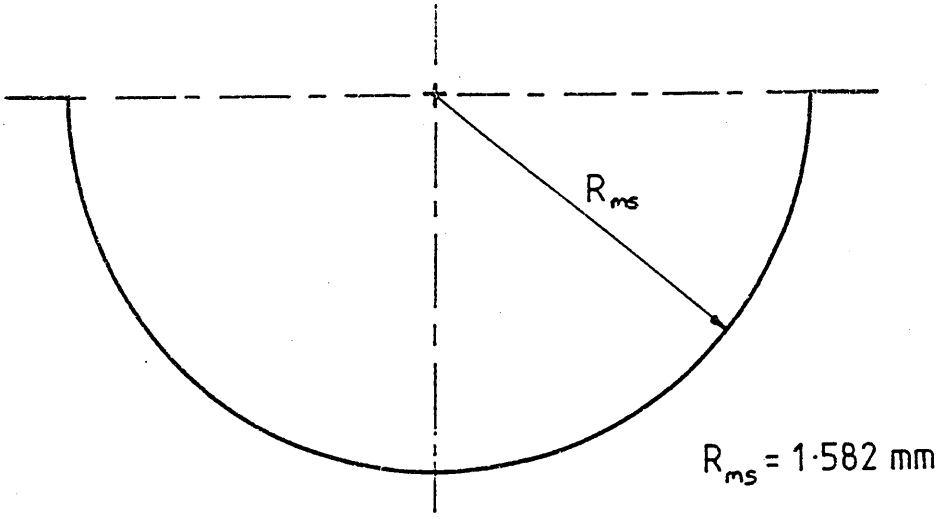

Fig 2.5 U Notch Profile NE8

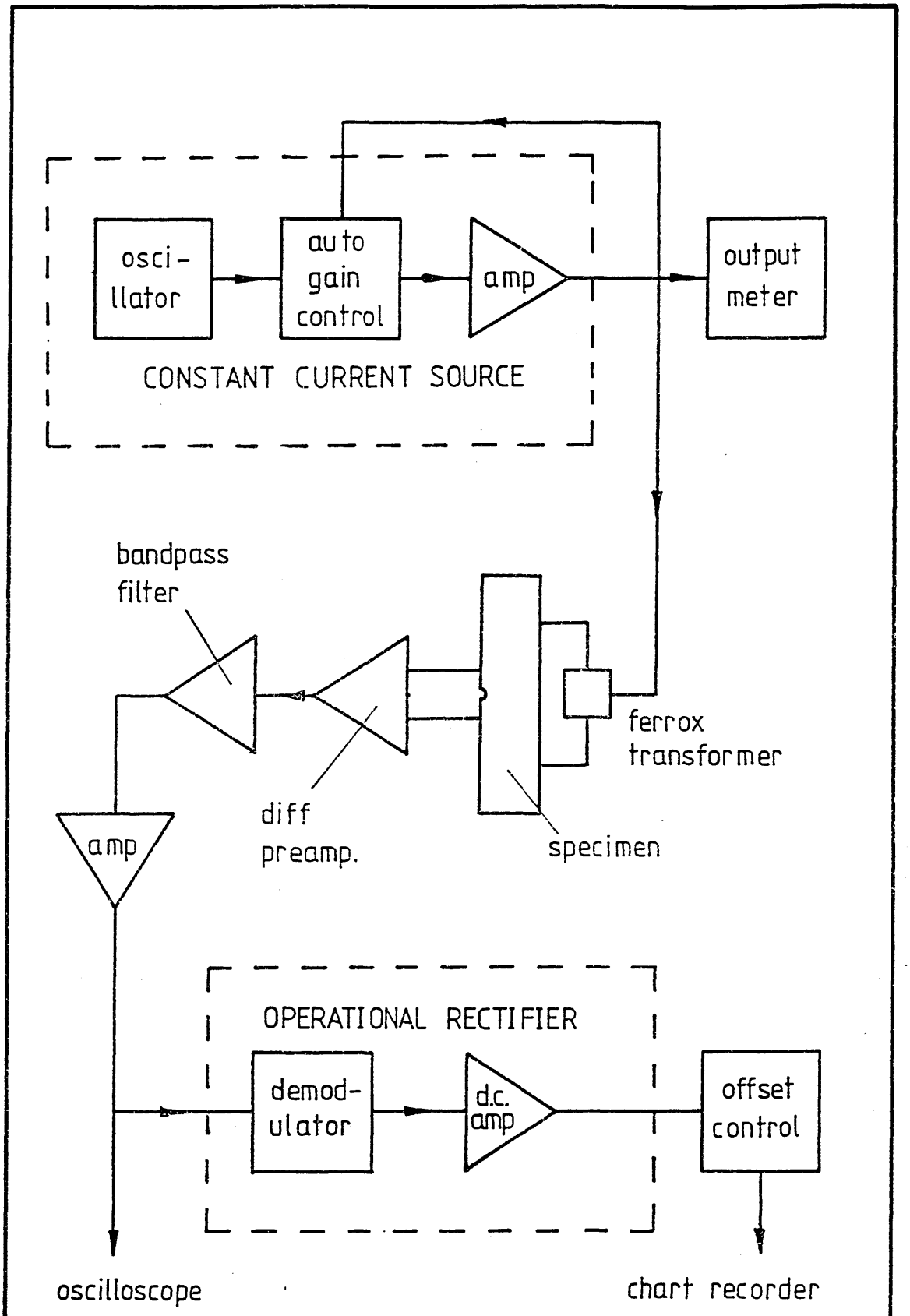

Fig 2.6 Schematic Representation of CPD3 Crack Detection System

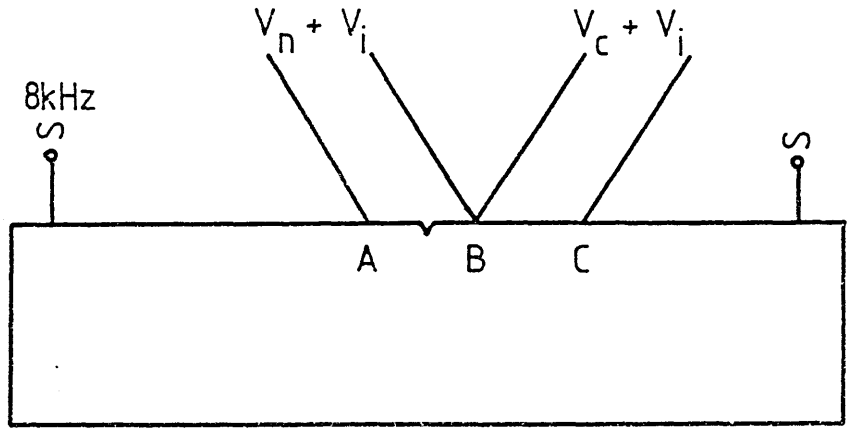

pathlength AB>BC specimen earthed

V_i = induced signal

V_n = voltage across notch

V_c = voltage across plain material

V = voltage output

G = gain

Fig. 27 Signal Notation for Material Compensation

DIN NO.

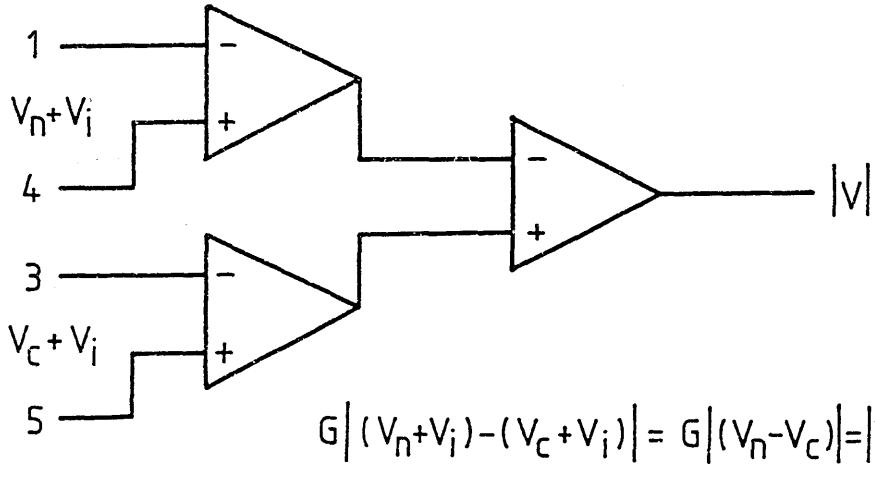

Fig. 2.8 Signal Processing for Material Compensation

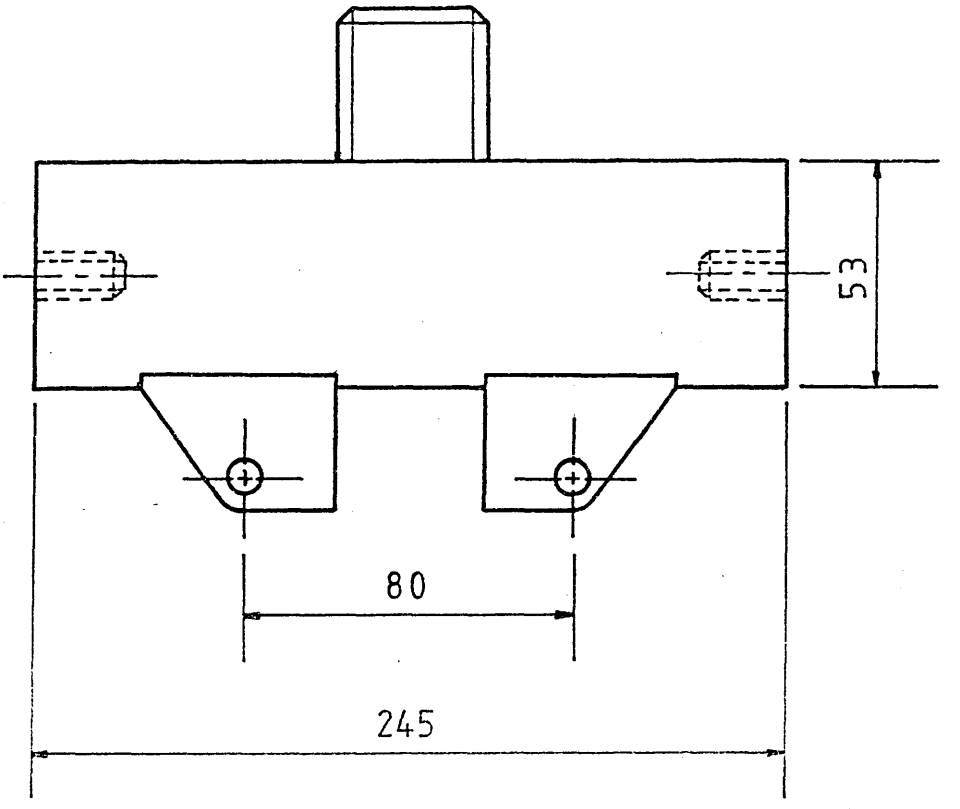

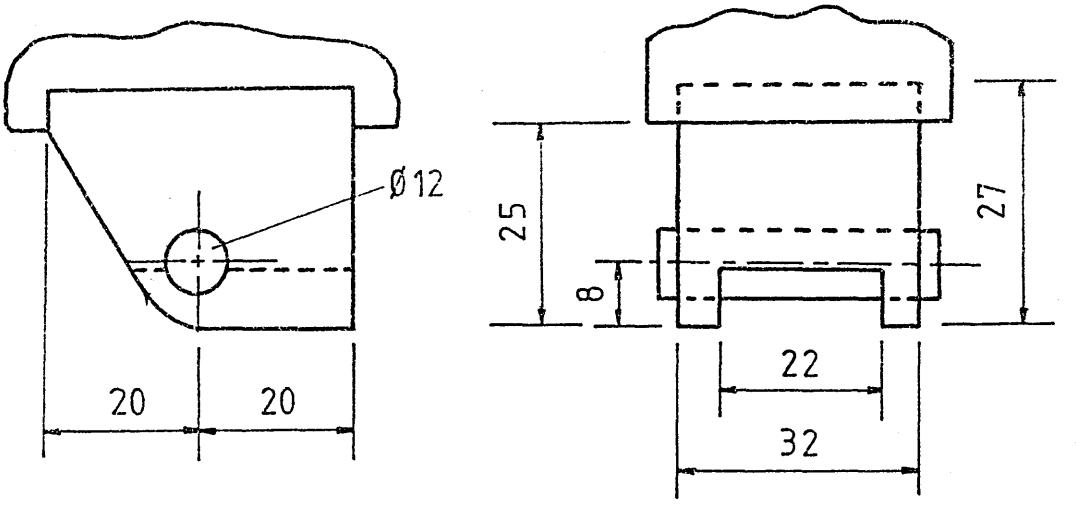

(not to scale: all dimensions in mm)

Fig 2.9 Upper Part of Testrig
and Roller Details

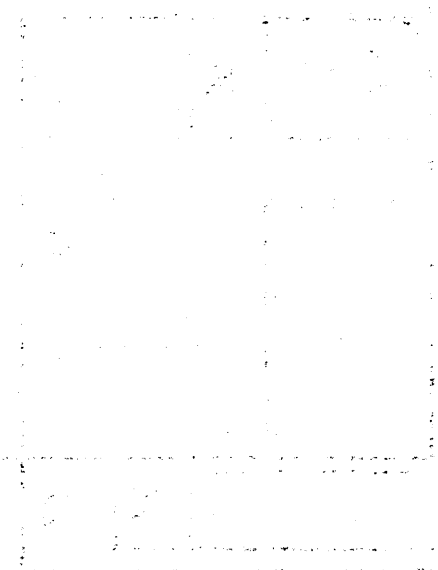

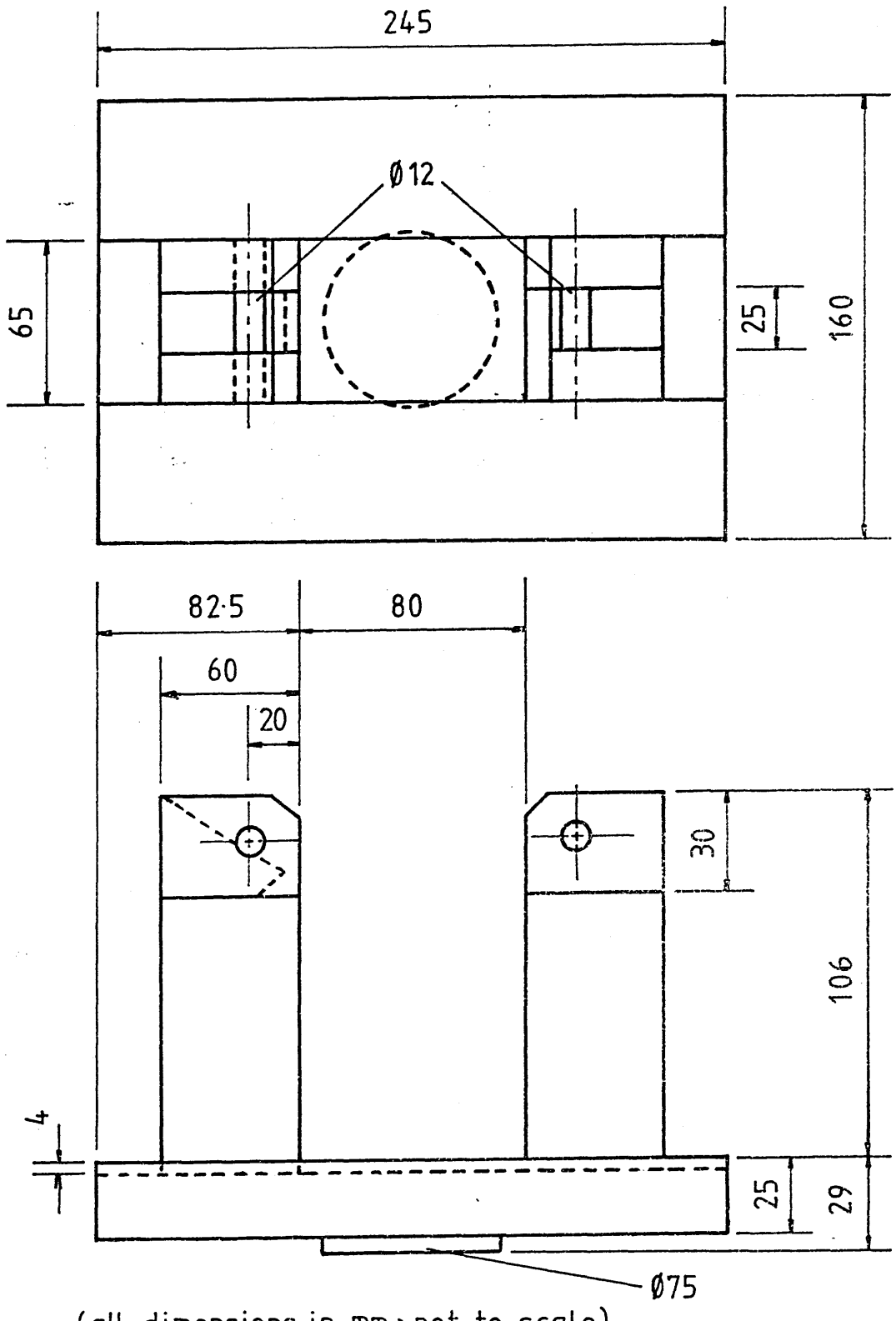

Fig 2.10 Lower Part of Testrig

Plate 2.1
Front panel of CPD3 crack monitoring system

Figure 5.1
Front panel of CRD3 crack monitoring system

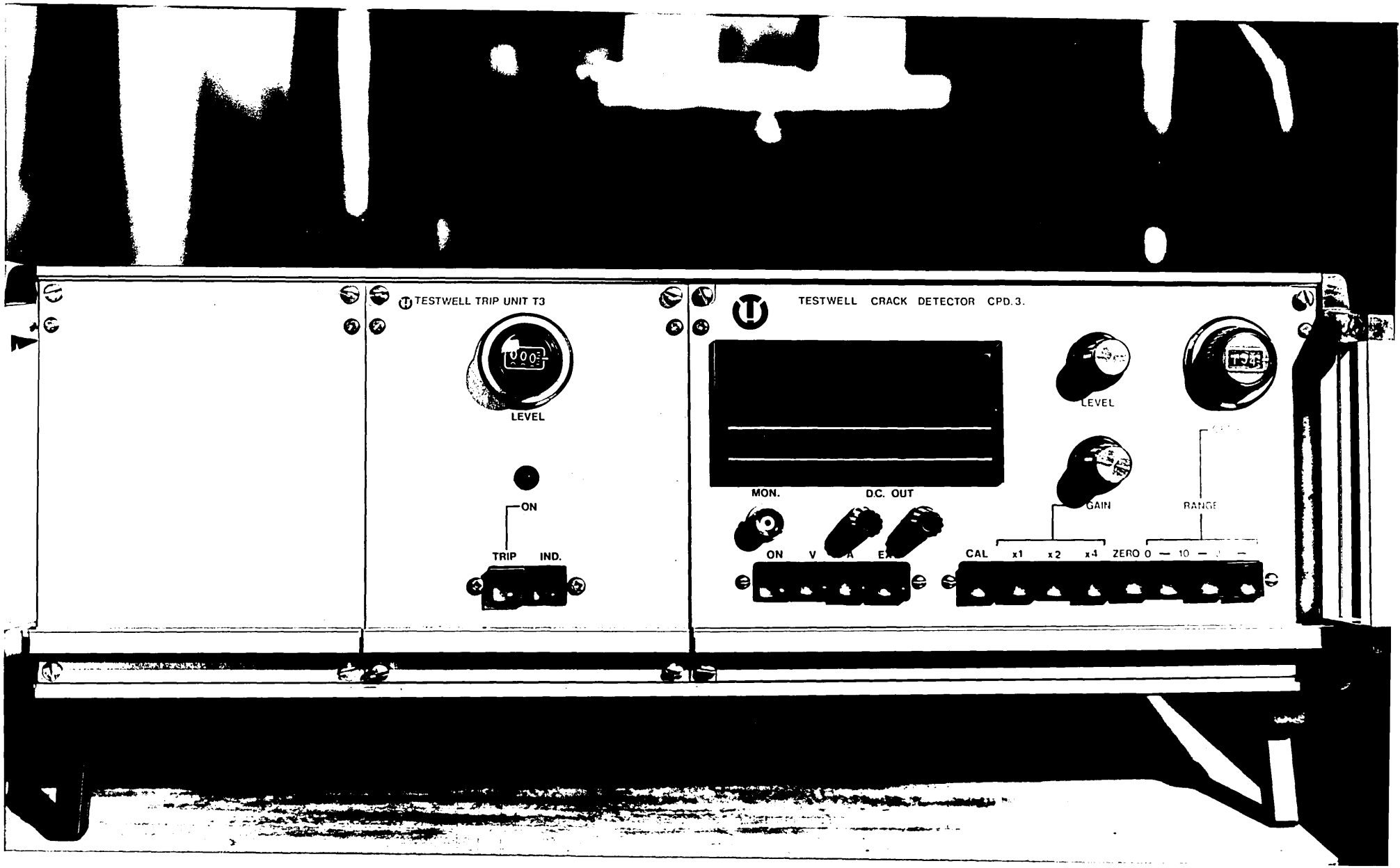
TESTWELL TRIP UNIT T3
LEVEL
ON
TRIP IND.
TESTWELL CRACK DETECTOR CPD.3.
LEVEL
MON.
D.C. OUT
GAIN
RANGE
ON
CAL
x1
x2
x4
ZERO 0 — 10 —

CHAPTER 3 - MEASUREMENT OF THE ACPD RESPONSE IN NOTCHED EN1A MILD STEEL SPECIMENS

3.1 INTRODUCTION

Prior to the experimental work described in this section a preliminary series of experiments were conducted using several V notched EN1A specimens to assess the basic characteristics and magnitude of the ACPD response.

The notch profile was machined using a Standard Charpy 60° V cutter. This profile was chosen because it was known to have good stress concentration properties. These preliminary tests involved an applied load of 50 kN maximum, half that of some of the later tests. The choice of load level was made after several yield load calculations using simple bending theory with an allowance for the notch stress concentration effects and the prerequisite of only localised yielding. The maximum load was applied as both a continuous ramp load and a series of 2.5 kN steps to full load. During each load step the PD measured across the notch drifted slightly under constant load, a steady value being reached after approximately 30s. This was attributed to the metallic lattice requiring a finite length of time to reach a state of equilibrium displaying steady electrical and magnetic properties. Later experimental work employed step load application exclusively to give a quasi-static stress distribution around the notch tip at each load level.

Optimisation of instrument current and gain settings was also possible during these preliminary tests. Suitable values were determined to be a gain of 4000 and an AC input signal of 5A, transmitted at a fixed energising frequency of 8 kHz. Continuing from this initial series of tests a more rigorous series of experimental work was

undertaken to produce a set of more readily quantifiable results. Employing the ACPD monitoring technique developed and refined in the initial experimental work measurements of PD variation with strain and deformation were conducted in a series of notched mild steel (EN1A) and aluminium alloy (NE8) specimens. The EN1A test programme is detailed in the following section and the NE8 testing in section 4.

3.2 SPECIMEN PREPARATION

After machining, all the specimens were annealed to maximise material homogeneity and remove any residual stresses introduced during manufacture. Any resultant surface scale or tarnish was removed with light use of fine emery cloth. To reduce the level of surface oxidation the mild steel specimens were coated with the de-oxidant 'Berkatekt' before heat treatment. The notch profiles were then examined on a shadowgraph machine to help determine an average notch profile suitable for the finite element (FE) model and to provide a check on notch tolerance.

Monitoring of the PD response across the notch required the careful attachment of a series of current input and voltage pick-up leads. All leads were located centrally across the width of specimen. The voltage pick-up leads consisted of four single strand enamelled copper wires. All the wires were spot-welded directly onto the surface of the specimen at spacings of AB = BC = 9mm from the notch centre-line. The relative positions of these together with the earthing leads can be seen in figure 3.1. To allow for a good electrical contact the surface was prepared with light emery cloth and an aerosol degreasant.

The current input leads were not attached directly to the specimen but via a small section of ordinary paperclip soldered onto the end of each of the current lead wires. These were then spot-welded onto the specimen at positions 45 mm either side of notch centreline. At these distances the electric field distribution across the central portion of the notch could then be assumed linear, with distance proportional to PD. Such conditions allowed the initial application of the one-dimensional field solution in order to interpret the voltage readings. After spot-welding all leads were protected and reinforced using Araldite cement. This was allowed to harden completely prior to any mechanical testing. Several precautions were taken to reduce the risk of introducing induced EMF's into the external monitoring system. Both the current and pickup leads were taken off opposite sides of the specimen, and the pick-up leadwires were twisted closely together (see plate 3.1). Each specimen was drilled and tapped at both ends to allow the attachment of earthing straps via two small allen screws. A suitable earthing point for the specimen was chosen as the upper ram of the Mayes testing machine to which the earthing straps were then attached.

As an aid to correct location of the specimen in the loading rig a series of alignment marks were scribed onto each side of the specimen. These marks corresponded to the position of the upper loading rollers (see figure 3.2).

3.3 EXPERIMENTAL PROCEDURE

The following section outlines the experimental procedure followed during the determination of the PD response across the notch in the mild steel EN1A specimens. The procedure is also intended as a

general guide to any similar investigations of ACPD response in other, strongly ferromagnetic, materials.

(i) Prior to any testing the CPD3 crack detection system was switched on, usually 45 minutes beforehand, and the circuitry allowed to warm up. This precaution helped reduce the risk of current fluctuation during testing. Current and gain values of 5A and 4000 respectively were selected on the CPD3.

(ii) The specimen was wired up and the Araldite reinforcing cement allowed to set well before testing began. The specimen was then placed in the rig and aligned correctly. All necessary electrical connections to the CPD3 were then made and examined carefully to ensure that there were no faulty connections in the external monitoring system. The voltage and current lead wires were then taken off opposite sides of the specimen and secured to the rig using electrical insulating tape. These two precautions minimised the size of the current loop and prevented lead wire movement thereby reducing the risk of introducing extraneous voltage signals into the monitoring system. The loading rig with specimen in situ and all the necessary electrical connections can be seen in plate 3.2.

(iii) The POSITION module on the front panel of the Mayes, controlling the displacement of the ram, was then selected. The rollers of the loading rig were brought toward the specimen until contact was just made. Examination of the uniformity of roller contact was then made to ensure even specimen loading with all four rollers. If necessary it was then possible to place shims below the loading pillars to give an even contact before any load was applied to the specimen. The ram was then lowered away from the specimen.

(iv) The LOAD module of the Mayes was then selected together with the appropriate load range. The load ranges used during testing were either 0-50 kN or 0-100 kN with the maximum load corresponding to 10 V Mayes output signal. The load was monitored via a DVM connected to the output terminals of the Mayes. The output from the CPD3 was also monitored by another DVM connected into the DC out terminals. This provided a more accurate evaluation of the PD response than the in-built DVM of the CPD3, see plate 3.3. The current and gain settings of the CPD3 were again checked and any necessary adjustments made. A note of all instrument settings, load range and initial PD was then made. The complete monitoring and loading system can be seen in plate 3.4.

(v) A slight load of $\simeq$ 0.7 kN was then applied to bring the ram into contact with the specimen. Once contact had been made the CPD3 settings were again checked. At this point there would have been substantial leadwire movement and the specimen electric field may have been disturbed on roller contact.

The load was then applied in a series of load increments using the manual load control facility of the Mayes. The magnitude of each load step was typically 2.5-5.0 kN. After each load step, 30s was allowed for the PD signal to steady and then the datapoint was recorded. The load was then increased in a similar manner to the maximum level. Unloading of the specimen was a reversal of the loading procedure. For subsequent loading cycles (2nd, 3rd etc) the load was not allowed to go to zero on unloading but kept a small positive value to maintain roller contact. The output from the Mayes and CPD3 was recorded onto a

Bryans X-Y plotter as a plot of PD against load. Additionally each of the coordinate PD/load points was recorded manually to ensure accuracy and note any fluctuations in response not shown on the plotter.

3.4 RESULTS AND DISCUSSION

In all cases the absolute voltage measured across the notch using the compensation method has been plotted against load. The size of the standing voltage across the specimen was quite consistent with all results being in the range 100-200 μV. The PD response to increasing load in the case of the V notched mild steel specimens can be seen in figures 3.3-3.8. These plots are not the complete series of results but are considered a representative selection.

The results exhibit several interesting characteristics. Consider the first load cycle shown in figures 3.3 and 3.4. The loading and unloading responses were quite distinct with the unloading response being at a generally higher level of PD. In all cases the PD initially fell 10-20 μV to a local minimum at 6-9 kN then increased by 15-25 μV reaching a maximum value at a loading of 30-35 kN before finally beginning to level out or even fall off up to the 50 kN maximum load level. These two turning points could be clearly identified on all of the results. Unloading of the specimens generally gave a higher PD response than during loading. As the load decreased from the 50 kN maximum the PD increased 10-22 μV up to 30 kN and then steadily decreased to a value at zero load typically 15-30 μV less than its initial unloaded value.
(NB Strictly speaking the difference could not be measured at zero but only at a slight positive value of load).

Although it was possible to observe several distinctive features in all the first cycle loading responses there was some variation particularly in the relationship between the loading and unloading responses. This is clearly seen by contrasting figure 3.5 with figures 3.3 and 3.4. The loading and unloading responses each displayed very similar characteristics but unlike those shown in figures 3.3 and 3.4 the unloading response, seen in figure 3.5, was at a generally lower level of PD than the loading response. However the same distinct turning points and general trends could be clearly identified in each. Subsequent load cycles were very consistent and showed a quite similar response to the first cycle, see figures 3.4-3.6. Again the loading and unloading responses were still quite separate and not coincident over any extended interval of the load range. However unlike the first cycle there was a clearly definable PD origin at zero load and no large initial decrease of 15-20 μV in PD as the re-load commenced. This produced a notable characteristic in the response, with the PD / load curve tracing a stable hysteresis loop on second and subsequent cycles.

Considering the results obtained from the U notch specimens. These results were overall slightly more consistent than the equivalent V notch ones. The initial loading of the specimens was very repeatable, unloading also produced a reasonably consistent response.

Figures 3.8-3.10 show the initial loading response in the case of the U notch. The response displayed similar maxima and minima to the V notches and also the generally higher unloading response and as a consequence there were few clearly marked differences separating the two notches. The only exception to this was a slightly lower drop of PD, 5-15 μV, with the U notches over the initial 10 kN

loading. The separate loading/unloading responses were again quite distinct with a noticeable drop in PD response at zero load. This shift was in general not as large as the V notch, with 10-20 μV being typical.

Subsequent to the first load cycle a very high level of repeatability was again observed in all the plots, see figures 3.10-3.12. Similar to the V notch results a recognisable origin to the PD response could be identified together with a clear, but somewhat different, hysteresis loop having a much greater variation of PD, 20-30 μV, over the reloading cycle with a clearly defined maximum.

Contrasting the results from both notch profiles several interesting points arise.

Firstly the similarity in the initial loading response in both cases, but with this similarity being lost in subsequent cycles where each of the notches developed a distinct and stable hysteresis loop with clearly defined fixed end points (see figures 3.6, 3.7 and 3.11, 3.12).

The response of the two notch profiles each display distinct and separate characteristics after the first load cycle. In each case the unloading response was at a generally higher PD level than loading. In all cases the curves exhibited one or more turning points and changes in gradient. This implies there can be no direct correspondence between strain or deformation since both these parameters are monotonically increasing functions of load, see section 4. Further, since the nature of the response precludes any simple direct characterisation in terms of strain levels etc, explanation must be sought in terms of the more complex electrical and magnetic properties.

An indication of the significance of the variation in PD observed during a load cycle can be seen in figures 3.13-3.16. The PD response has been interpreted by the one-dimensional electric field solution, see section 1.2.2, in terms of an apparent cracklength. This has been done for the second load cycle only where a clearly identifiable zero load potential exists. This was necessary to obtain an estimate of the electrical potential gradient along the surface of the specimen from which to compute crack depth estimates. It can be seen that although no crack is present an apparent crack of up to 0.6 mm may be detected.

In conclusion these results clearly show that strain and plastic deformation have an appreciable influence on PD in such a strongly ferromagnetic material.

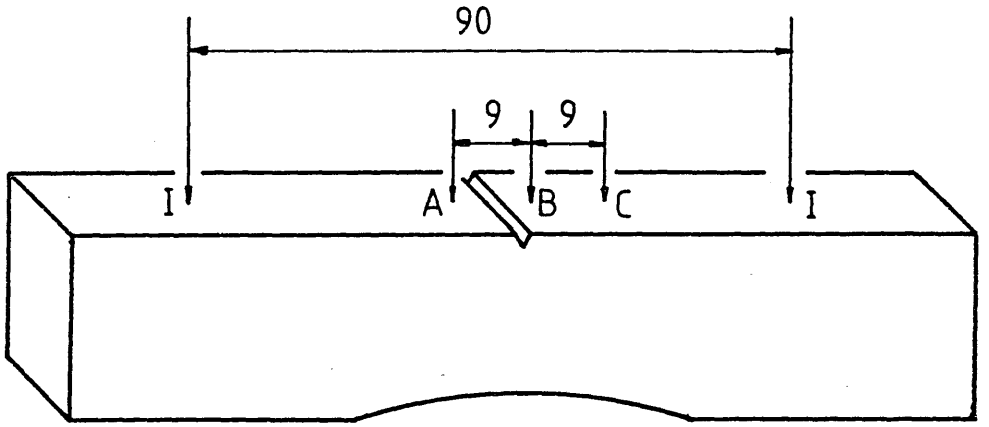

A,B – pick-up leads

B,C – compensation leads

I – current inputs

Fig 3.1 Location of Current Input and voltage pick-ups

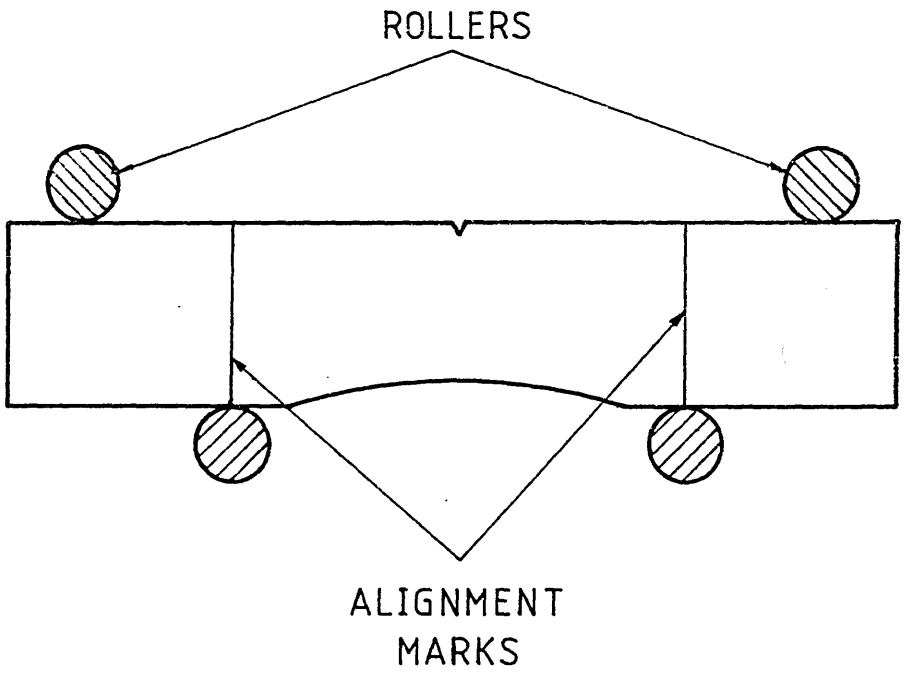

Fig 3.2 Position of Specimen Alignment Marks

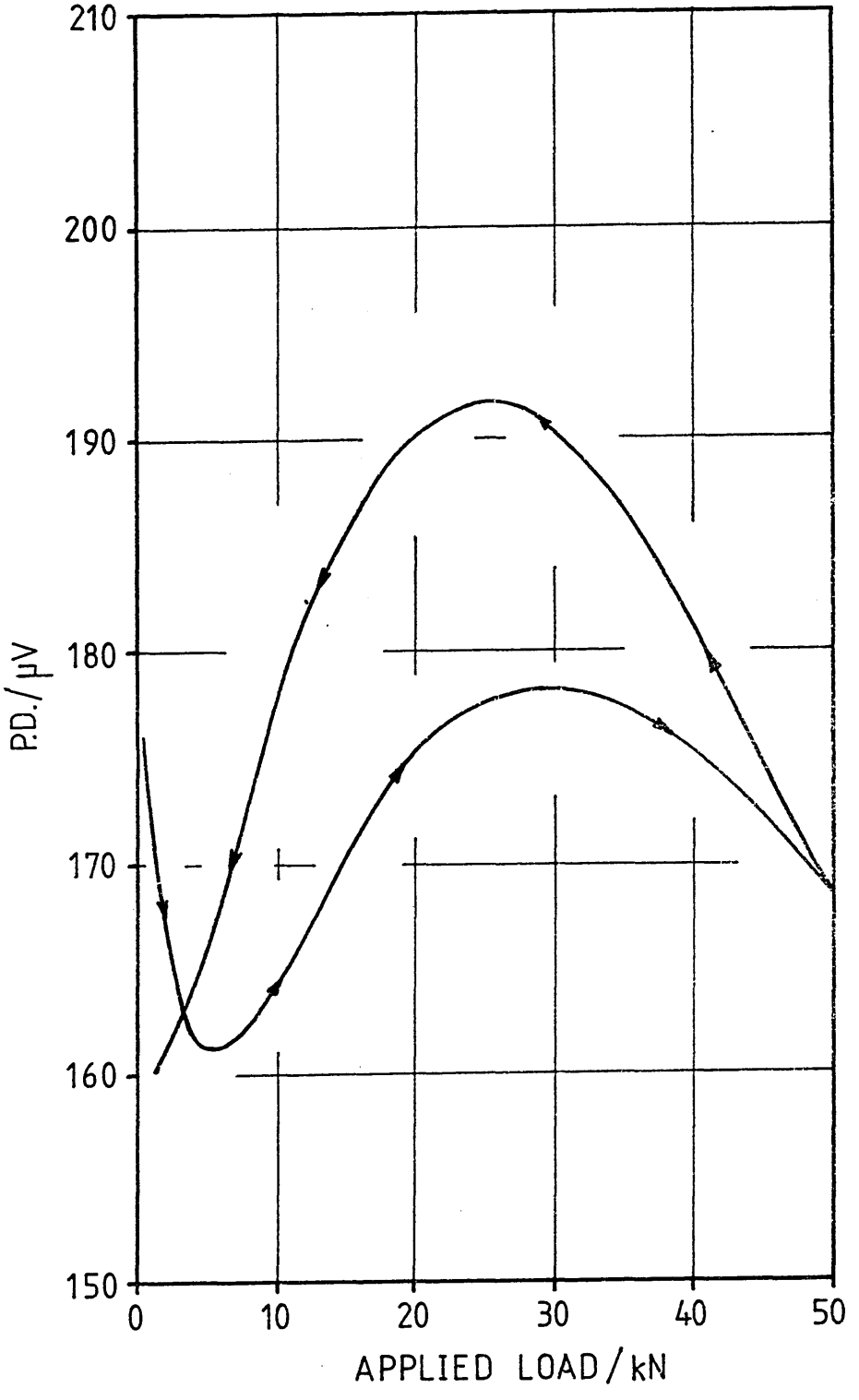

Fig 3.3 ACPD Response : EN1A V Notch :

Specimen VM2 : First Load Cycle

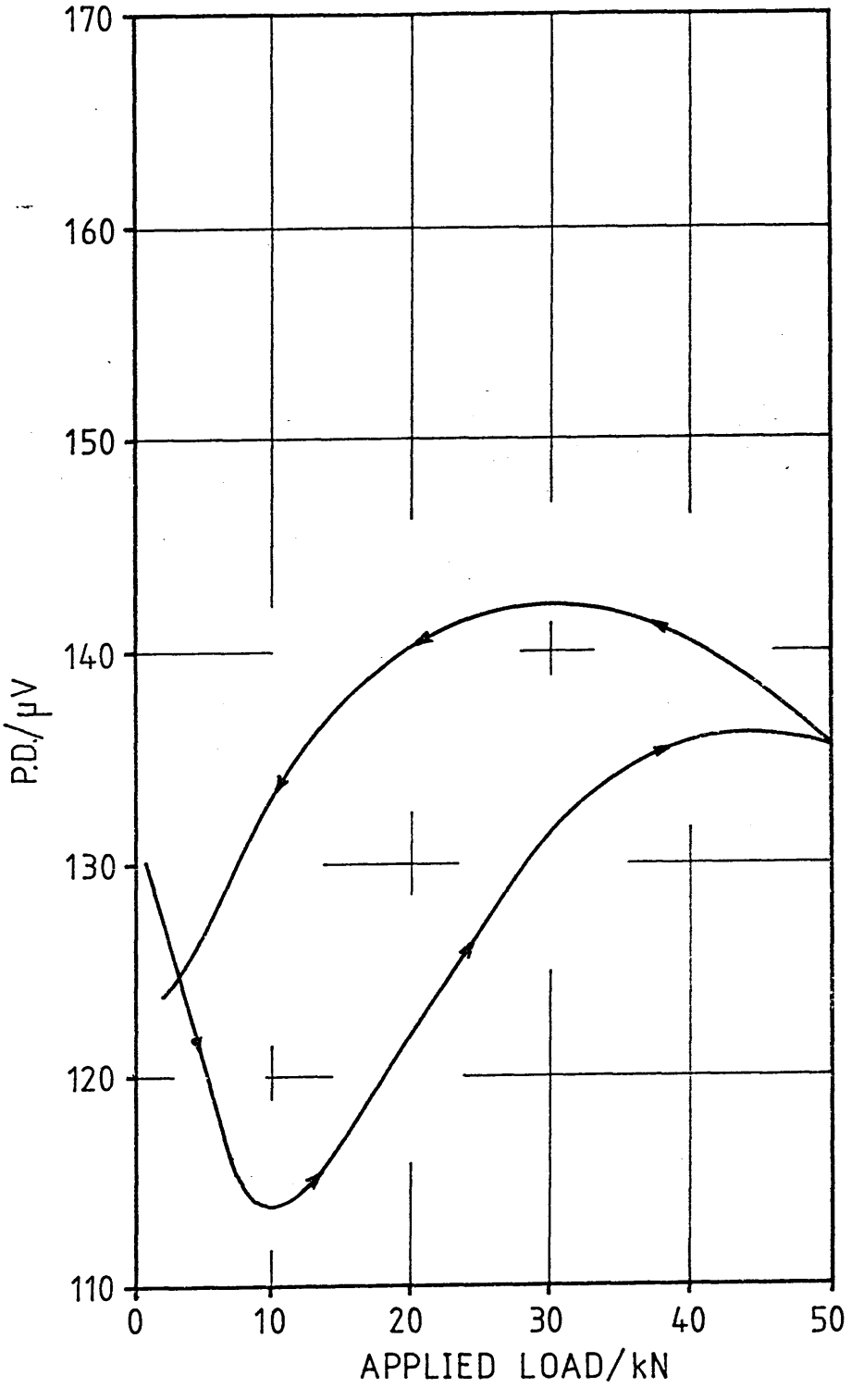

Fig 3.4 ACPD Response : EN1A V Notch :

Specimen VM3 : First Load Cycle

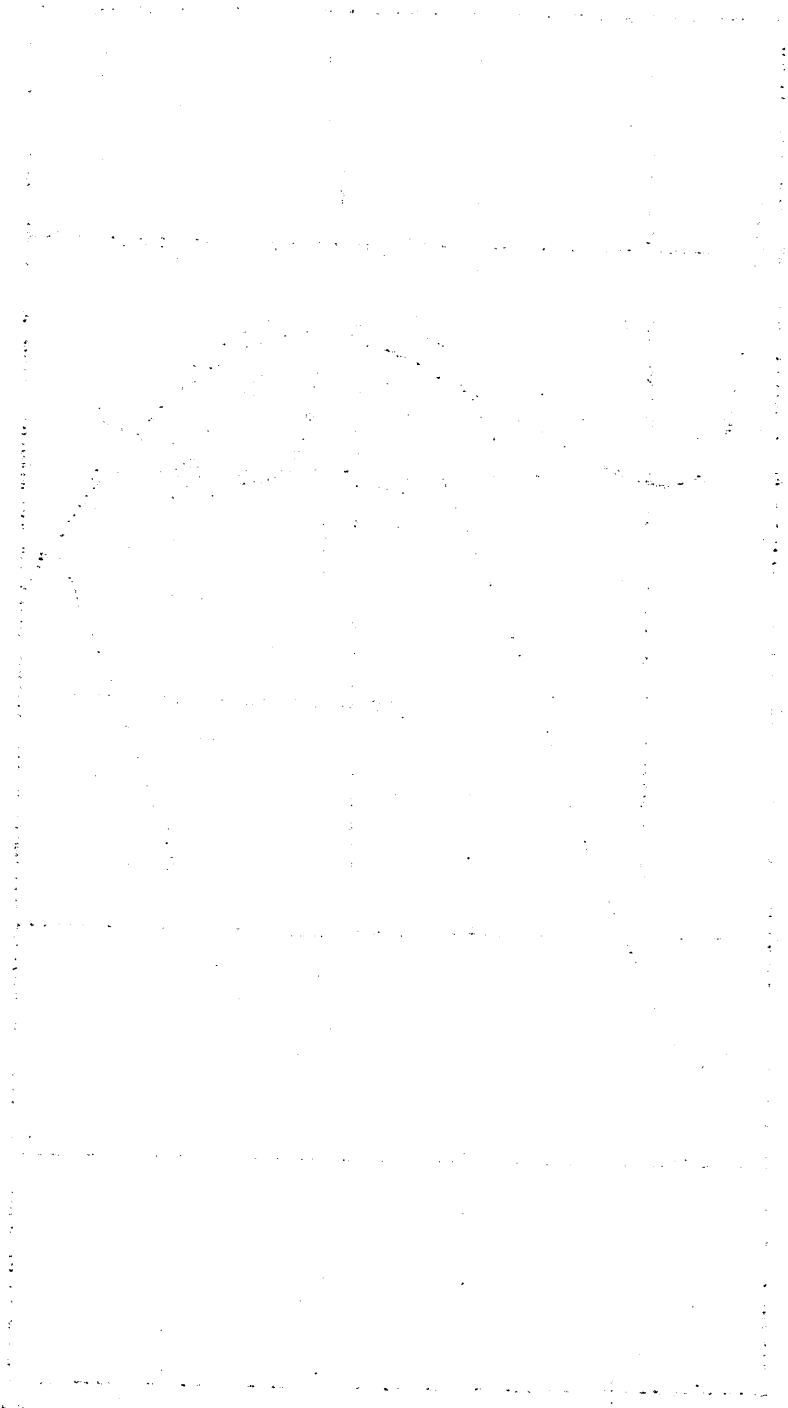

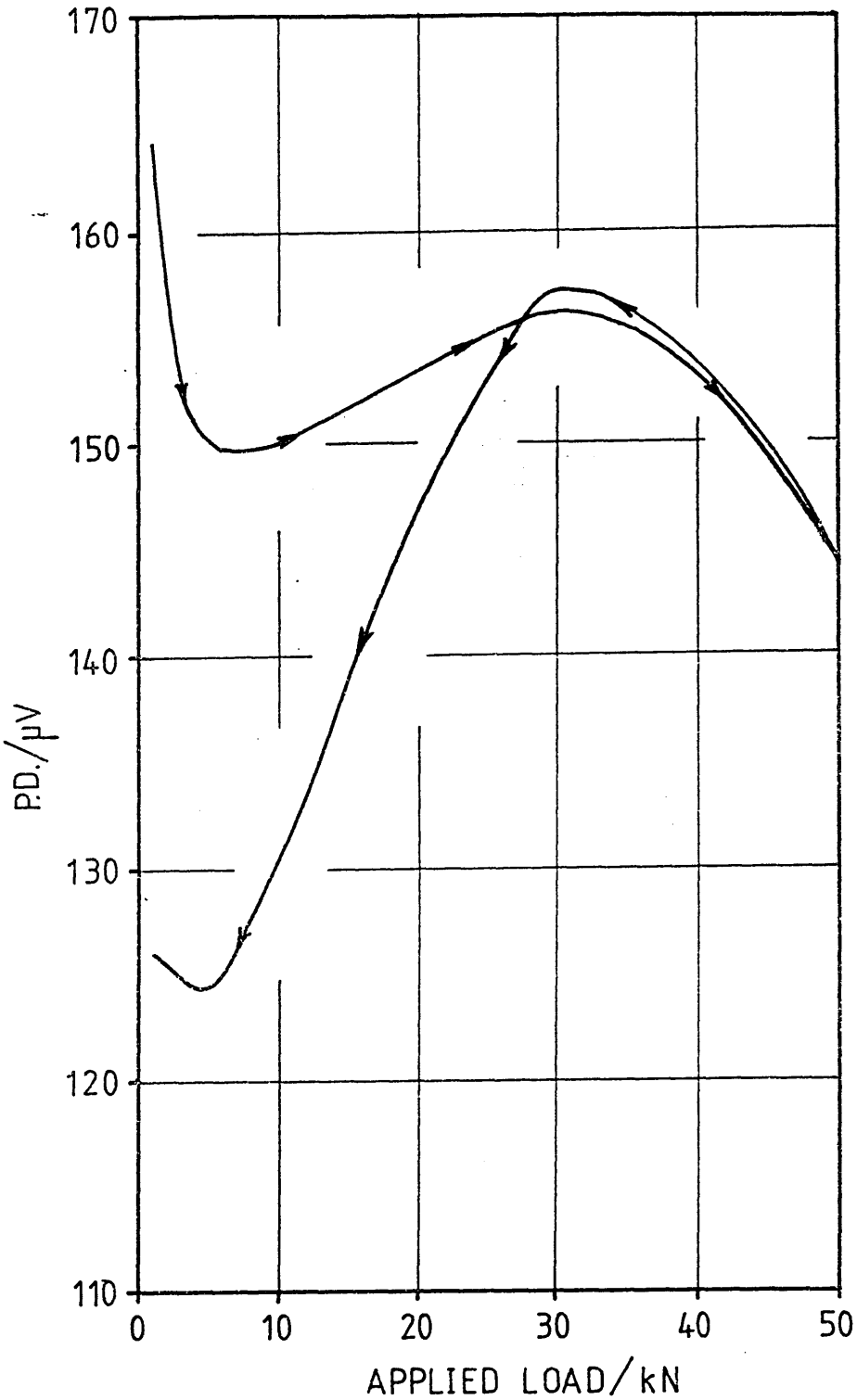

Fig 3.5 ACPD Response : EN1A V Notch :

Specimen VM6 : First Load Cycle

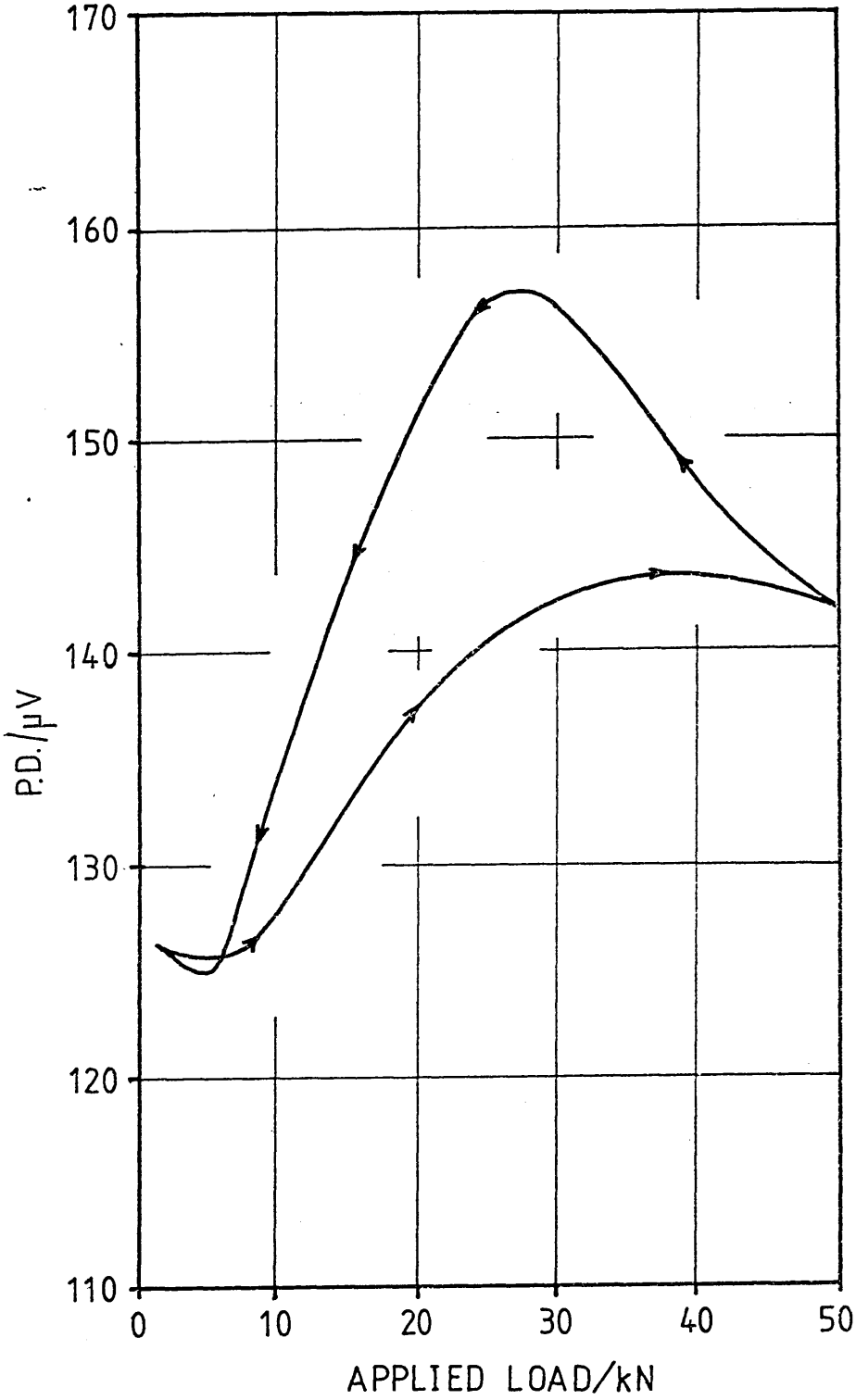

Fig 3.6 ACPD Response : EN1A V Notch :

Specimen VM6 : Second Load Cycle

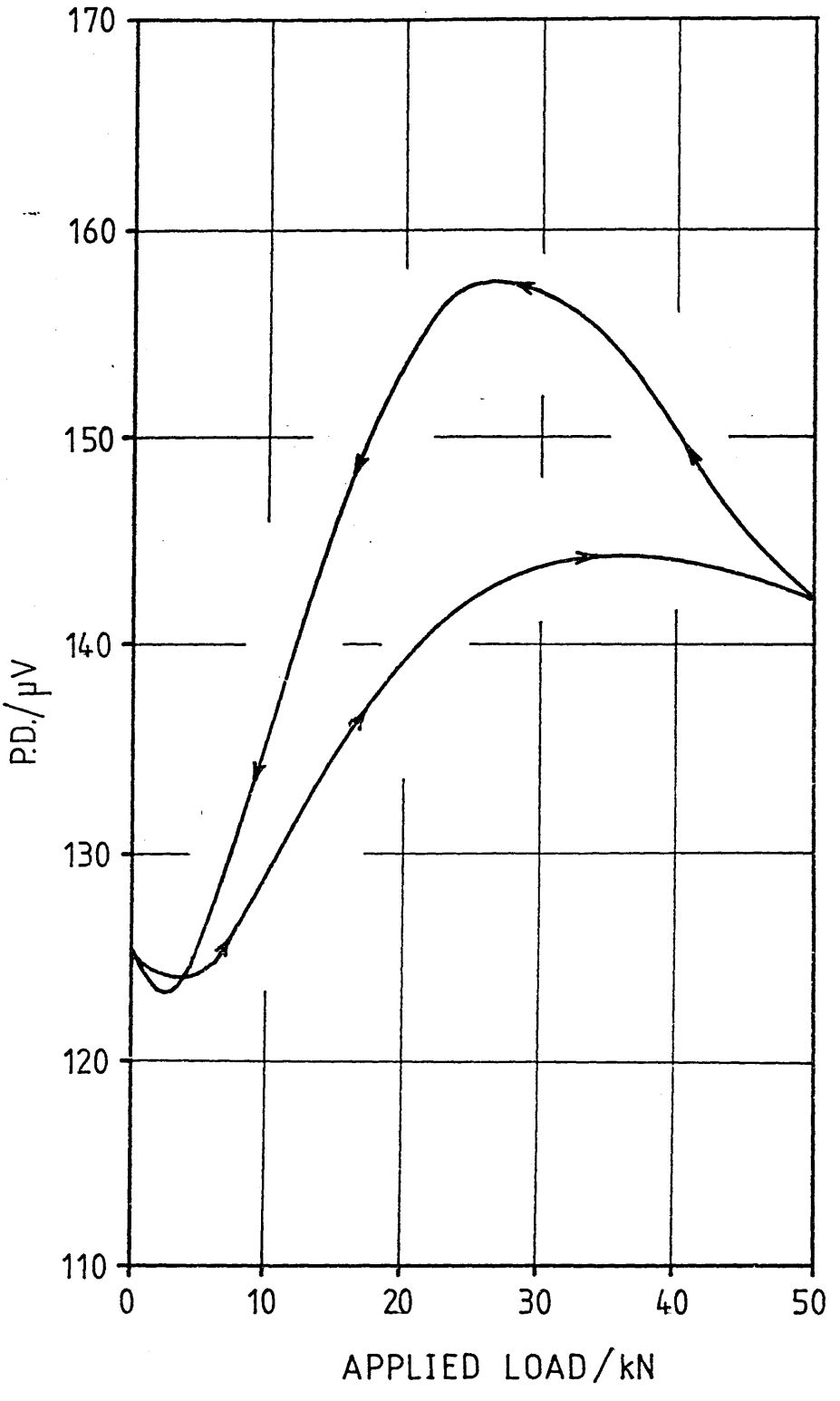

Fig 3.7 ACPD Response : EN1A V Notch :

Specimen VM6 : Third Load Cycle

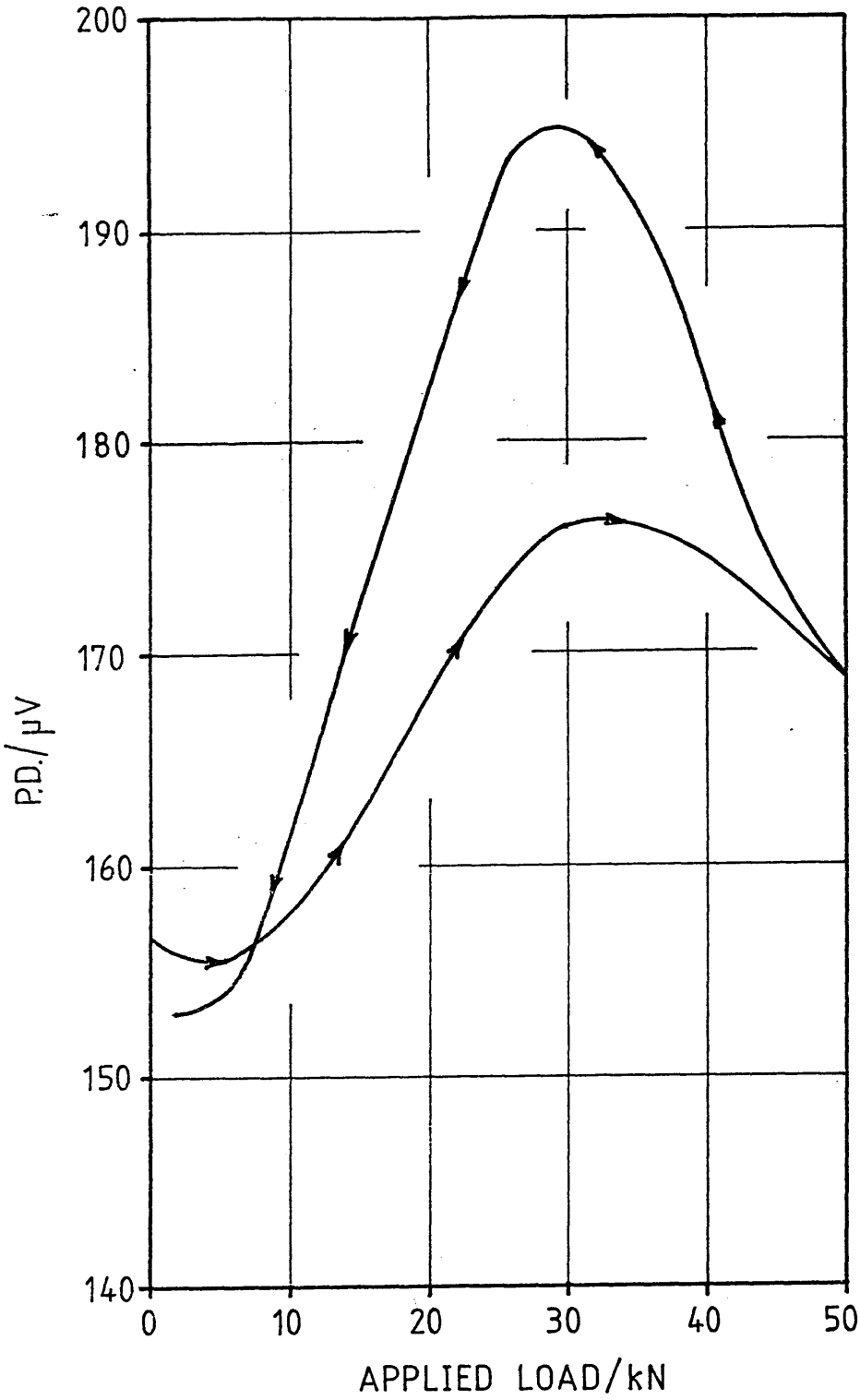

Fig 3.8 ACPD Response : EN1A U Notch :

Specimen SM1 : First Load Cycle

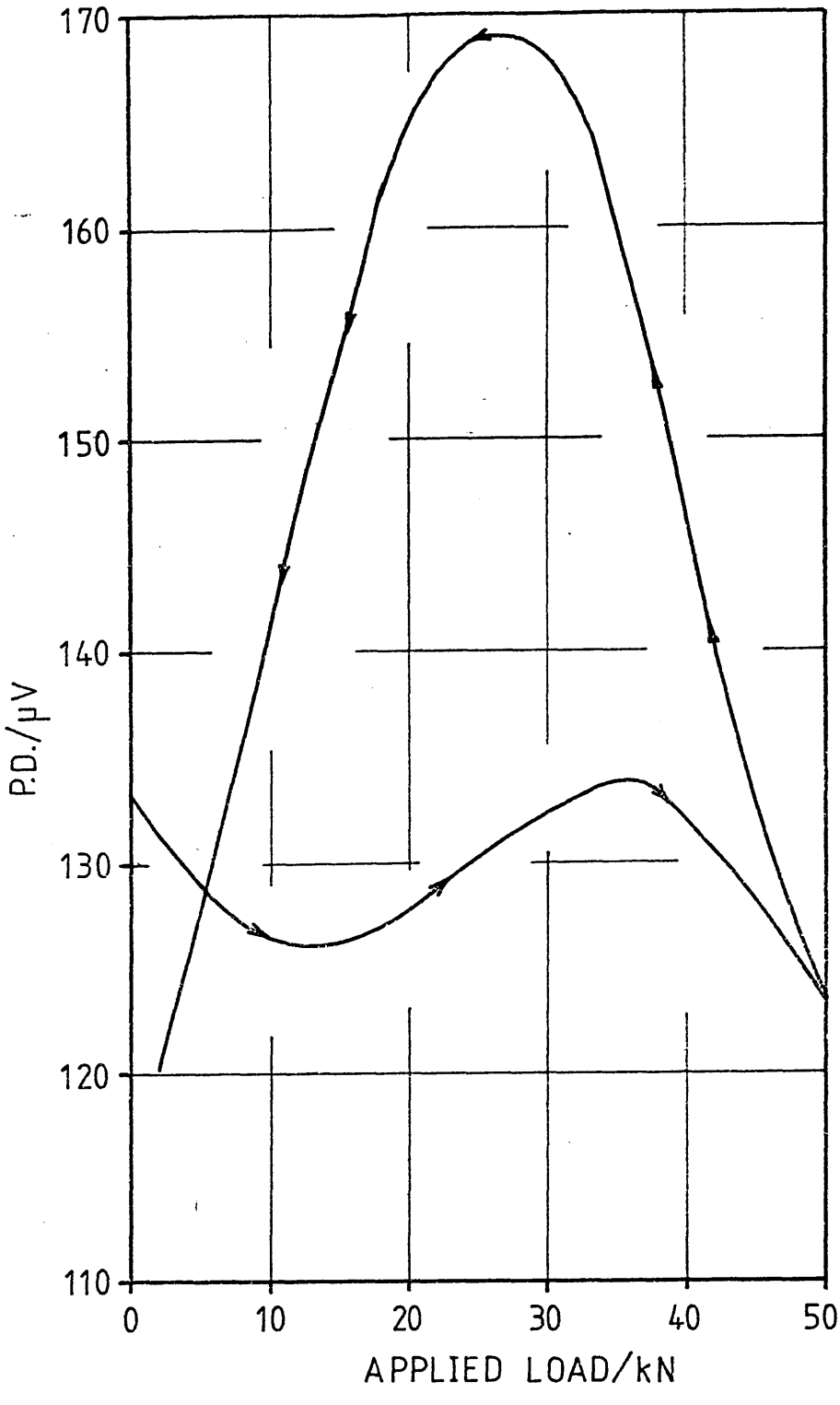

Fig 3.9 ACPD Response : EN1A U Notch :

Specimen SM5 : First Load Cycle

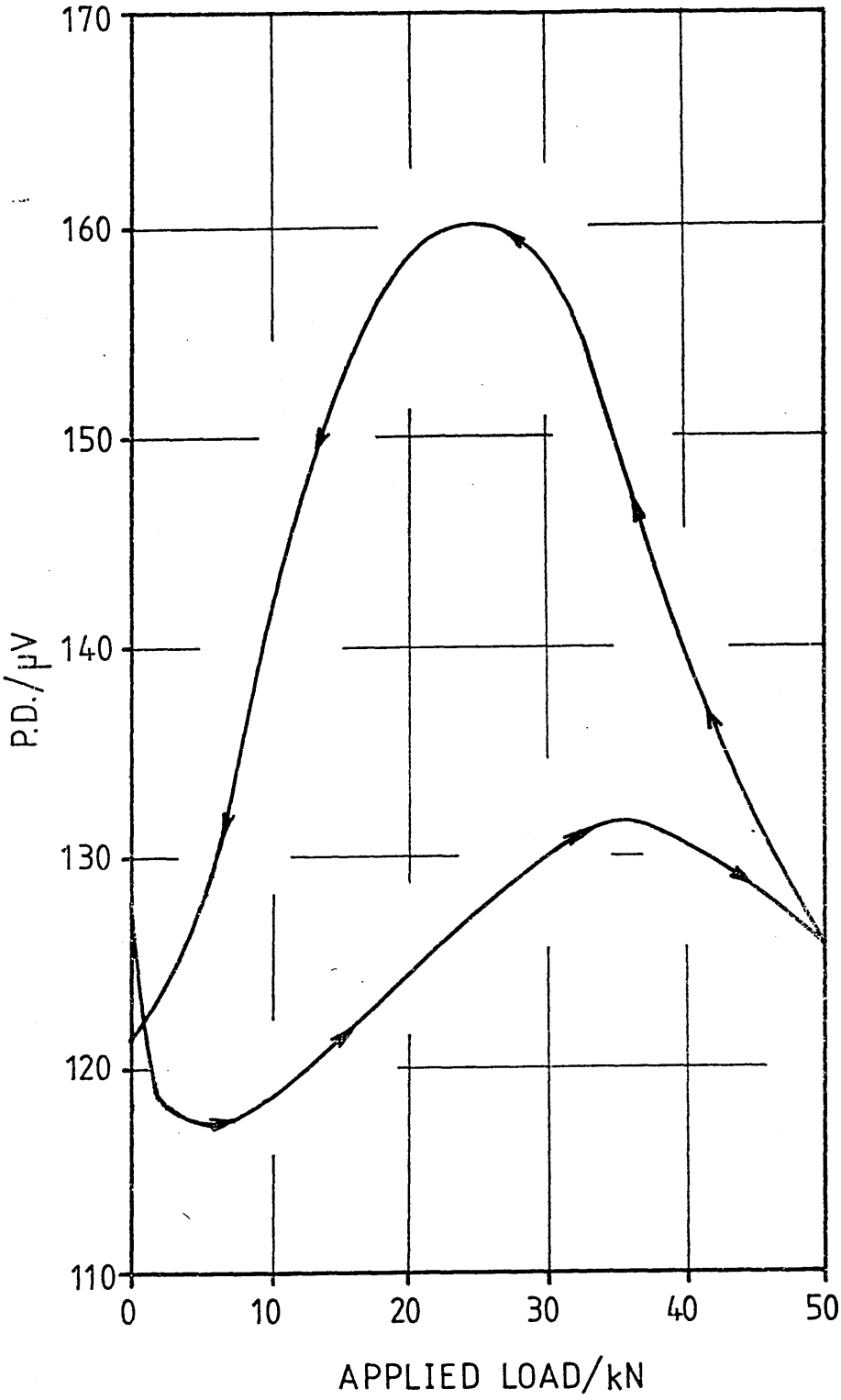

Fig 3.10 ACPD Response : EN1A U Notch :

Specimen SM9 : First Load Cycle

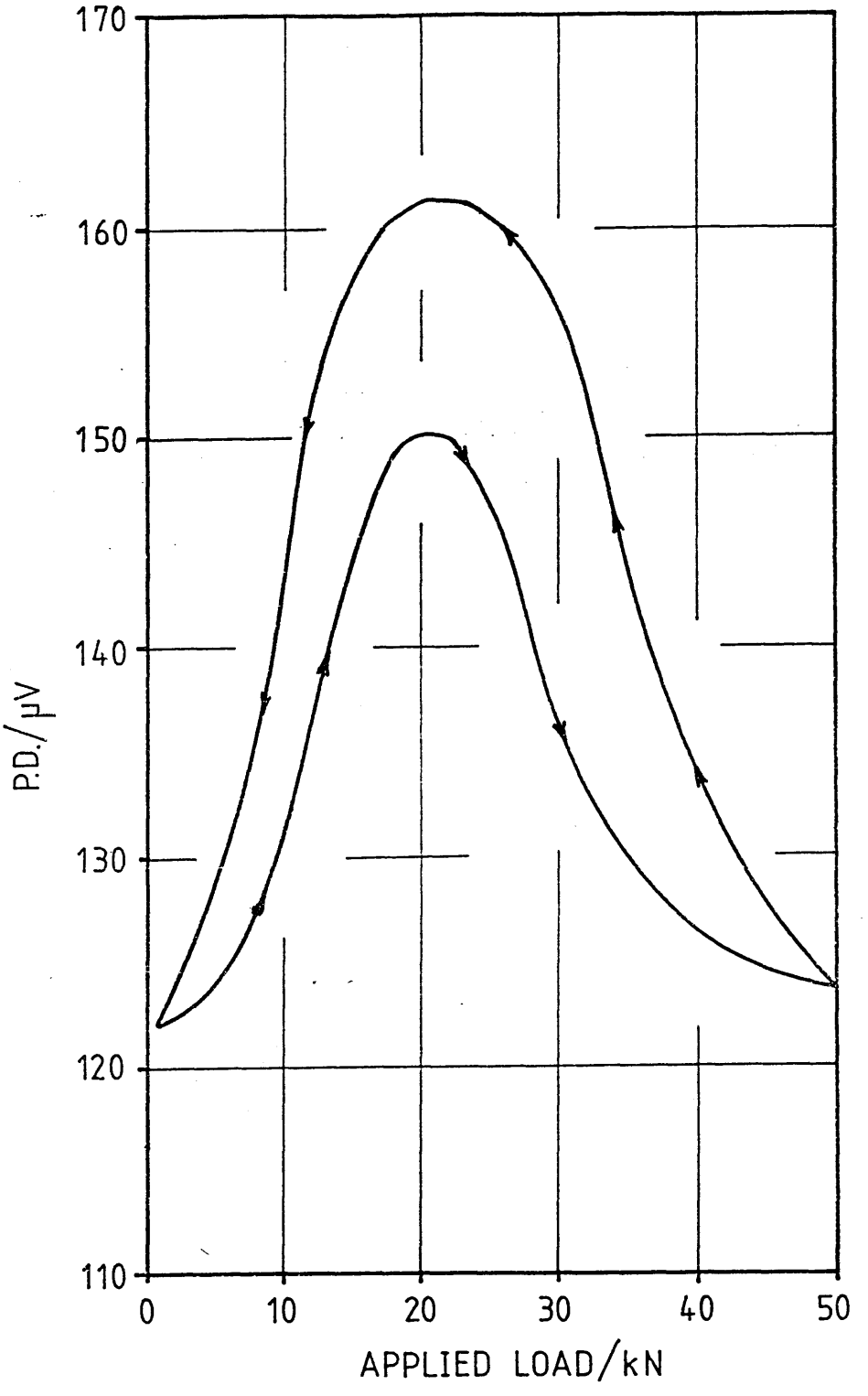

Fig 3.11 ACPD Response : EN1A U Notch :

Specimen SM9 : Second Load Cycle

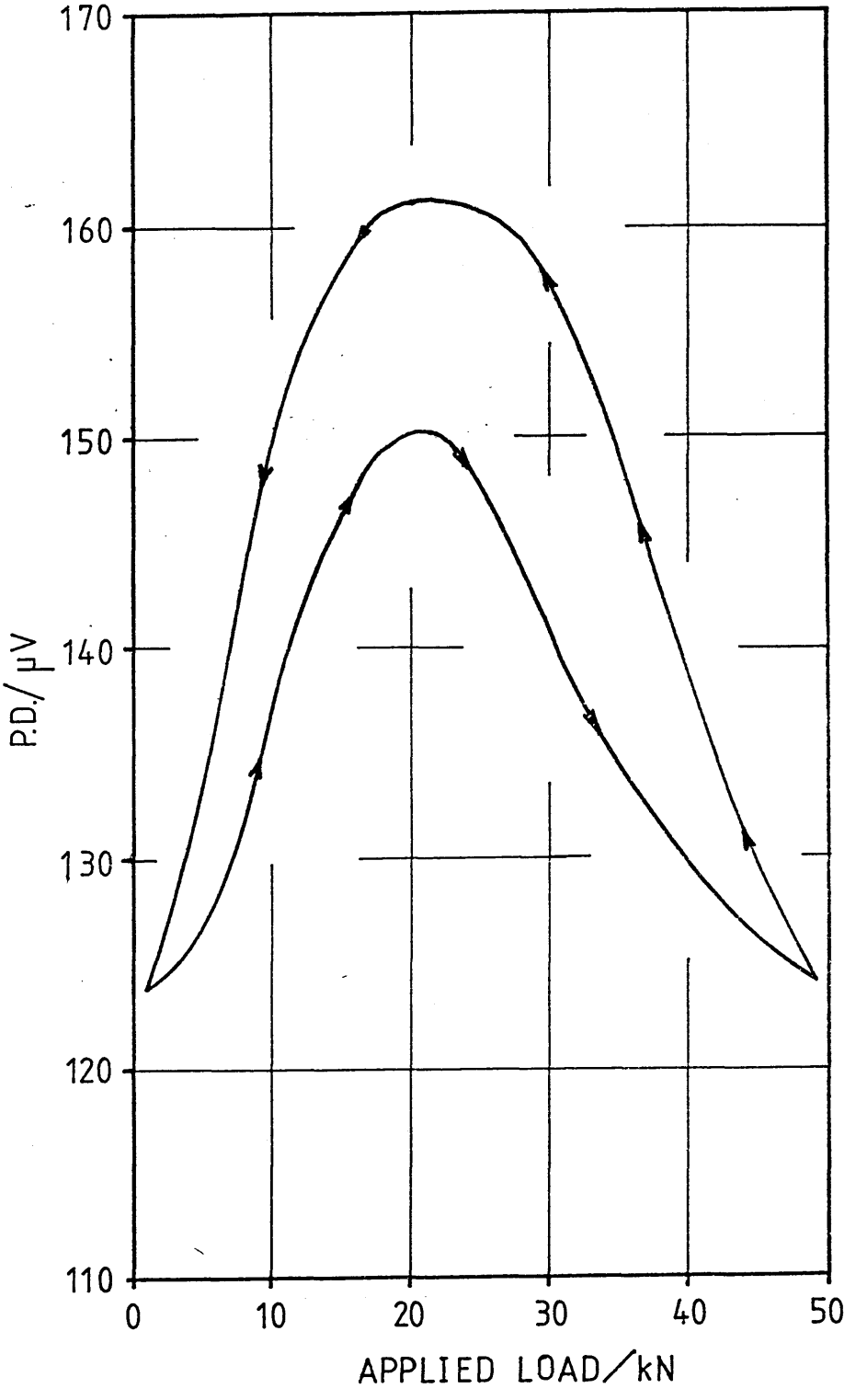

Fig 3.12 ACPD Response : EN1A U Notch :

Specimen SM9 : Third Load Cycle

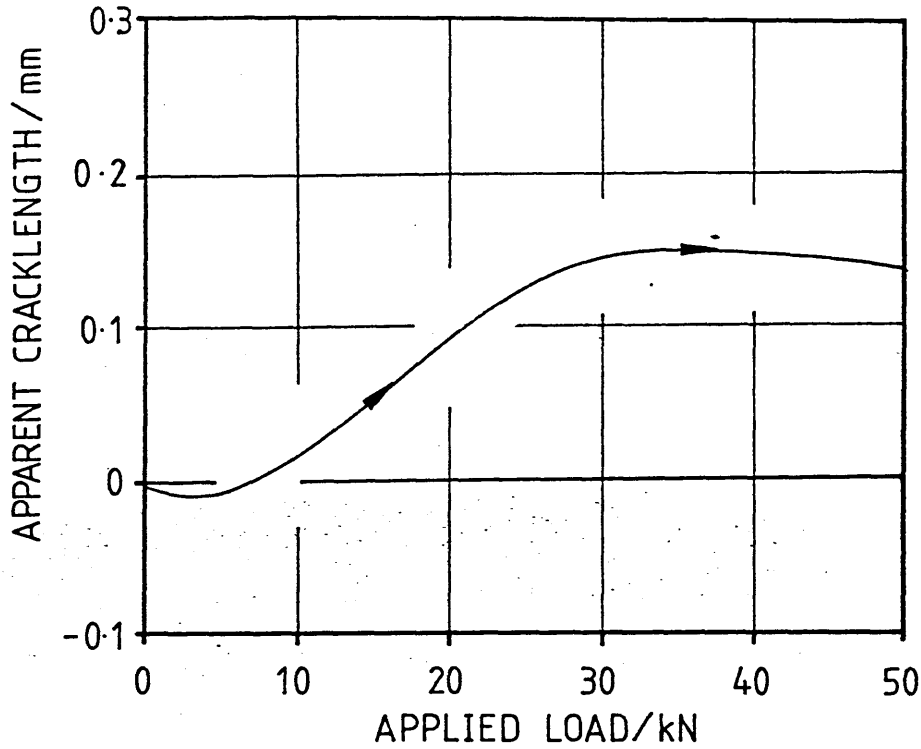

Fig 3.13 EN1A V Notch : Apparent Crack Depth During Second Load Cycle : Load Increasing.

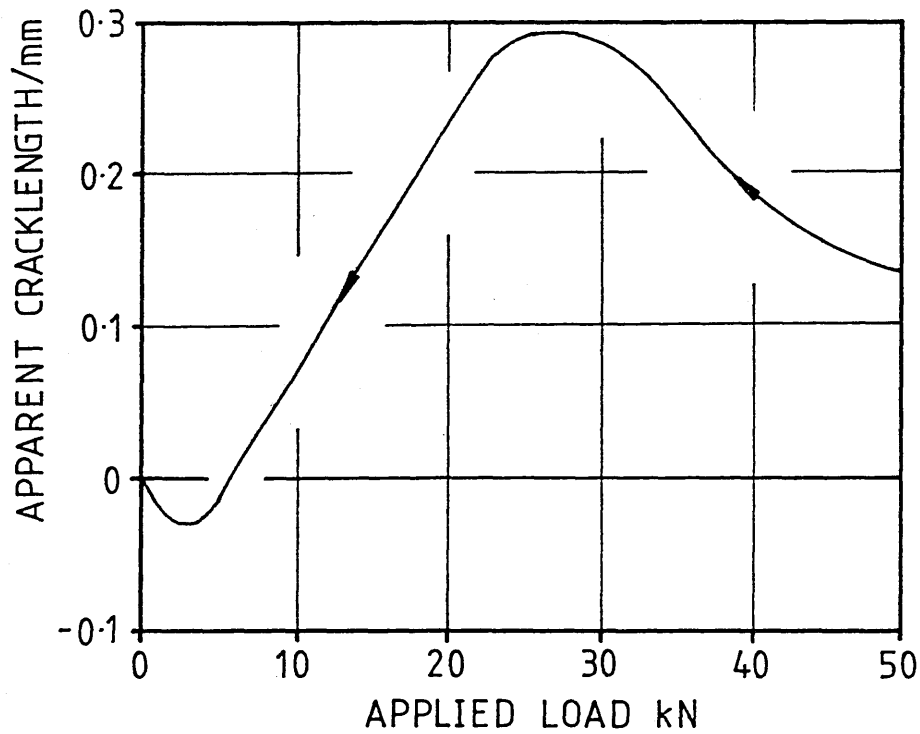

Fig 3.14 EN1A V Notch: Apparent Crack Depth During Second Load Cycle : Load Decreasing

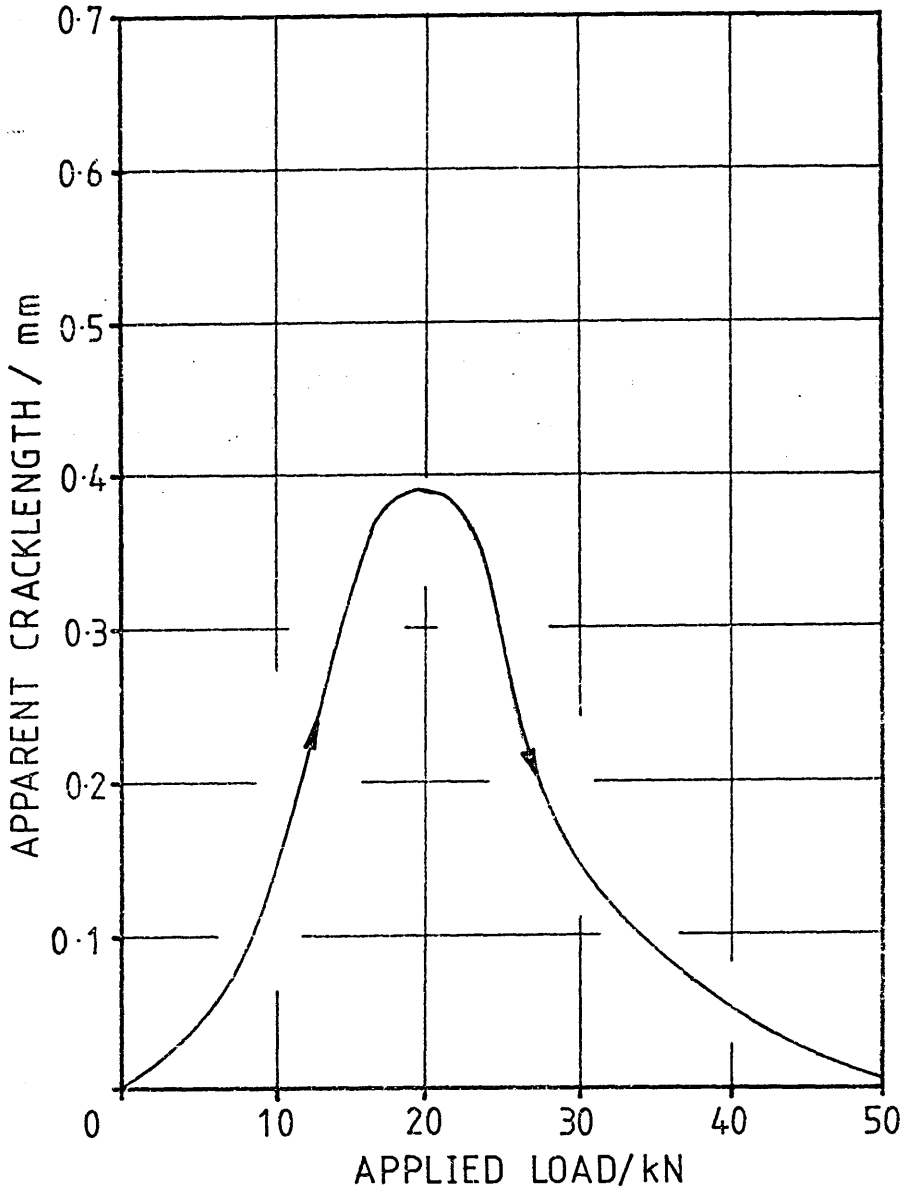

Fig 3.15 EN1A U Notch : Apparent Crack Depth During Second Load Cycle : Load Increasing

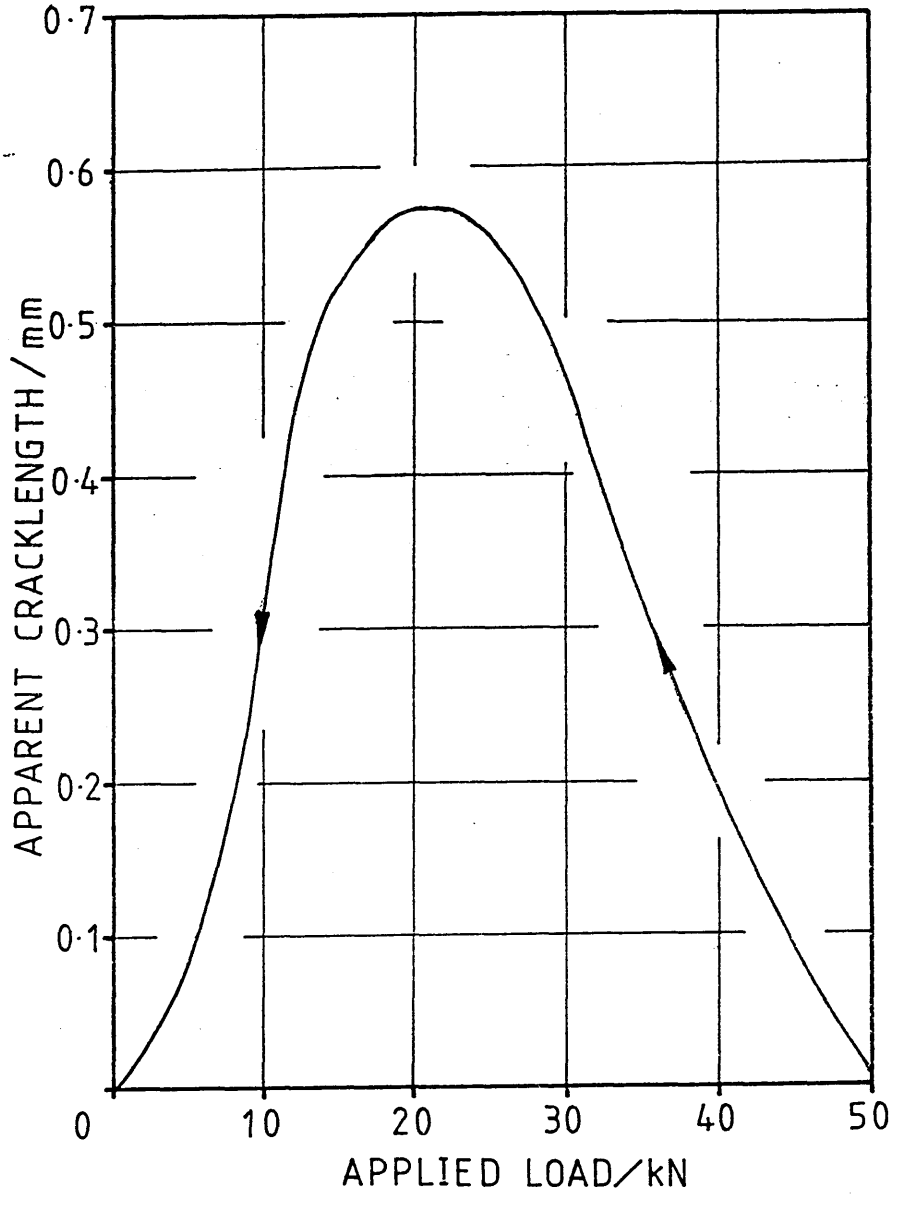

Fig 3.16 EN1A U Notch : Apparent Crack Depth During Second Load Cycle : Load Decreasing

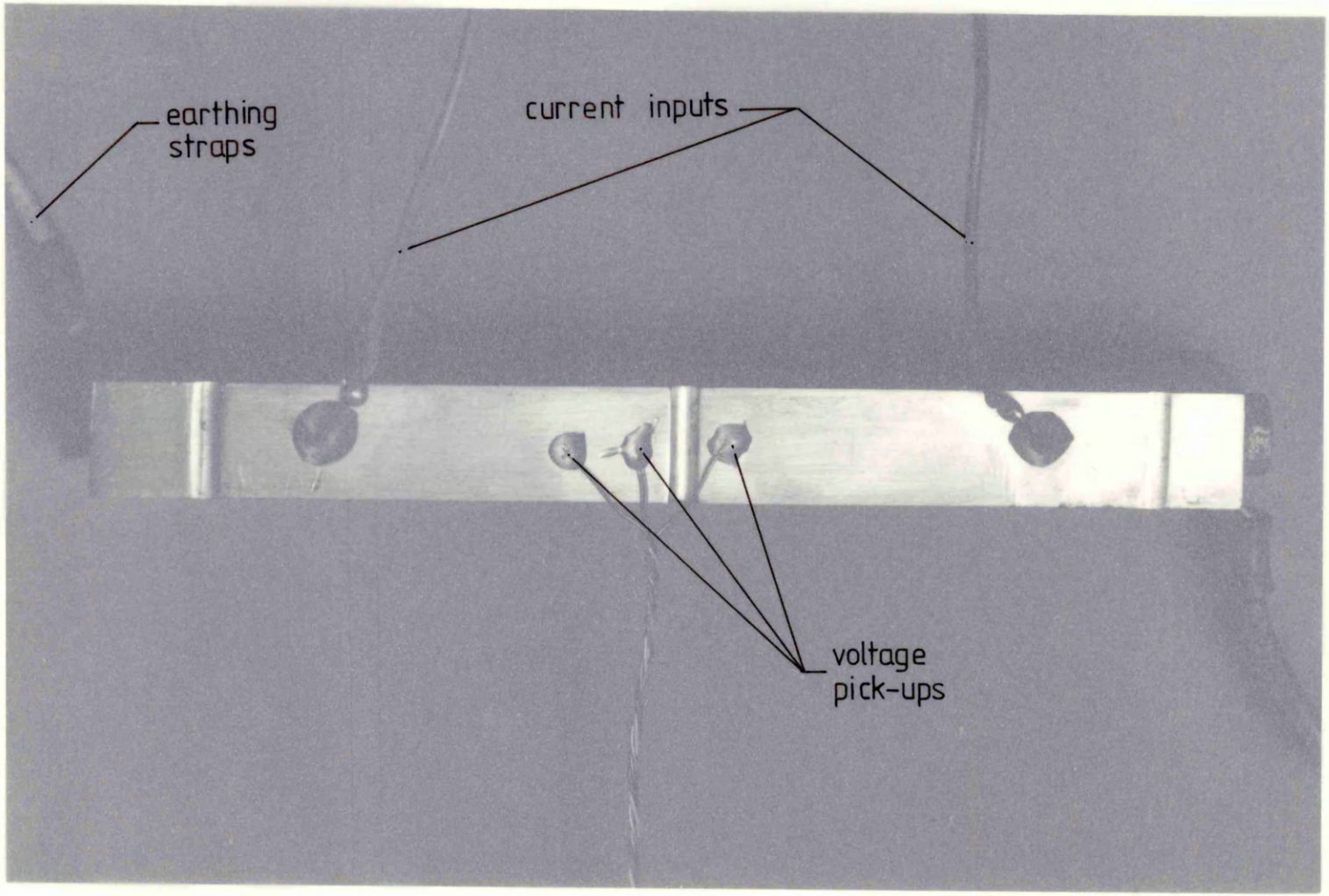

Plate 3.1
Attachment of current input, voltage pick-ups and
specimen earth for EN1A specimens

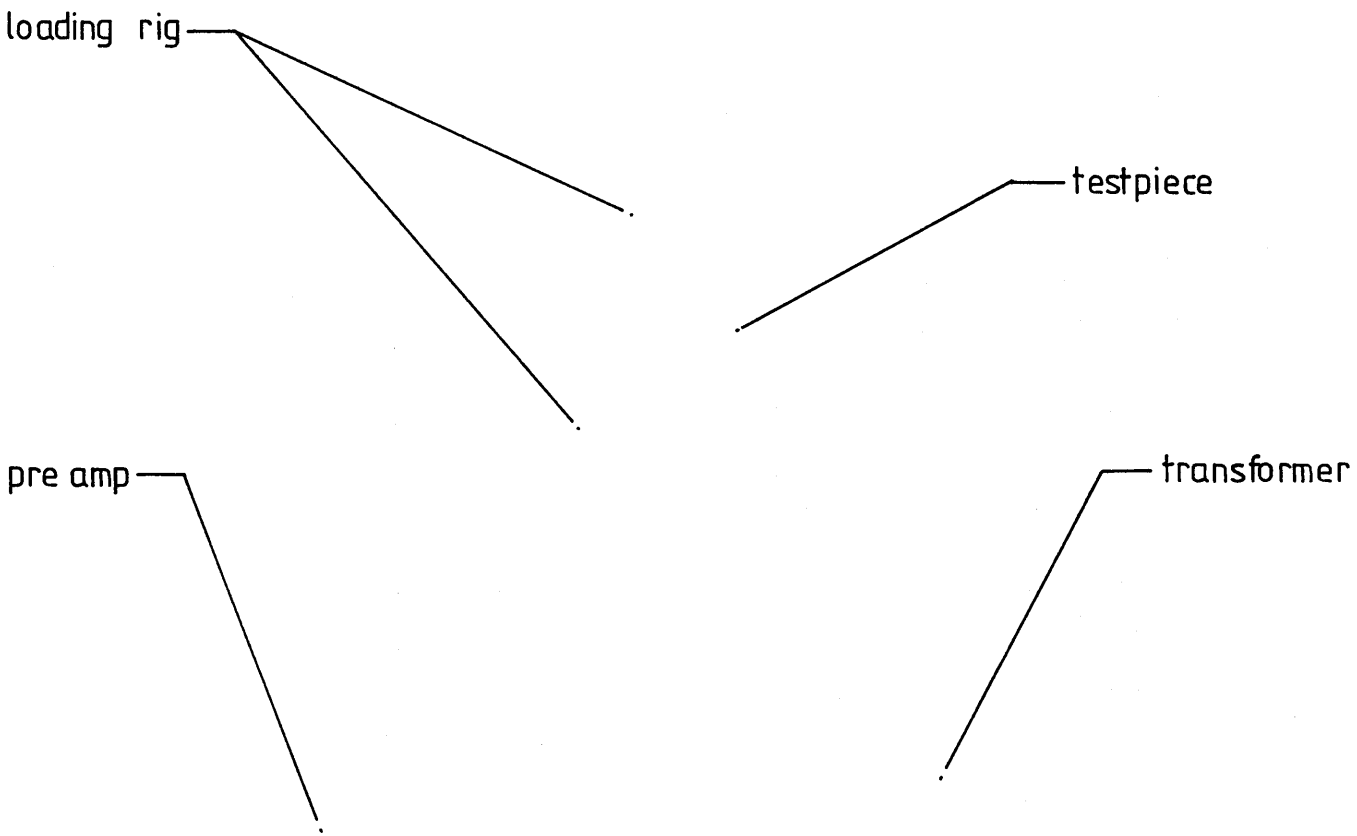

Plate 3.2
EN1A specimen in situ in loading rig

EMA specimen in grip in loading rig

Figure 3.5

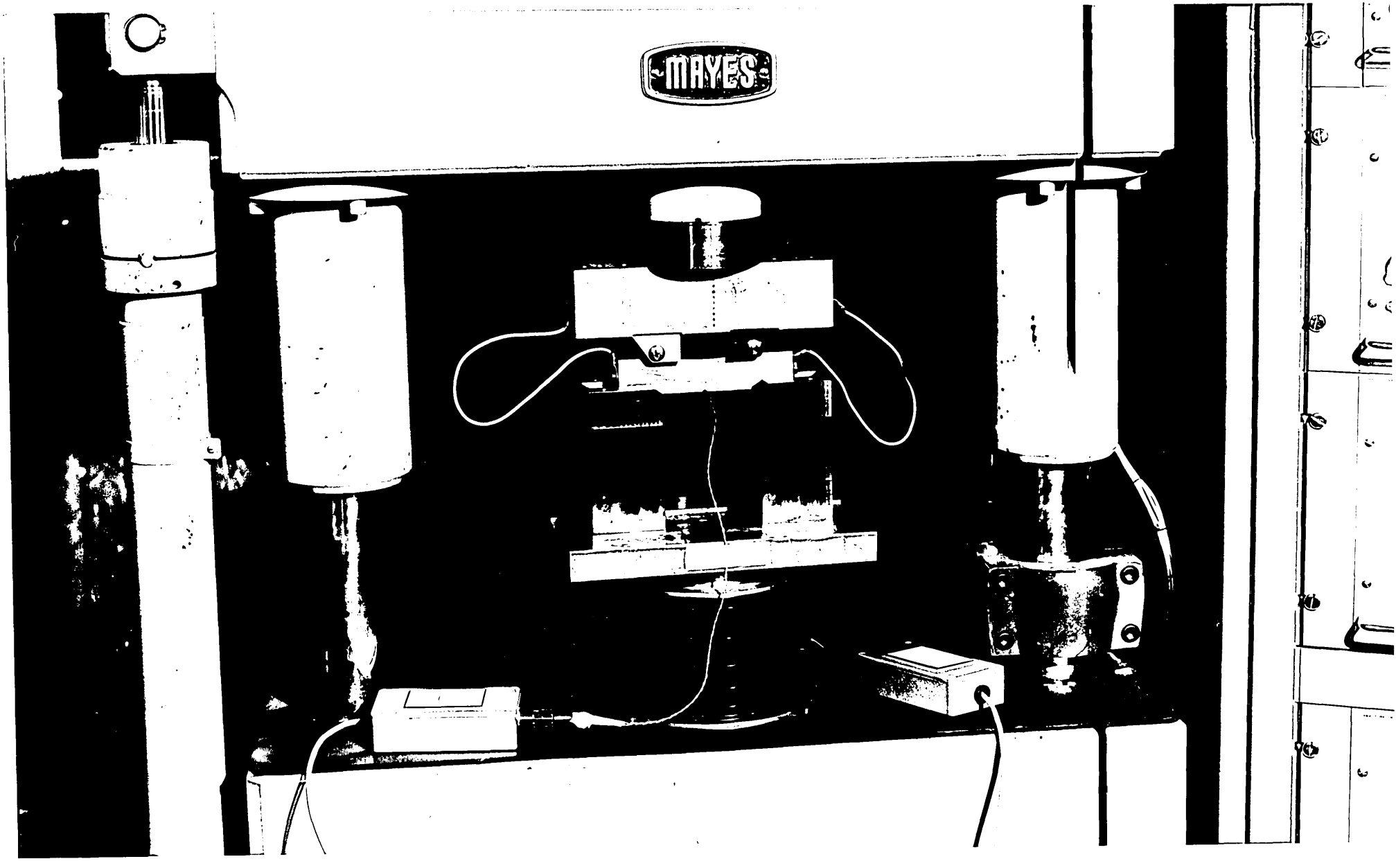
MAYES

Plate 3.3
Monitoring of CPD3 output voltage via DVM

Monitoring of CCD3 output voltage via DVM
Figure 3.3

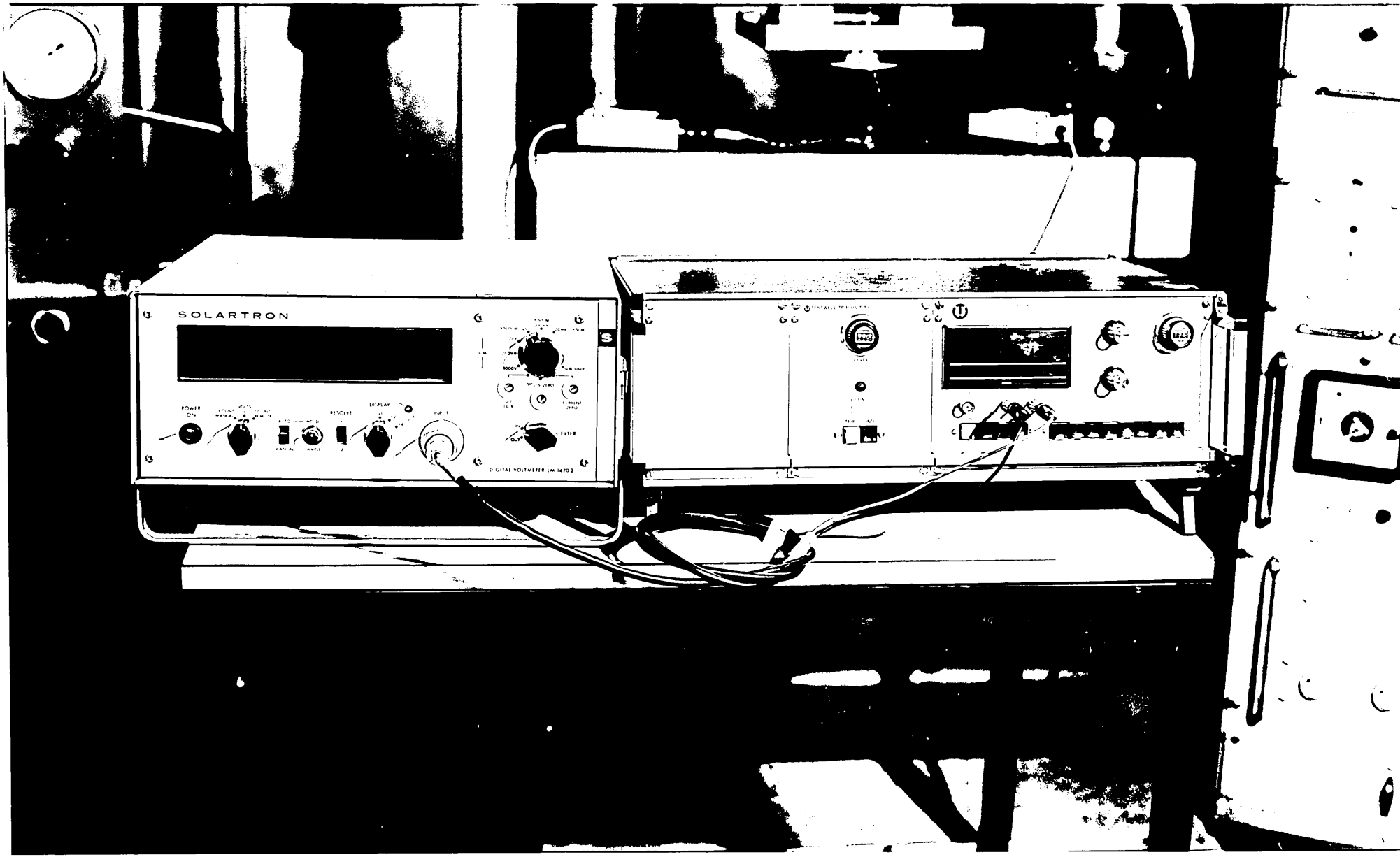
SOLARTRON

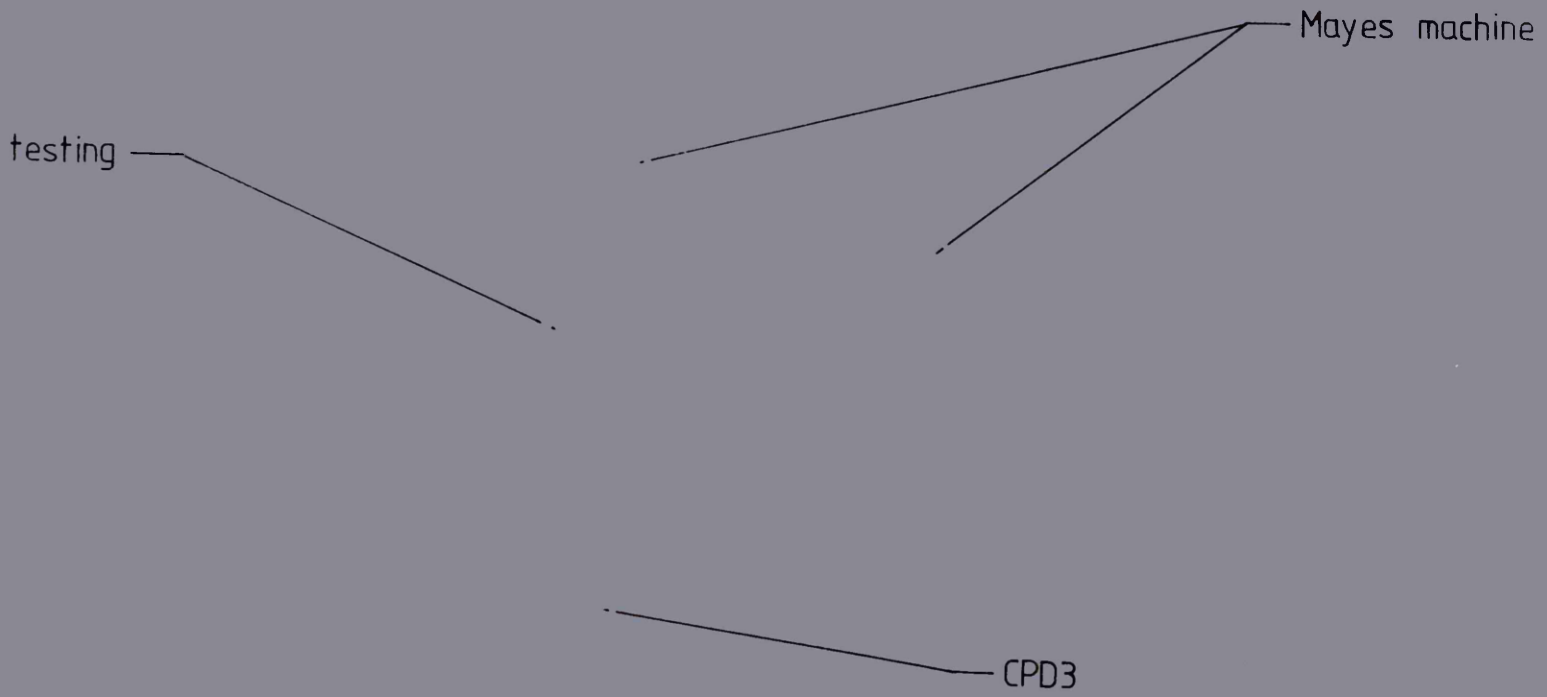

Plate 3.4
Complete monitoring and loading system for
testing of EN1A specimens

Plate 3.4

Complete monitoring and loading system for
environmental AUV to grips
testing

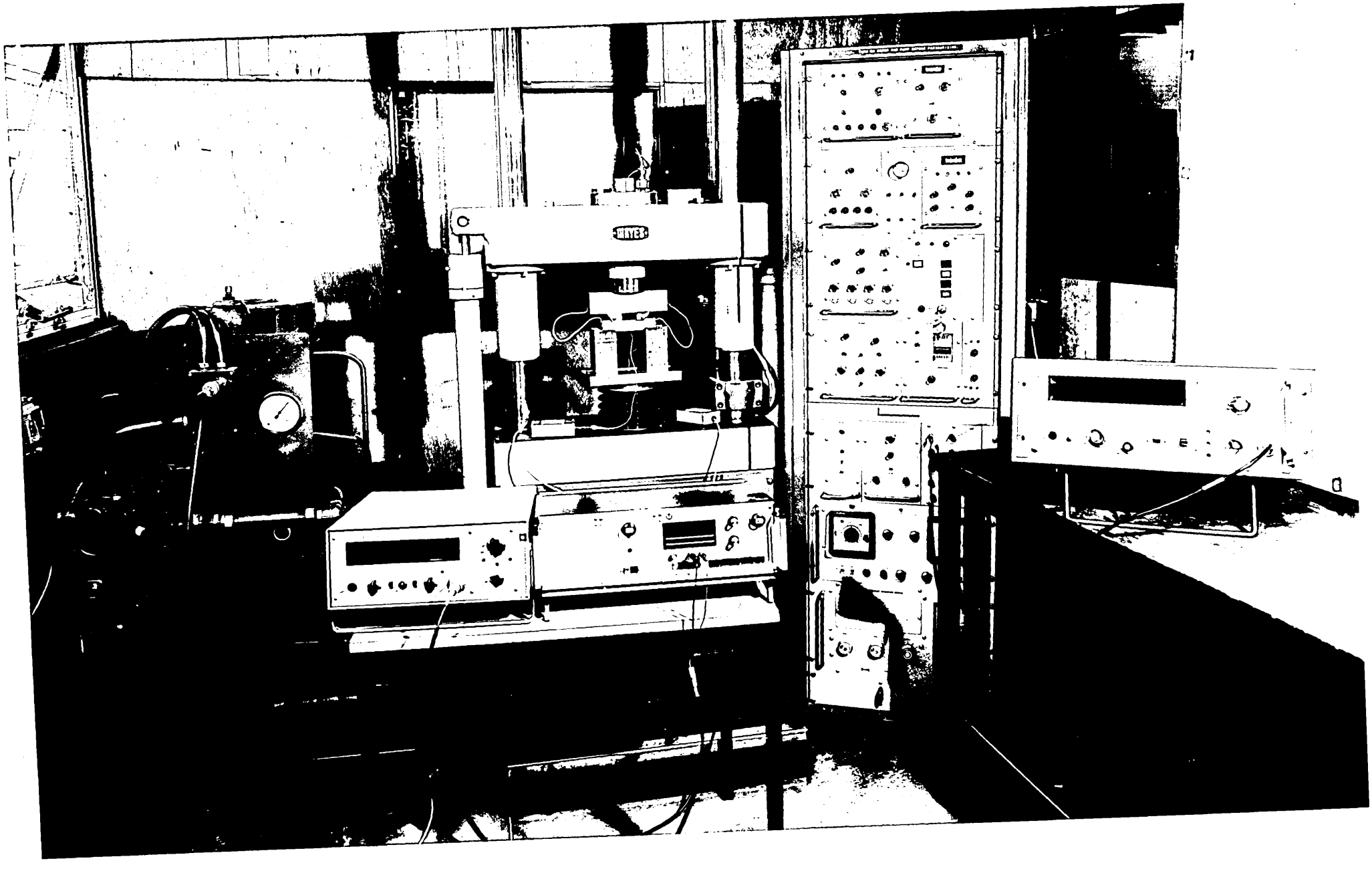
MAYES

CHAPTER 4 - MEASUREMENT OF THE ACPD RESPONSE IN NOTCHED NE8 ALUMINIUM ALLOY SPECIMENS

4.1 INTRODUCTION

In addition to the testing of the mild steel specimens described in the previous section, a complementary programme of experimental work using notched NE8 aluminium alloy specimens was also undertaken.

From examination of equation 1.7 it can be seen that dominant terms in the expression for the skin depth are the magnetic permeability ($\mu=\mu_r\mu_o$) and the electrical resistivity (ρ). In a strongly ferromagnetic material, such as mild steel EN1A, both these parameters are significant in determination of the ACPD response. Hence the EN1A experimental work essentially examined the effect of strain on both these parameters collectively. An additional series of experiments using the aluminium alloy NE8 allowed the examination of ρ in isolation. This alloy was chosen because of its good ductile properties and weak magnetic characteristics typical of all non-ferrous alloys. Such materials have a constant value of relative magnetic permeability (μ_r) close to unity and ρ is the only material parameter affecting the ACPD response.

To provide a realistic comparison of results the NE8 experimental programme was based very closely on that of the EN1A testing. The same current value of 5A at the fixed operating frequency of 8 kHz was again used. However due to the relatively weak skin effect in the NE8 alloy a much higher value of basic system gain was necessary to produce a reasonable PD output response from the CPD3 monitoring system. This consideration also presented additional difficulties with the PD measurements not encountered previously.

At very high values of gain (the CPD3 allows gains of up to 70000) electrical noise becomes a very real problem. In an effort to avoid this, the original pre-amplifier and current transformer were replaced with much higher quality components having enhanced noise rejection capabilities.

As stated earlier the experimental work closely followed that of the previous EN1A programme. Preceding the main NE8 experimental work an initial series of tests were required to determine an appropriate value of system gain and verify the suitability of the test procedure for non-ferrous materials. However it was found largely unnecessary to modify the EN1A test procedure significantly.

4.2 SPECIMEN PREPARATION

Subsequent to the machining of the specimens and prior to lead and pick-up wire attachment the complete batch of specimens were heat treated. The annealing procedure chosen increased specimen homogeneity and removed any residual stresses that may have been introduced during manufacture. (see section 2.1.2)

The levels of surface oxidation were considerably less than in the case of the mild steel specimens, therefore leadwire attachment required little preparation of the material surface.

Following heat treatment, the notch profiles were then examined using a shadowgraph machine to check notch tolerances. Additionally, close examination provided an accurate estimate of the "average" notch profile suitable for input into the PAFEC datafiles during the finite element analysis.

The nominal positions of the current input and voltage pick-ups remained the same as for the mild steel specimens. The current

inputs were located sufficiently far apart to allow the assumption of a linear electric field distribution over the central region of the notch. The largest difference in specimen preparation was the method of lead attachment and specimen earthing. The relative positions of the lead and pick-up wires can be seen in figure 4.1.

During the NE8 testing the introduction of a higher quality pre-amplifier necessitated a different method of specimen earthing via pin number 2 of the DIN connector. This was accomplished using a fifth pickup lead wire attached at position B, see figure 4.1 and plate 4.1. Similar to the mild steel testing the pick-up wires consisted of 27 SWG single strand enamelled copper wire.

A different method of lead and pick-up wire attachment was also required with the aluminium alloy specimens due to the difficulty of spot-welding successfully directly onto this material. An alternative method of attachment was accomplished via electrical matrix pins. A series of small holes slightly smaller than the pin diameter were drilled at the required positions and pins inserted to cause an interference fit. A small centrepunch mark was then made alongside to burr the metal over and secure the pins. Lead and pick-up wires were then soldered directly onto the heads of the pins in the normal manner, see figure 4.2. This mode of attachment also precluded the necessity of reinforcing the leadwire to specimen connection with Araldite cement.

To minimise the risk of induced EMF's both the current leads and pickup wires were taken off on opposite sides of the specimens.

The method of specimen alignment, in the loading rig, using scribe marks corresponding to the positions of the upper loading rollers was continued from the mild steel experimental work.

4.3 EXPERIMENTAL PROCEDURE

The experimental method adopted during the NE8 testing was based closely on that of the EN1A procedure. Details of the loading rig with the specimen in situ and the necessary electrical connections can be seen in plate 4.2 and the complete monitoring and loading system in plate 4.3. Since the two materials had totally contrasting magnetic characteristics the PD response in each case could be expected to be equally distinct. The response observed in the NE8 was likely to be much less marked and hence some optimization of the CPD3 instrument settings was required before the experimental work could begin. The values of current and frequency were already predetermined and could not be altered without violating the comparability of the results. Hence it was necessary to determine a suitable value of gain that would provide sufficient resolution of the PD response and produce a reasonable set of results.

Using a V notched specimen a wide range of gain values, from 2000 to 70000, were investigated. An increasing bending load was applied to the specimen, in the manner detailed later in this section, as a sequence of 5 kN steps up to 50 kN maximum. At each load step the gain was switched across a series of levels up to 70000 and the PD response noted. Knowing the gain and DC offset, the absolute value of PD in μV was calculated at each load level for all values of gain. Theoretically all should have been the same at each load level but in practice this was not so. The results can be seen plotted in figures 4.3 and 4.4. As can be seen above, a gain of 30000, excellent signal resolution was available. Stability of the signal was also very good with a very low level of noise even at the highest levels of gain. From these results it was decided to employ a basic system gain of 70000 together with an input current of 5A at a fixed operating frequency of 8 kHz.

The experimental procedure adopted for the U and V notched specimens was very close to that used previously with the En1A specimens.

The procedure followed in the NE8 testing given below is in the form of an addendum to the EN1A procedure detailed in section 3.3.

(i) As for section 3.3(i), except an instrument gain of 70000 was selected.

(ii) As for section 3.3(ii), except it was unnecessary to allow time for the Araldite cement to harden since the current and voltage pick-up leads were soldered directly onto the specimen via electrical matrix pins.

(iii) As for section 3.3 (iii)

(iv) As for section 3.3 (iv)

(v) As for section 3.3 (v)

4.4 RESULTS AND DISCUSSION

The results of the NE8 experimental work can be seen in figures 4.5-4.14 and in all cases the absolute voltage measured across the notch using the compensation method has been plotted against increasing load. The selection of results presented is not the whole set but is considered to be a representative sample typifying the responses observed.

Examination of these results reveals several interesting features.

The most striking aspect of all the results was the uniformity of the ACPD response to increasing notch tip strain and deformation. The size of the standing voltage measured across the specimen was also quite consistent with all the results being in the 20-40 μV range. This was in contrast to the EN1A testing where the standing voltage

was much higher, 100-200 μV. This large difference was due to the much higher value of μ_r for the strongly ferromagnetic EN1A.

Irrespective of notch profile an almost constant PD response was recorded as the bending load increased, see figures 4.5-4.7 and 4.10-4.12. Even the unloading response displayed a remarkably similar pattern resulting in an overlapping of the two responses during each load cycle. This overlapping was seen clearly on the first load cycle but on second and subsequent cycles the effect was even more marked with the loading and unloading responses being virtually inseparable, see figures 4.8, 4.9, 4.13 and 4.14. Although not shown in the selection of results presented a slight deviation from the constant response during the first loading cycle of some of the specimens was recorded. However the deviation was not dramatic with the unloading response displaced 5-10 μV from the loading response. For both notch profiles this discrepancy disappeared completely in subsequent cycles giving the more usual overlapping response.

Although the unloading response of the first load cycle closely followed that of loading there was generally a small difference in the PD seen at zero load, with a slightly lower value of 2-3 μV on unloading, see figures 4.5-4.7 and 4.10-4.12. A similar phenomenon was also observed with the EN1A but the discrepancy was much higher, 30 μV.

The lack of any major change in PD during either loading or unloading allows several immediate conclusions to be drawn concerning the nature of the response.

Contrasting the responses observed in the two materials the differences are dramatic. The most likely mechanism through which to explain the

difference is the effect of strain and deformation on the value of μ_r of both materials. The skin depth and hence PD responses in the non-ferrous NE8 is largely governed by ρ. Combined with the PD response observed in this material it is reasonable to conclude that ρ is not a crucial factor in determining the PD response to increasing elastic and plastic strain. This also implies that when using ACPD systems with non-ferrous materials strain levels and material deformation will not significantly affect crack depth estimates. Care must be exercised in extrapolation of these deductions to systems operating at appreciably different frequencies from the 8 kHz employed in the current programme. However since most commercial systems operate close to this level this consideration should not present too many problems.

Clearly the magnetic permeability dominates the PD response and from consideration of the form of the response in EN1A there is no simple strain/PD relationship available. From these deductions it is clear that in strongly ferromagnetic materials where crack tip plasticity is appreciable the influence of strain on the value of μ_r is a significant factor in determining PD response.

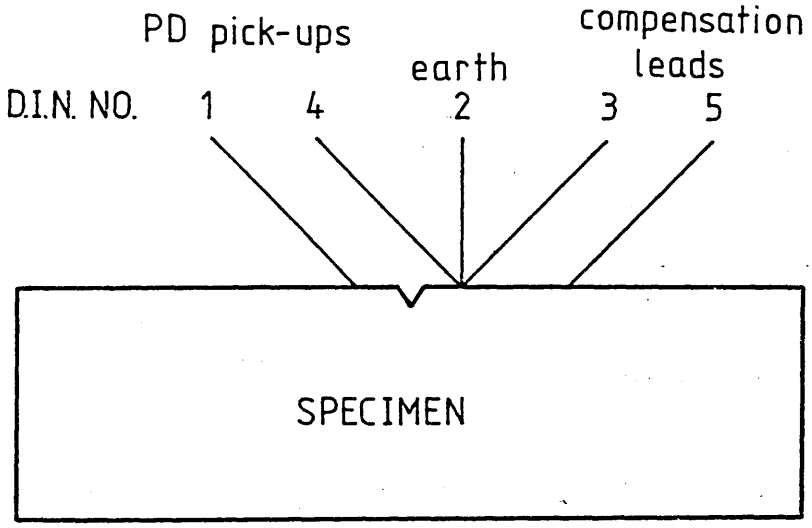

PIN NO.2 NEW SPECIMEN EARTH

Fig 4.1 Position of current input, voltage pick-ups and specimen earthing via pin no 2 of DIN Connector

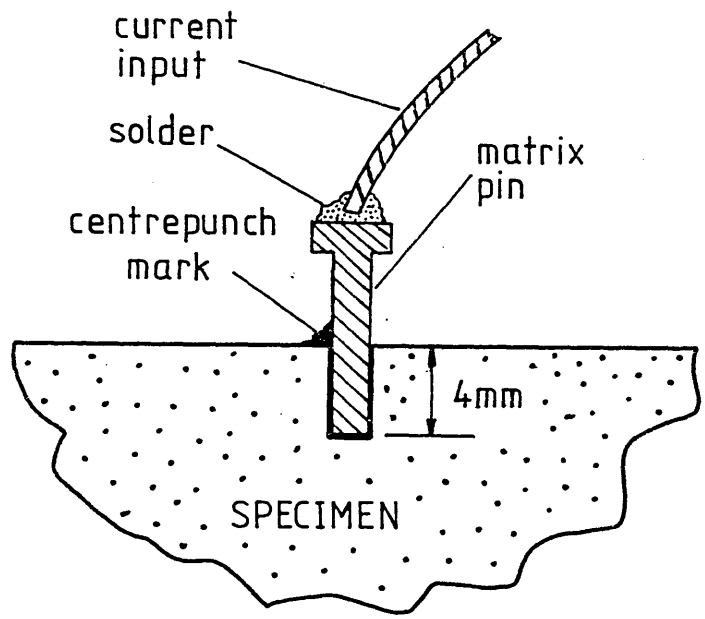

Fig 4.2 Attachment of current input leads onto NE8 specimens via electrical matrix pins

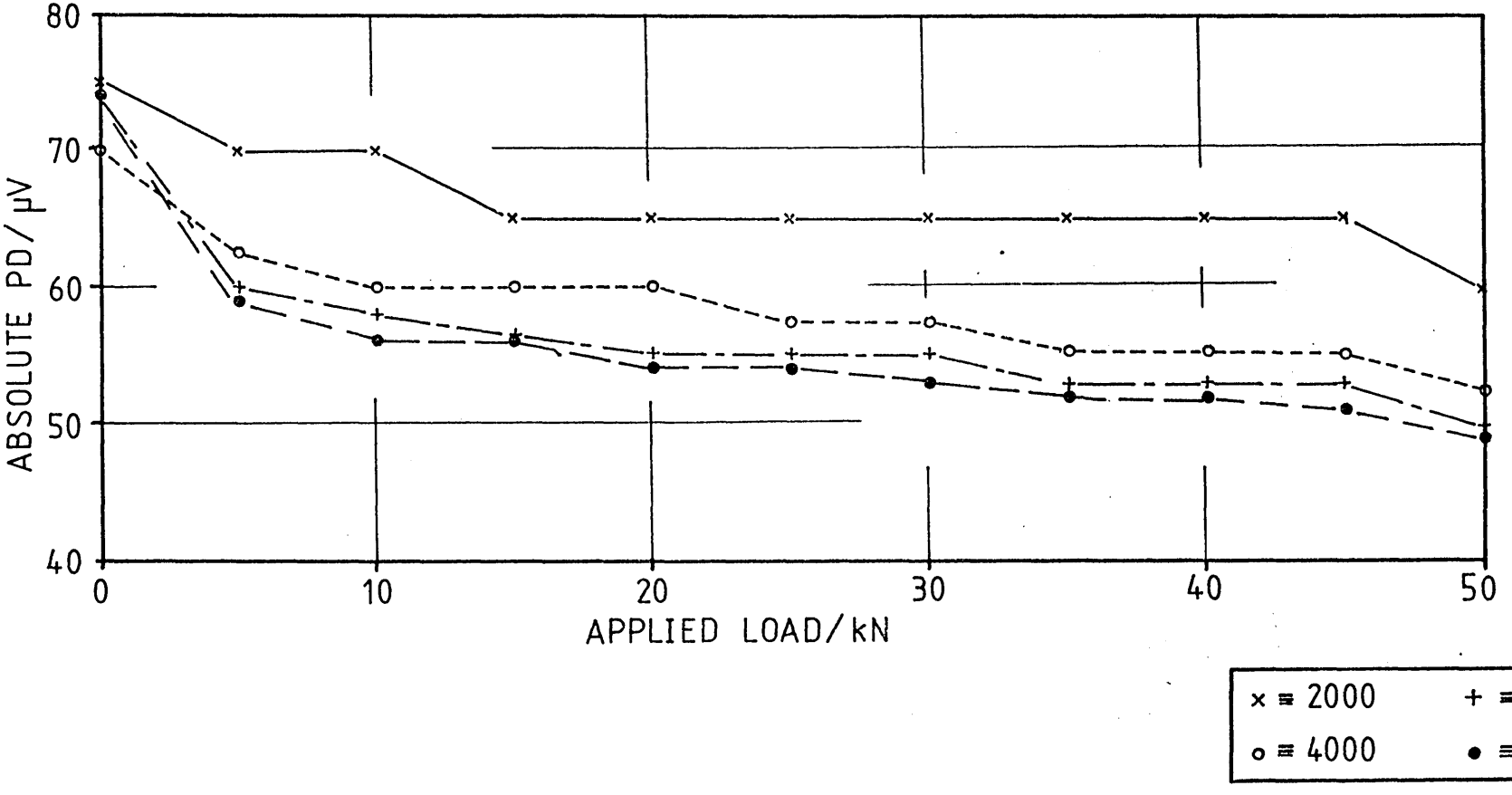

Fig 4.3 Resolution versus gain characteristics of the CPD3 with NE8 Aluminium Alloy

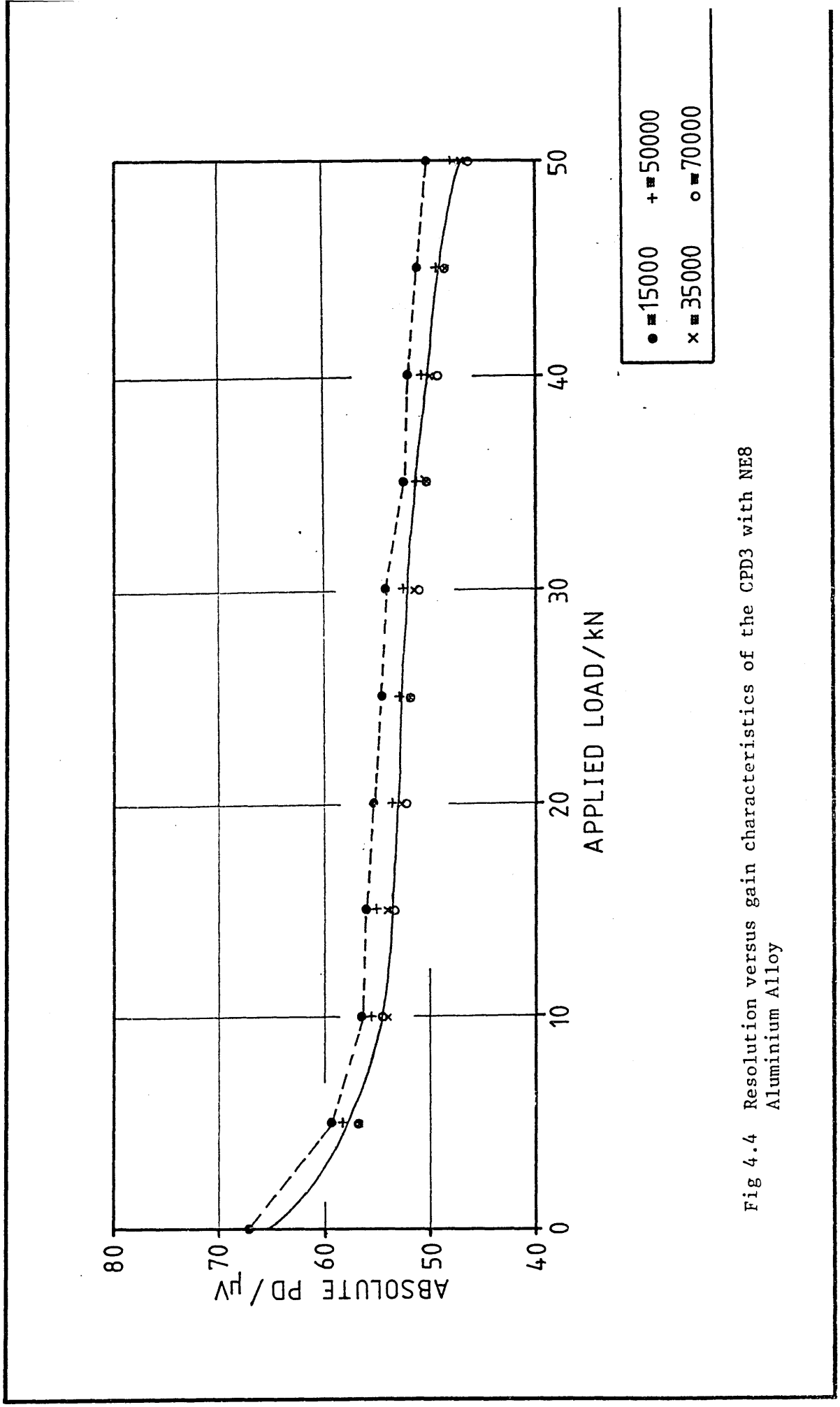

Fig 4.4 Resolution versus gain characteristics of the CPD3 with NE8 Aluminium Alloy

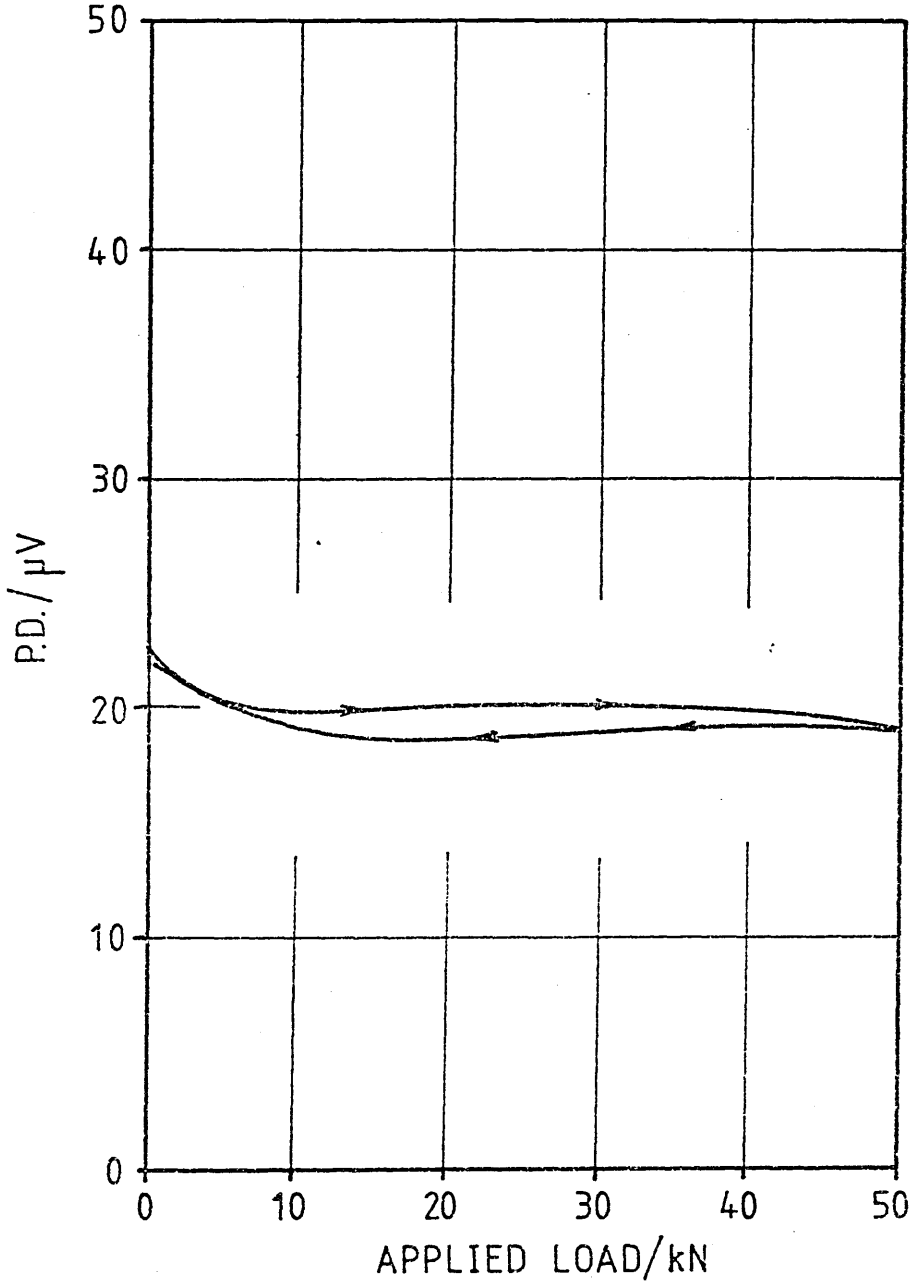

Fig 4.5 ACPD Response : NE8 V Notch :

Specimen VA10 : First Load Cycle

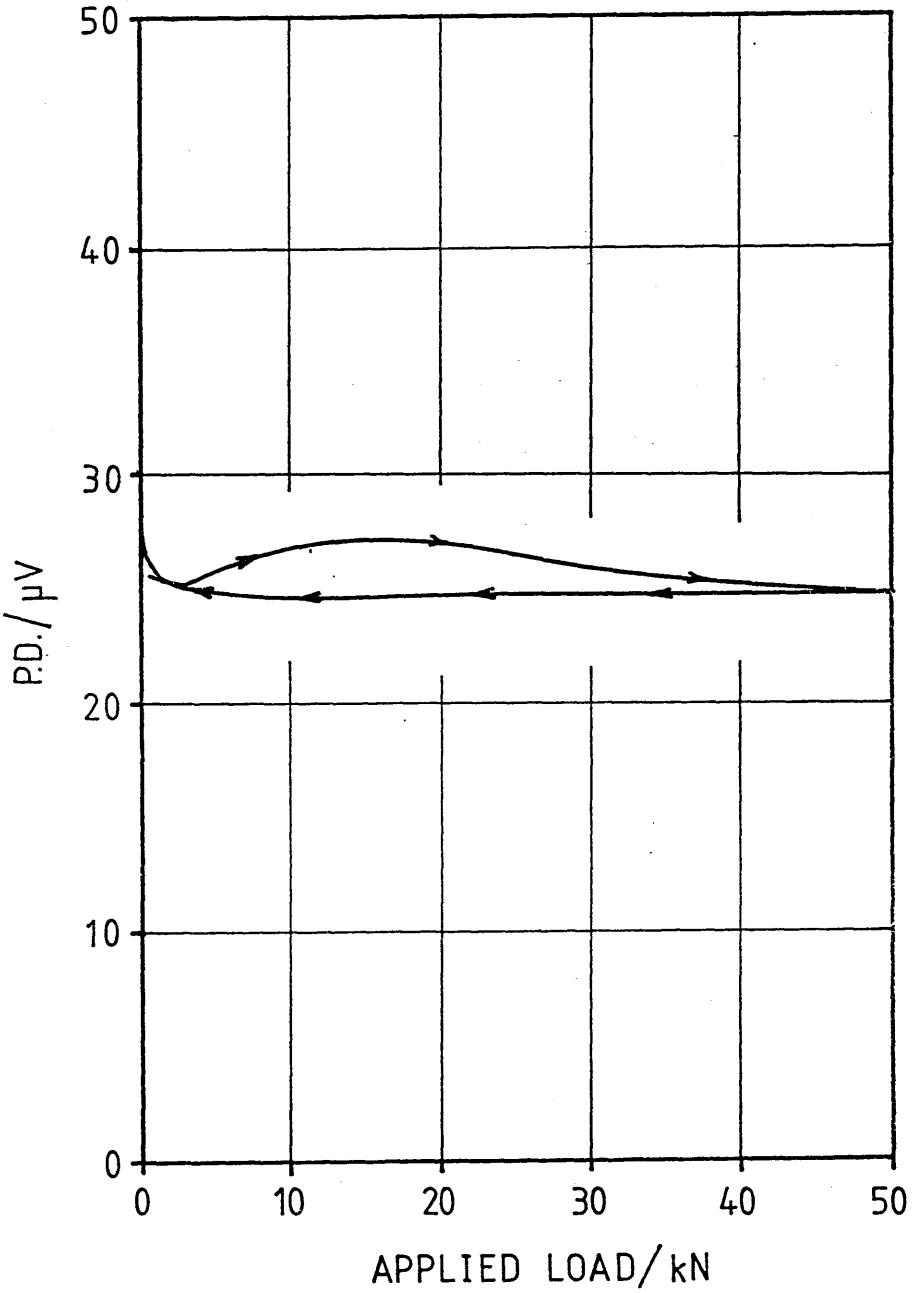

Fig 4.6 ACPD Response : NE8 V Notch :

Specimen VA8 : First Load Cycle

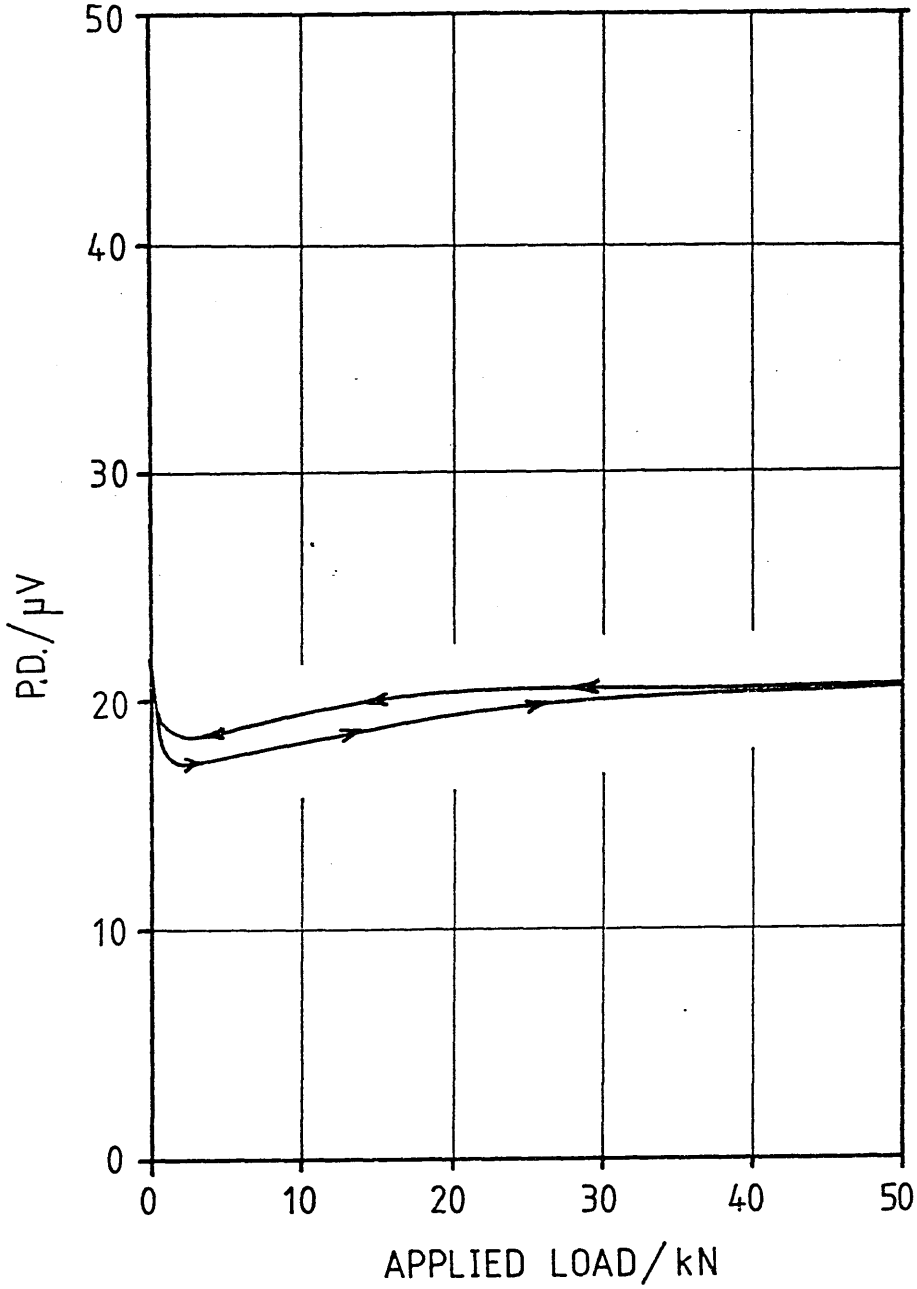

Fig 4.7 ACPD Response : NE8 V Notch :

Specimen VA9 : First Load Cycle

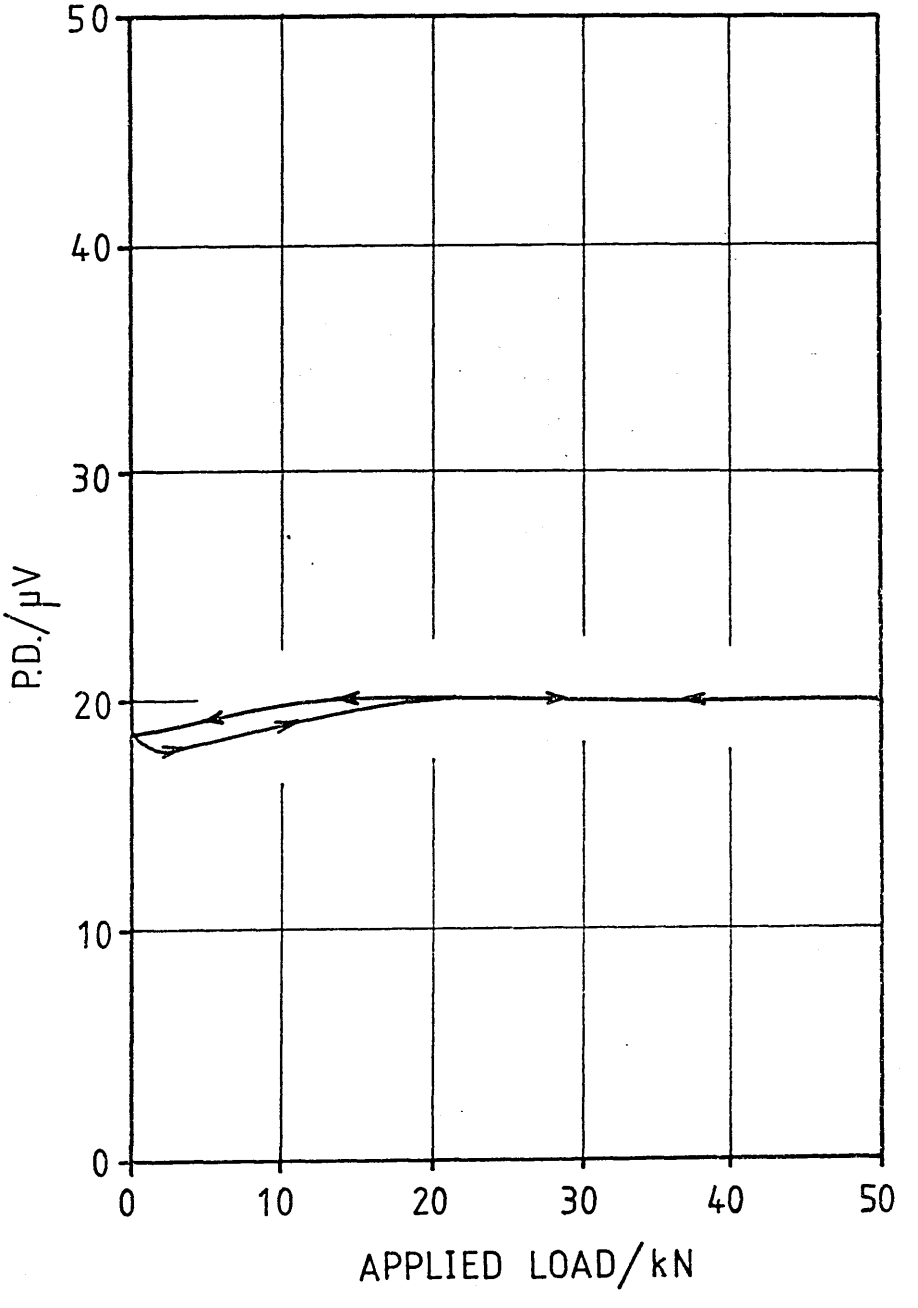

Fig 4.8 ACPD Response : NE8 V Notch :

Specimen VA9 : Second Load Cycle

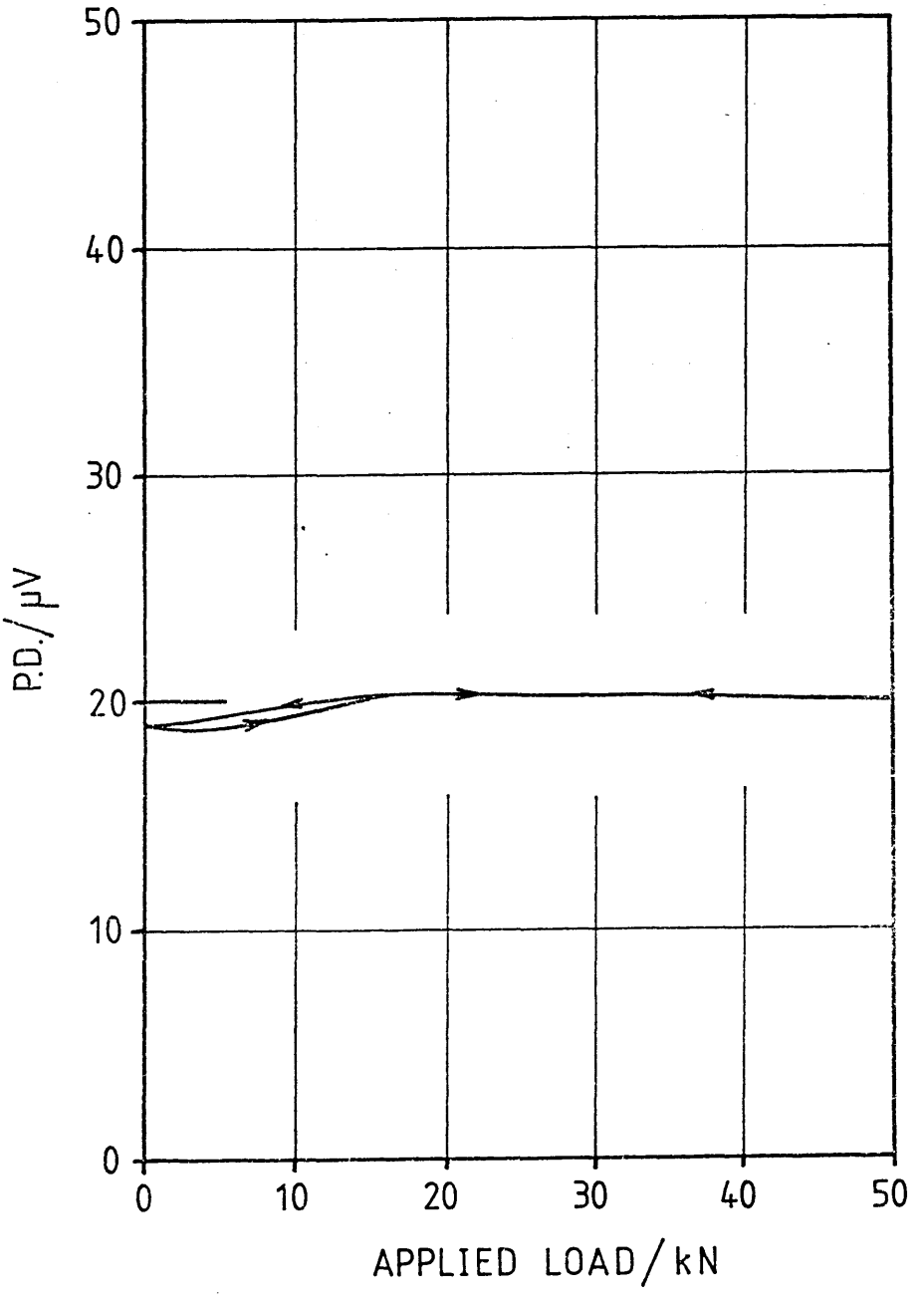

Fig 4.9 ACPD Response : NE8 V Notch :

Specimen VA9 : Third Load Cycle

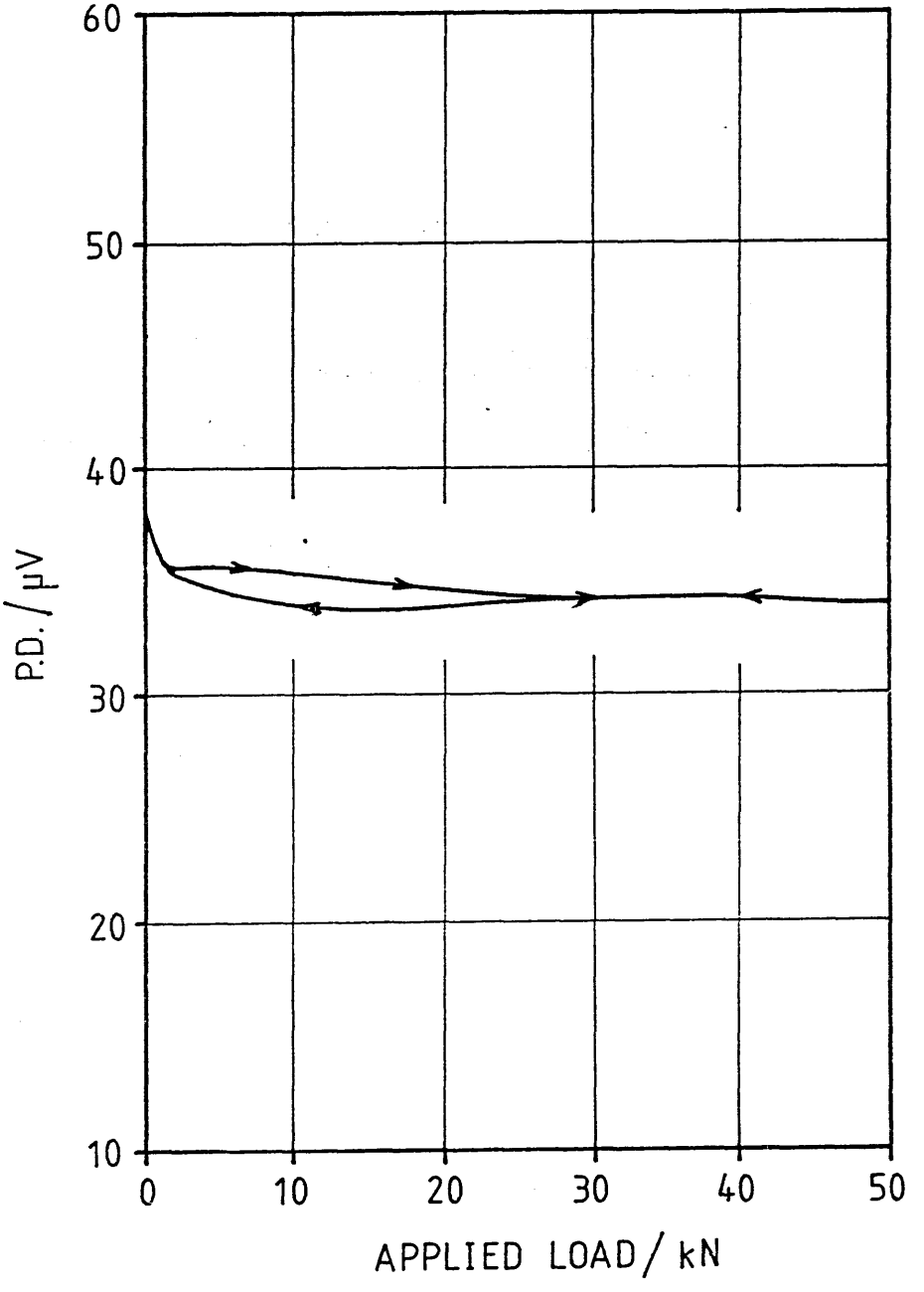

Fig 4.10 ACPD Response : NE8 U Notch :

Specimen SA10 : First Load Cycle

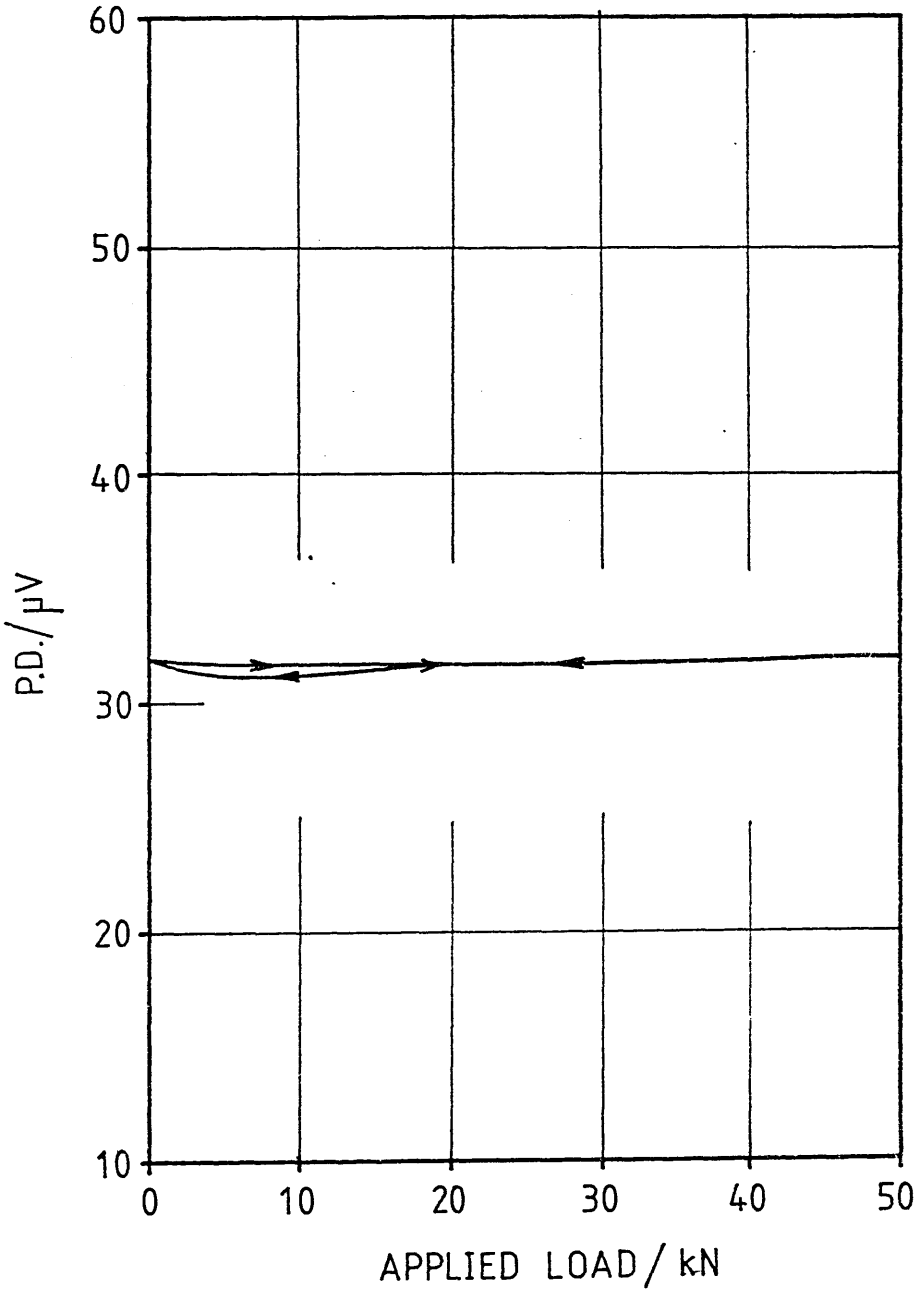

Fig 4.11 ACPD Response : NE8 U Notch :

Specimen SA11 : First Load Cycle

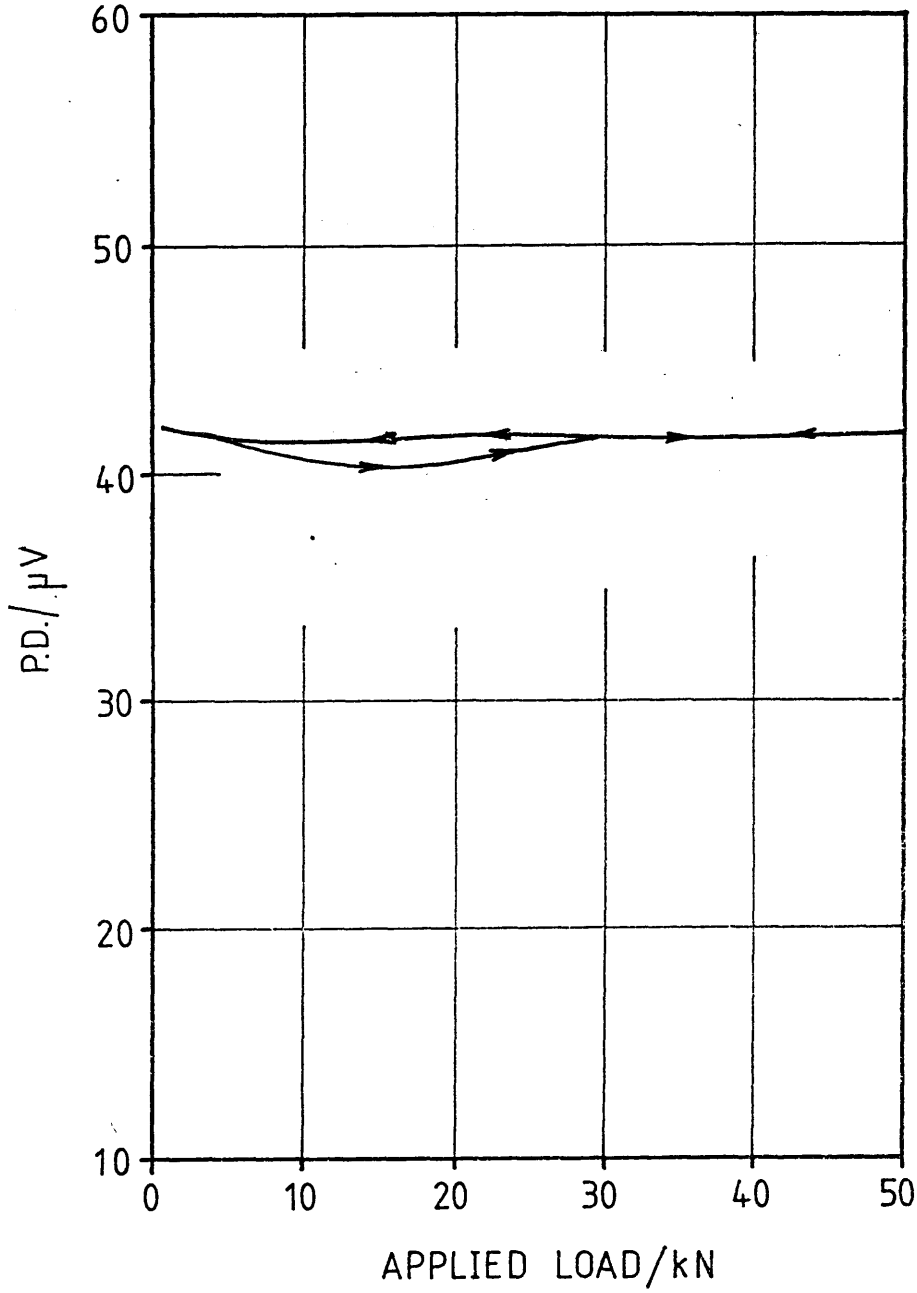

Fig 4.12 ACPD Response : NE8 U Notch :

Specimen SA8 : First Load Cycle

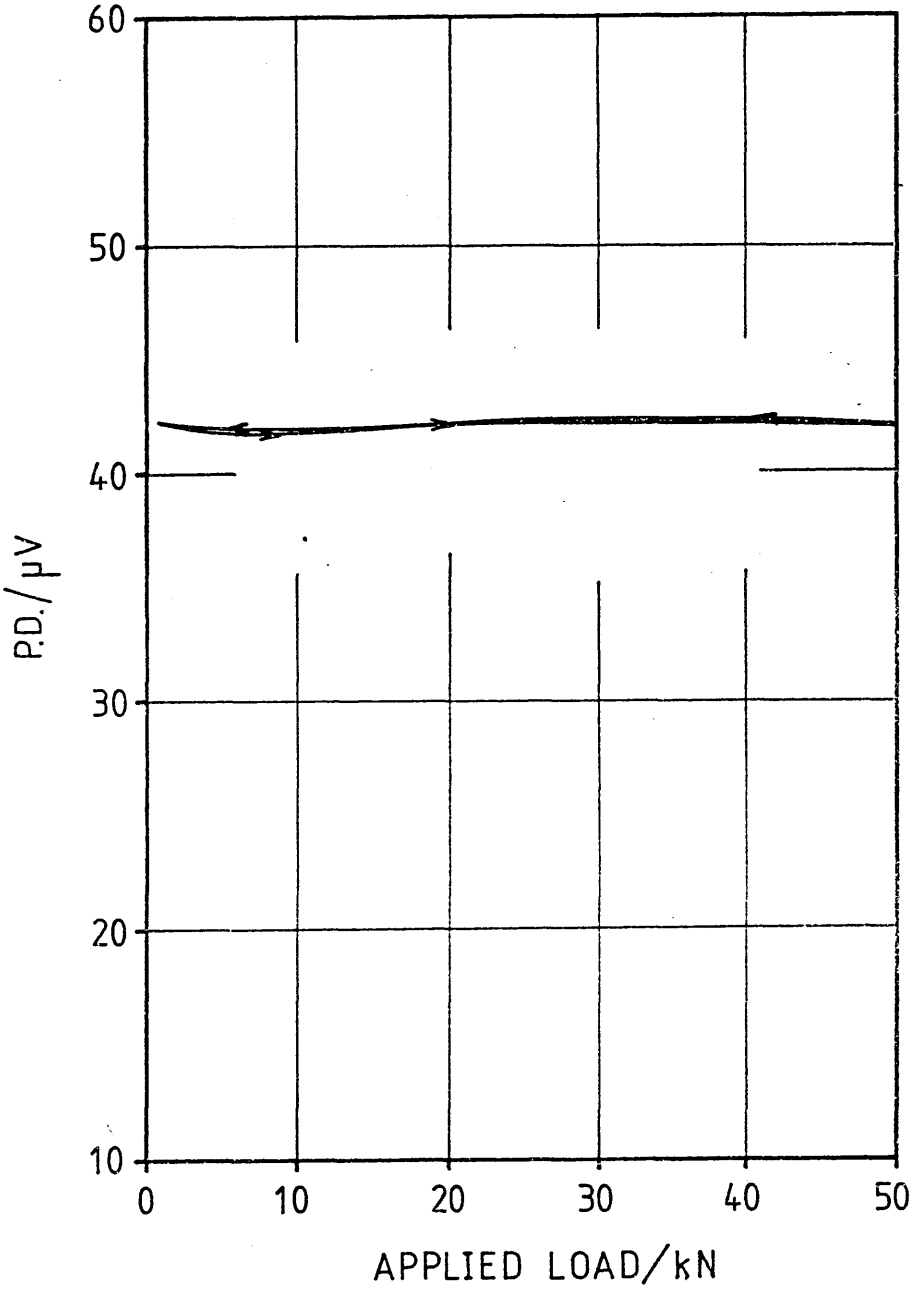

Fig 4.13 ACPD Response : NE8 U Notch :

Specimen SA8 : 2nd Load Cycle

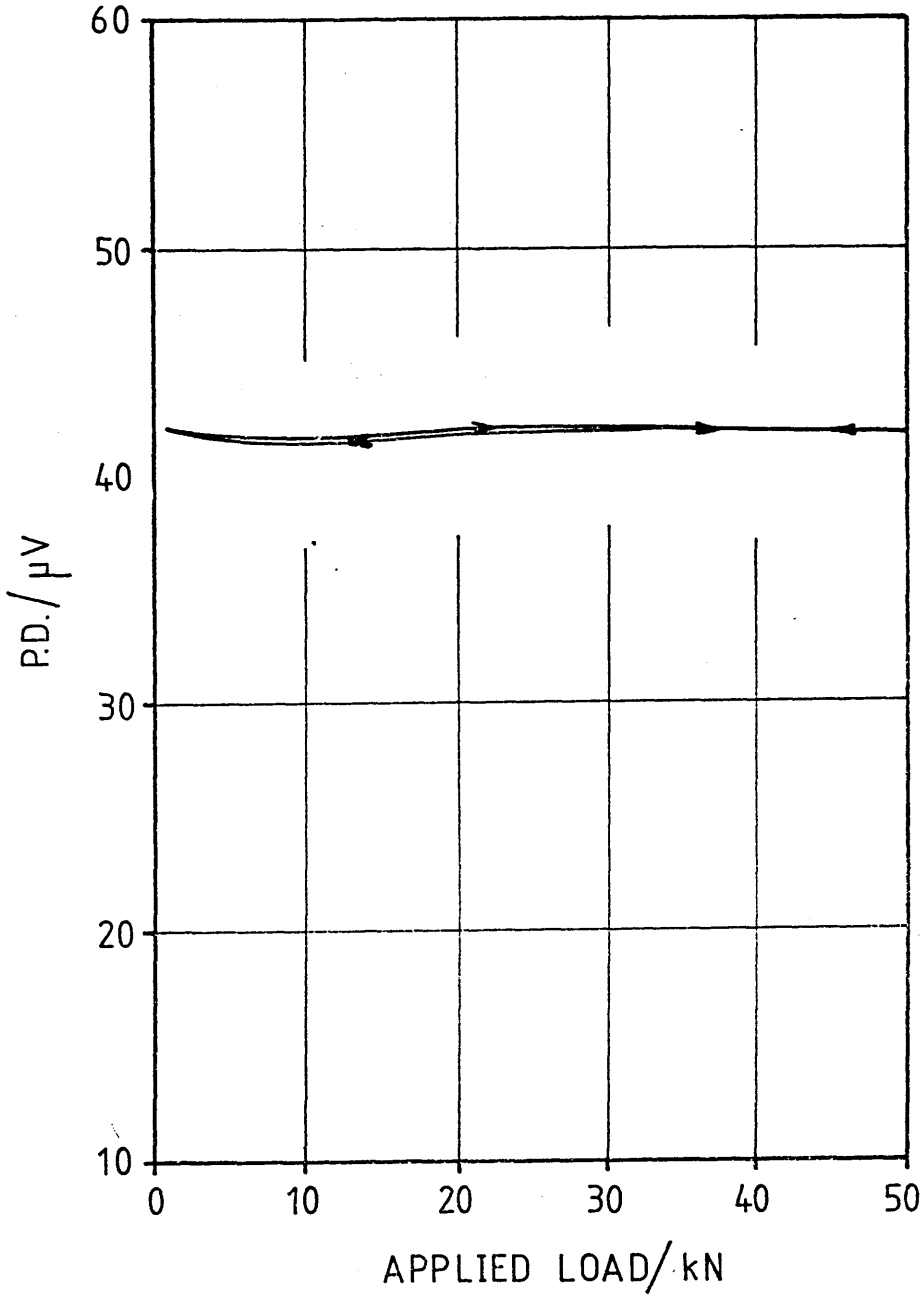

Fig 4.14 ACPD Response : NE8 U Notch :

Specimen SA8 : Third Load Cycle

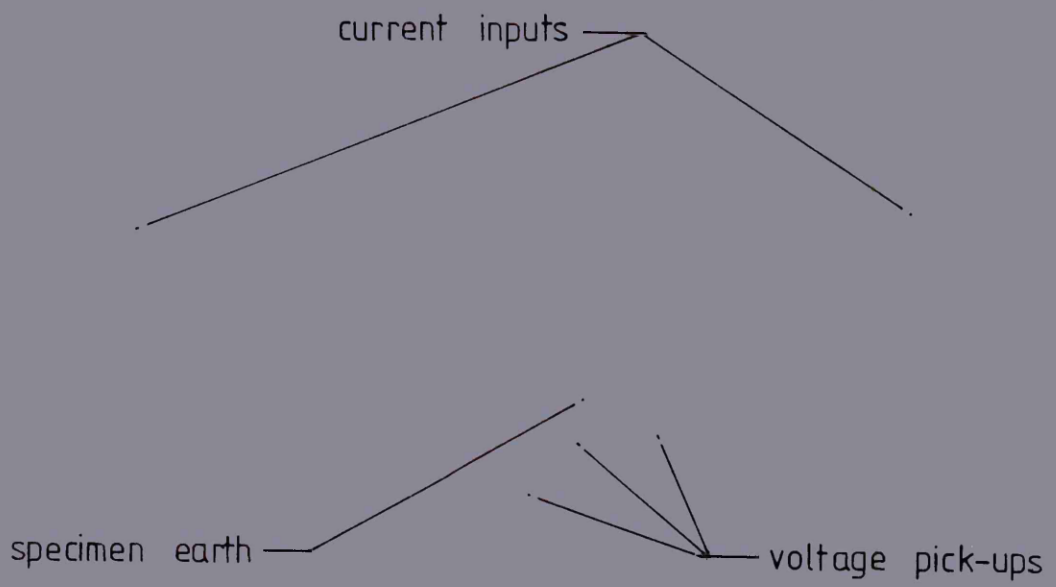

Plate 4.1
Attachment of current input, voltage pick-ups and specimen earth for NE8 specimens

Plate 4.1

Variation of transient current to earth fault for HEB specimens
examined by voltage pick-ups and spectrum

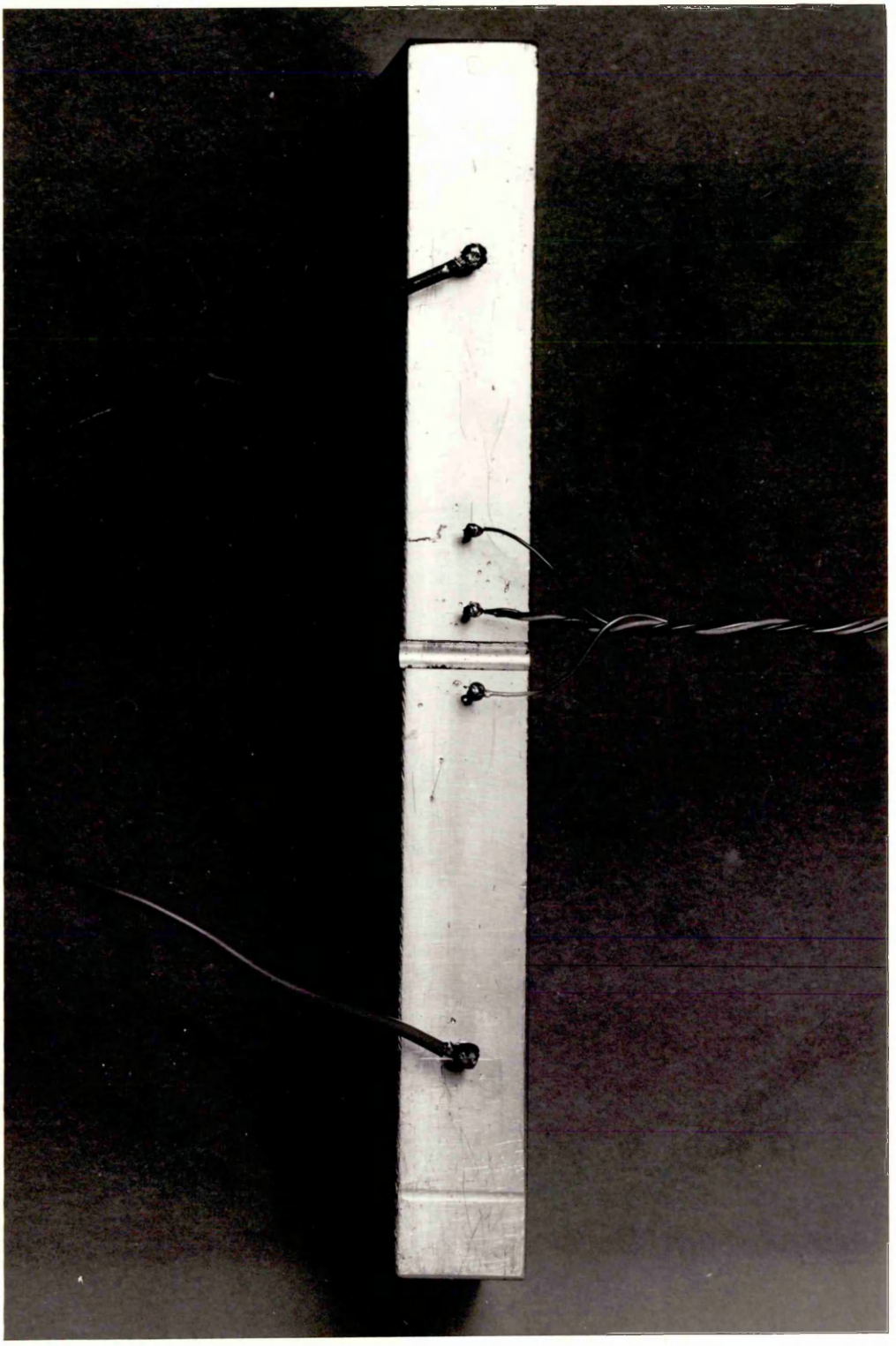

Plate 4.2
NE8 specimen in situ in loading rig

WE8 specimen in grips loading rig
Figure 4.2

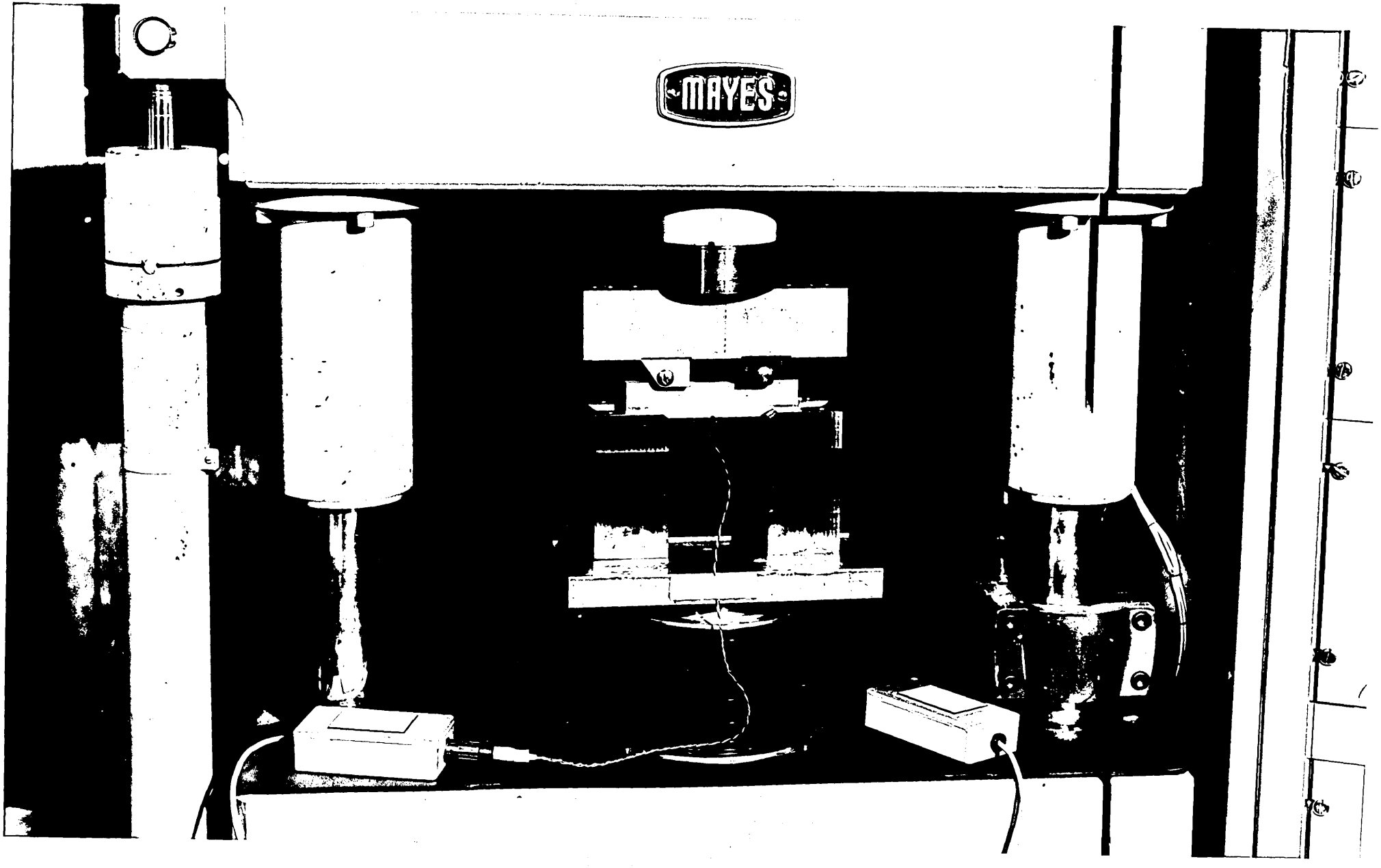
MAYES

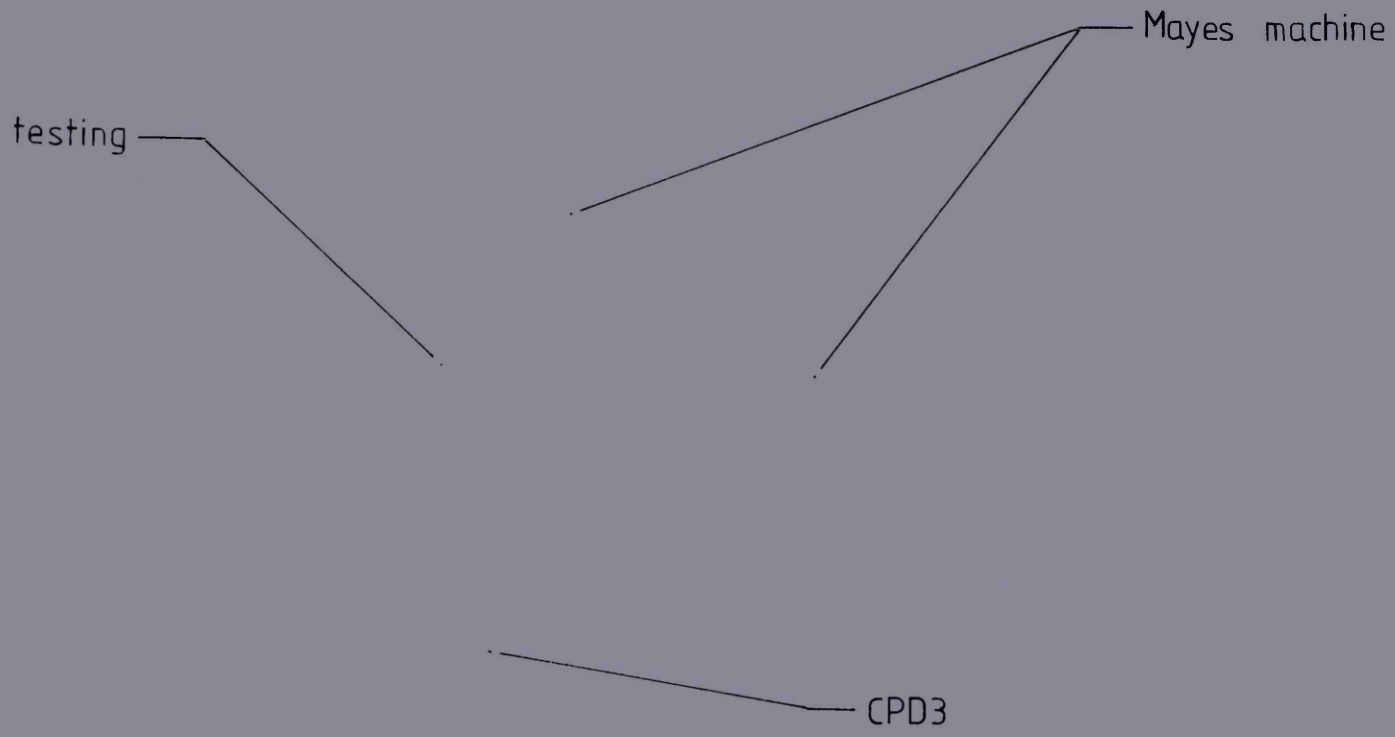

Plate 4.3
Complete monitoring and loading system for testing
of NE8 specimens

Figure 4.3

Computer monitoring and logging system for research and diagnostic purposes of ME8 spectrums

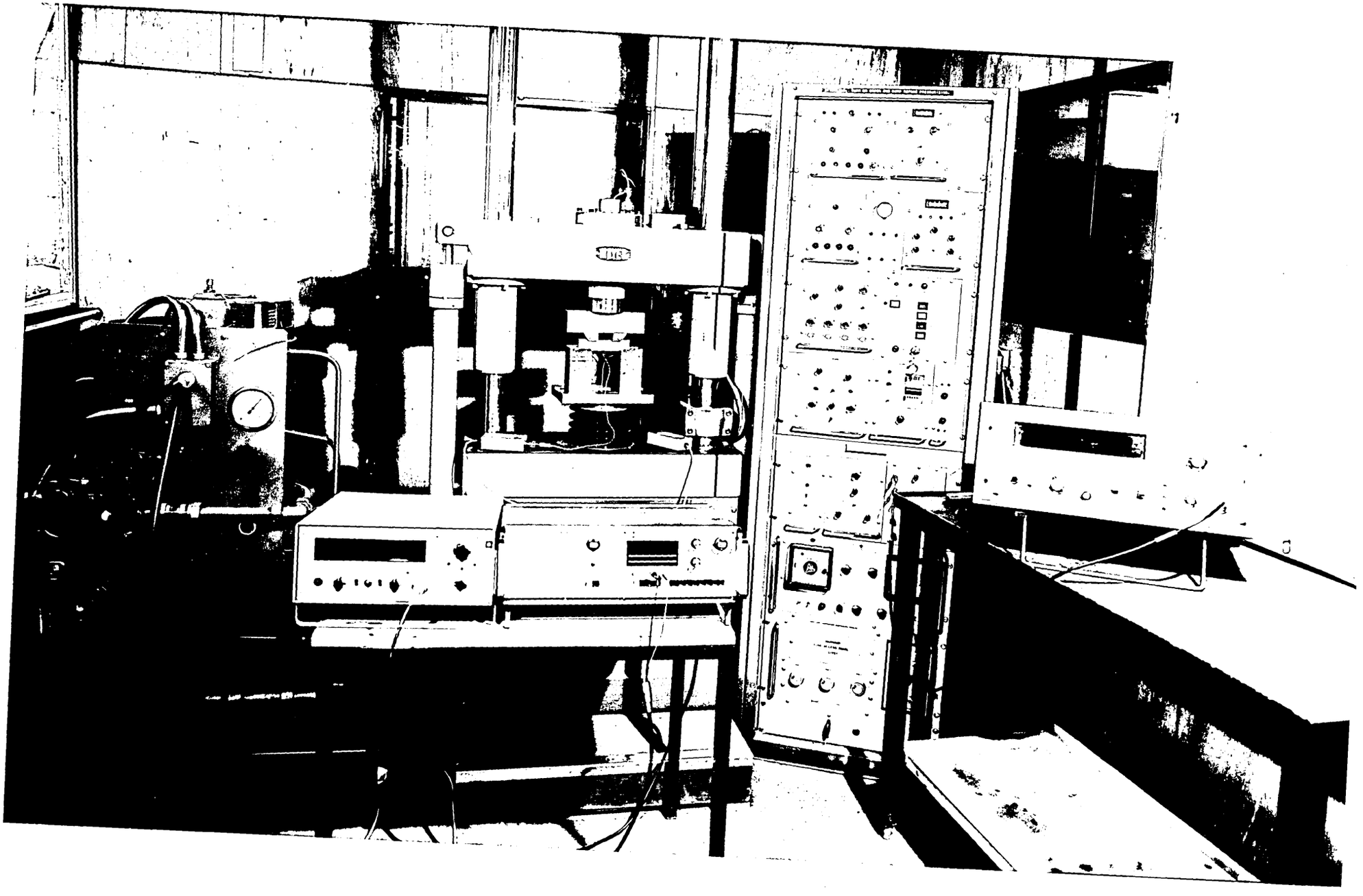

CHAPTER 5 - THEORETICAL FINITE ELEMENT STRESS ANALYSIS

5.1 INTRODUCTION

The aim of the present programme of work was to understand and quantify the influence of localised elastic and plastic deformation at the tip of a notch on measurements made using the ACPD method. In understanding such a study it was therefore necessary to have a reliable, detailed description of the notch tip deformation and stress field under both elastic and post-yield conditions with which to correlate the experimentally determined ACPD response.

Several experimental stress analyses were also attempted to supplement the finite element (FE) analysis but were very difficult in application. Strain gauges located along the notch centreline proved unsatisfactory. It was only possible to position a maximum of four elastic gauges and one post-yield gauge close to the notch root. The results in themselves seemed contradictory and differed greatly from strains predicted by simple bending theory. Following the lack of success in such methods a numerical finite element (FE) stress analysis was undertaken to determine the notch tip stress field.

The FE method has been developed and refined continuously since its initial introduction in the late 1960's and with the growing availability of cheap and powerful computing facilities the method has found many areas of application and has been used by many researchers to great effect [22, 23, 24]. One of its main areas of application has been that of stress analysis where it has proven a very useful numerical tool providing

an accurate picture of the strain and deformation in any stressed engineering component. However, the FE method is only a numerical process and as such the answers are totally dependent on the model and initial data input by the user. In order to ensure the accuracy and reliability of the numerical solution careful modelling of the structure and loading conditions are necessary.

The FE analysis of the notches was run in two separate but interdependent stages. Firstly an elastic analysis was conducted where the stress components were assumed not to exceed the yield stress of the material and only linear material behaviour was considered. This was a necessary first step and provided an insight into the validity of the FE model itself and also indicated the load at which yielding would first occur at the notch root. The second stage was the extension to a full elastic/plastic analysis and the consideration of non-linear material behaviour with the stresses around the notch root being well above the yield point of the material. This latter stage was far more costly in terms of CPU time and it was therefore wise to conduct the elastic analysis first to ensure the validity of the model and of the solution.

5.2 DESCRIPTION OF SOLUTION MODEL

5.2.1 Specimen Geometry and Material Properties

The overall specimen dimensions and details of notch geometries can be seen in figures 2.1-2.5. As commented upon previously in section 2 after machining a slight variation was discovered between the mild steel (EN1A) and aluminium alloy (NE8) U and V notch profiles. To minimise the risk of introducing possible sources of error and inaccuracies into the analysis

each notch geometry was modelled separately. This necessitated the separate consideration and modelling of four different notch profiles, but did not unduly increase the complexity of the modelling since equivalent U and V notch profiles were still very similar.

The material properties necessary for input into the PAFEC datafiles were determined from tensile tests on both materials in their annealed condition. Details of the elastic material properties are given below.

EN1A MILD STEEL

Young's Modulus, E = 209GPa

Uniaxial Yield Stress = 254MPa

Poisson's Ratio = 0.30

NE8 ALUMINIUM ALLOY NE8

Young's Modulus, E = 58GPa

Uniaxial Yield Stress = 163 MPa

Poisson's Ratio = 0.33

During the non-linear (plastic) analysis stage of the FE analysis the material stress/strain curve had to be entered in a suitable form. To accompish this it was necessary to discretize the whole of the curve into a series of straight sections and describe it in a piecewise linear form, each section being defined by a pair of stress/strain values. The FE formats of the curves together with the co-ordinates defining each linear section can be seen in figures 5.1, 5.2 and tables 5.1 and 5.2.

5.2.2 Computational Details

The finite element package PAFEC (Program for Automatic Finite Element Calculations) level 4 mounted on an IBM 4341 mainframe computer together with the complementary graphics suite PIGS was initially adopted for the analysis, [25-28]. This proved an adequate system for the elastic analysis and restricted plastic analyses with a small number of load increments and few elements allowed to yield, the case pertaining to the U notch profiles.

In the situation of extensive plasticity and severe stress gradient, present with the V notches, this system presented considerable limitations to solution accuracy. In these cases much smaller load increments and large numbers of yielding elements, due to the necessarily small size of the notch tip elements, were needed to prevent divergence of the solution. The extent of the non-linear analysis required large amounts of CPU time unobtainable on the IBM 4341. This necessitated the use of the PRIME 9750 computer for the plastic analysis of the V notch profiles. With this system the jobs could be sent to batch and run overnight without significant CPU time restrictions. In addition level 6 of PAFEC was available on the PRIME together with a higher level of PIGS capable of providing enhanced and more detailed output than was available with the IBM 4341.

5.2.3 Development of the FE Model

The aim of the FE analysis was to correctly model and predict the stresses and strains in a notched four point bend specimen, see figure 2.1, as the bending load increased and localised

yielding occurred. The most rigorous treatment of the situation would have necessitated the generation of a very complex three-dimensional FE mesh. There would have been, however, significant penalties in undertaking such an approach.

Restrictions on element geometry present considerable constructional difficulties in any 3-D analysis. Within such a complex mesh it is difficult to avoid the generation of elements which violate the basic elemental geometric rules. Distorted elements even far removed from the region of immediate interest can lead to the introduction of quite considerable inaccuracies into the results. In addition the vast number of elements and nodes generated in such an extensive analysis would have been prohibitively expensive in terms of computer time. The greatest restriction, however, was that plasticity was not readily available with level 6 of PAFEC for 3-D elements. Due to these limitations a relatively less complex 2-D analysis was undertaken to determine the notch tip stress/strain field.

Initially the state of stress predominating was indeterminate and the analysis was conducted assuming conditions of both plane stress and plane strain. In reality a state of plane stress was likely to prevail at the surface and more closely approximate that of plane strain toward the interior of the specimen.

The FE mesh was constructed using standard eight-noded isoparametric (36210) 2-D plate elements available under the PAFEC system. These elements are very versatile and are capable of accurately modelling a cross element quadratic stress distribution.

In the vicinity of the notch tip, particularly in the case of the V, the stress gradient was likely to be very severe and certainly not quadratic. To closely approximate this rapid local variation of stress it was necessary to use a high density of small elements. Accurate prediction of notch tip stresses and strains was vital since it was assumed a priori that these were most likely to govern the variation of PD observed across the notch during the experimental work. Larger elements were employed moving away from this region where a more uniform distribution of stress was likely to exist. Collectively a total of twelve FE meshes were developed to model the elastic stress distribution around each of the two notch profiles in each of the two materials, EN1A and NE8. In general the ratio of the number of elements in the meshes was in the ratio 3:2:1 and were termed fine, medium and coarse.

Comparison of the results from each of the three elastic analyses revealed no significant differences in predicted stress values at selected critical node locations. Examination of stress continuity demonstrated that not all the meshes were adequate in this respect. The U notch meshes proved excellent with even the coarsest 67 element mesh giving a cross element stress discontinuity < 1.0% for both materials. This allowed the coarse mesh to be employed in the non-linear analysis to help reduce both the complexity of the analysis and necessary computer time. During the non-linear analysis the discontinuity was slightly higher (= <2.6%) but still well within acceptable limits (<10.0%). Results from the elastic analysis of the

V notches revealed several inadequacies in the coarser meshes (= <114 elements) giving a worst case discontinuity of 21.0%. It was therefore necessary to use a very fine mesh in these cases (258 elements, NE8; 186 elements, EN1A) for both the elastic and plastic analyses to reach the required levels of stress continuity, for the elasticity analysis the discontinuity was <3.0% and in the non-linear case ≈2.0%.

Due to the symmetry of the specimen and loading conditions it was only necessary to model one half of the structure. To simulate the action of the "missing" half it was necessary to restrict the movement of the notch centreline nodes accordingly, see figure 5.3. Nodes were located at positions corresponding to the bending rig rollers. Equal and opposite point loads were then applied to these nodes to simulate a four point bending action. Although the rollers were of cylindrical form a point load approximation was considered an accurate loading simulation, being sufficiently far removed from the notch to have negligible effect on the notch tip stress field.

5.3 RESULTS FROM THE ELASTIC ANALYSIS

The elastic analysis formed a necessary first step to the complete non-linear analysis and was vital in ensuring the validity and accuracy of the solution.

For both notch profiles in each of the materials three separate meshes were generated. All twelve meshes were employed during the elastic analysis, though in general only the results for the fine meshes are given in the following sections. Detailed illustrations of mesh geometry and configuration used to compute

the elastic results given in this section can be seen in figures 5.4-5.9. These clearly illustrate the philosophy adopted during mesh generation with a high density of smaller elements surrounding the notch and larger elements moving away from this region. The results from each case provided checks on mesh accuracy and reliability, details of which are given in section 5.6. In addition the elastic analysis also allowed for the calculation of the yield load in each case and the notch tip elastic stress concentration factor.

The elastic stress gradient along the notch centreline has been given in all cases to illustrate the different stress concentration effects of each of the notch profiles and their influence on the overall specimen stress distribution and can be seen in figures 5.10-5.13.

The stress gradient has been expressed in terms of the dimensionless elastic stress concentration factor, K_t, plotted against distance below the notch root. The stress concentration factor has been given as the ratio of the maximum principal stress to a chosen nominal stress. The nominal stress was taken as the largest absolute value of principal stress on the opposite, smooth, side of the specimen to the notch and on the notch centreline. This was chosen to represent the value of stress without the presence of the notch. Strictly speaking a state of multiaxial stress prevailed locally at the notch root with the magnitudes of all the principal stresses being influenced to some degree by the stress raising effects of the notch. However the maximum principal stress dominated the other stress terms and was taken to reflect most realistically the magnitude

of the influence of the notch on the local stress field. The distribution has been given up to 3 mm from the notch root, since at greater distances the distribution became linear, decreasing to a zero value at the neutral axis (approximately on the longitudinal axis of the specimen). In every case the peak value of K_t at the notch root has also been given.

Contours of Von-Mises elastic yield zones can be seen in figures 5.14-5.21. These gave a useful indication to the extent of yielding that could be expected in the non-linear analysis, presenting in effect a lower bound to the extent of plasticity. Brown and Kfouri [29], during crack propagation studies under conditions of plain strain, remarked that the "elastic yield" zone predictions correlated well with those predicted through a complete non-linear analysis. Comparison of the Von-Mises yield zones and plastic zones predicted during this analysis therefore presented a useful check on the validity of their suggestion.

5.4 RESULTS FROM THE PLASTIC ANALYSIS

Following the preliminary elastic analysis it was necessary to predict the post-yield stresses and strains around the notch as the bending load was increased and plastic deformation spreads form the notch tip.

During the non-linear analysis the material stress/strain curve was input into the PAFEC datafiles in a piecewise linear form. Appropriate details of the curves may be seen in figures 5.1, 5.2 and tables 5.1, 5.2.

For the solution of plasticity problems PAFEC adopts the Prandtl-Reuss equations together with the Von-Mises yield criterion. The Prandtl-Reuss equations are based upon increments of strain and correspondingly this dictates that the final load must also be applied in a series of load increments. For every load increment the stresses and strains are calculated via

an iterative technique at the element Gauss points and extrapolated to the nodes. The size of the load increments depends very much on the circumstances of each analysis.

For the U notch profiles, load steps of 5 kN proved adequate but for the V notch profiles smaller steps of only 1 kN were necessary to prevent divergence of the solution. In each of the aluminium alloy NE8 and the mild steel EN1A analyses the final loads applied during the plasticity analysis were different. With the mild steel it was possible to apply a final load of 50 kN and plastic deformation was still predominantly localised around the notch tip. However in the case of the NE8 Aluminium alloy, at loads >37.0 kN, plasticity developed along the upper and lower surfaces of the specimen. At these load levels a situation of general yield was approached and the spread of plasticity could no longer be considered to be determined through notch geometry. Accordingly the final load applied in the case of NE8 was limited to 40 kN. In all cases the initial load increment corresponded to the load causing the onset of yield at the notch root.

During the linear analysis each of the twelve meshes generated provided satisfactory continuity of stress with a mismatch of stress across adjacent element boundaries <10%. However discontinuity was accentuated during the plasticity analysis and in the case of the V notches, particularly the NE8 aluminium alloy, only the finest meshes were sufficiently refined to produce reliable non-linear results. The necessarily fine mesh and small load increments greatly increased the CPU time required for these analyses. As commented upon in section

5.2.2 this prompted the transferral of the job from the IBM 4341 computer to a newly acquired PRIME and job execution via a batch system overnight.

In the case of the U notches the stress gradient was comparatively gentle around the notch allowing the coarsest mesh (67 elements, see figures 5.22 and 5.23) to be adopted with a consequent saving on computer time, a more important consideration than in the elastic analysis.

The plastic stresses and strains given in the results are all expressed in terms of equivalent values. The equivalent stress is given as,

$$\sigma_{eq} = \frac{1}{\sqrt{2}} \cdot \{(\sigma_{xx} - \sigma_{yy})^2 + (\sigma_{zz} - \sigma_{xx})^2 + (\sigma_{yy} - \sigma_{zz})^2 + 6(\sigma_{xy}^2 + \sigma_{yz}^2 + \sigma_{zx})^2\}^{\frac{1}{2}} \qquad 5.1$$

During computation the equivalent strain is divided into elastic and plastic parts, with the elastic parts related to the equivalent stress by Hooke's Law,

$$\varepsilon_{eq\ el} = \frac{\sigma_{eq}}{E} \qquad 5.2$$

and the plastic parts given by the sum of increments of equivalent plastic strain,

$$\delta\varepsilon_{eq\ pl} = \frac{1}{1.5x\sqrt{2}} \cdot \{(\delta\varepsilon_{xxpl} - \delta\varepsilon_{yypl})^2 + (\delta\varepsilon_{zzpl} - \delta\varepsilon_{xxpl})^2 + (\delta\varepsilon_{yypl} - \delta\varepsilon_{zzpl})^2 + 1.5(\delta\varepsilon_{xypl}^2 + \delta\varepsilon_{yzpl}^2 + \delta\varepsilon_{zxpl}^2)\}^{\frac{1}{2}} \qquad 5.3$$

Although more detailed output was available with level 6 of PAFEC the equivalent stress and strain values were considered to be the most suitable single parameter representing the state of stress and deformation at each node. This assumption greatly reduced the complexity of characterising the notch/loading conditions in terms of the individual stress and strain components.

Figures 5.24-5.31 illustrate the spread of plasticity away from the notch as the load was incremented up to the respective maximum load level for each material. The plastic zones in the NE8 aluminium alloy were extensive at a load of 35 kN. Above these load levels plasticity spread even more rapidly and extensively, general yielding, and consequently could not be shown on the diagram.

A more quantitative assessment of the extent of plasticity at each load increment can be seen in figures 5.32-5.39. U and V notch profile results of each material are given together to allow easy comparison.

Important parameters governing ACPD response were thought likely to be the values of stress and strain at the notch root. It has been suggested previously, see Bozorth [6], that elastic and plastic strain have different effects on ACPD response and correspondingly equivalent notch tip elastic and plastic strains have been plotted separately. The variation of these parameters with increasing load can be seen in figures 5.40-5.47. An extension to the notch tip characterisation can be seen in figures 5.48-5.71. Here the notch tip elastic strain, plastic strain and stress gradients have been plotted

along the notch centreline at representative load levels.

5.5 DISCUSSION OF THE RESULTS

The elastic stress gradients given in figures 5.10-5.13 confirmed the expected stress concentration effects of the two differing notch profiles. In either material the V notch had a much higher Kt value at the notch root (5.4 EN1A; 6.7 NE8) than the U profiles (2.6 for both materials). The difference in V notch values suggested that the difference in notch root radii did have an appreciable effect on the notch root stress field. In all cases the peak elastic stress and hence strain occurred at the notch root and increased in proportion to the applied load up to yield. Below the notch the distribution of stress became linear at between 1.2 mm and 1.5 mm along the notch centreline in all cases.

Comparison of the Von-Mises yield zone estimates from the elastic analysis, figures 5.14-5.21, and the plastic zones predicted via the plastic analysis, figures 5.24-5.31, showed striking similarities. Best agreement was found under conditions of plane strain, a point which tended to confirm the proposals of Brown et al mentioned in section 5.3. There were however several slight differences common in all cases. The elastic analysis produced a conservative estimate of plastic zone size, with yielding extending less rapidly below the notch in comparison with the predictions of the non-linear analysis.

Contrasting the plastic results for the U and V notch profiles, figures 5.24-5.31, revealed several characteristics common to both materials. Plasticity spread far more extensively

along the surface of the U notch (1.0 - 1.5 mm) than in the V notches (< 0.5 mm). In both cases the spread of plasticity along the notch surface attained a steady value soon after yield with a gradual increase below the notch.

The variation of stress and strain at the notch tip for EN1A is given in figures 5.40-5.43. The notch tip stress reached a peak value corresponding to roughly that of the yield stress, 256 MPa, at loads of 8 kN and 16 kN for the V and U notch profiles respectively. This value and hence the elastic strain then remained constant (1500 $\mu\varepsilon$) as the load was increased. The plastic strain at the notch root increased rapidly after yield and continued to do so with increasing load. The resultant plastic strains at final load dominated the corresponding elastic strain at the notch root. This was accentuated with the V profiles where the plastic strain was three times that of the U notch but with roughly equal elastic strain levels.

Figures 5.40-5.43 also reveal that the stresses and elastic strains remained constant, once the yield values had been reached, throughout the plastic zone. Ahead of the plastic zone there was however an appreciable stress and elastic strain gradient with the greatest value at the elastic/plastic interface. The plastic strain was not constant however, but with a considerable plastic strain gradient across the whole plastic zone and the peak value at the notch root.

As expected the behaviour of the aluminium alloy NE8 was quite dissimilar to that of the mild steel EN1A in many respects. Unlike the EN1A the notch stress did not reach a constant

value after yield but continued to increase, figures 5.44-5.47. This trend was also reflected in the elastic strain. Similarly with the stress and elastic strain gradients away from the notch. Both the stress and elastic strain showed a considerable variation across the plastic zone at all load levels, figures 5.60-5.71. The plastic strain, represented in the total strain, behaved as in the case of the mild steel EN1A. The notch root value increased continuously after yield with a rapid decrease directly below the notch root.

In general the levels of stress, elastic strain and plastic strain were considerably higher in the aluminium alloy NE8 with in particular intense plastic strain at the notch root at higher load levels. A similar trend could also be seen between the two different notch profiles.

5.6 CHECKS ON THE ANALYSIS

An assessment of the errors involved in the solution obtained from a finite element analysis is in most instances an extremely difficult task. The most simple estimate of the errors involved in the numerical solution would be a straightforward comparison with existing analytical and experimental solutions. Usually, however a FE analysis would not be undertaken in the first instance if such solutions existed, hence this is not often a viable approach. It was therefore necessary to adopt a different approach in the validation of the solution.

Since no absolute checks exist on solution accuracy a number of precautions were taken to greatly increase confidence in the numerical solution obtained. These can be roughly divided

into two groups dealing with separate aspects of the analysis and solution.

(1) Suitability of the Mesh

This aspect is concerned with considering the influence of changes in FE mesh configuration, density and size of elements. These in their turn influence the continuity of stress across adjacent element boundaries and also convergence of the solution in the case of non-linear analyses.

(2) Modelling of Physical Conditions

This aspect considers the application of loads, pressures, restraints etc to the FE model and how closely the real physical situation is being modelled. For instance the use of point loads in the FE model is not the same as a real load bearing roller, however if the region of interest is sufficiently far from the position of loading then this is a reasonable approximation.

Both (1) and (2) need to be considered in the validation of any FE solution. In the present study checks were conducted throughout the analysis to reduce the risk of accumulative errors in the solution. Errors introduced at an early stage into the computation would tend to produce ever more inaccurate results. Consideration of (i) and (ii) and their application to the present study are given below. This is also hoped to provide a guide to validation of other FE analyses.

(i) Suitability of the Mesh

(ii) Convergence of the Solution

The finite element approach is a numerical approximation to the real structure and loading conditions. The structure is modelled as a discrete series of elements of somewhat arbitrary size and distribution. Since the finite element method may be considered a numerical procedure for extremising a given functional the FE solution will tend to converge to the true value with increasing fineness of mesh subdivision. It should therefore be possible to use several meshes containing different numbers of elements and compare the solutions. If by comparison it was found that the results from the coarser meshes were very close to those of the finer meshes then it could have been concluded that the number of elements was sufficient and both models had converged close to the true solution. On the other hand if quite different answers were obtained then further computer runs would have been necessary with meshes of finer subdivision to ensure convergence of the solution.

In the present study there were, in total, eight different elastic analyses. Each analysis being undertaken with at least three separate meshes of differing degrees of fineness.

Following completion, results from each were contrasted to determine which of the meshes were satisfactory. The results are plotted in figures 5.72-5.79 for each of the separate elastic analyses. The maximum principal stress, σ_1, has been plotted against increasing number of elements.
N.B. Implicit with increasing number of elements is the reduction in size of element in the critical region of the notch tip.

The terms "nominal" and "peak" have been used for particular values of stress. The "nominal" value was taken as that defined previously in section 5.3 and the "peak" value as the value of the maximum principal stress at the notch root. The values of stress have been given for an applied bending load of 1 kN.

As can be seen from all the plots there was a slight variation with the coarser (81, 92 element) meshes in the case of the V notches. Although even in these cases the discrepancy was minimal. Hence during the analysis of the V notches only the finer (187, 250 element) meshes were used to ensure the reliability of the solution. There was very little variation with increasing number of elements in the case of the U notches and therefore any of the meshes would have given satisfactory answers.

The comparison of the solutions has only been undertaken for the elastic analyses, but it was reasonable to extend any conclusions to the case of the plastic analysis.

As a summary it was found that all the meshes were sufficiently refined to give reasonable results. However in the case of the V notches the slight discrepancy in results suggested it was prudent to only use the finer meshes to ensure convergence of the solution and hence the validity of the results.

(ii) Continuity of Stress

A very important aspect when considering the suitability of any FE mesh is the continuity of stress across the boundaries of adjacent elements. The continuity (or discontinuity) reflects the ability of the mesh to accurately model the true stress

distribution in the structure. The eight-noded isoparametric (36210) elements used throughout the present analysis are designed with a quadratic cross element stress distribution. To model more complex distributions smaller sized and greater numbers of elements need to be used. By investigation of the magnitude of the discontinuity of stress across elements it is possible to quantify how well the true stress distribution has been approximated (see figure 5.80).

As a guide, if the discontinuity of stress was > = 10% then the stress values in that region could not be relied upon to be very accurate. This aspect is discussed in further detail in section 5.2.3 of this chapter. The stress continuity for all the meshes proved to be well within the acceptable limits with, at most, a 3.0% mismatch of stress across adjacent elements. Hence it could be concluded that the FE models used were sufficiently refined to model the true stress distribution within the notched bend specimen to well above the acceptable limits of accuracy.

(2) Modelling of the Physical Conditions - Elastic Stresses

Often no exact analytic solution exists with which to compare the stresses predicted by the numerical FE solution. However, simplifying assumptions can usually be applied to the structure and loading conditions and straightforward analytic calculations be made to provide a check on the magnitude of the stresses likely to be expected.

As an example consider the case of the U notched EN1A specimen in plane stress bending.

From the elastic FE analysis using the 186 element mesh the stresses at the notch root node (node number 2) and its opposite counterpart on the smooth side of the specimen (node number 35) were as follows:

Node No. 2	Node No. 35
σ_1 = 31.0 MPa	σ_1 = -0.029 MPa
σ_2 = 0.171 MPa	σ_2 = -11.82 MPa

The negative values at Node no. 35 indicating, correctly, that this node was under compression.

At both nodes the stress distribution was very nearly uniaxial as expected.

N.B. In the case of the V notches the stress state at the notch root exhibited a slight degree of biaxiality due to the influence of the notch.

Consider the stresses predicted at node no. 35. This was situated on the smooth side of the specimen and may be considered sufficiently remote from the notch as to have been little influenced by its presence. Essentially the state of stress at this node could be considered the same as that in the outer "fibres" of a smooth beam, with the same nominal dimensions, subject to pure bending.

The depth, d, of the beam may be taken as either the distance from the notch root to the smooth side of the specimen, d' = 25.5 mm, or the nominal depth of the unnotched specimen, d" = 30.0 mm. These two values

should provide upper and lower bounds respectively to the predicted stress values.

From simple bending theory,

$$\frac{\sigma}{y} = \frac{M}{I} \qquad 5.4$$

and in the case of a rectangular beam of uniform cross-section,

$$I = \frac{bd^3}{12} \qquad 5.5$$

where, M = Applied Bending Moment

I = Second Moment of Area

y = Distance from Neutral Axis

σ = Stress at Distance y

b = Breadth of Beam

d = Depth of Beam

Combining equations 5.4 and 5.5 gives,

$$\frac{\sigma}{y} = \frac{M}{(bd^3/12)}$$

Hence,

$$\sigma = \frac{12My}{bd^3} \qquad 5.6$$

Now at the outer "fibres" of the beam, y = d/2.

Hence,

$$\sigma = \frac{12(d/2)}{bd^3} \qquad 5.7$$

$$\sigma = \frac{6M}{bd^2}$$

The breadth, b, of the beam is 15.0 mm.

Considering, for an applied load of 1 kN, the bending moment, M, at the point of interest, $M = 20 \times 10^3$ Nmm. Hence for thicknesses d' and d" the estimates of stress are,

$$\sigma' = \frac{6 \times 20 \times 10^3}{15 \times (25.5)^2}$$

$$= 12.30 \text{ MPa} \qquad 5.8$$

$$\sigma'' = \frac{6 \times 20 \times 10^3}{15 \times (30)^2}$$

$$= 8.89 \text{ MPa} \qquad 5.9$$

Clearly the value of stress of 11.82 MPa predicted from the FE analysis agrees very well with the two predictions given by 5.8 and 5.9, lying between the two analytical estimates.

σ' and σ'' are independent of material properties and strictly speaking only apply in cases of plane stress. However the two estimates above agree favourably compared with any of the predicted values of maximum principal stress, even under plane strain conditions, from any of the FE predictions.

These results confirm the validity of the FE models and simulation of loading conditions.

(ii) Structural Displacements

With similar simplifying assumptions to the geometry of the bend specimen it is also possible to check the elastic displacements due to bending.

Considering the beam to be smooth and of uniform cross-section, a simple relationship between the applied bending moment, M, and the geometry of deformation exists.

$$\frac{M}{I} = \frac{E}{R_{\alpha}} \qquad 5.10$$

where, M = Applied Bending Moment

I = Second Moment of Area

E = Young's Modulus of Material

R_{α}= Radius of Curvature of Deformed Beam

Now, combining equations 5.5 and 5.11,

$$\frac{M}{(bd^3/12)} = \frac{E}{R_{\alpha}}$$

$$R_{\alpha} = \frac{E}{M} \cdot \frac{bd^3}{12} \qquad 5.11$$

Considering the case of the U notched EN1A bar under plane stress bending as a representative example, where E for this material is 209 x 10^3 MPa.

Again two values of d seem appropriate to form bounds on the solution, d' = 25.5 mm and d'' = 30.0 mm.

Consider figure 5.85 showing the elastically deformed beam having radius of curvature $R_{\alpha}$and vertical deflection α. Node number 35 (N35) was the node directly below the notch root on the smooth side of the specimen and node number 44 (N44) corresponded to the position of the loading rollers.

The vertical displacement between nodes 35 and 44 predicted from the elastic FE analysis for an applied load of 1 kN was 2.5196 x 10^{-3}mm. This should therefore correspond to the distance α predicted from simple bending theory.

Now,

$$R_{\alpha}^2 = (R_{\alpha} - \alpha)^2 + (L/2)^2 \qquad 5.12$$

Hence, rearranging,

$$\alpha = R_{\alpha} - \{R_{\alpha}^2 - (L/2)^2\}^{\frac{1}{2}} \qquad 5.13$$

Also, $R_{\alpha} = \frac{E}{M} \cdot \frac{bd^3}{12}$ 5.14

Using the two estimates of d, d' = 25.5 mm and d'' = 30.0 mm,

$$R'_{\alpha} = \frac{209 \times 10^3 \times 15 \times (25.5)^3}{20 \times 10^3 \times 12}$$

$$= 216\ 594.21 \text{ mm} \qquad 5.15$$

$$R''_{\alpha} = \frac{209 \times 10^3 \times 15 \times (30.0)^3}{20 \times 10^3 \times 12}$$

$$= 352\ 687.50 \text{ mm} \qquad 5.16$$

Since (L/2) = 40.0 mm,

$$\alpha' = 216\ 594.21 - \{(216\ 594.21)^2 - (40)^2\}^{\frac{1}{2}}$$

$$= 3.8 \times 10^{-3} \text{ mm} \qquad 5.17$$

$$\alpha'' = 352\ 687.50 - \{(352\ 687.50)^2 - (40)^2\}^{\frac{1}{2}}$$

$$= 2.4 \times 10^{-3} \text{ mm} \qquad 5.18$$

Again it can be seen that the FE prediction of 2.5196×10^{-3} mm falls between the two analytical predictions given by 5.17 and 5.18. Similar results were obtained from all the elastic FE analyses further confirming the validity of the FE model.

Co-ordinate Number	Stress (MPa)	Strain (-)
1	254	0.0012153
2	262	0.0214
3	291	0.0298
4	332	0.0496
5	359	0.068
6	379	0.092

Stress/strain co-ordinates for elastic/plastic FE analysis of EN1A

Table 5.1

Co-ordinate Number	Stress (MPa)	Strain (-)
1	163	0.0028
2	212	0.0132
3	295	0.0460

Stress/strain co-ordinates for elastic/plastic FE analysis of NE8

Table 5.2

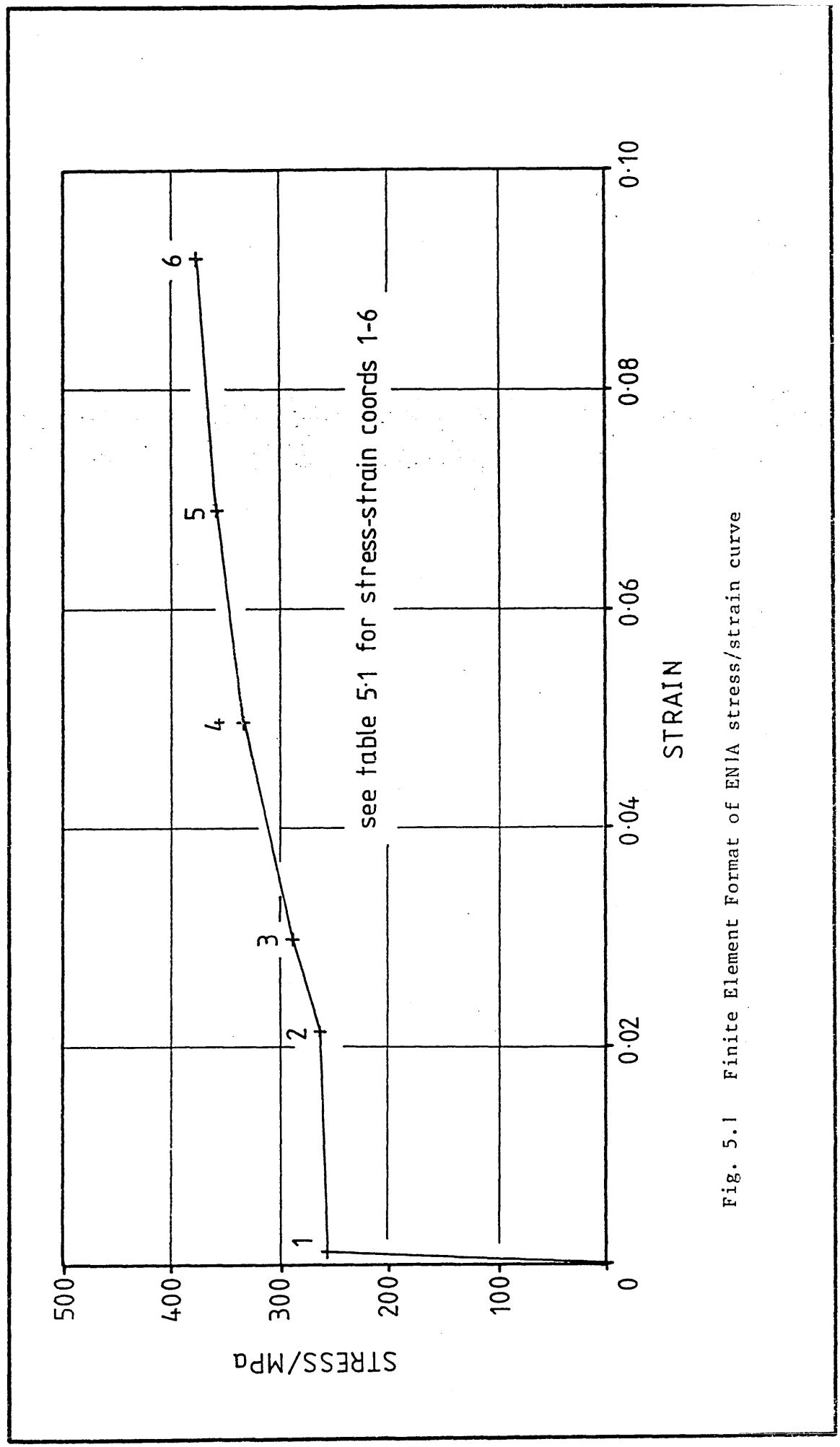

Fig. 5.1 Finite Element Format of EN1A stress/strain curve

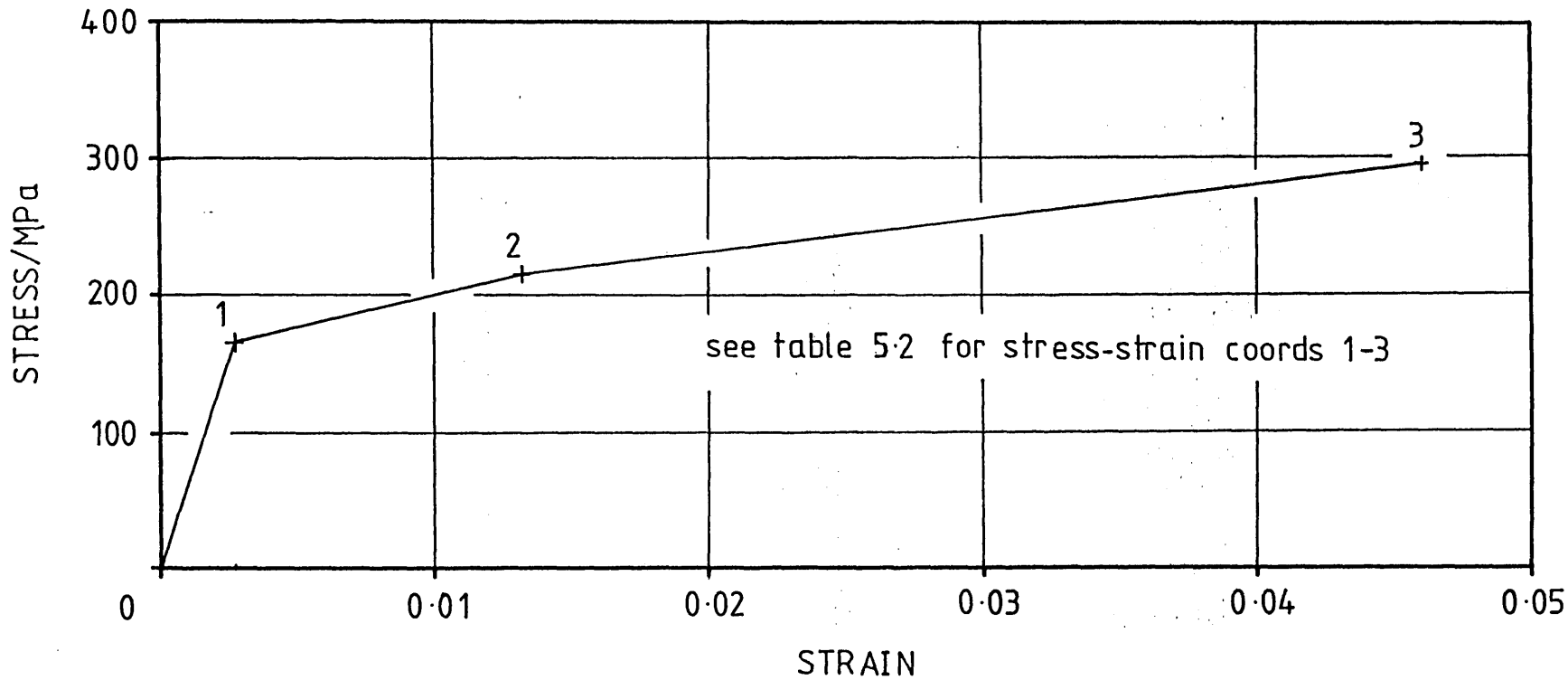

Fig. 5.2 Finite Element Format of NE8 stress/strain curve

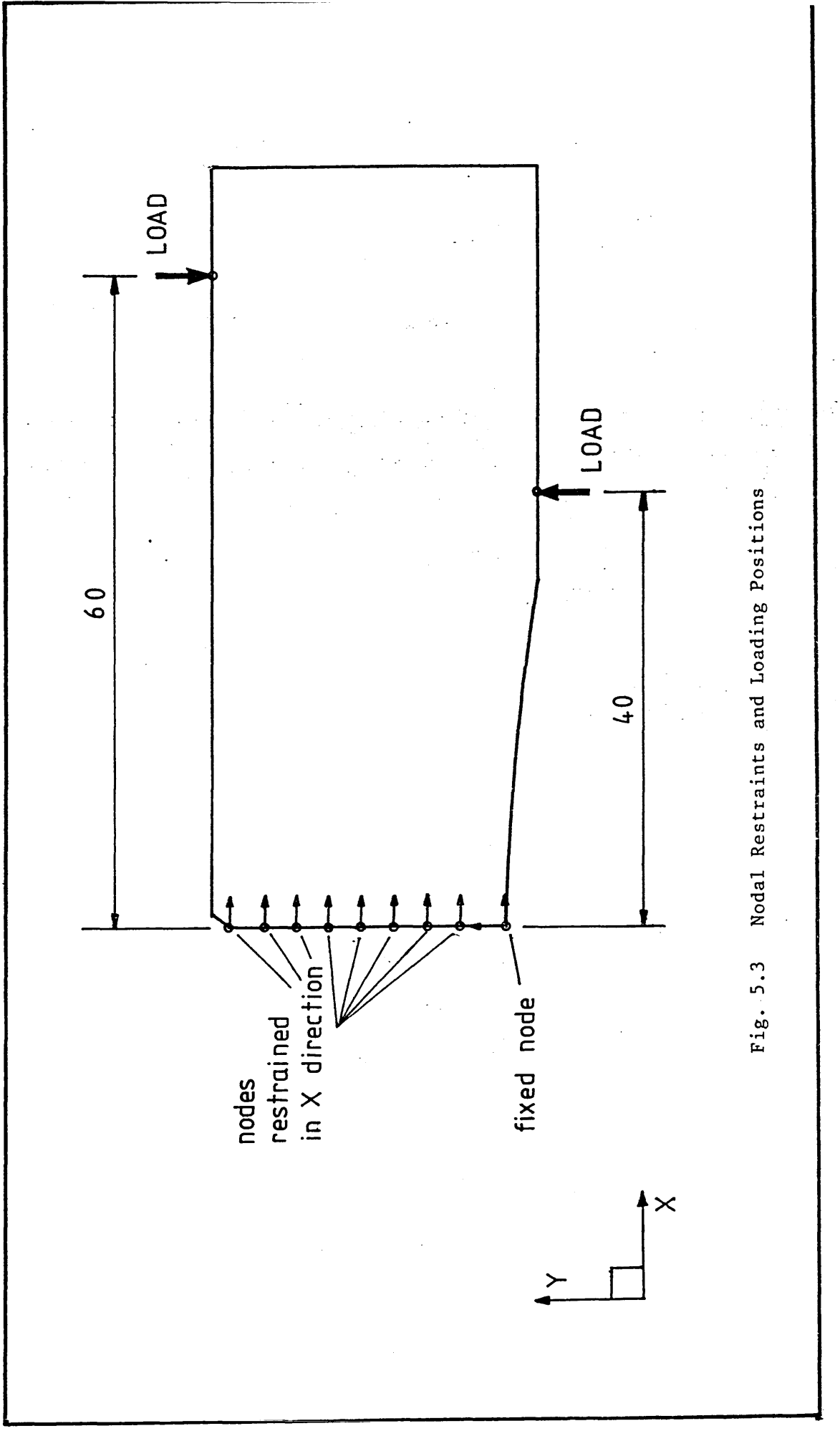

Fig. 5.3 Nodal Restraints and Loading Positions

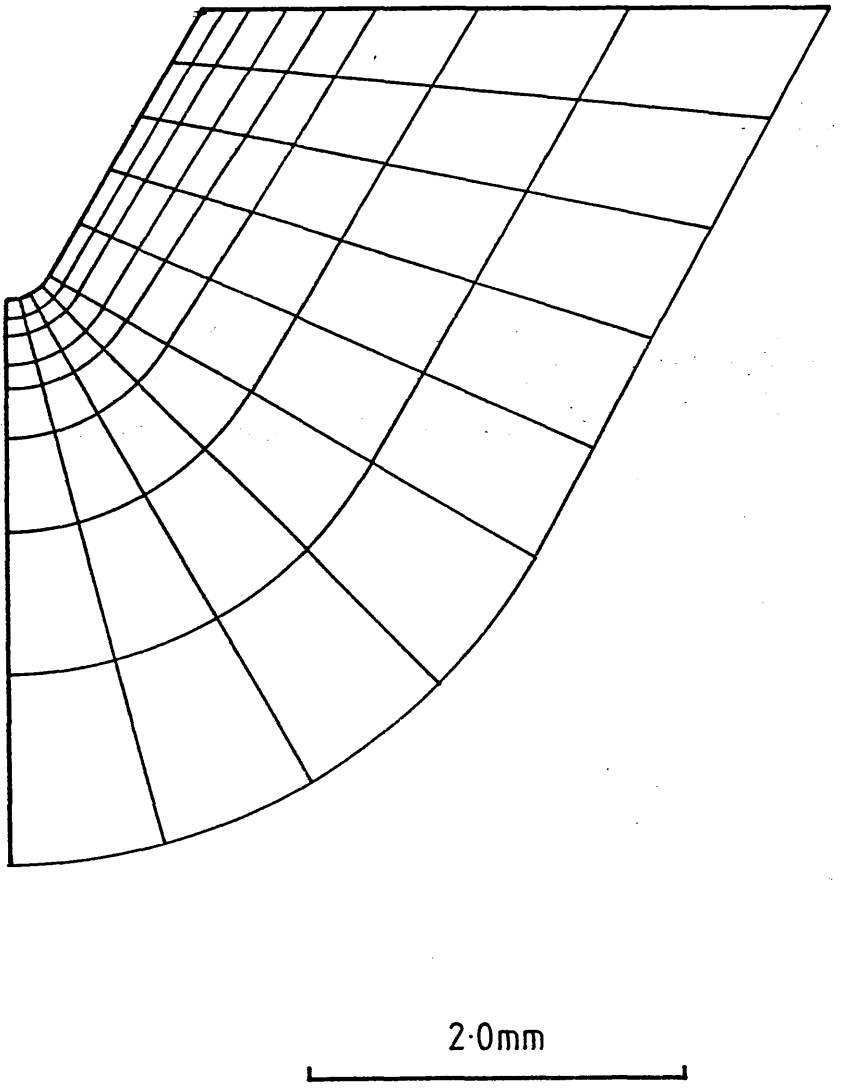

Fig. 5.4 Mesh Configuration for Elastic and Plastic FE Analysis of V Notch EN1A-Notch Root Details

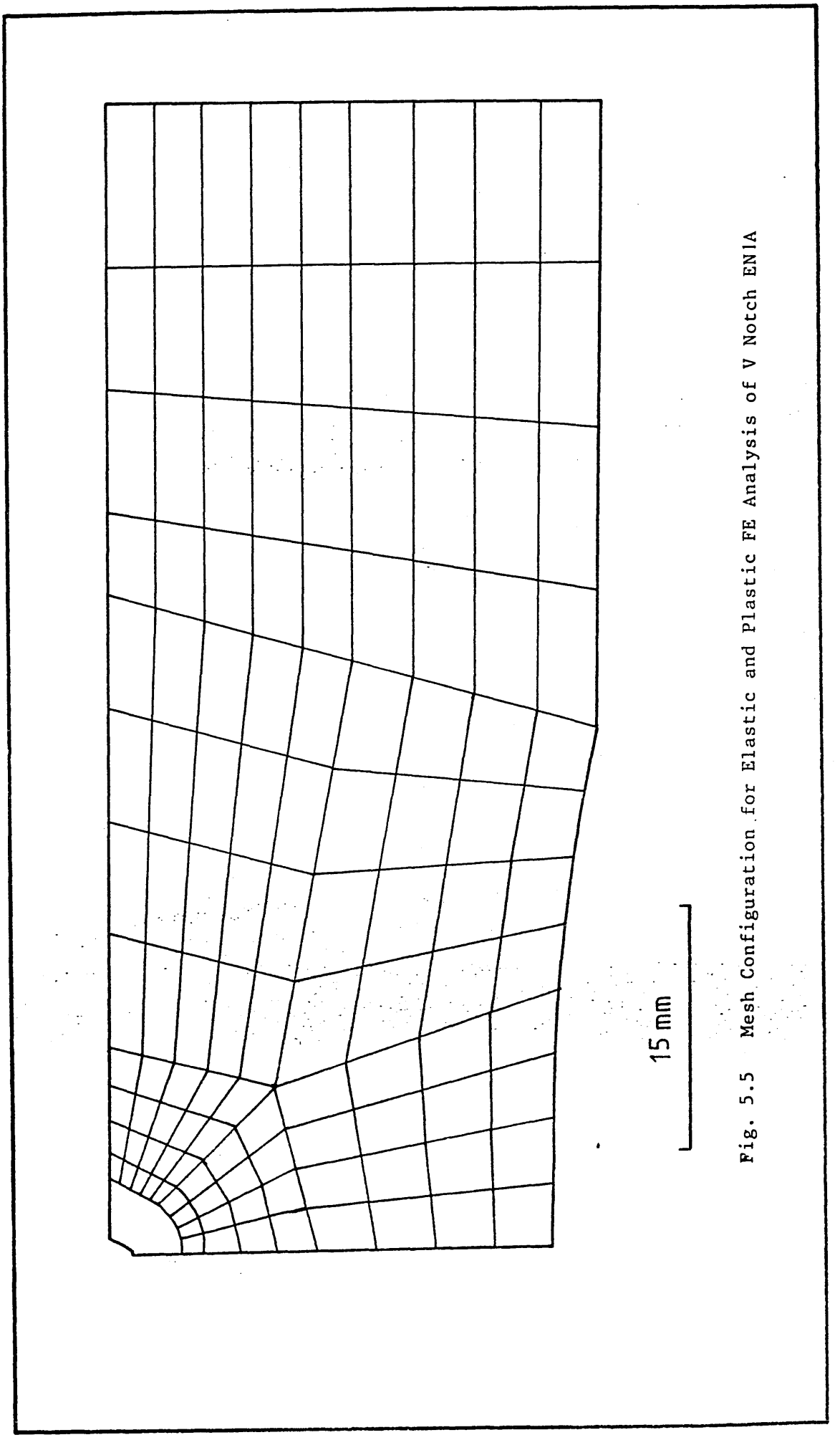

Fig. 5.5 Mesh Configuration for Elastic and Plastic FE Analysis of V Notch EN1A

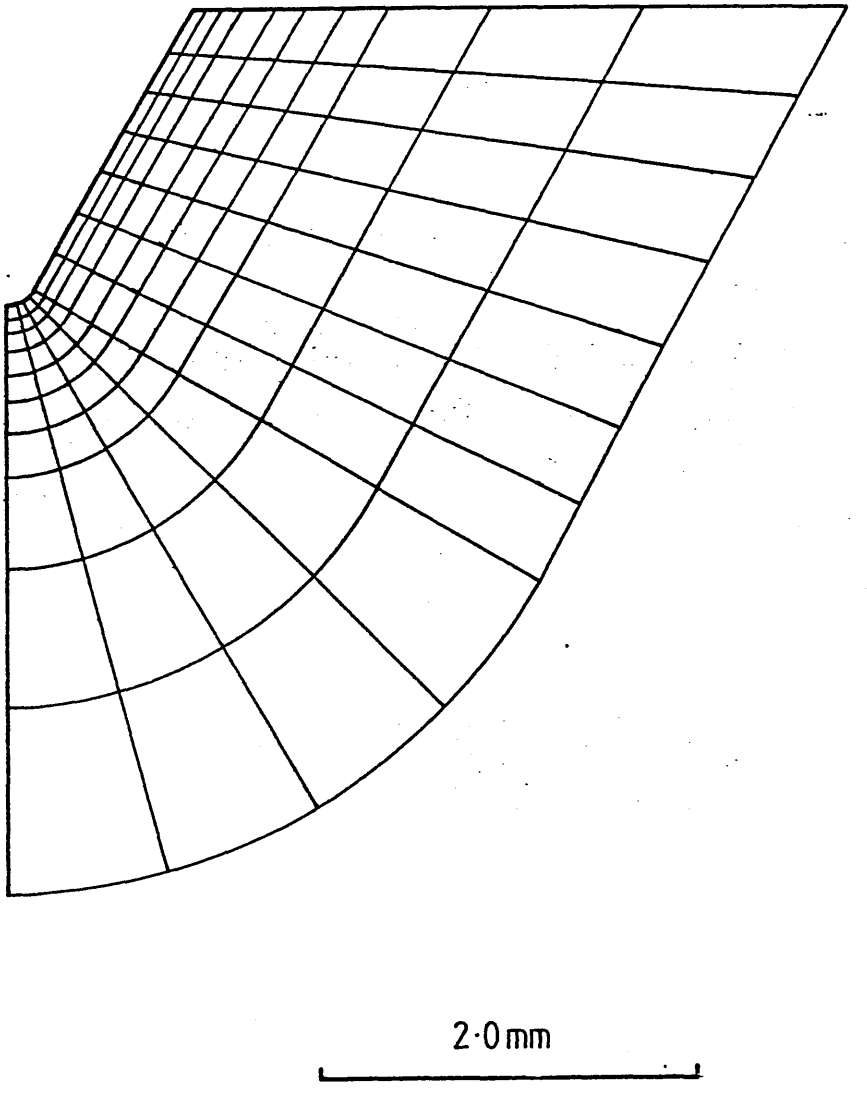

Fig. 5.6 Mesh Configuration for Elastic and Plastic FE Analysis of V Notch NE8 - Notch Root Details

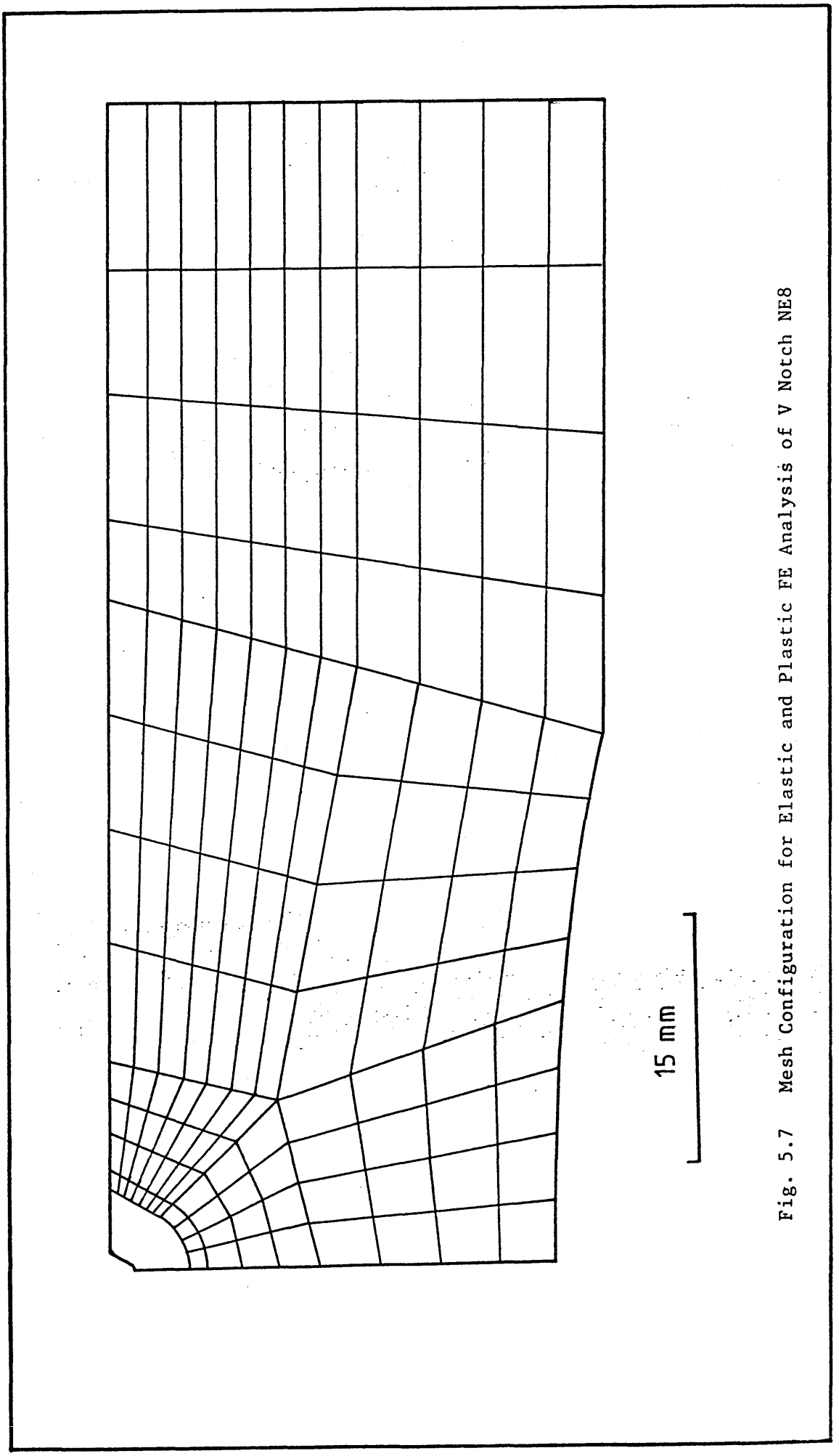

Fig. 5.7 Mesh Configuration for Elastic and Plastic FE Analysis of V Notch NE8

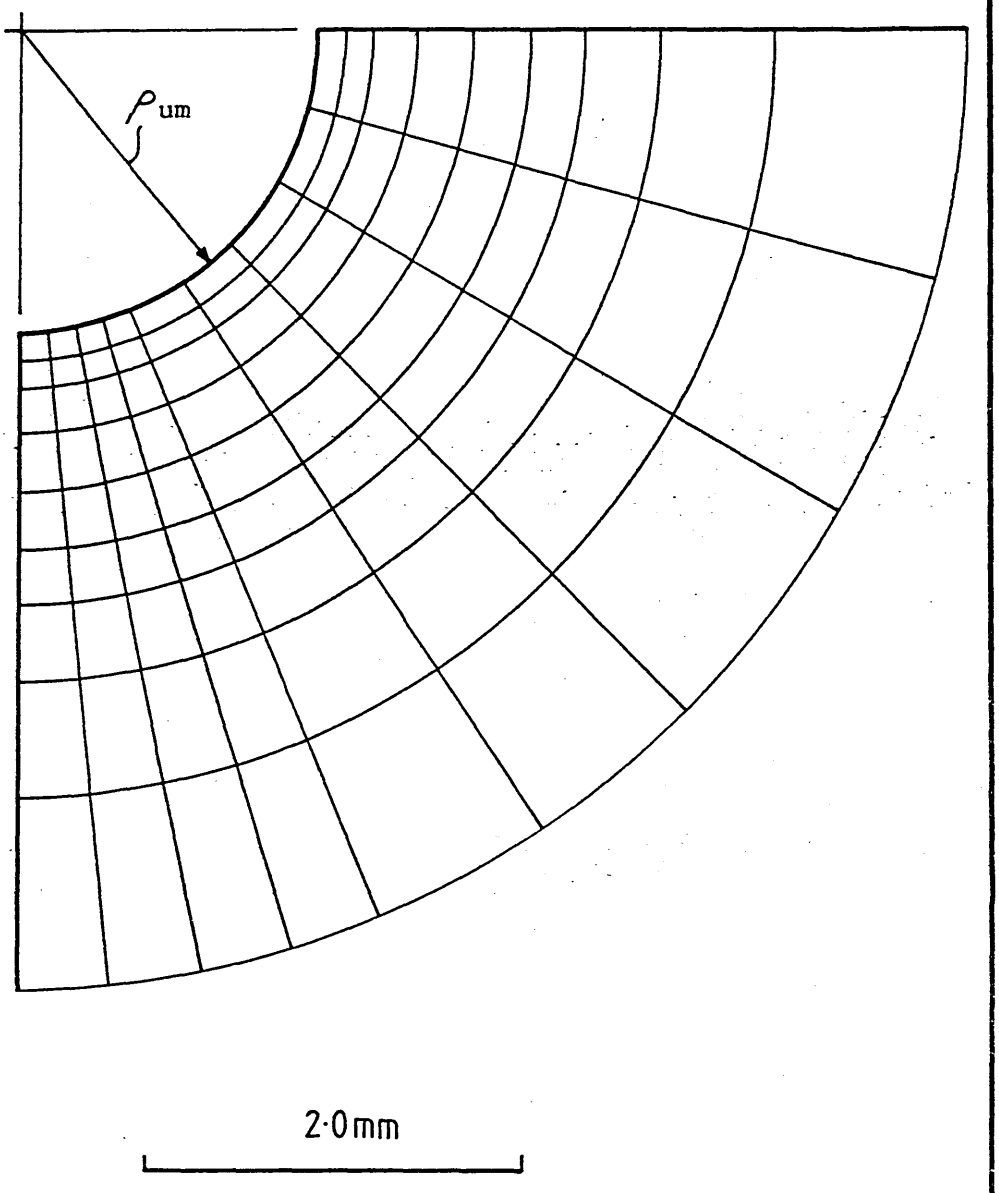

Fig. 5.8 Mesh Configuration for Elastic Finite Element Analysis of U Notch EN1A and NE8 - Notch Root Details

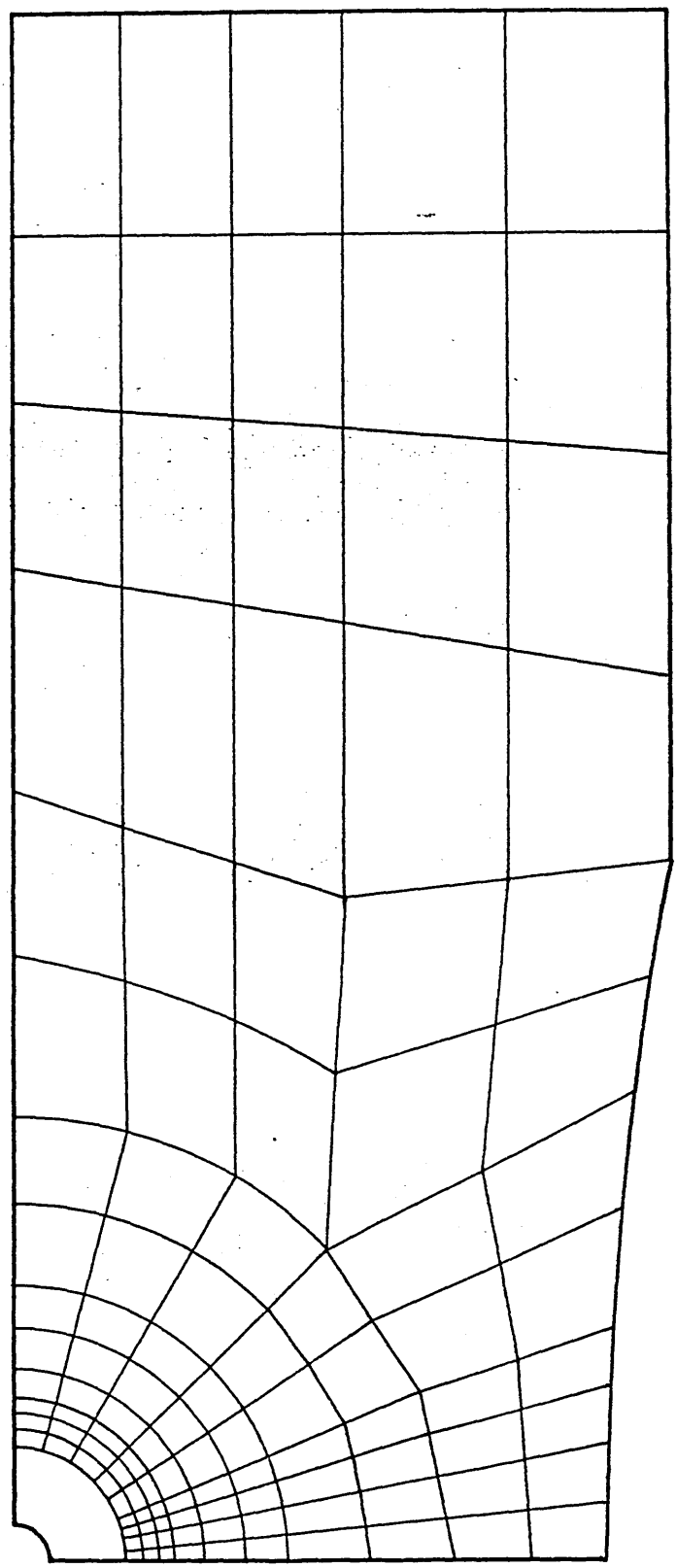

Fig. 5.9 Mesh Configuration for Elastic FE Analysis of U Notch EN1A and NE8

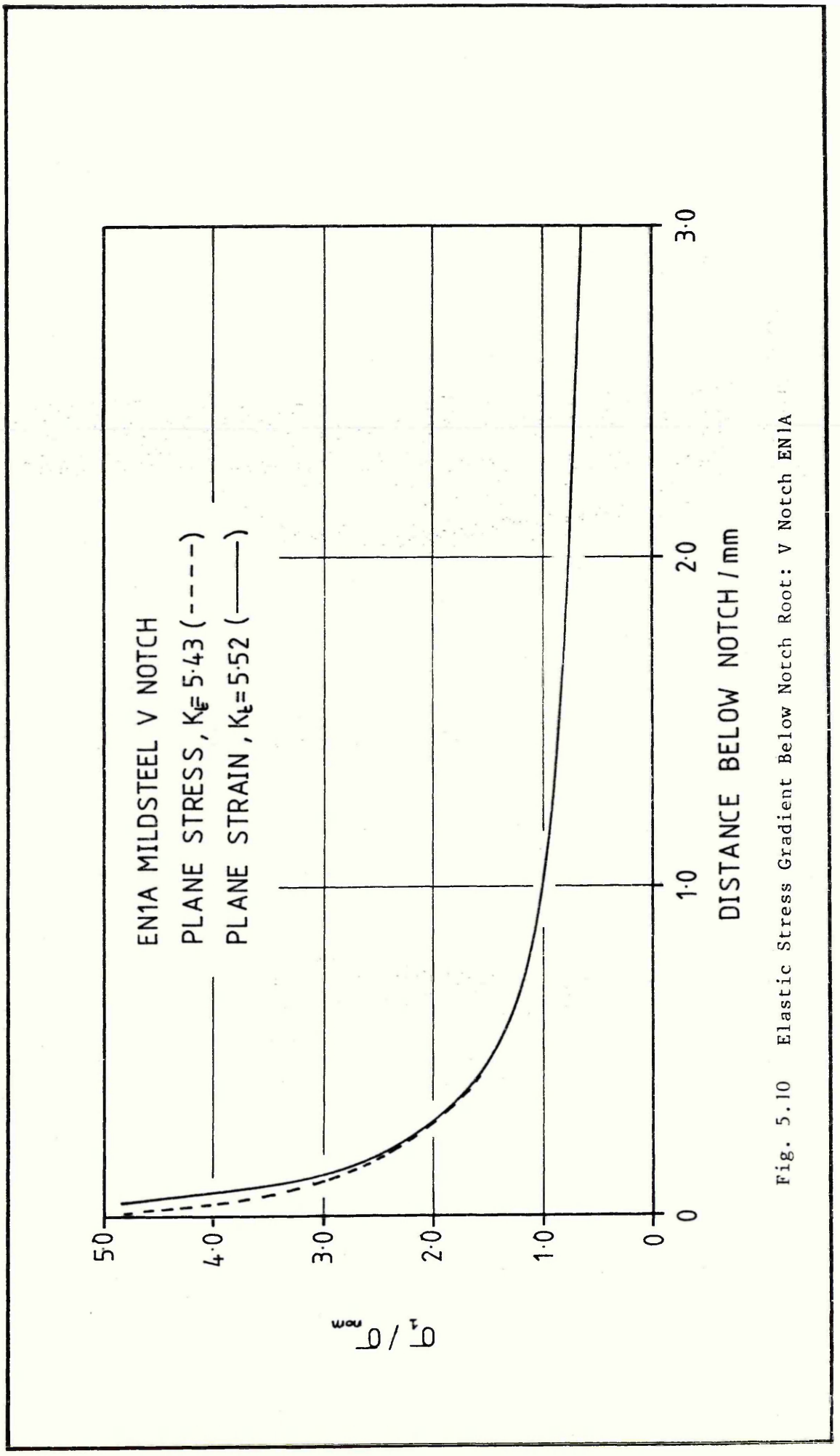

Fig. 5.10 Elastic Stress Gradient Below Notch Root: V Notch EN1A

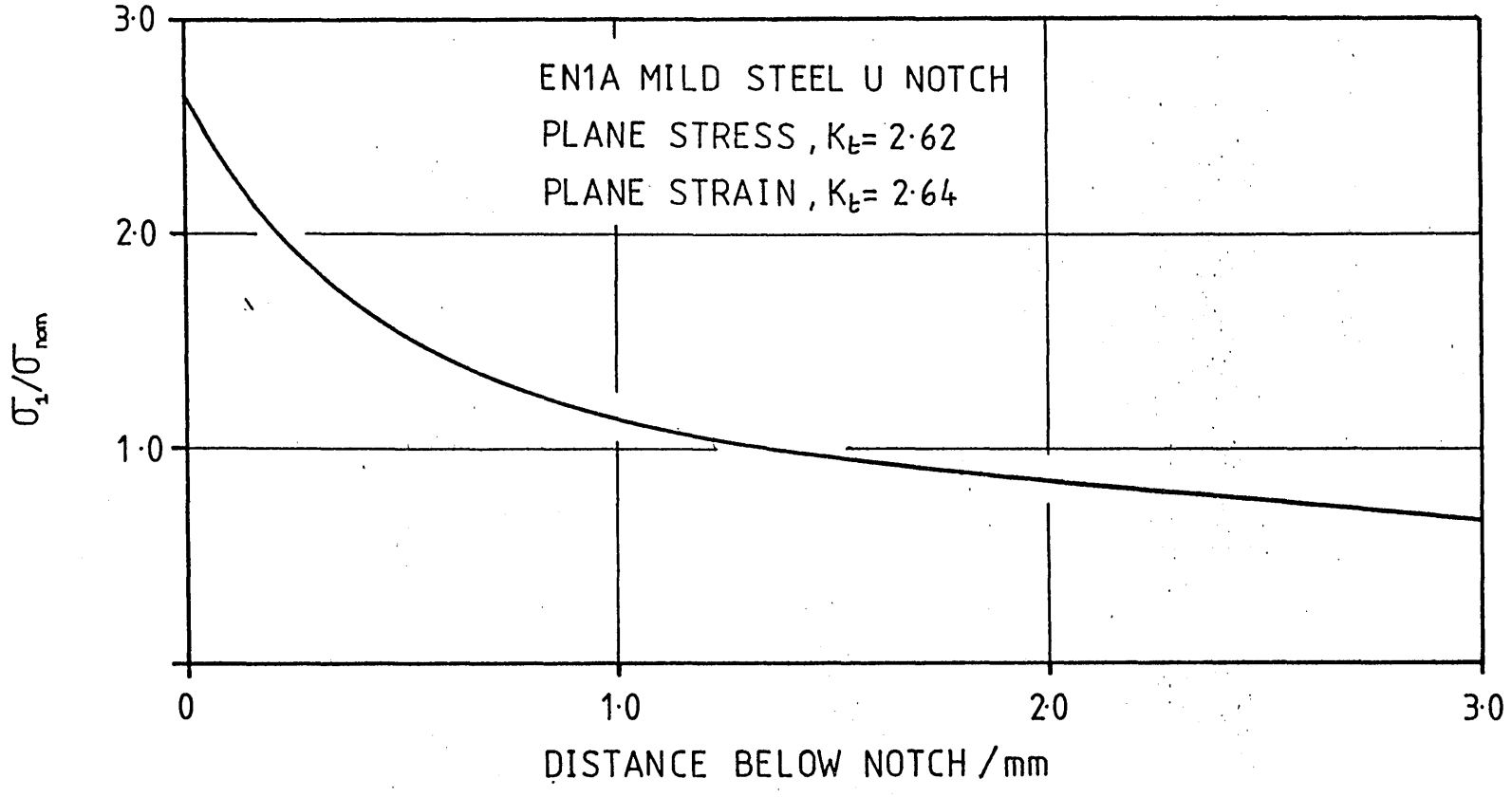

Fig. 5.11 Elastic Stress Gradient Below Notch Root: U Notch EN1A

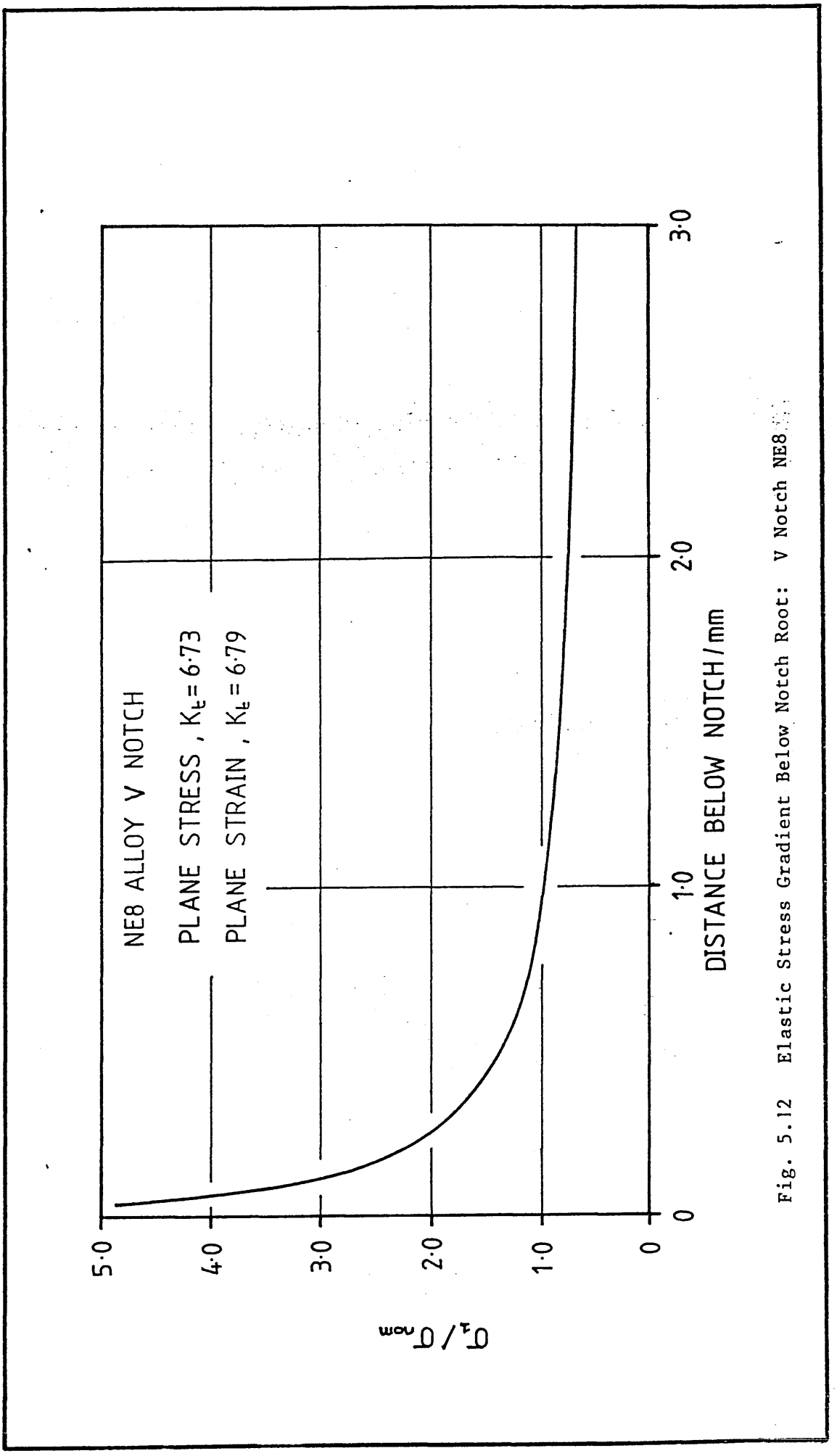

Fig. 5.12 Elastic Stress Gradient Below Notch Root: V Notch NE8

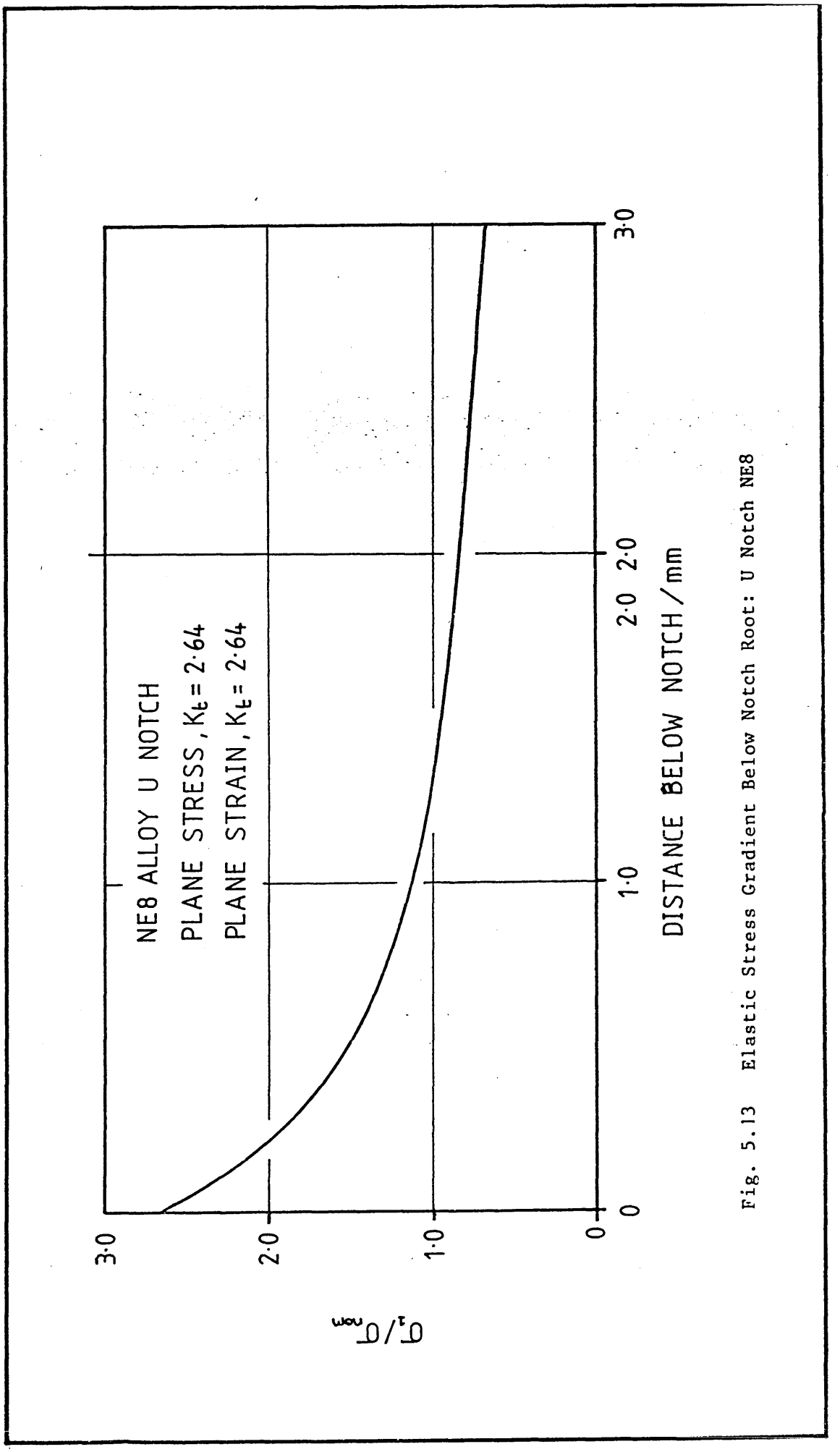

Fig. 5.13 Elastic Stress Gradient Below Notch Root: U Notch NE8

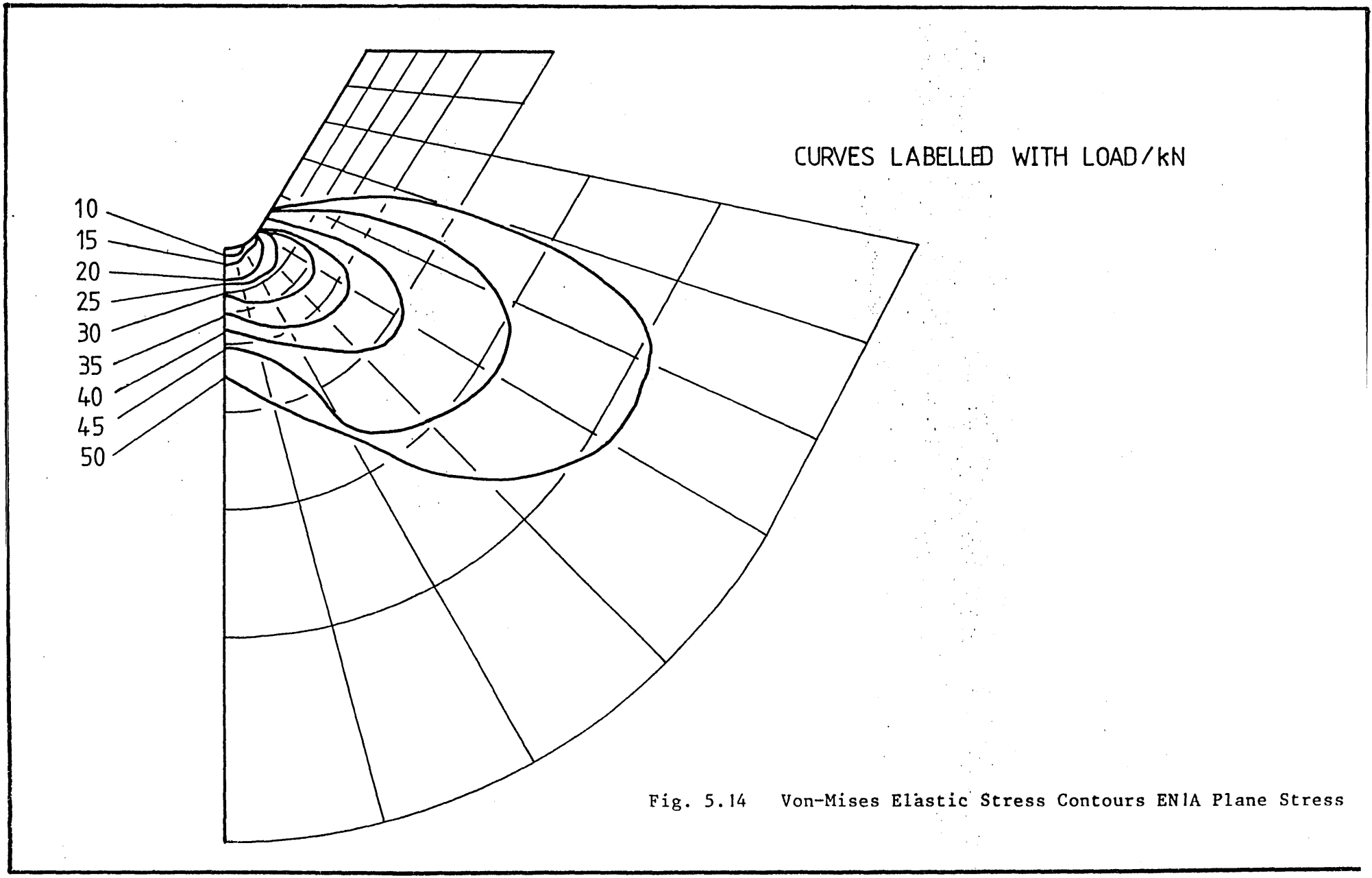

Fig. 5.14 Von-Mises Elastic Stress Contours EN1A Plane Stress

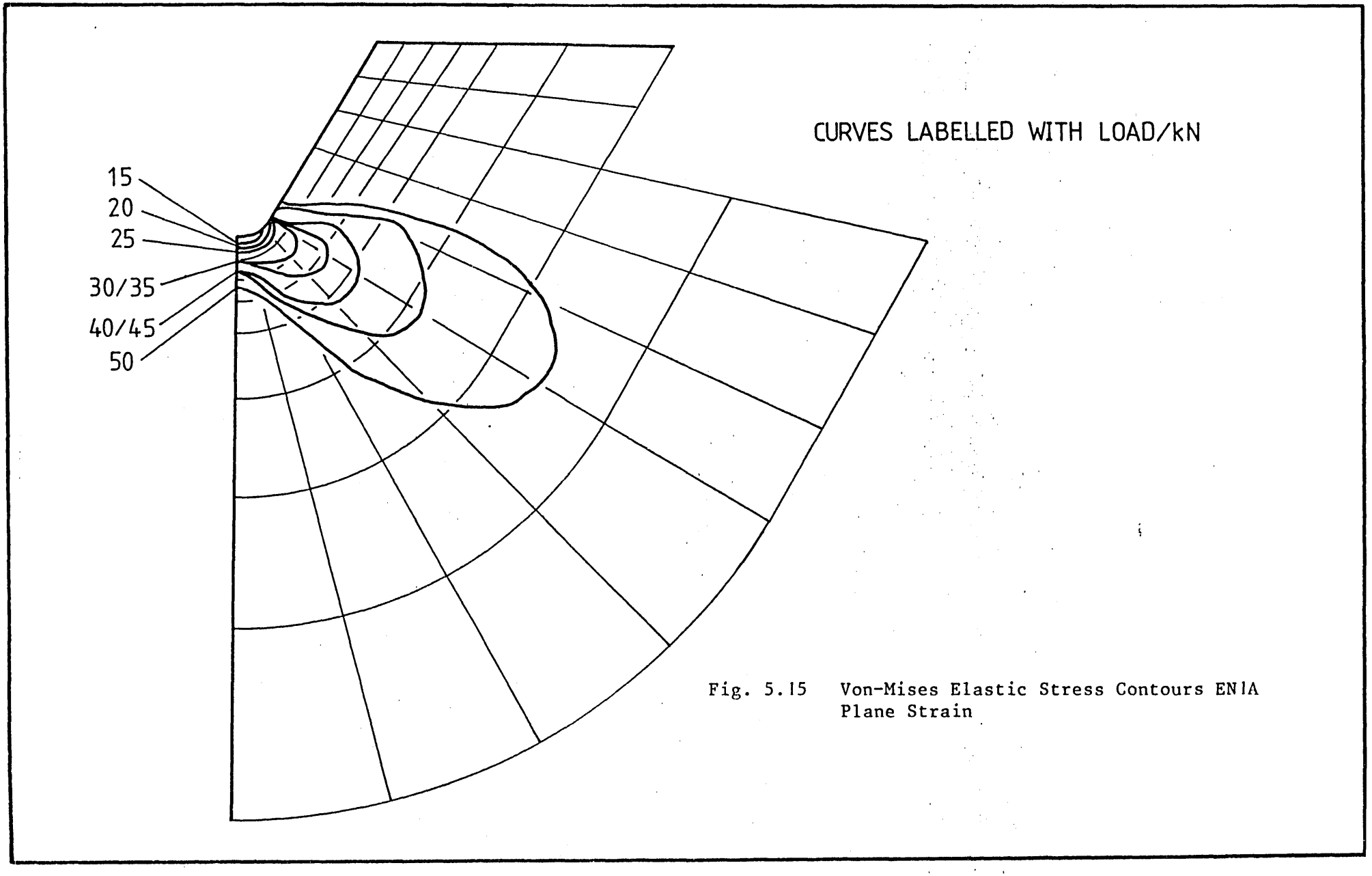

Fig. 5.15 Von-Mises Elastic Stress Contours EN1A Plane Strain

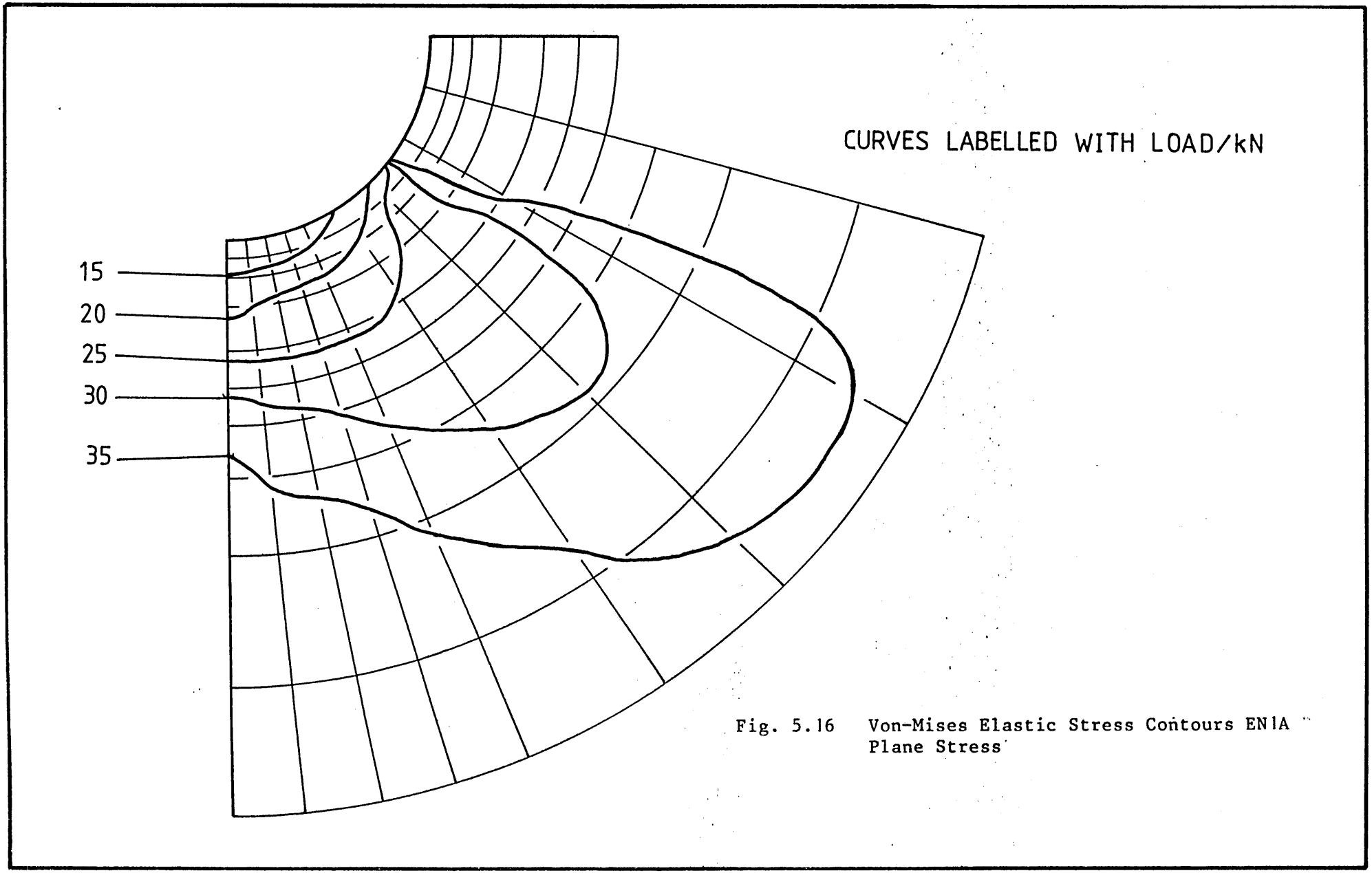

Fig. 5.16 Von-Mises Elastic Stress Contours EN1A Plane Stress

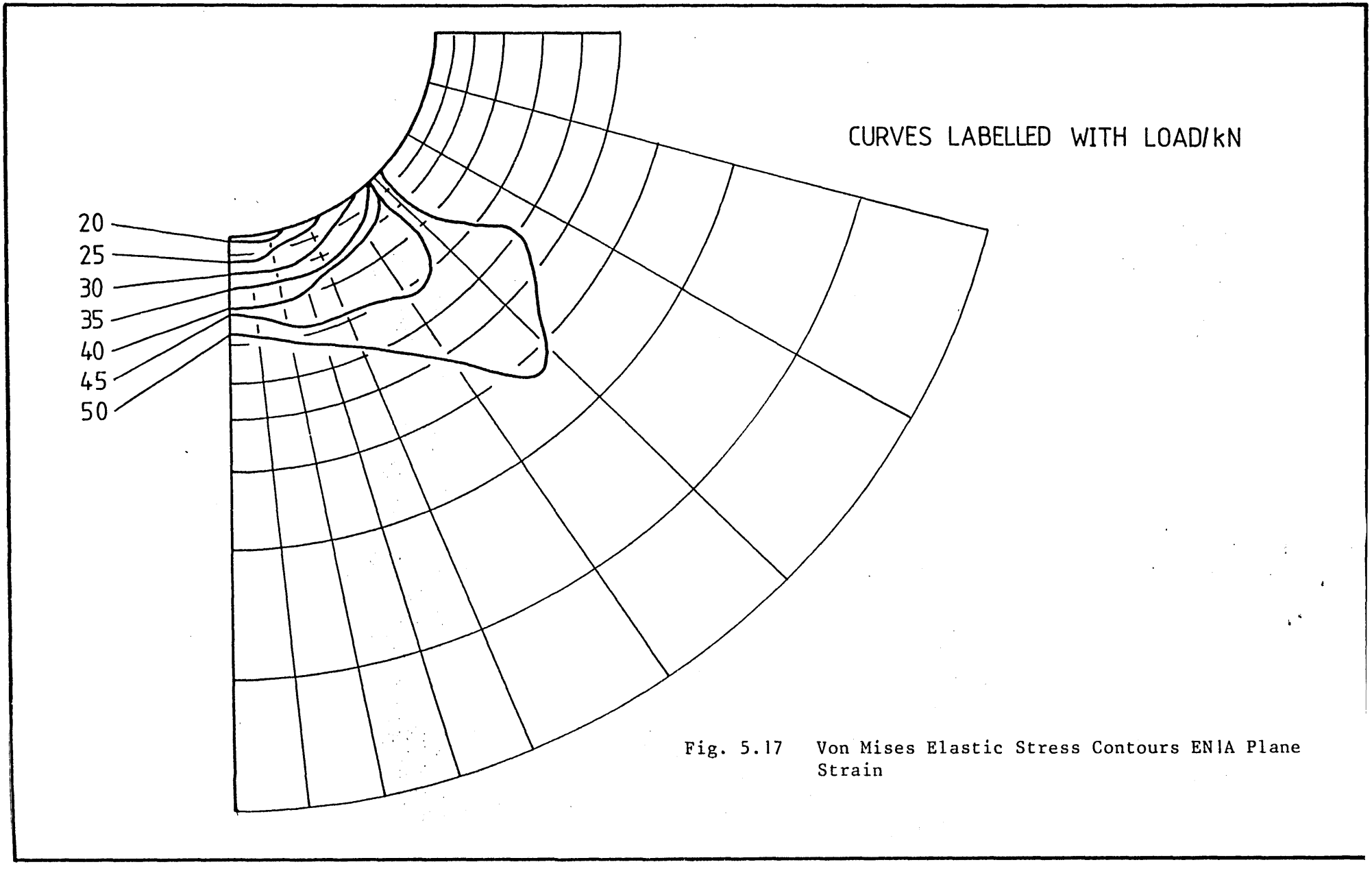

Fig. 5.17 Von Mises Elastic Stress Contours EN1A Plane Strain

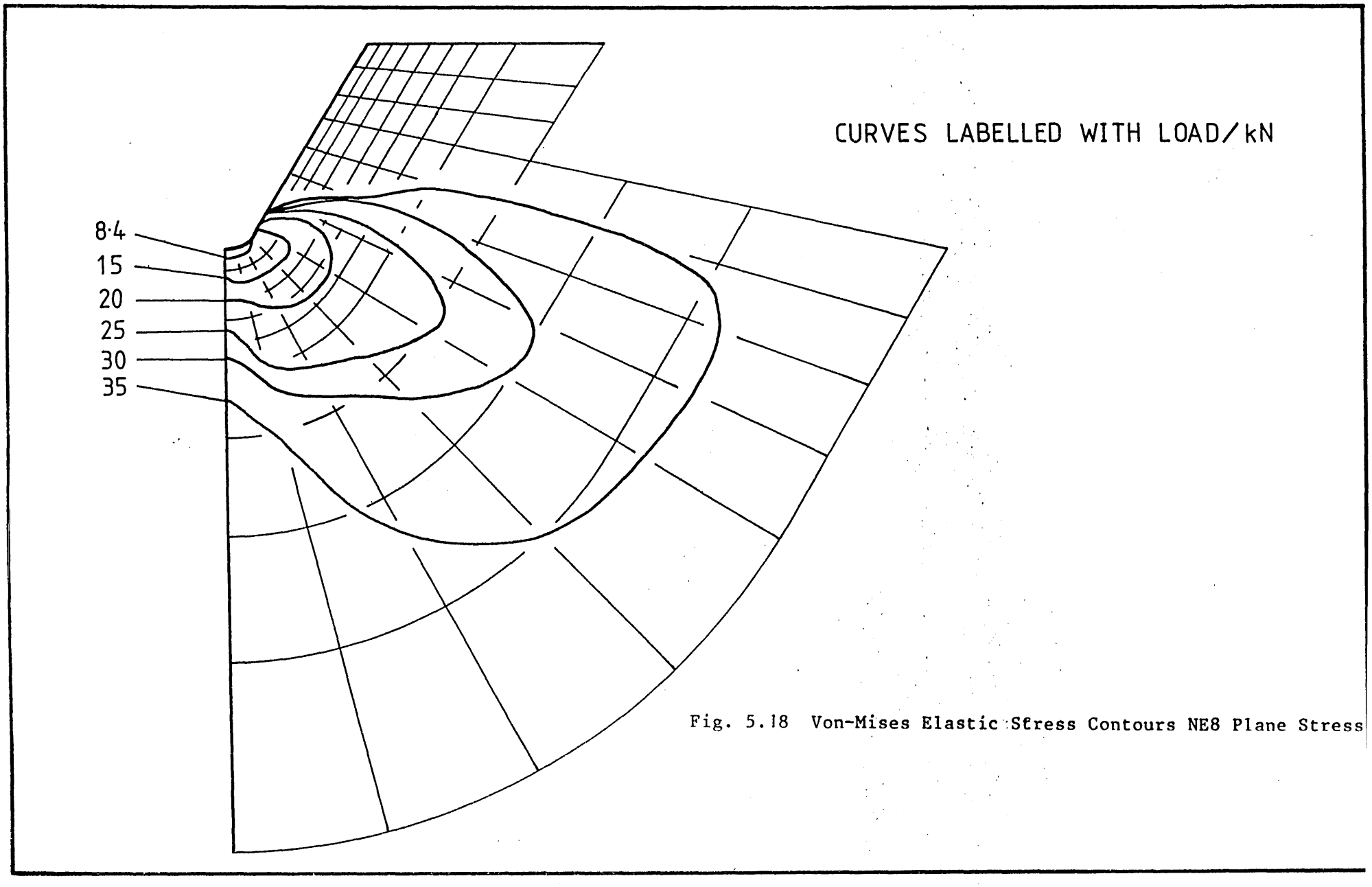

Fig. 5.18 Von-Mises Elastic Stress Contours NE8 Plane Stress

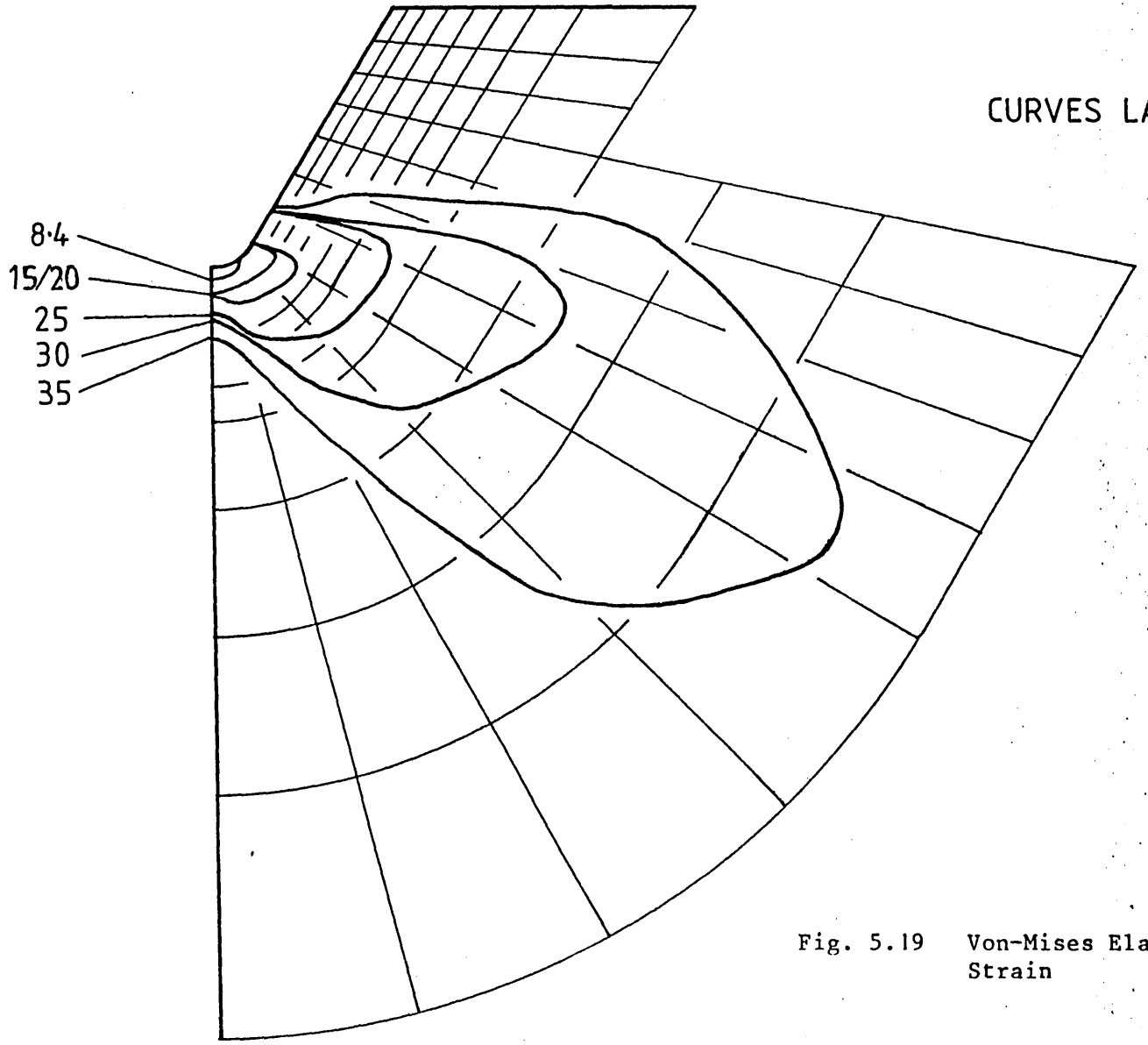

Fig. 5.19 Von-Mises Elastic Stress Contours NE8 Plane Strain

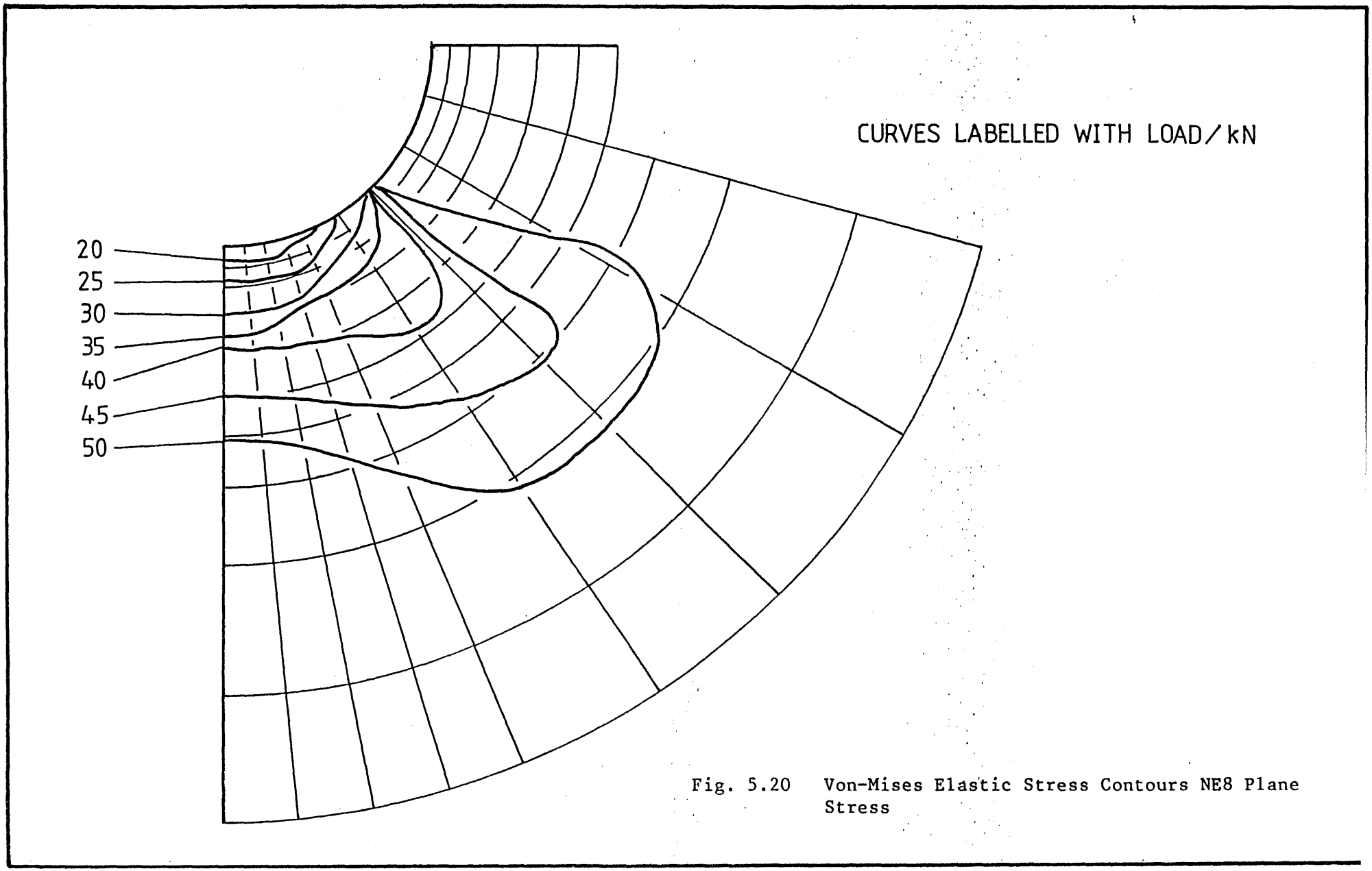

Fig. 5.20 Von-Mises Elastic Stress Contours NE8 Plane Stress

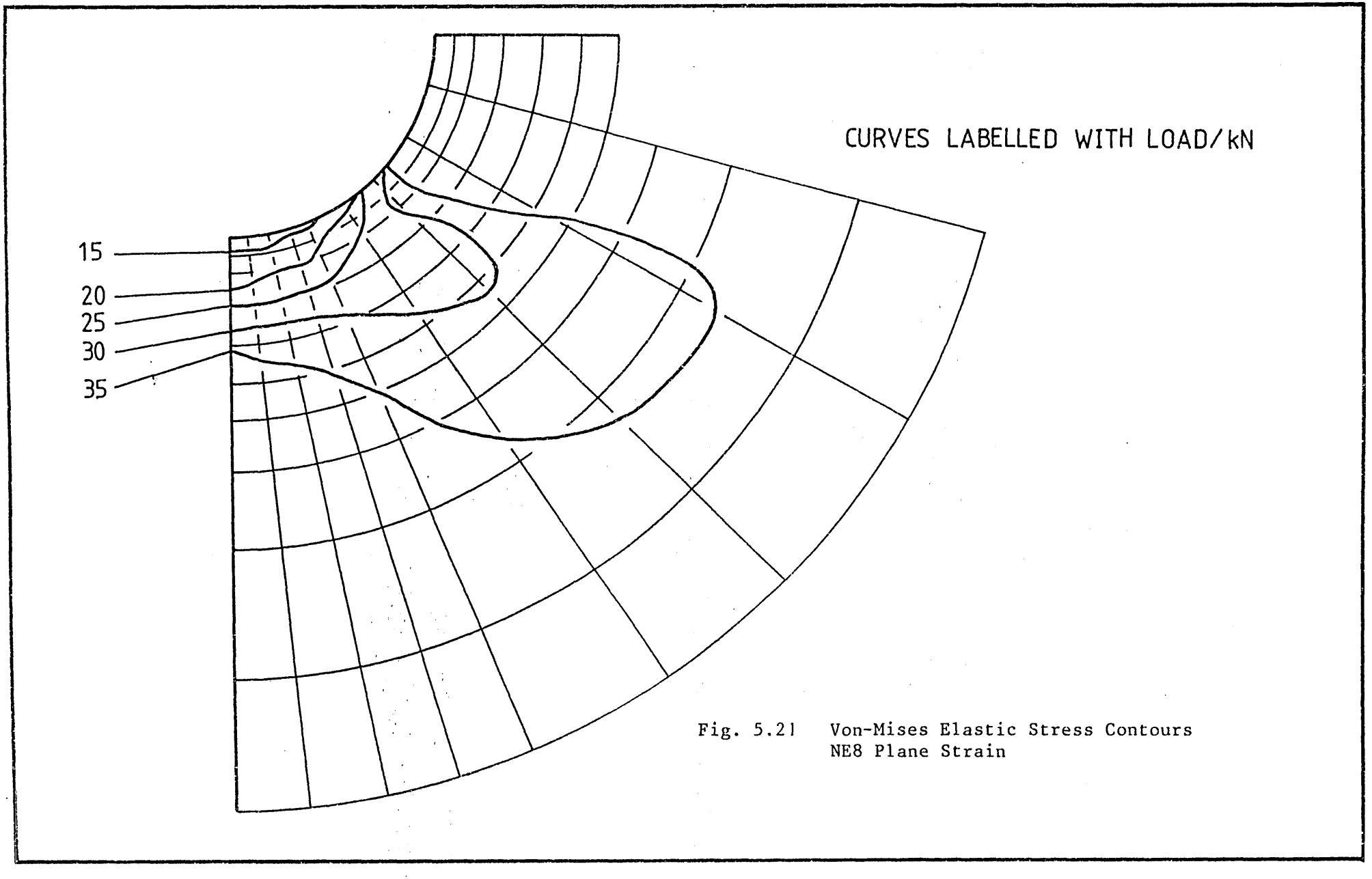

Fig. 5.21 Von-Mises Elastic Stress Contours
NE8 Plane Strain

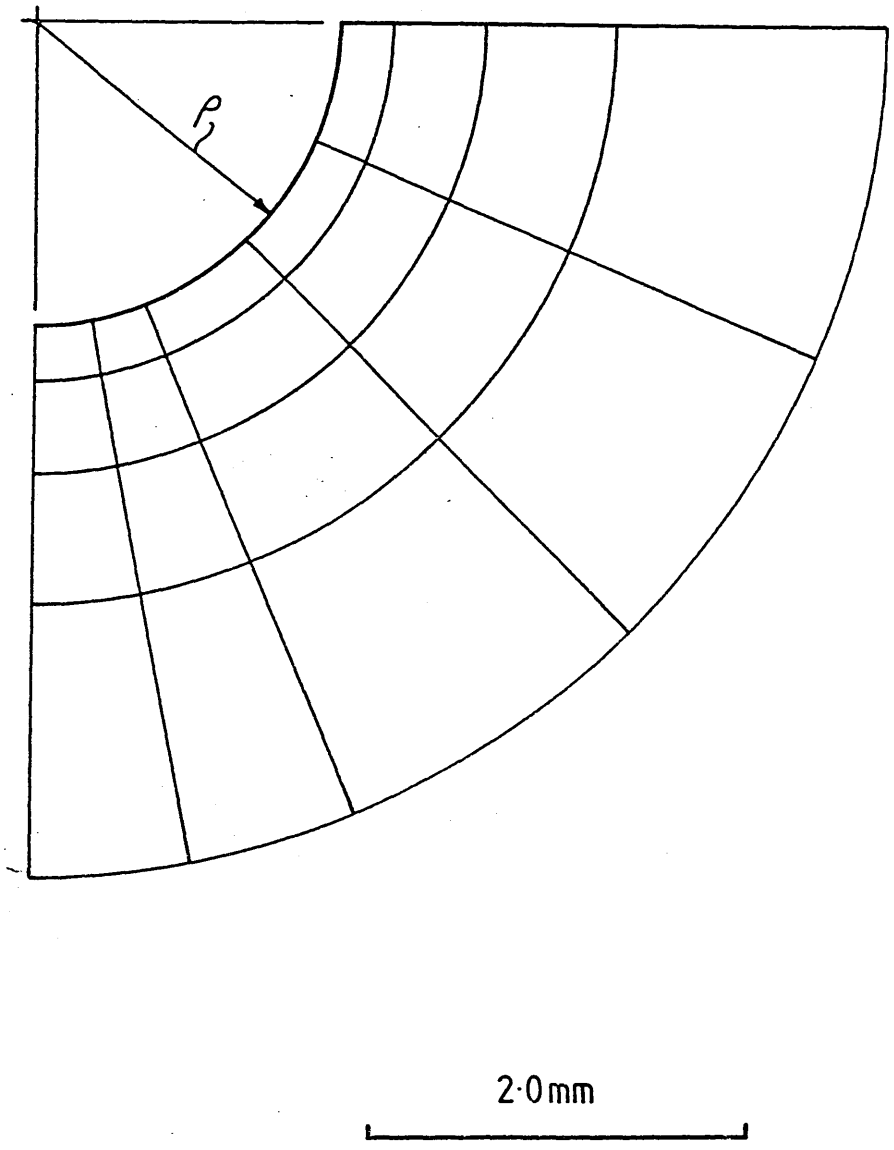

Fig. 5.22 U Notch Mesh Configuration for Plastic Analysis of EN1A and NE8 - Notch Root Details

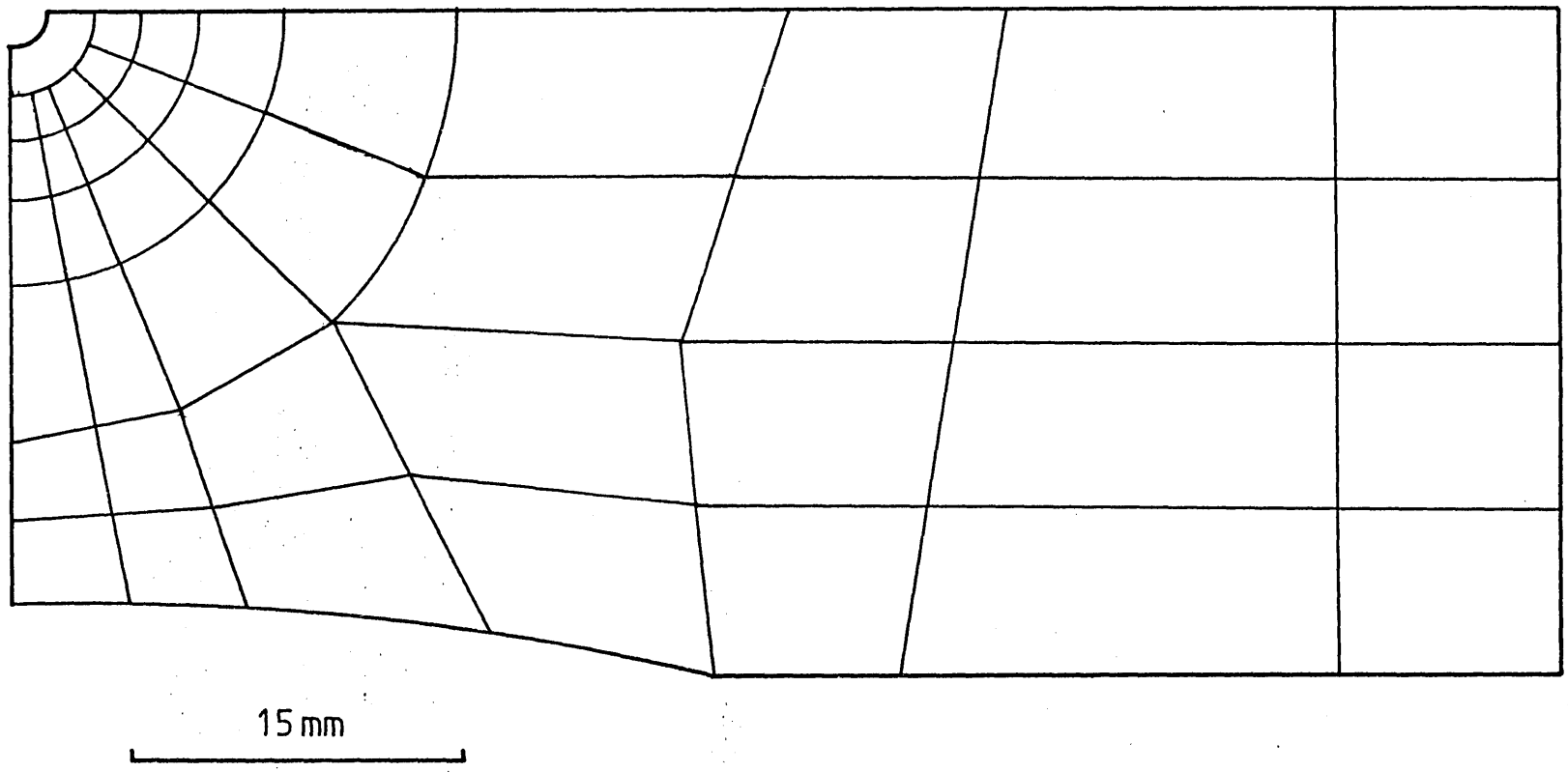

Fig. 5.23 U Notch Mesh Configuration for Plastic Analysis of EN1A and NE8

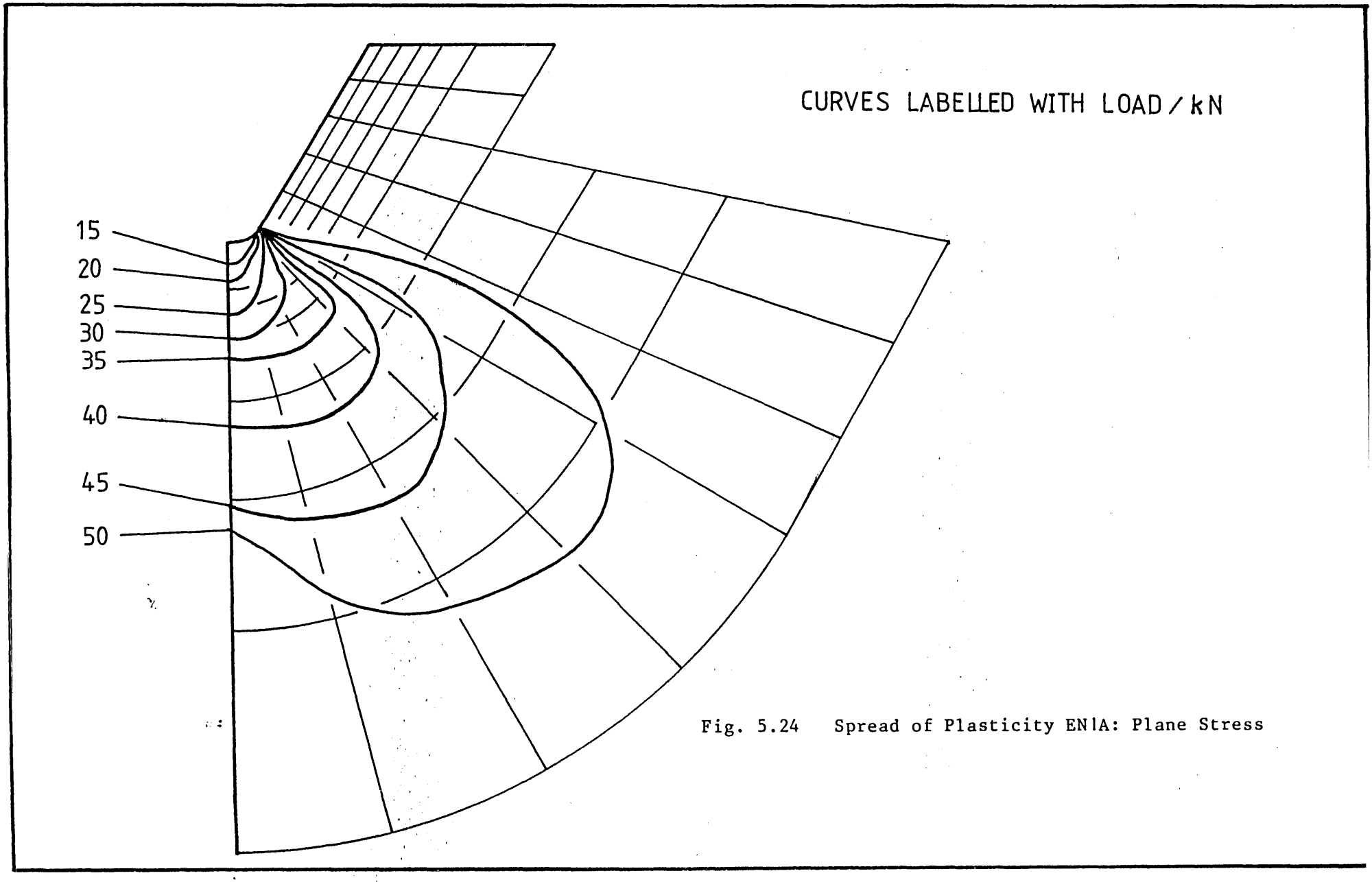

Fig. 5.24 Spread of Plasticity EN1A: Plane Stress

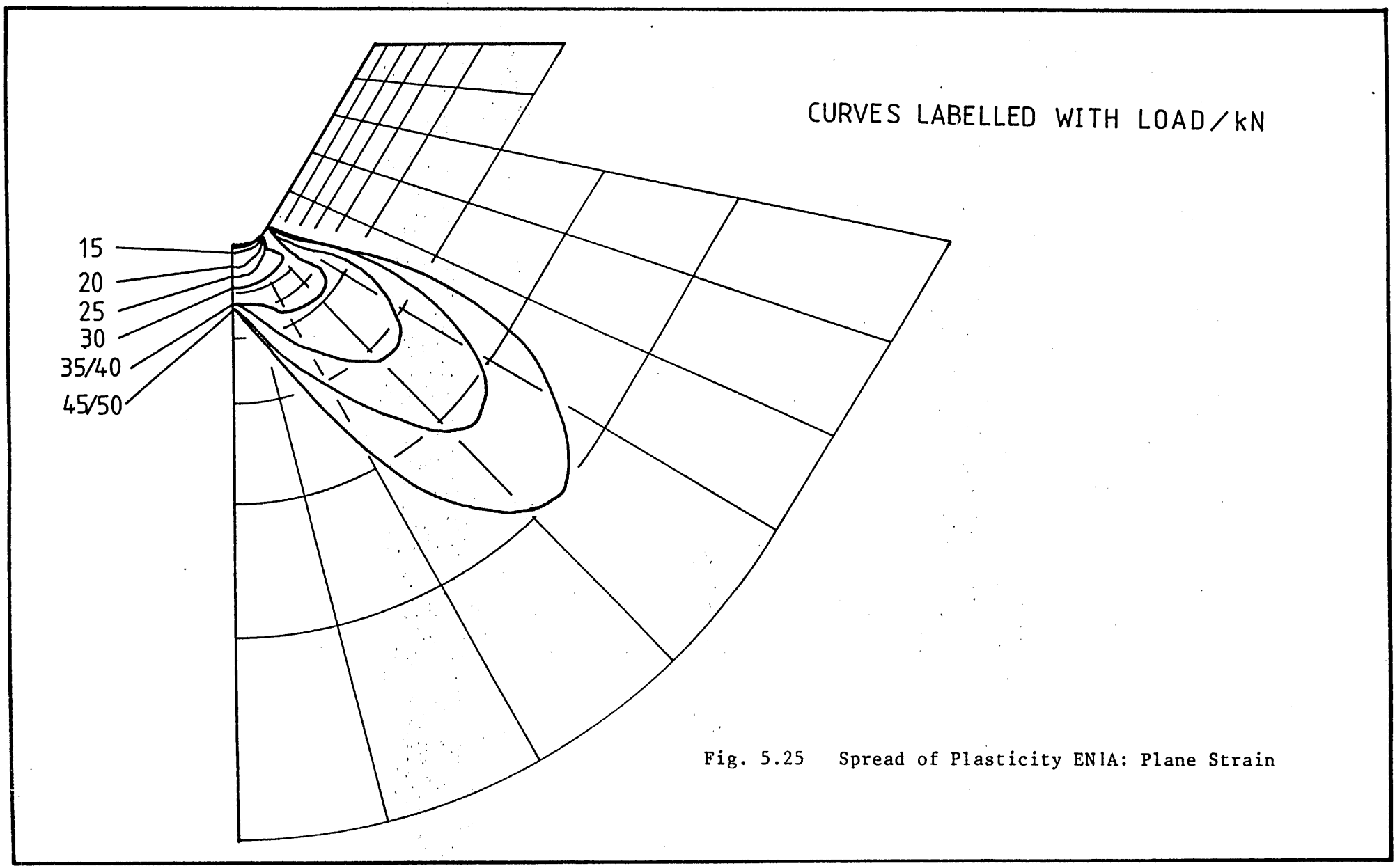

Fig. 5.25 Spread of Plasticity EN1A: Plane Strain

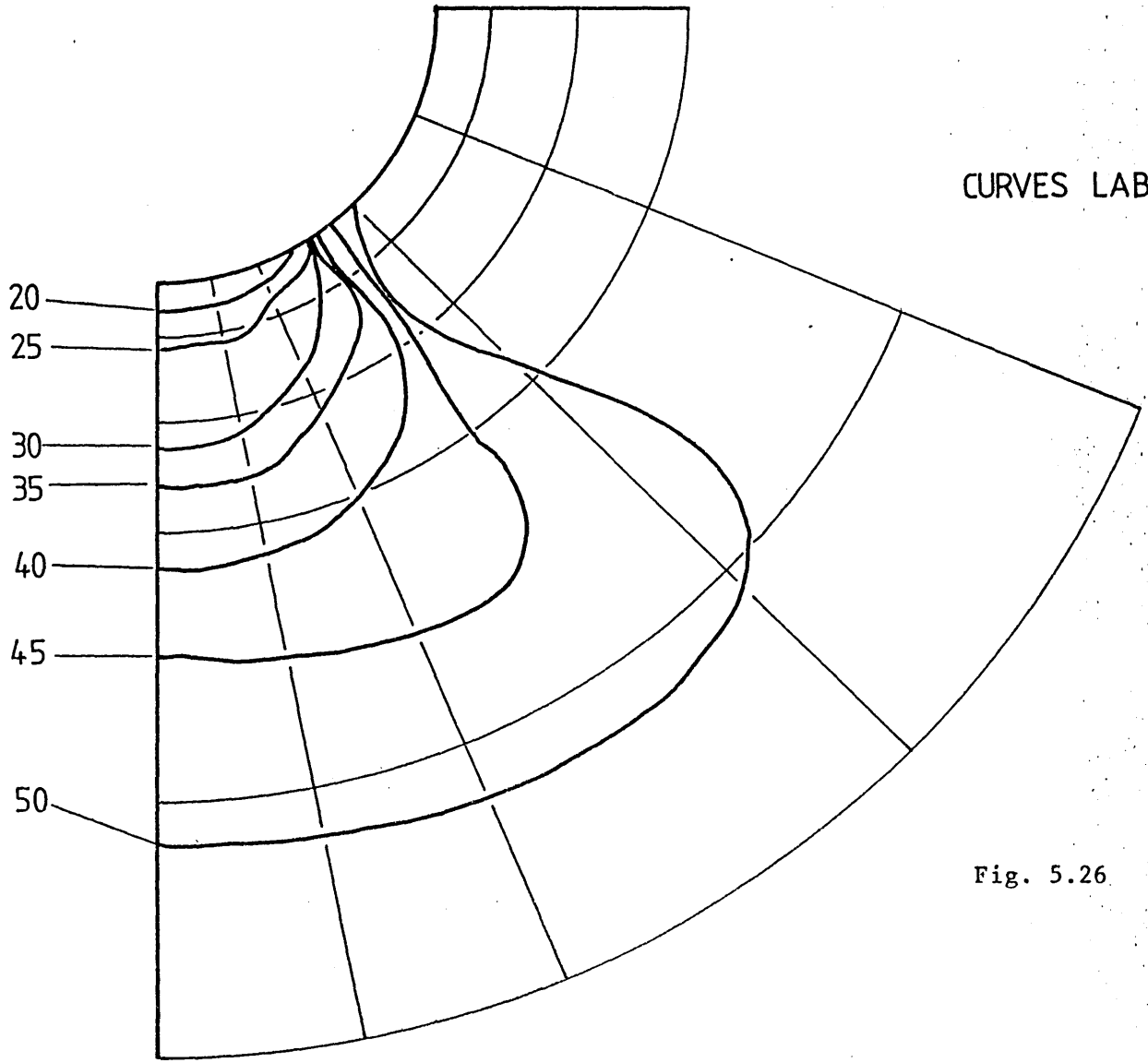

Fig. 5.26 Spread of Plasticity
EN1A: Plane Stress

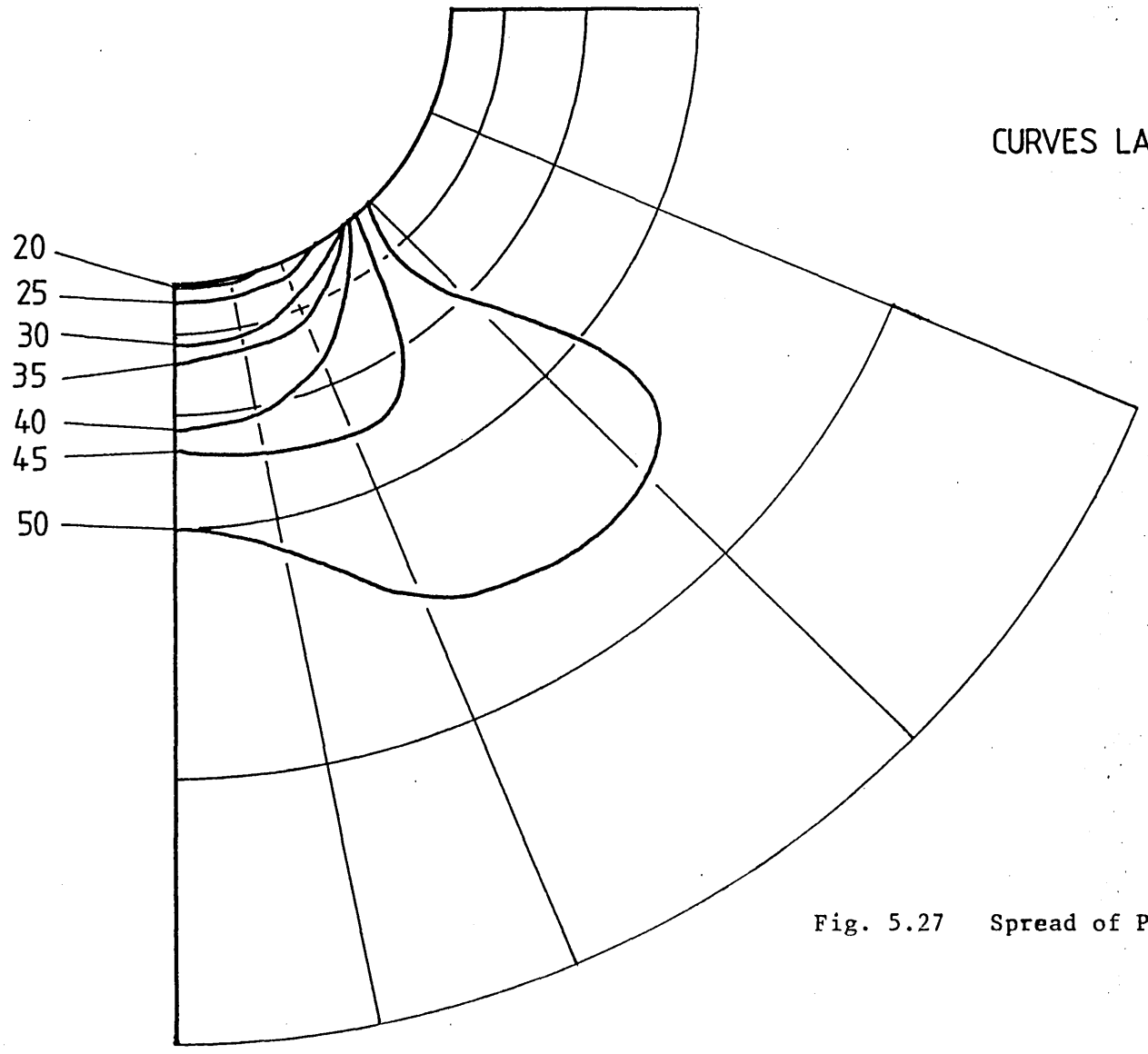

Fig. 5.27 Spread of Plasticity EN1A: Plane Strain

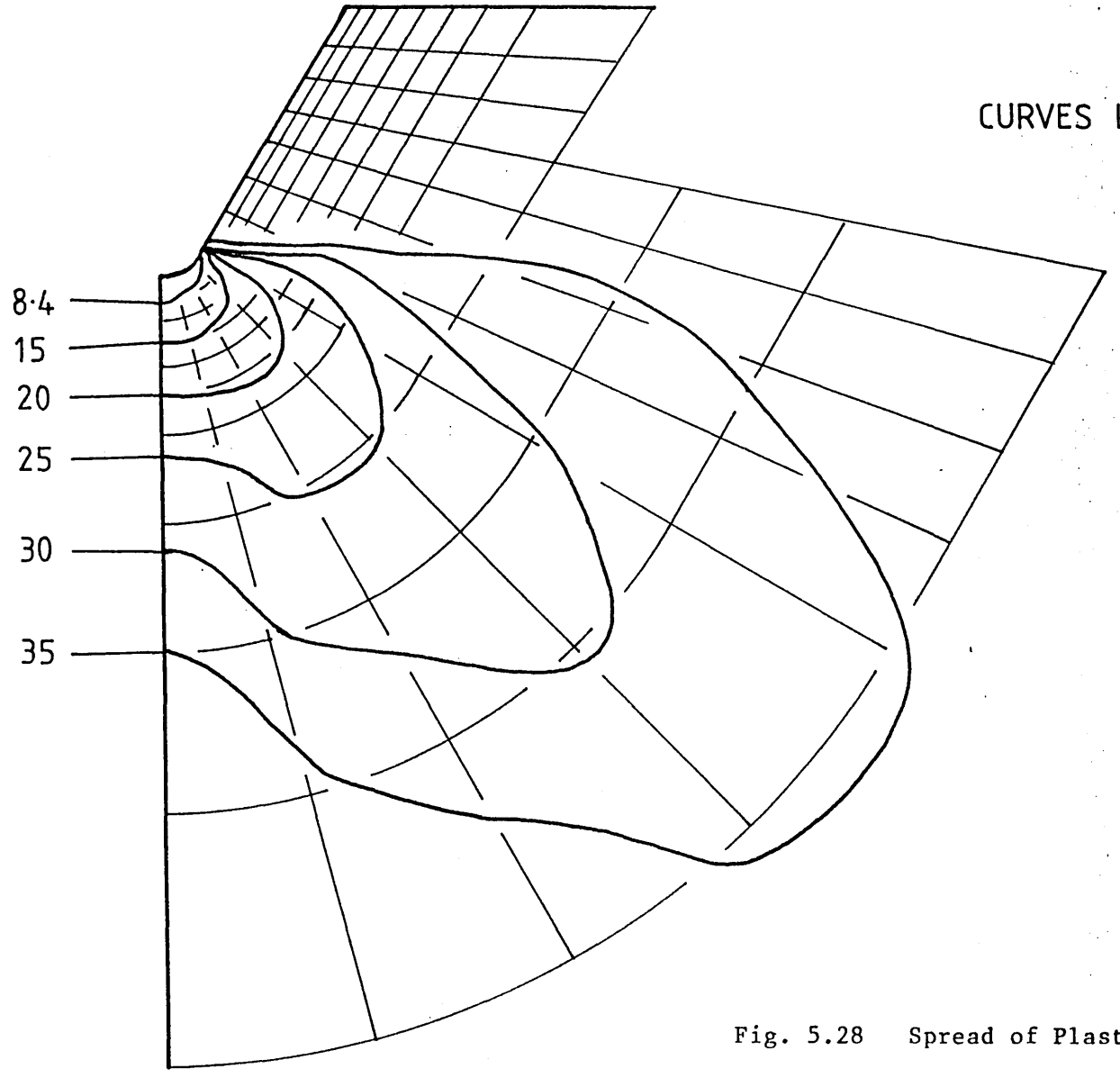

Fig. 5.28 Spread of Plasticity NE8 : Plane Stress

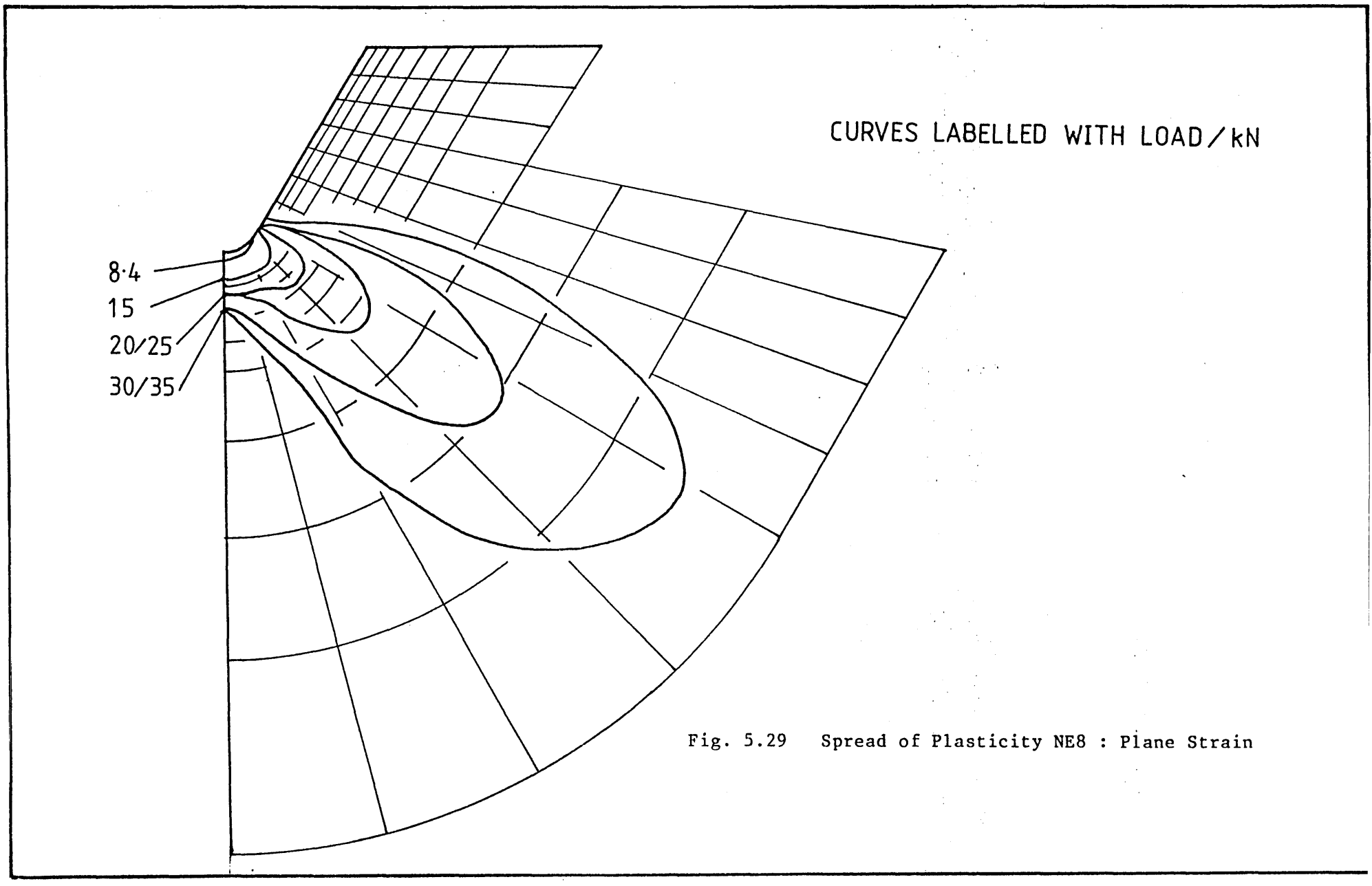

Fig. 5.29 Spread of Plasticity NE8 : Plane Strain

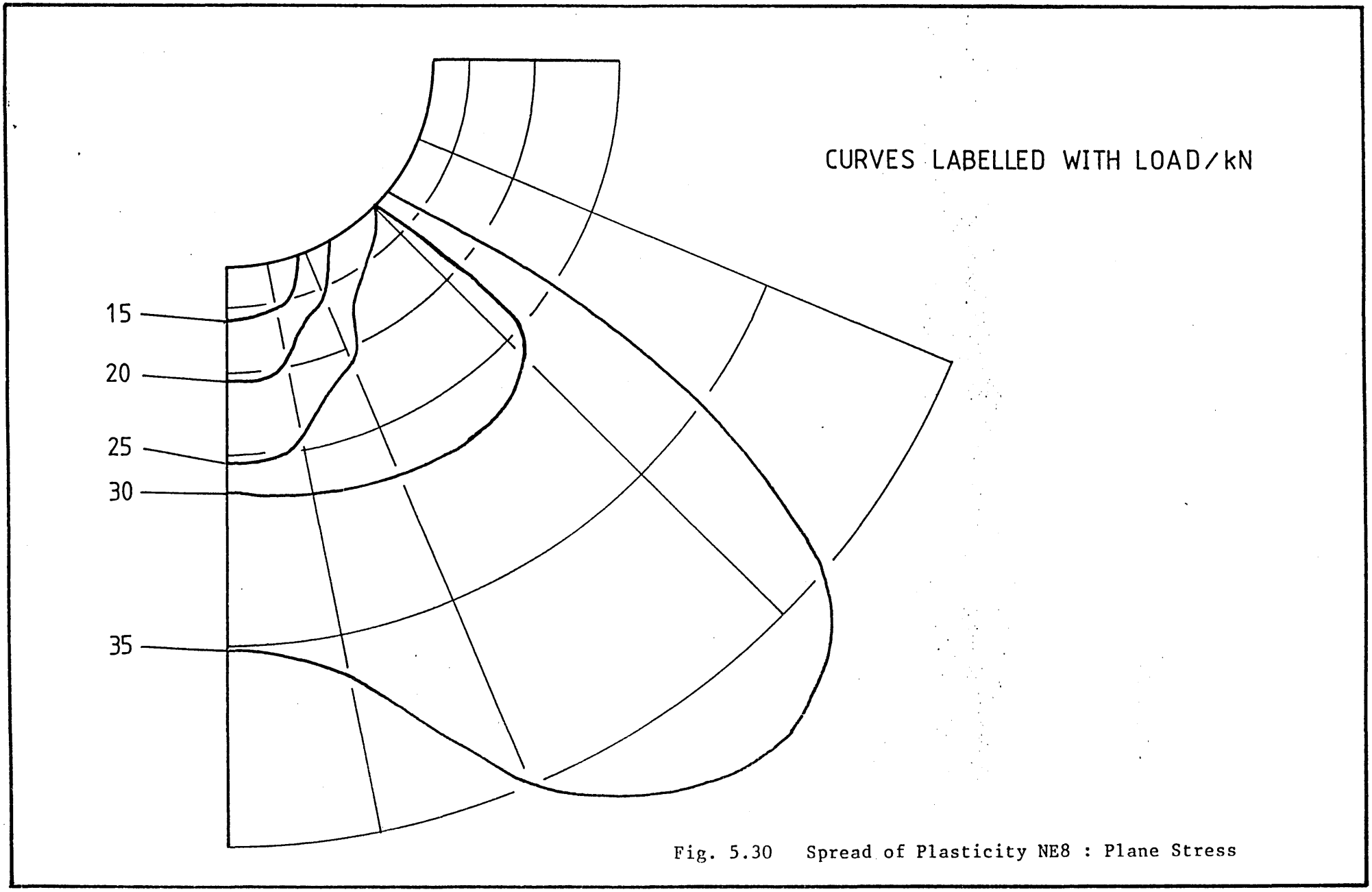

Fig. 5.30 Spread of Plasticity NE8 : Plane Stress

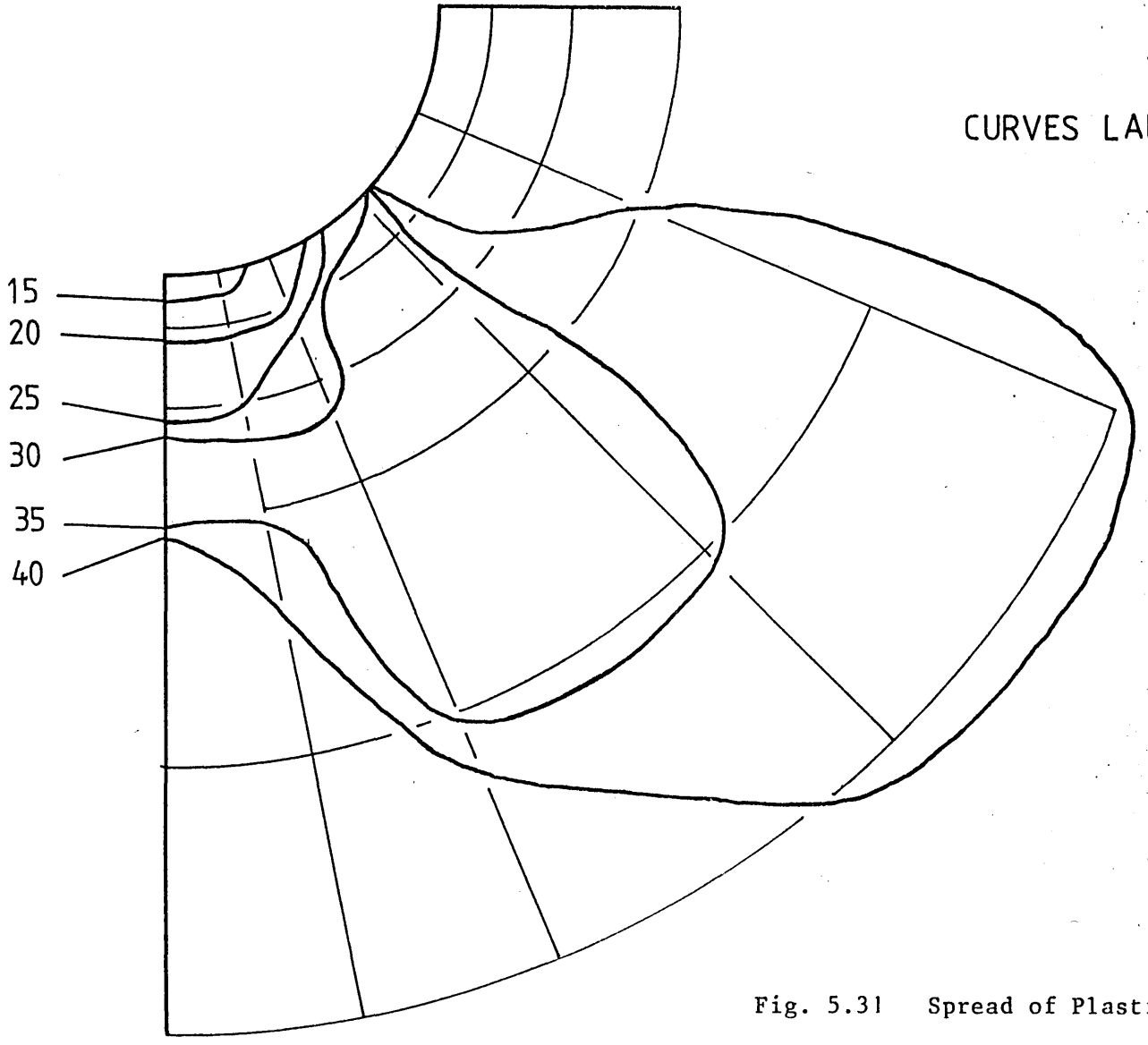

Fig. 5.31 Spread of Plasticity NE8 : Plane Strain

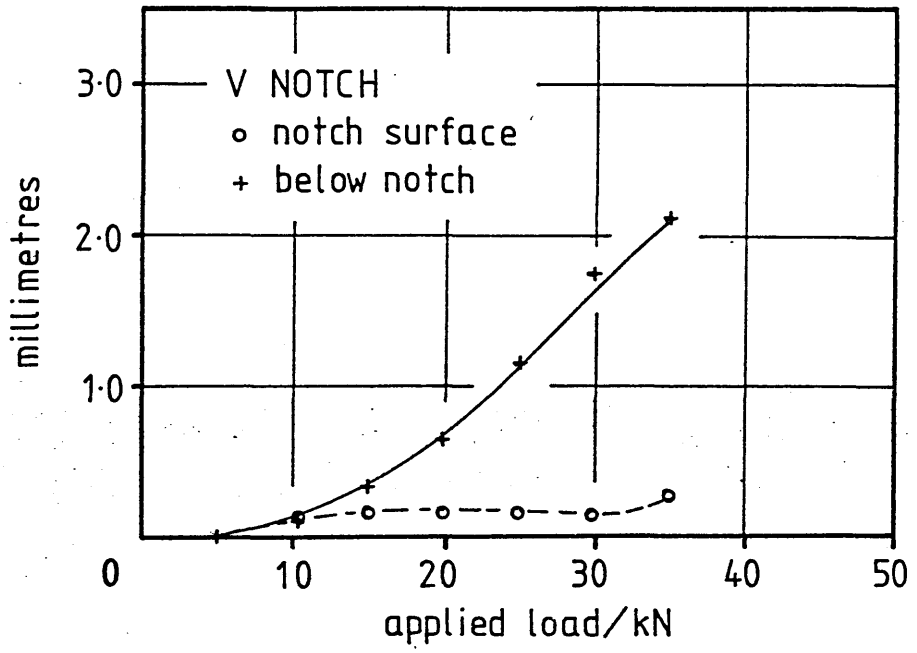

Fig. 5.32

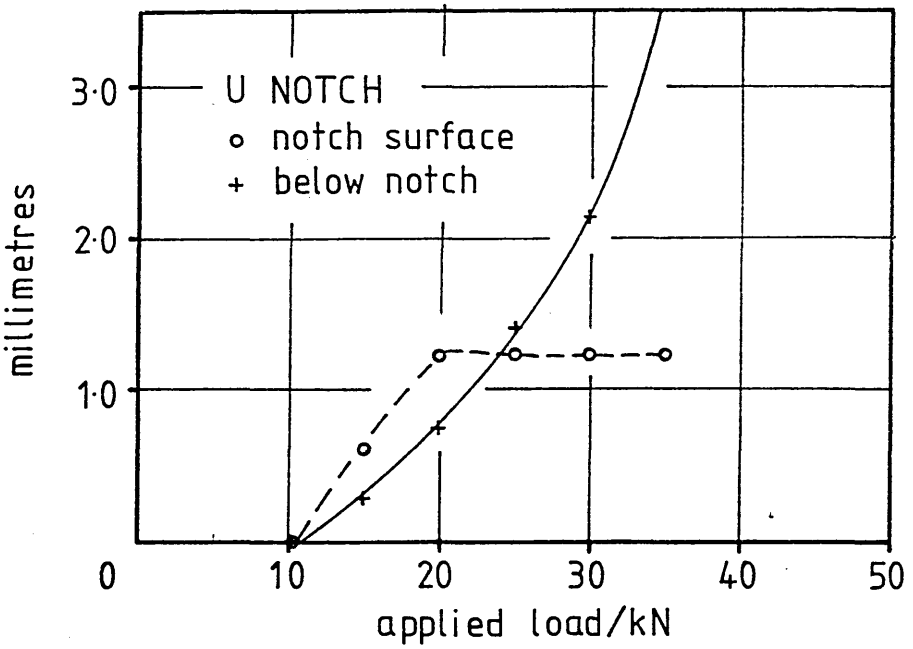

Fig. 5.33

Extent of Plastic Zone
EN1A : Plane Stress

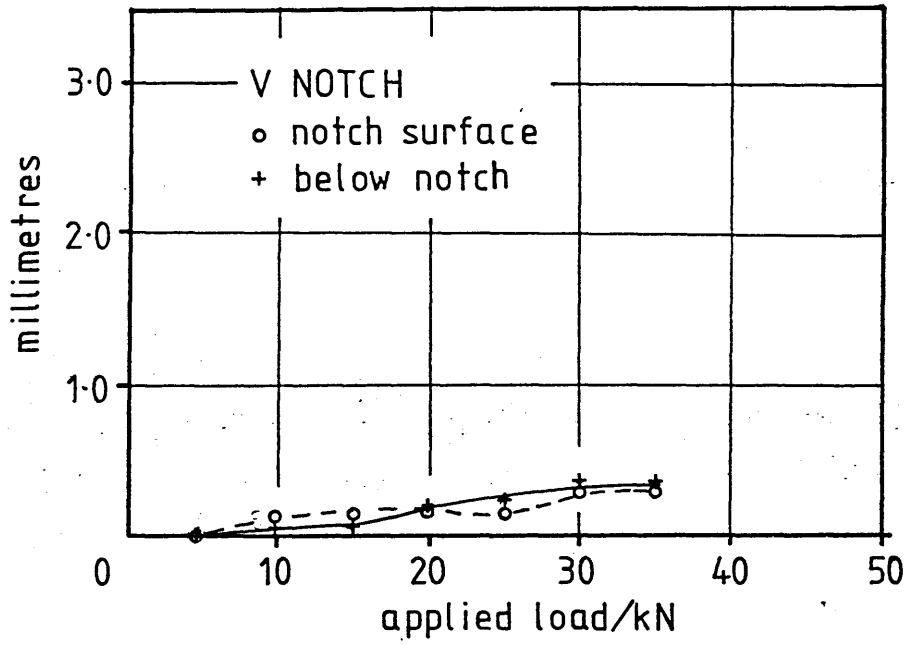

Fig. 5.34

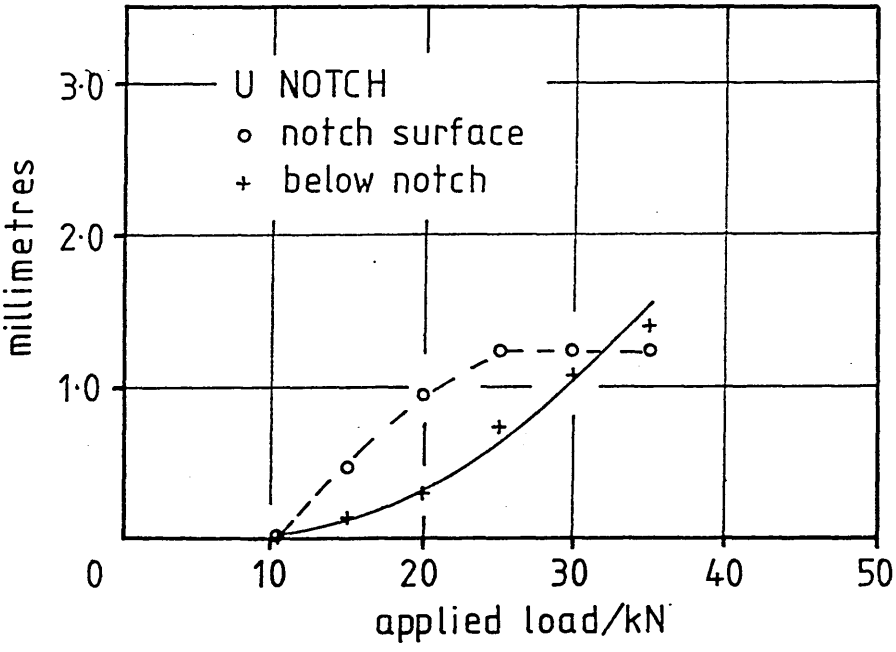

Fig. 5.35

Extent of Plastic Zone
EN1A : Plane Strain

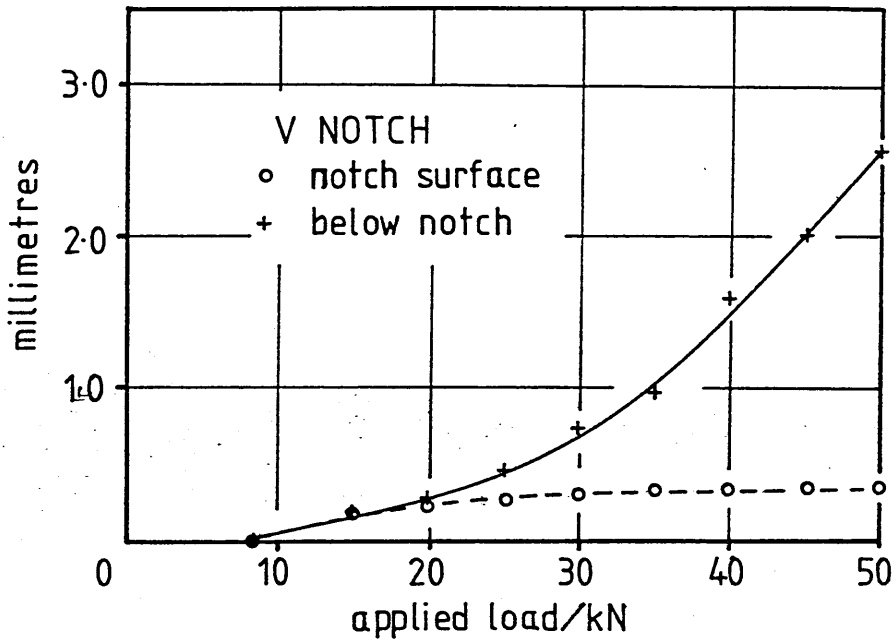

Fig. 5.36

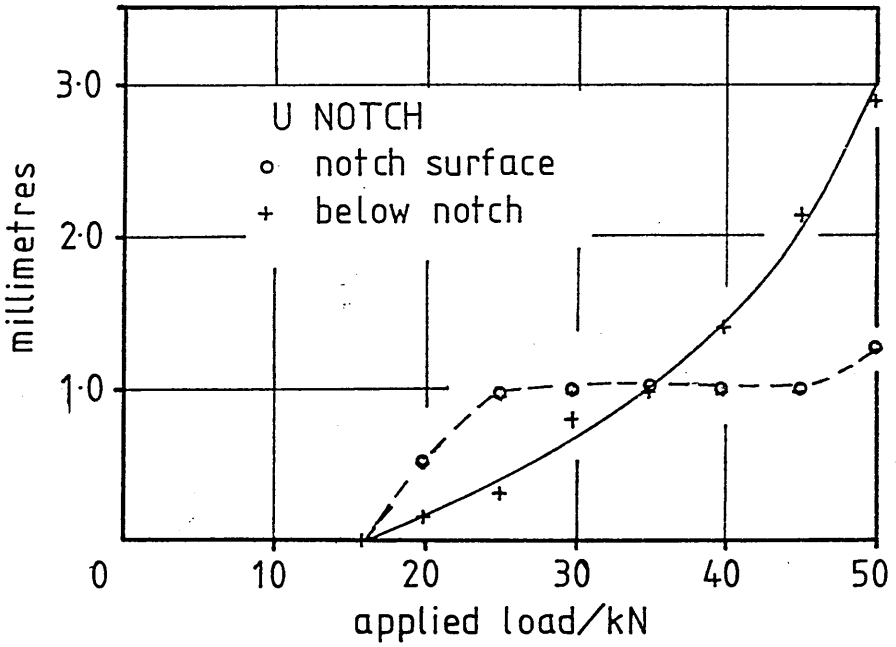

Fig. 5.37

Extent of Plastic Zone
NE8 : Plane Stress

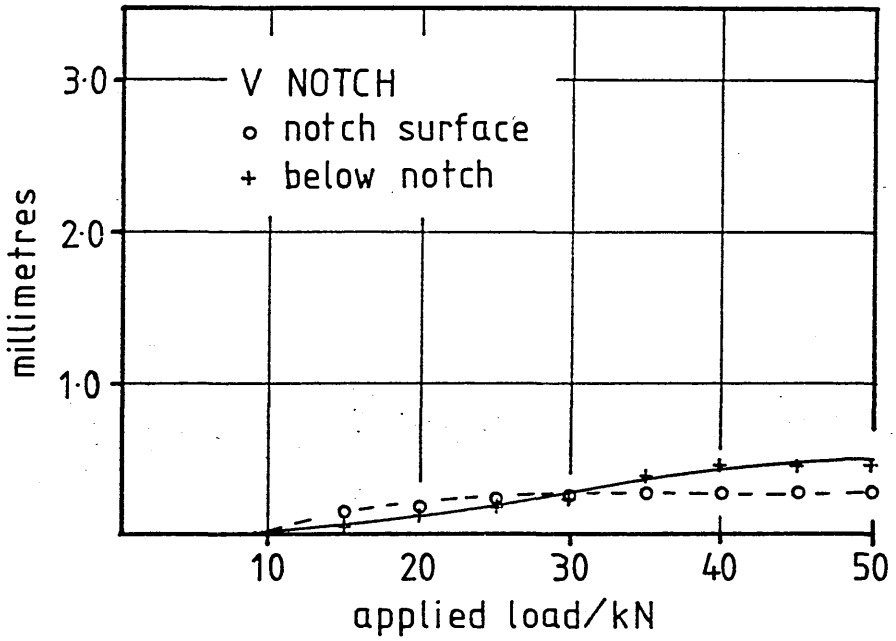

Fig. 5.38

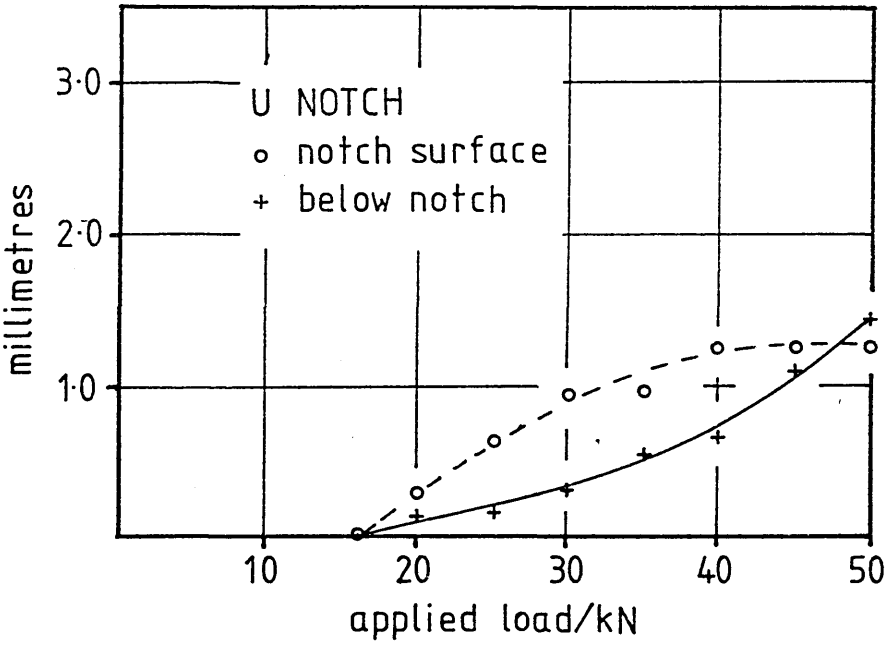

Fig. 5.39

Extent of Plastic Zone
NE8 : Plane Strain

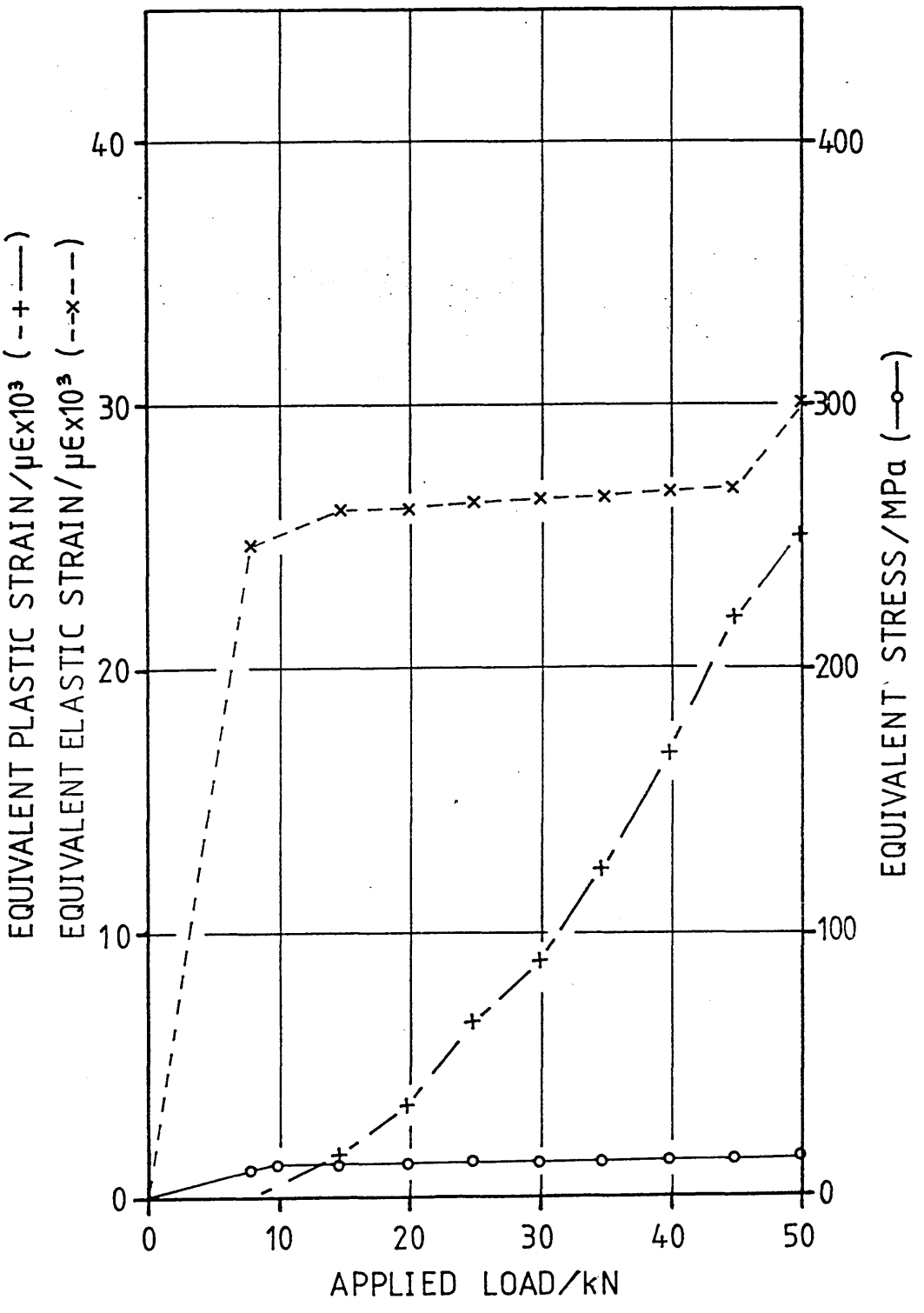

Fig. 5.40 EN1A Mild Steel V Notch Plane Stress
Notch Tip Stress Strain v Load

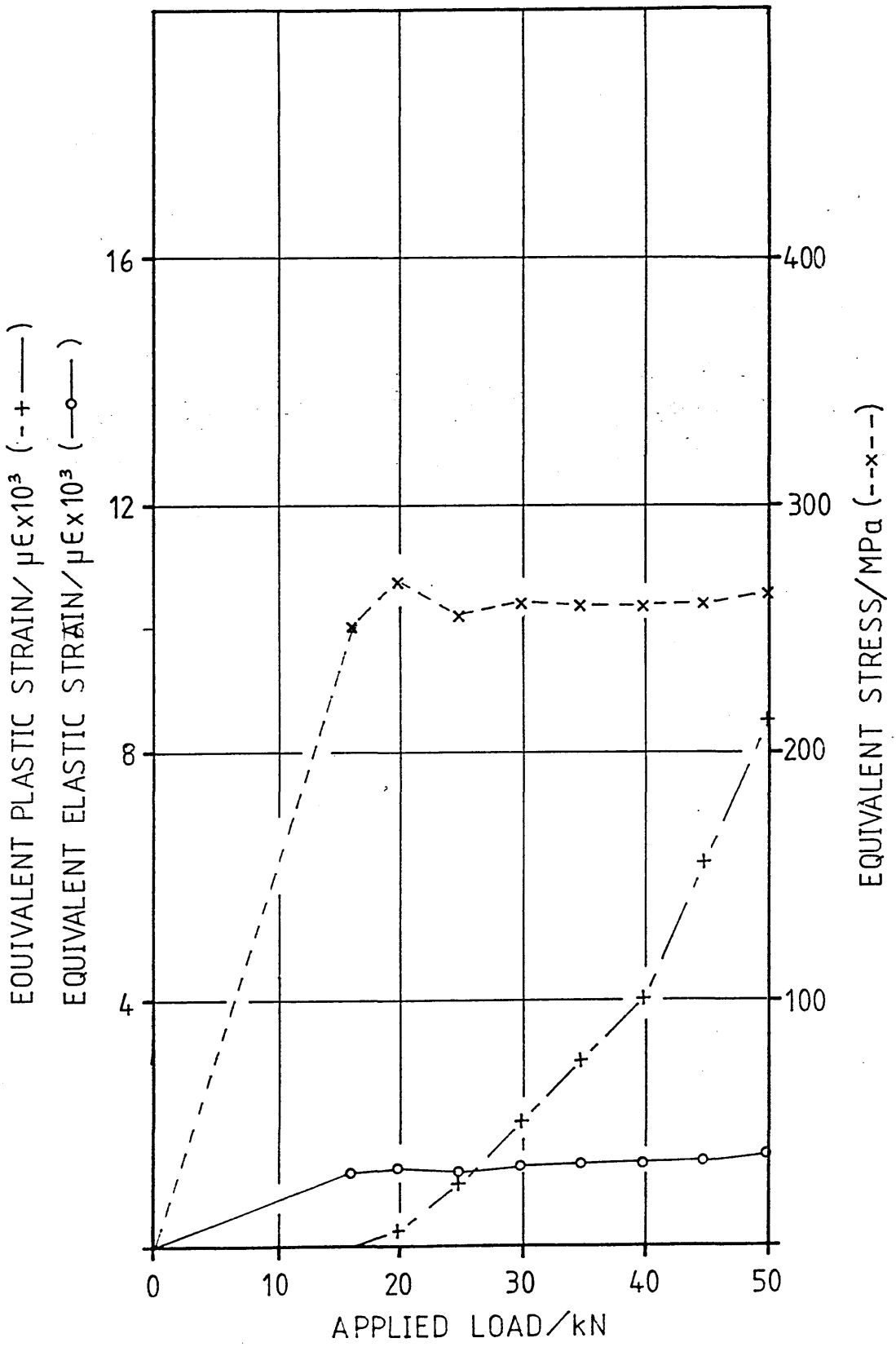

Fig. 5.41 EN1A Mild Steel U Notch Plane Stress
Notch Tip Stress Strain v Load

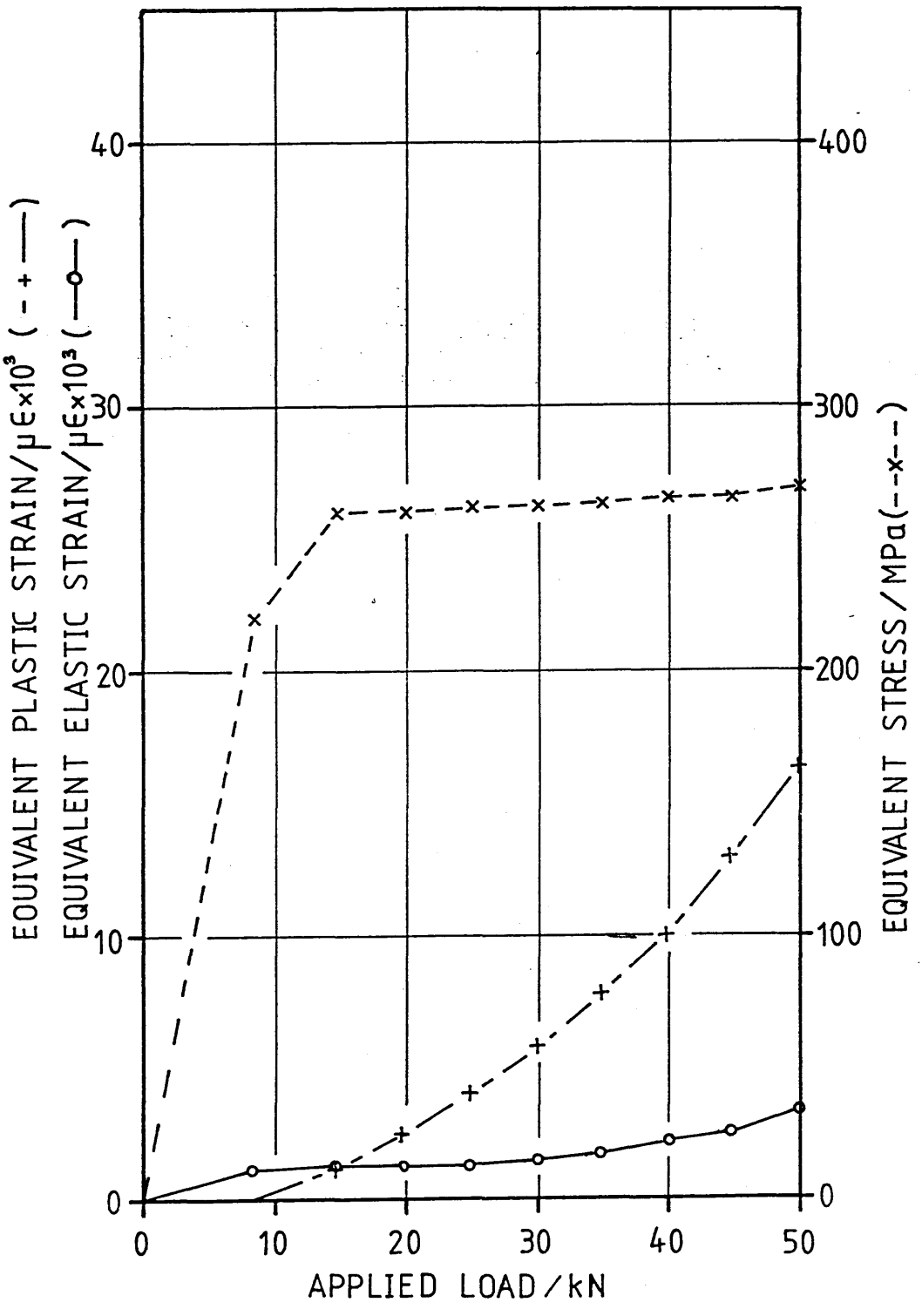

Fig. 5.42 EN1A Mild Steel V Notch Plane Strain
Notch Tip Stress Strain v Load

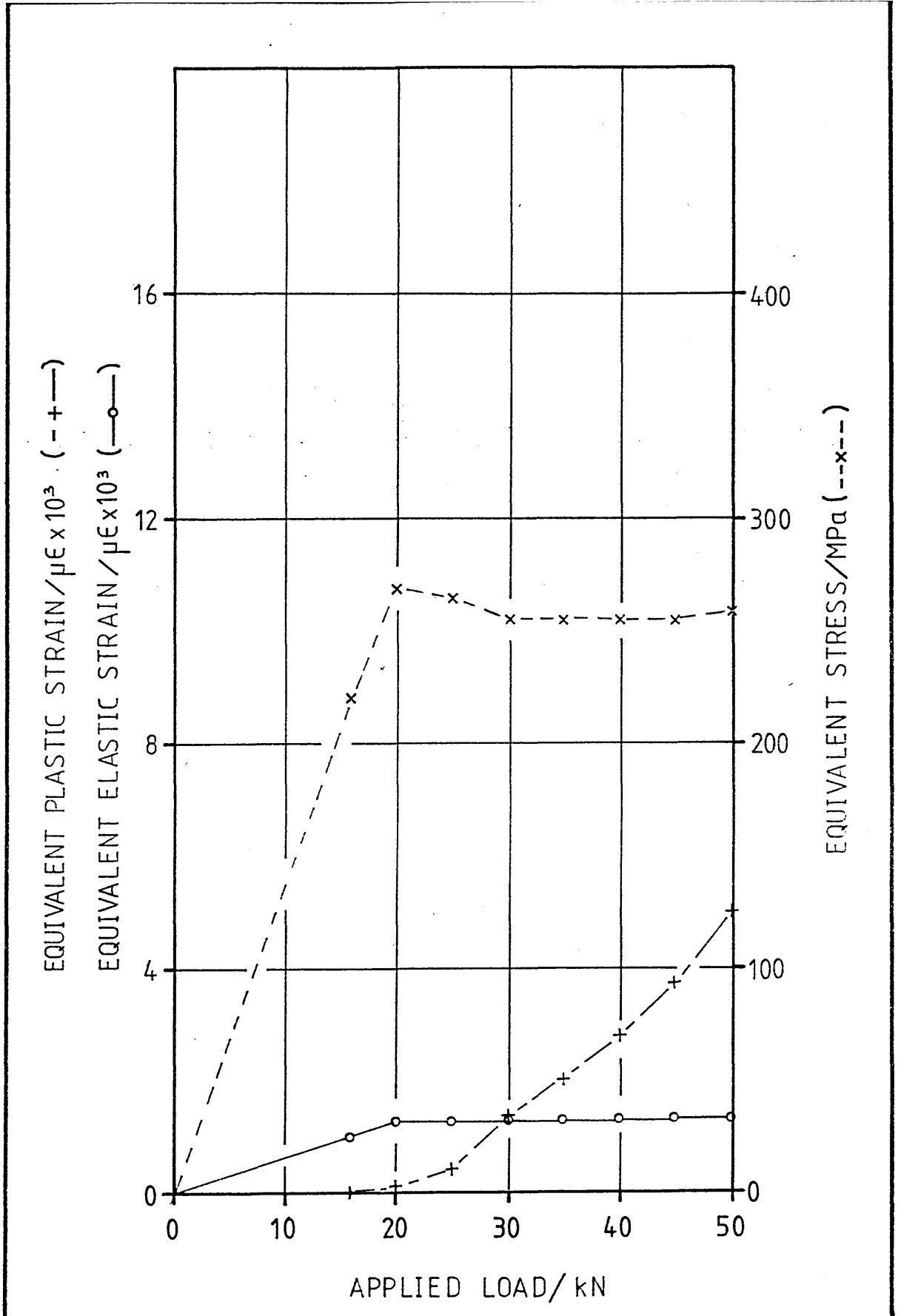

Fig. 5.43 EN1A Mild Steel U Notch Plane Strain
Notch Tip Stress Strain v Load

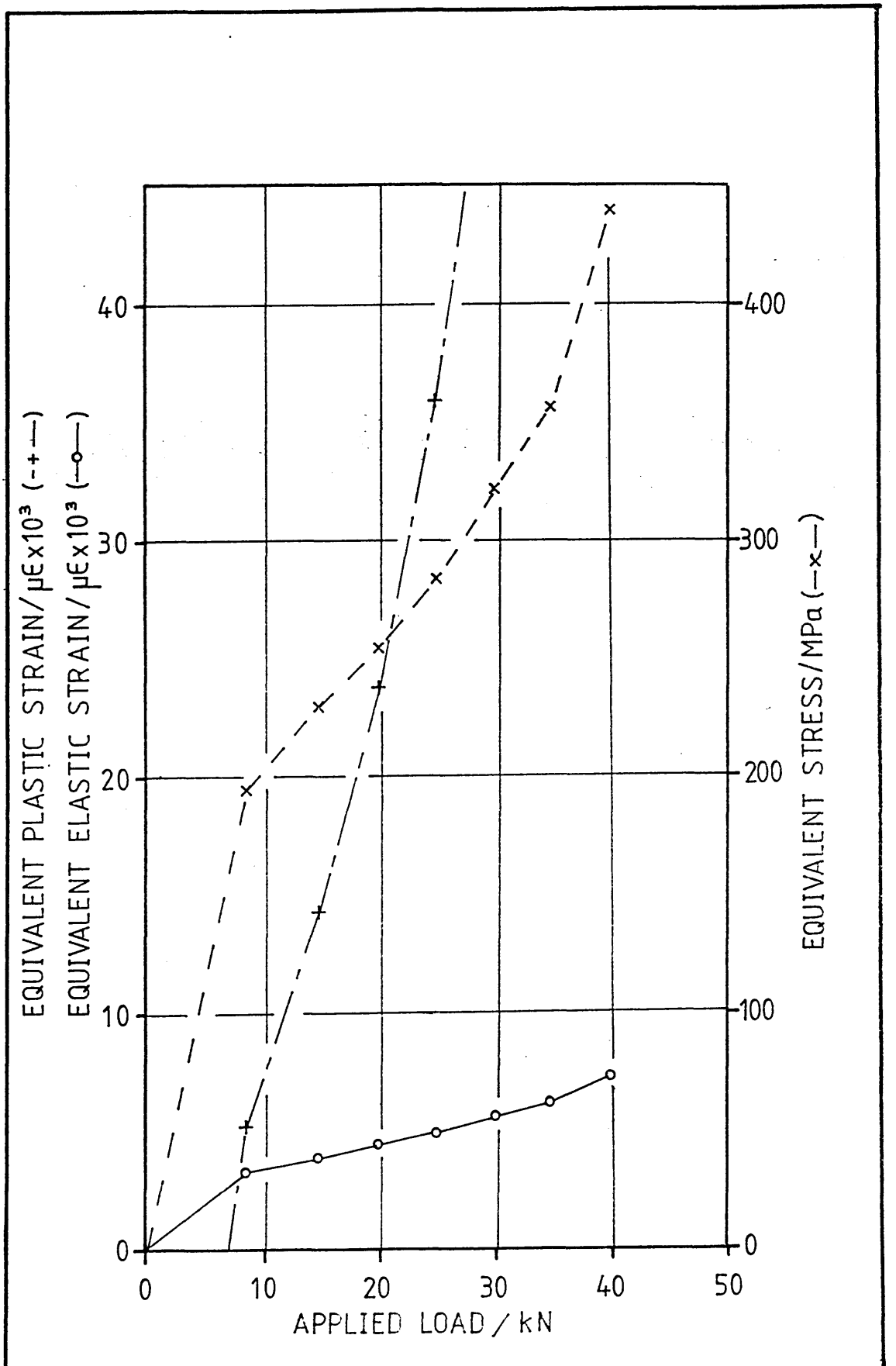

Fig. 5.44 NE8 Alloy V Notch Plane Stress
Notch Tip Stress Strain v Load

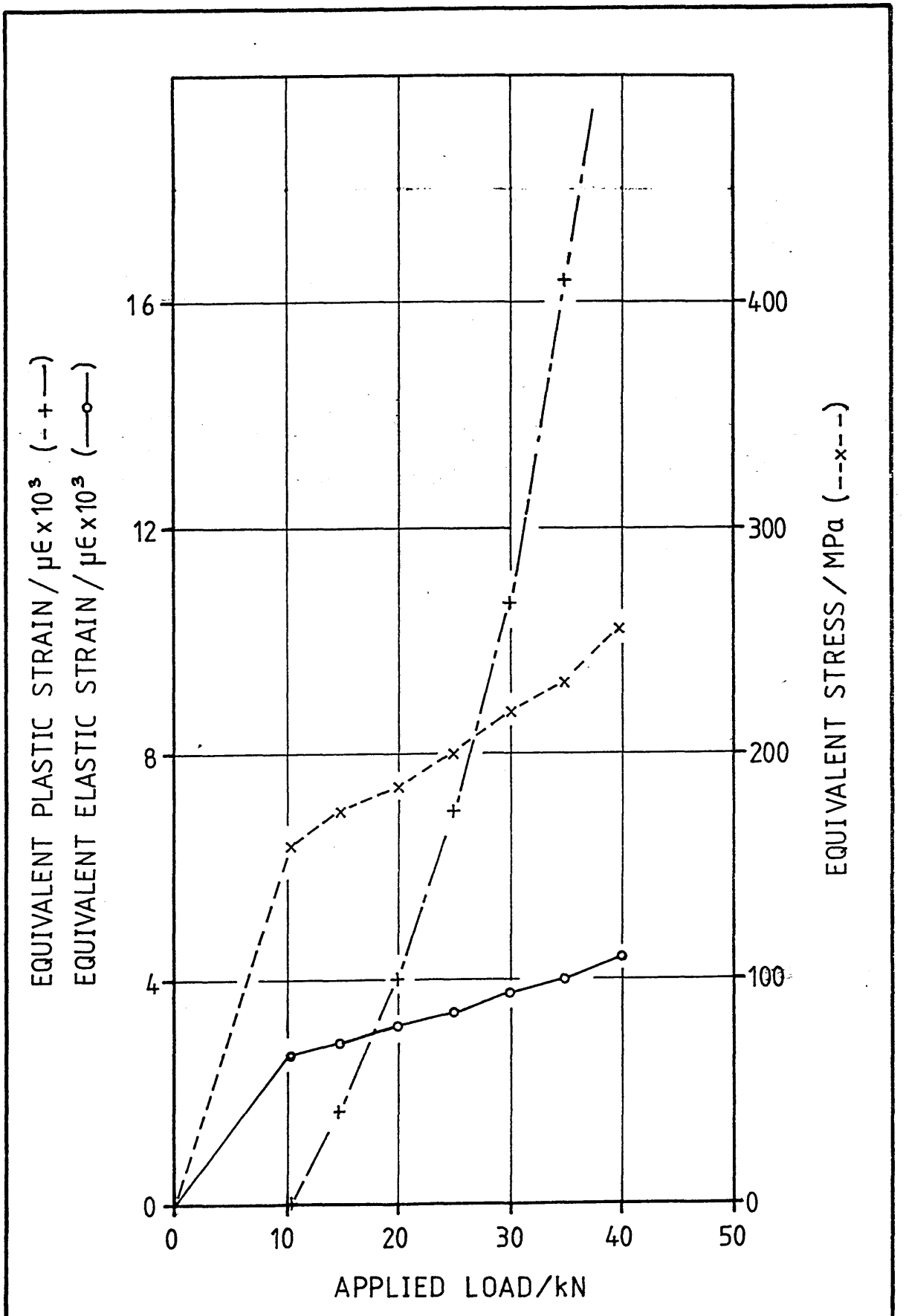

Fig. 5.45 NE8 Alloy V Notch Plane Strain
Notch Tip Stress Strain v Load

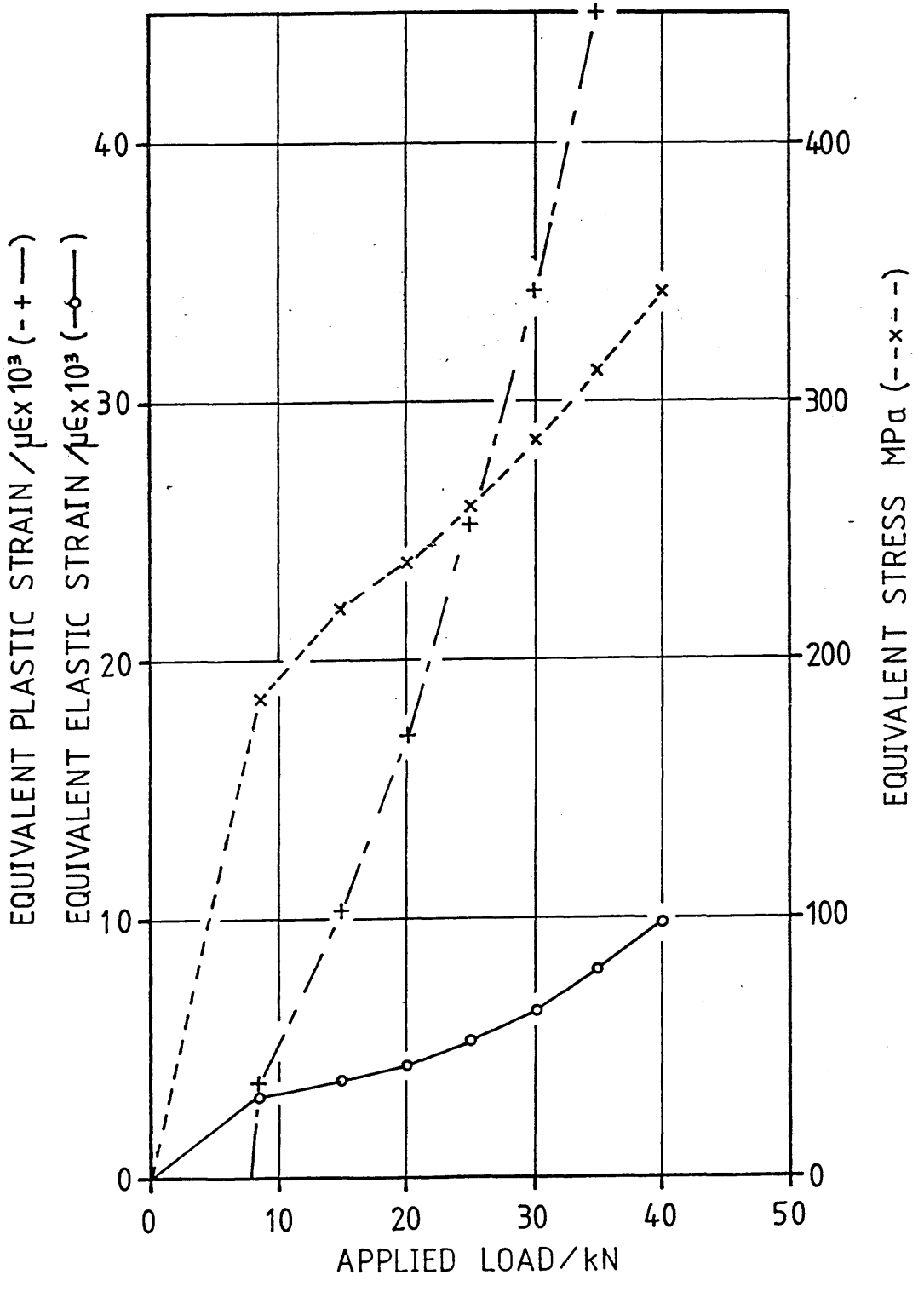

Fig. 5.46 NE8 Alloy U Notch Plane Stress
Notch Tip Stress Strain v Load

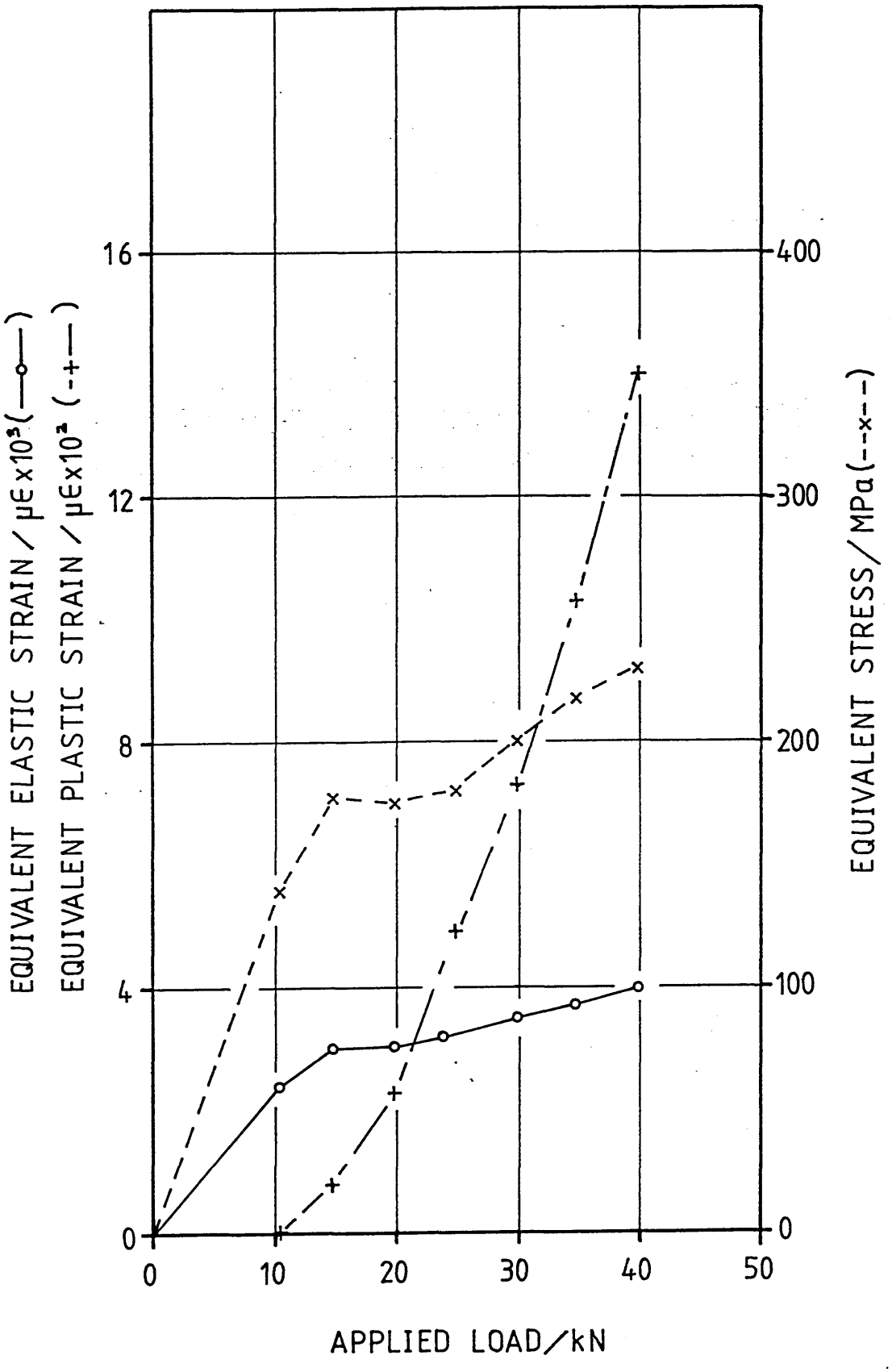

Fig. 5.47 NE8 Alloy U Notch Plane Strain
Notch Tip Stress Strain v Load

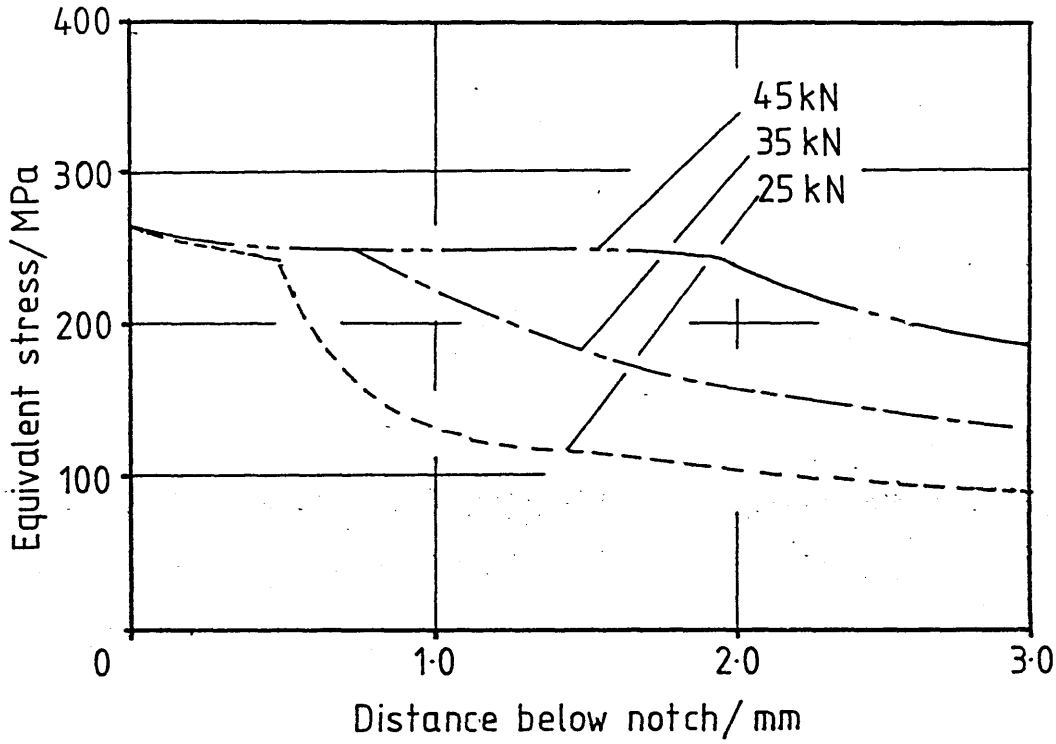

Fig. 5.48
V Notch EN1A

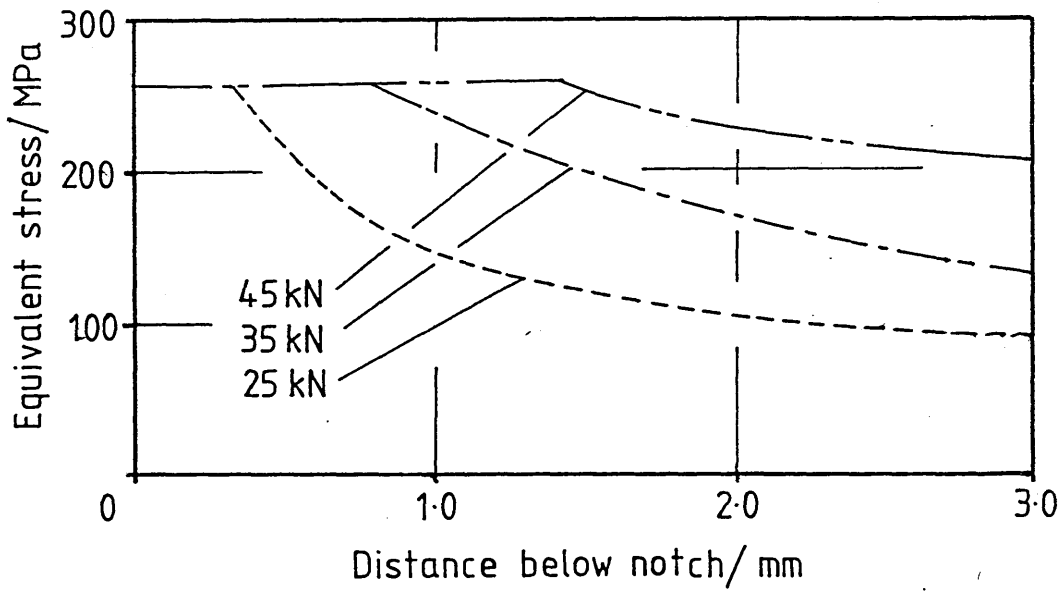

Fig. 5.49
U Notch EN1A

Stress Gradient Below Notch - Plane Stress

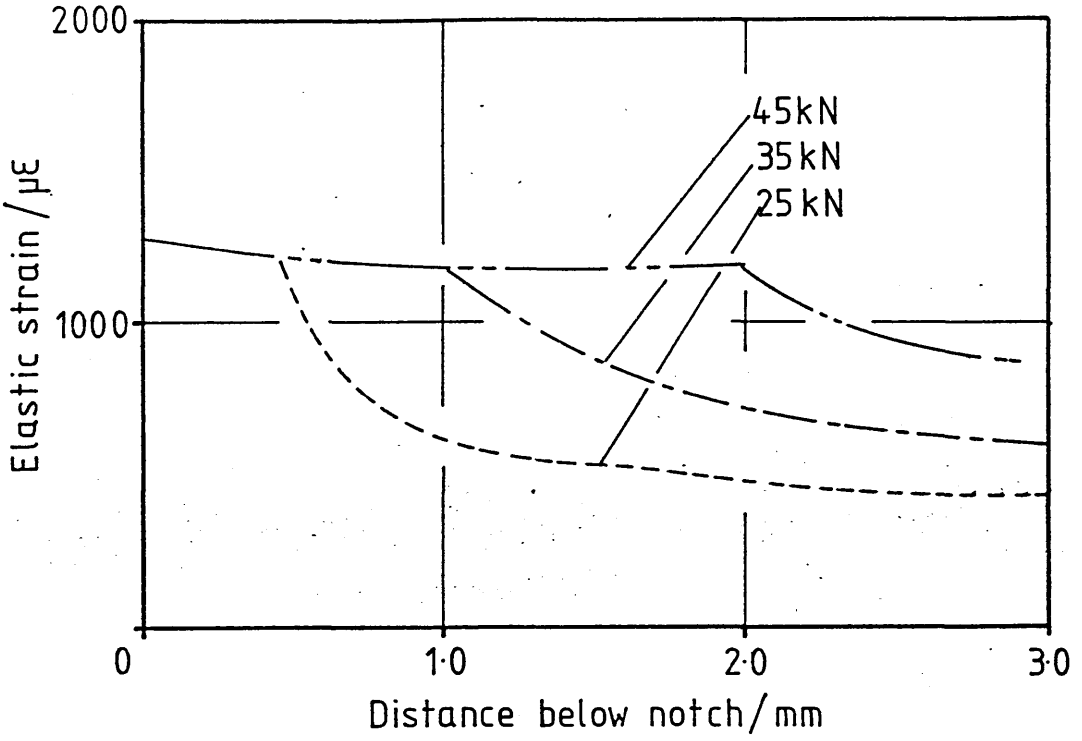

Fig. 5.50
V Notch EN1A

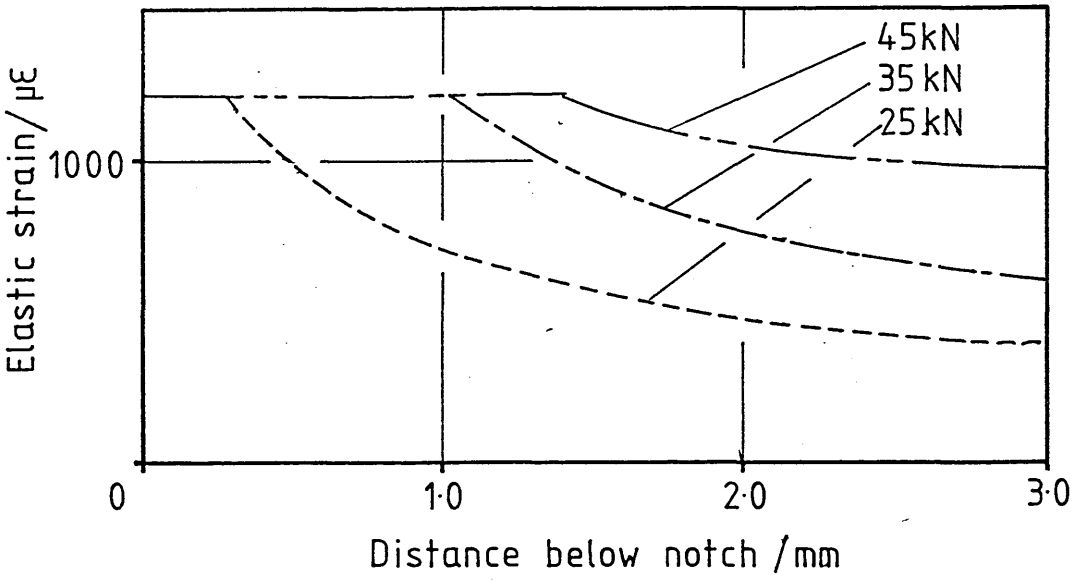

Fig. 5.51
U Notch EN1A

Elastic Strain Gradient Below Notch - Plane Stress

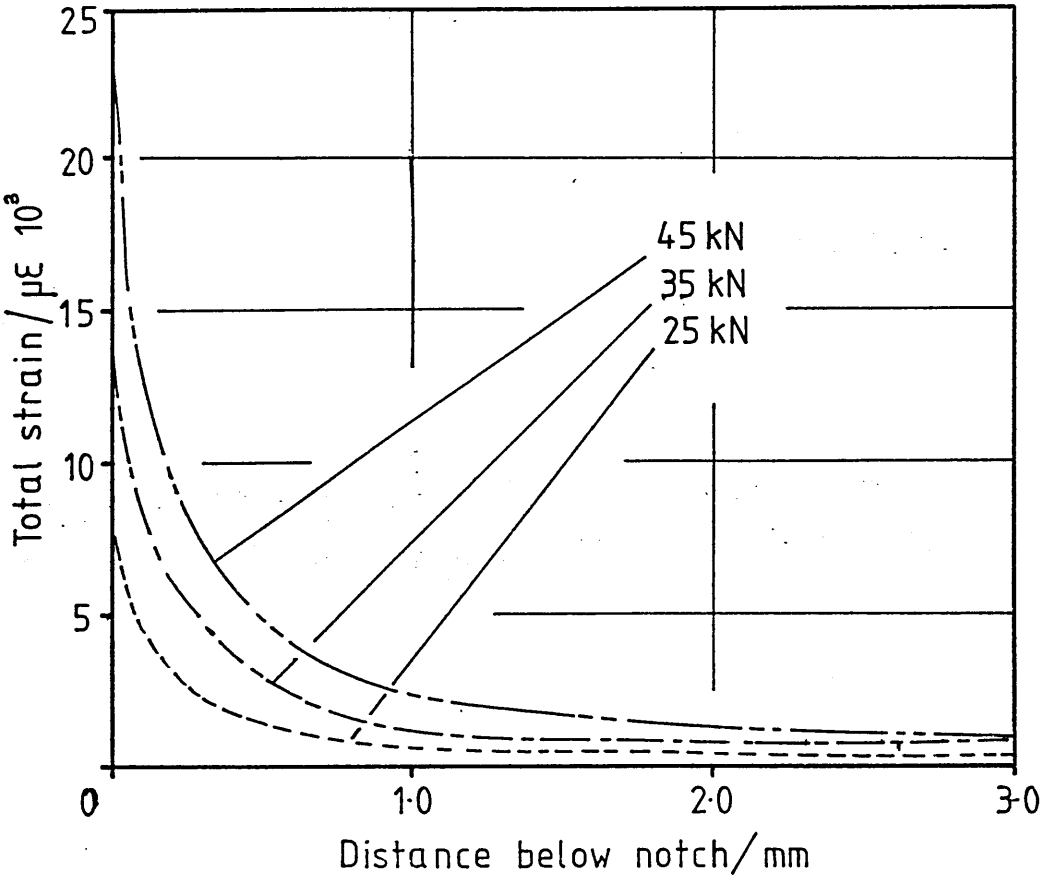

Fig. 5.52
V Notch EN1A

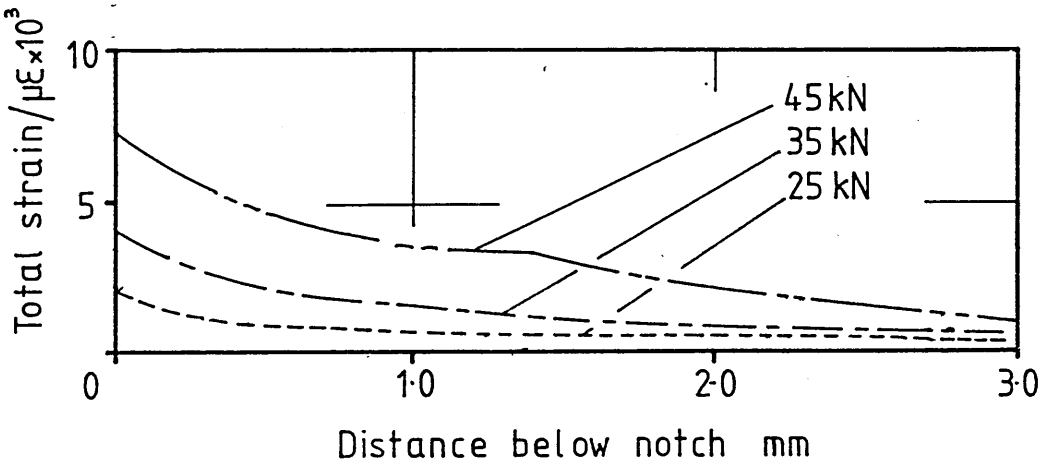

Fig. 5.53
U Notch EN1A

Total Strain Gradient Below Notch - Plane Stress

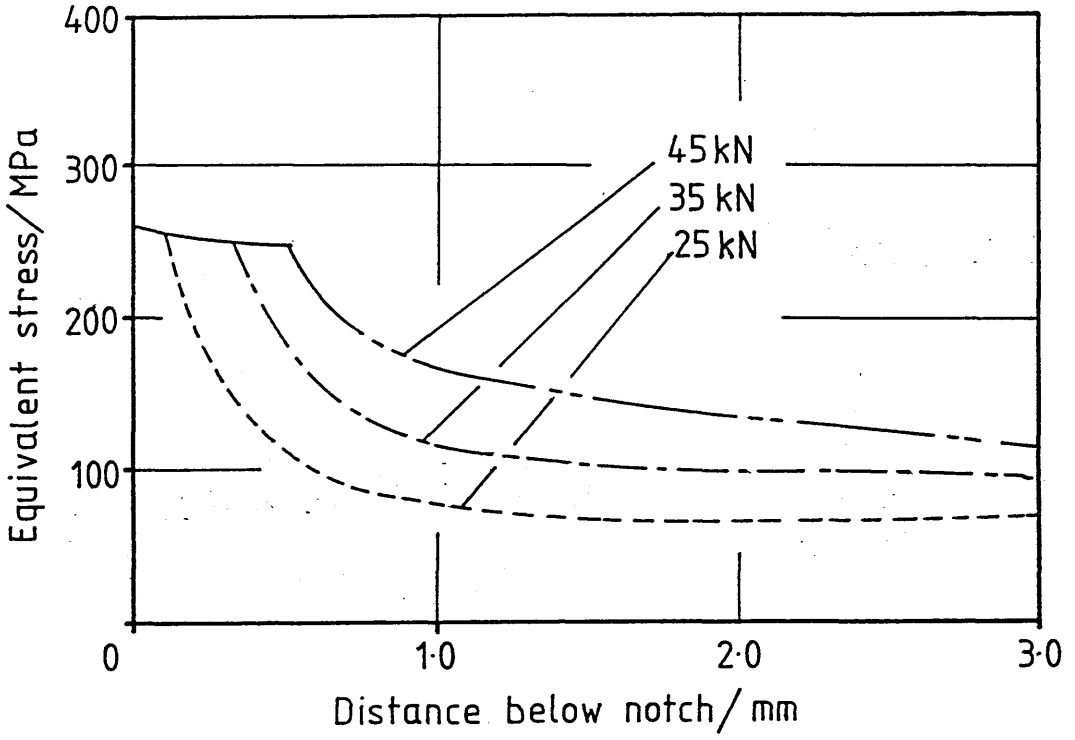

Fig. 5.54
V Notch EN1A

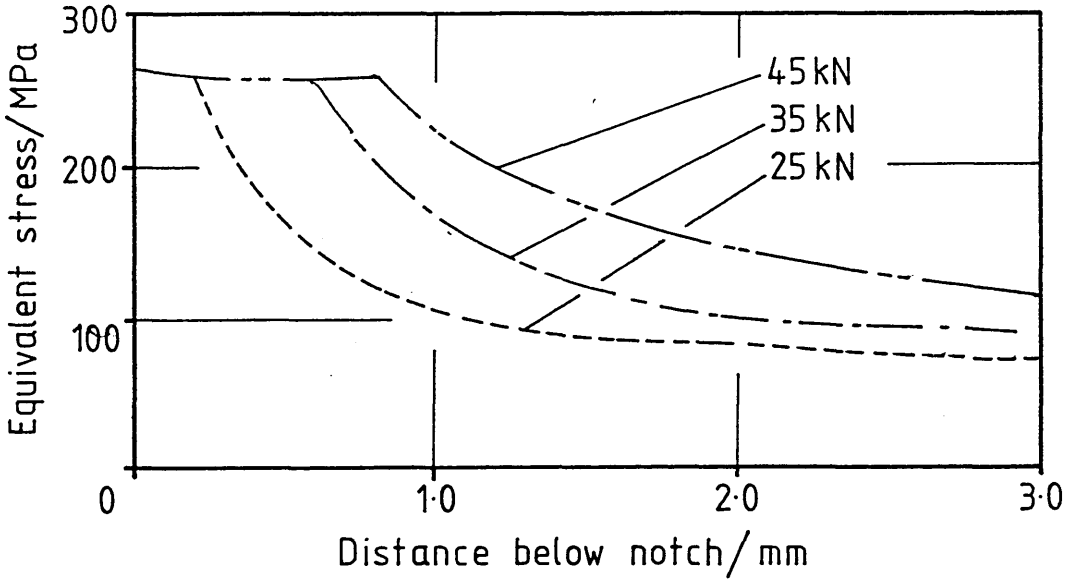

Fig. 5.55
U Notch EN1A

Stress Gradient Below Notch - Plane Strain

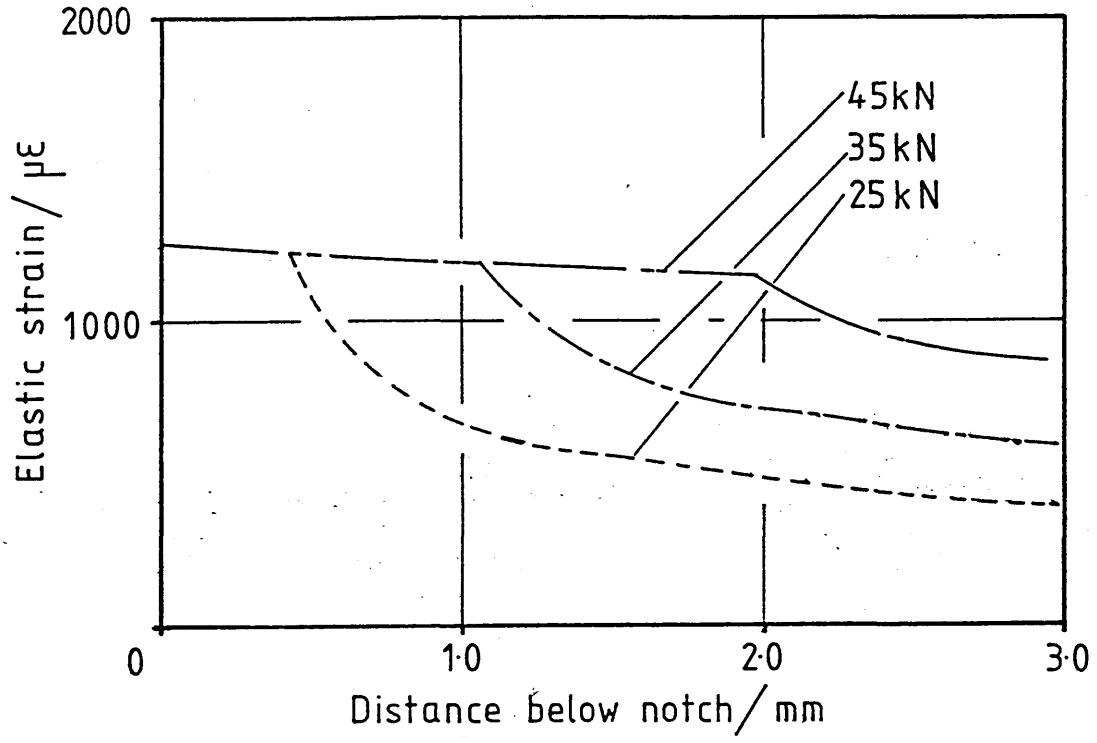

Fig. 5.56
V Notch EN1A

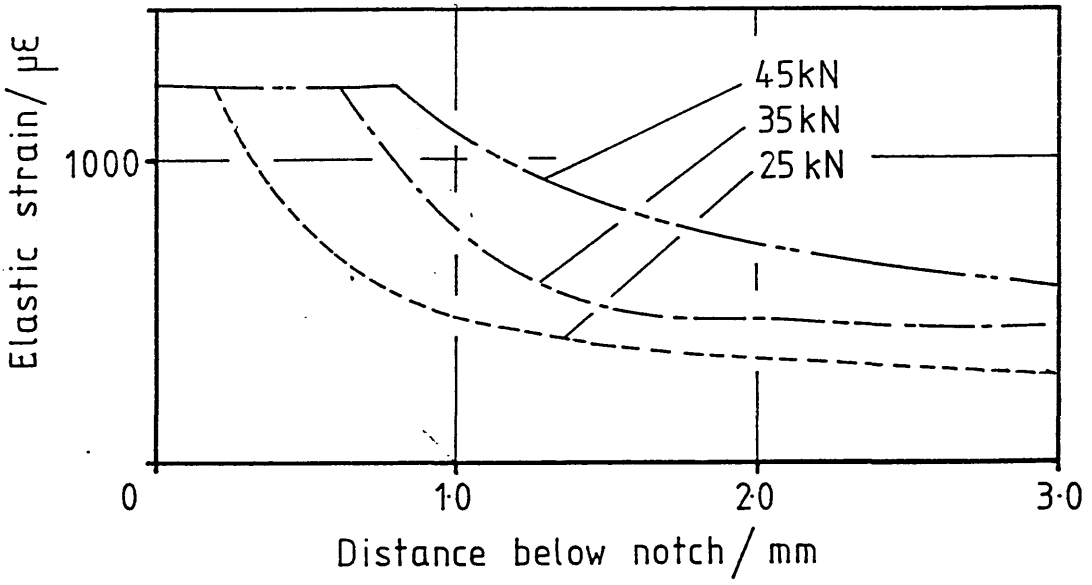

Fig. 5.57
U Notch EN1A

Elastic Strain Gradient Below Notch - Plane Strain

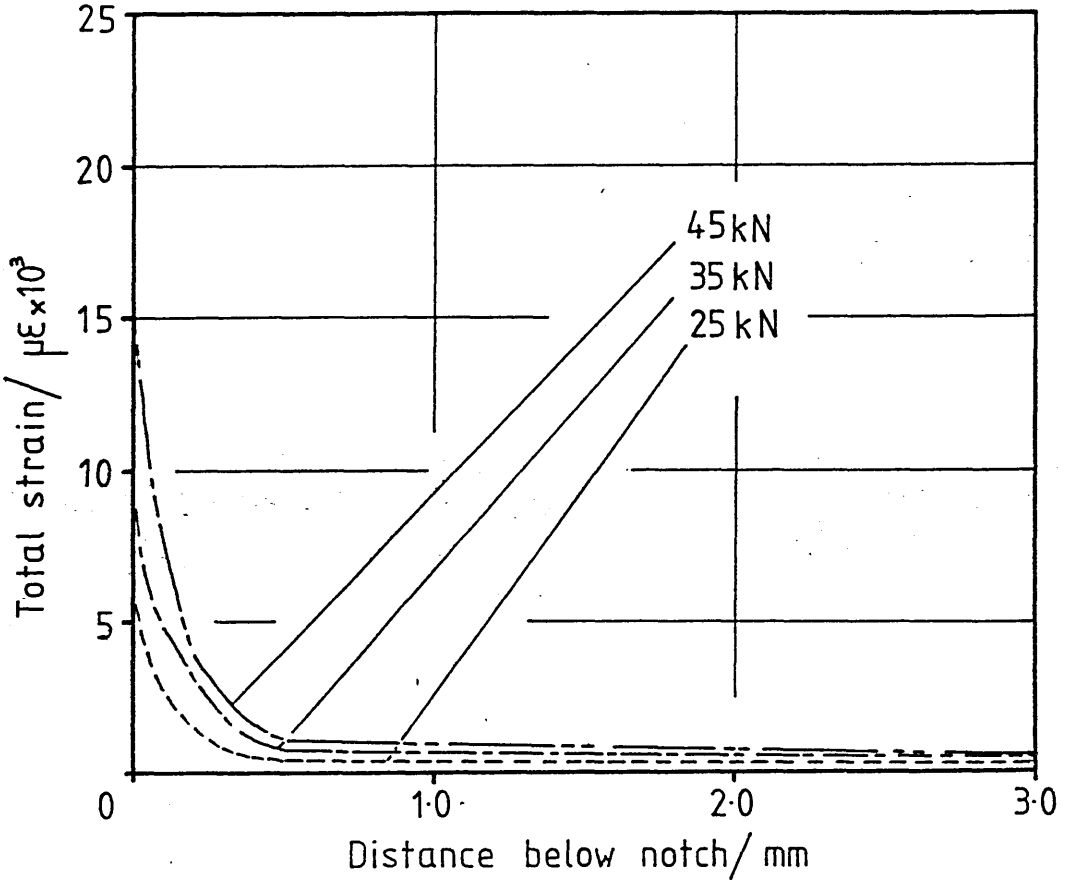

Fig. 5.58
V Notch EN1A

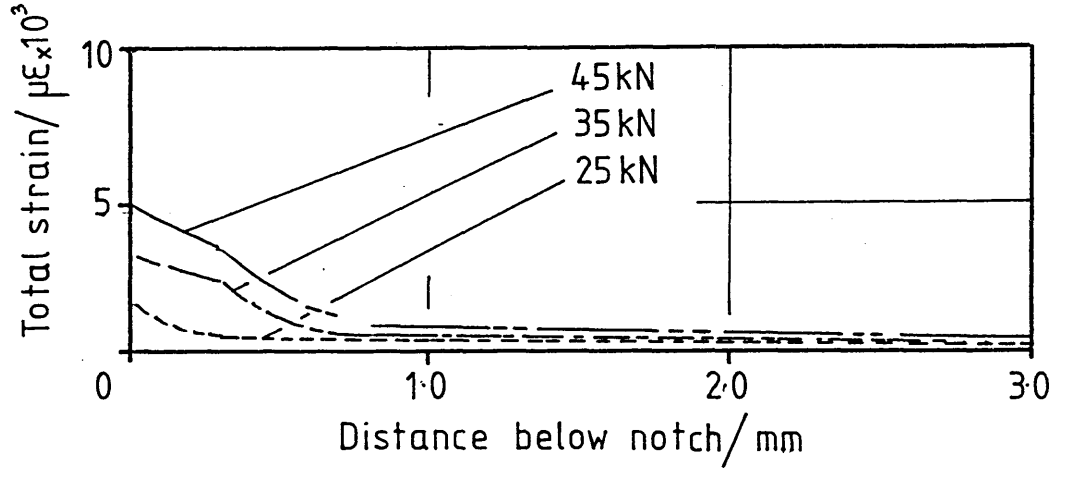

Fig. 5.59
U Notch EN1A

Total Strain Gradient Below Notch - Plane Strain

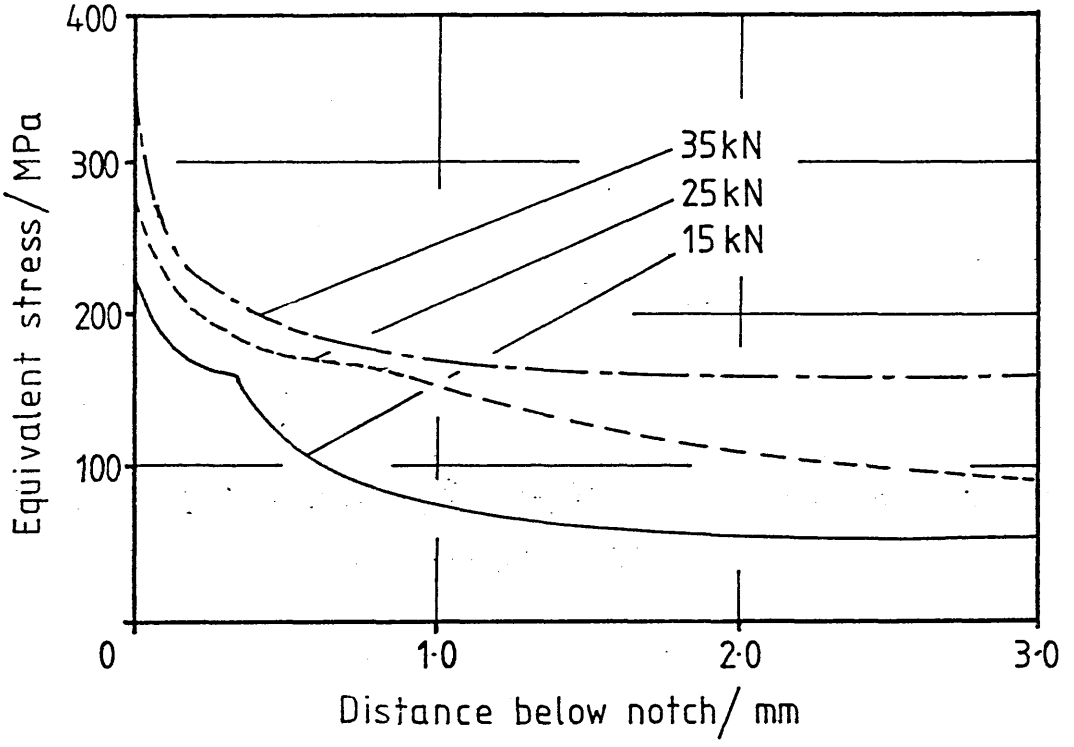

Fig. 5.60
V Notch NE8

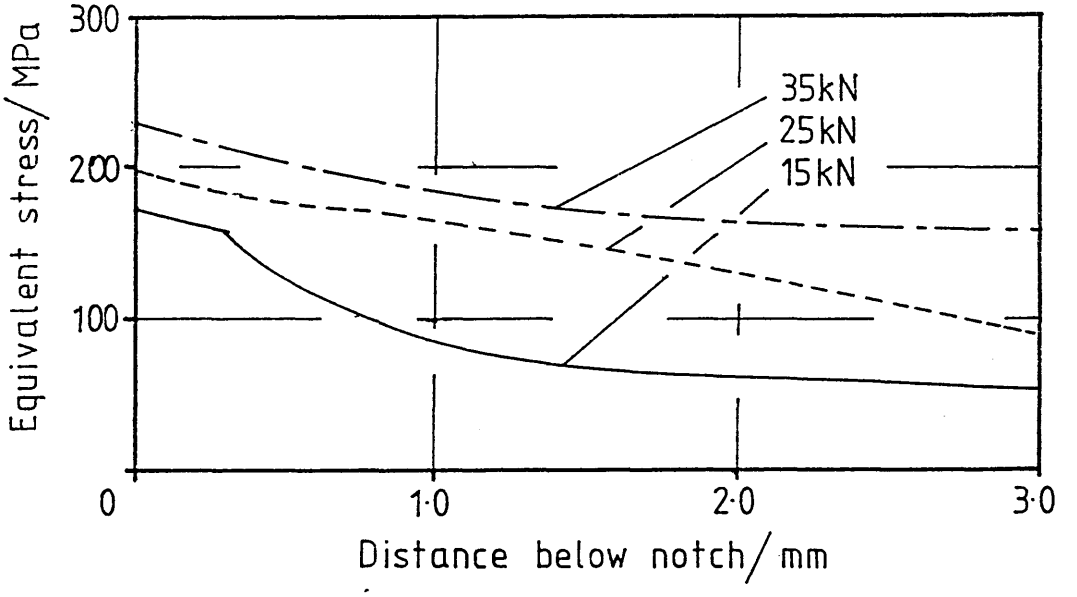

Fig. 5.61
U Notch NE8

Stress Gradient Below Notch - Plane Stress

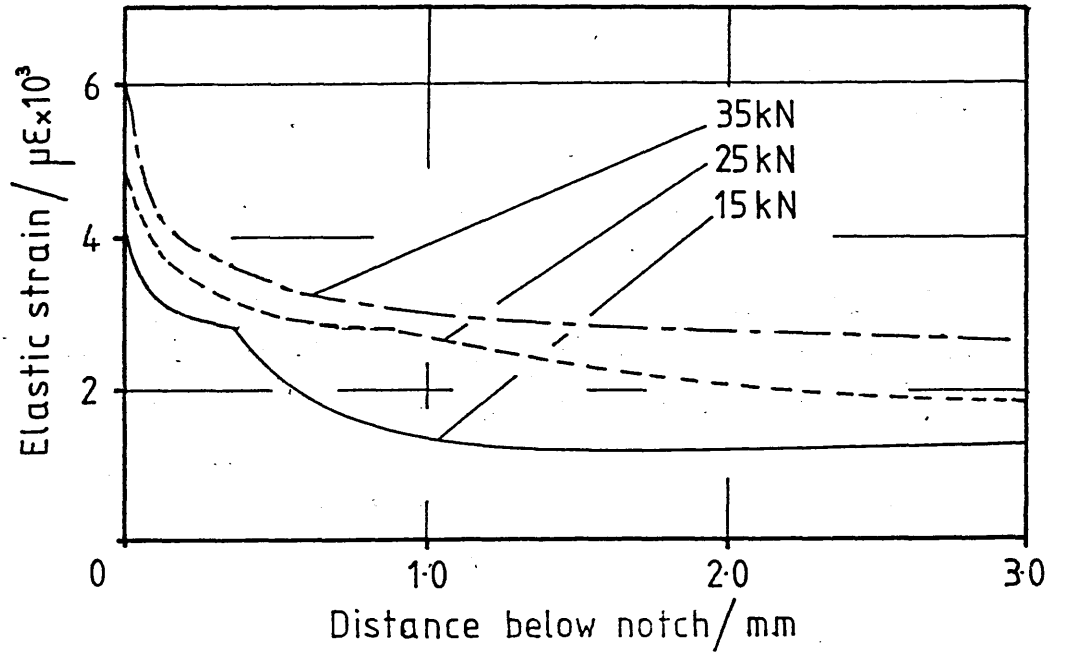

Fig. 5.62
V Notch NE8

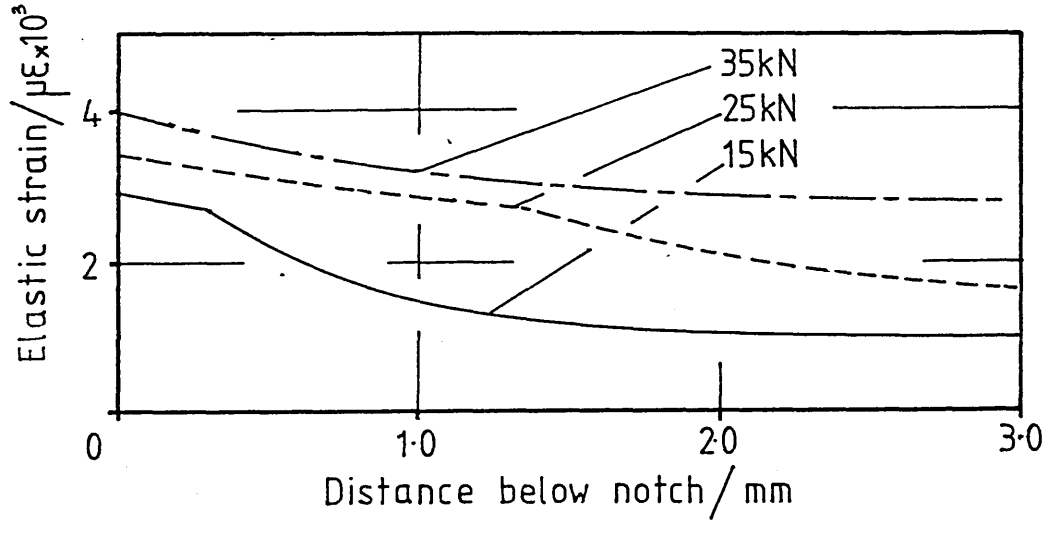

Fig. 5.63
U Notch NE8

Elastic Strain Gradient Below Notch - Plane Stress

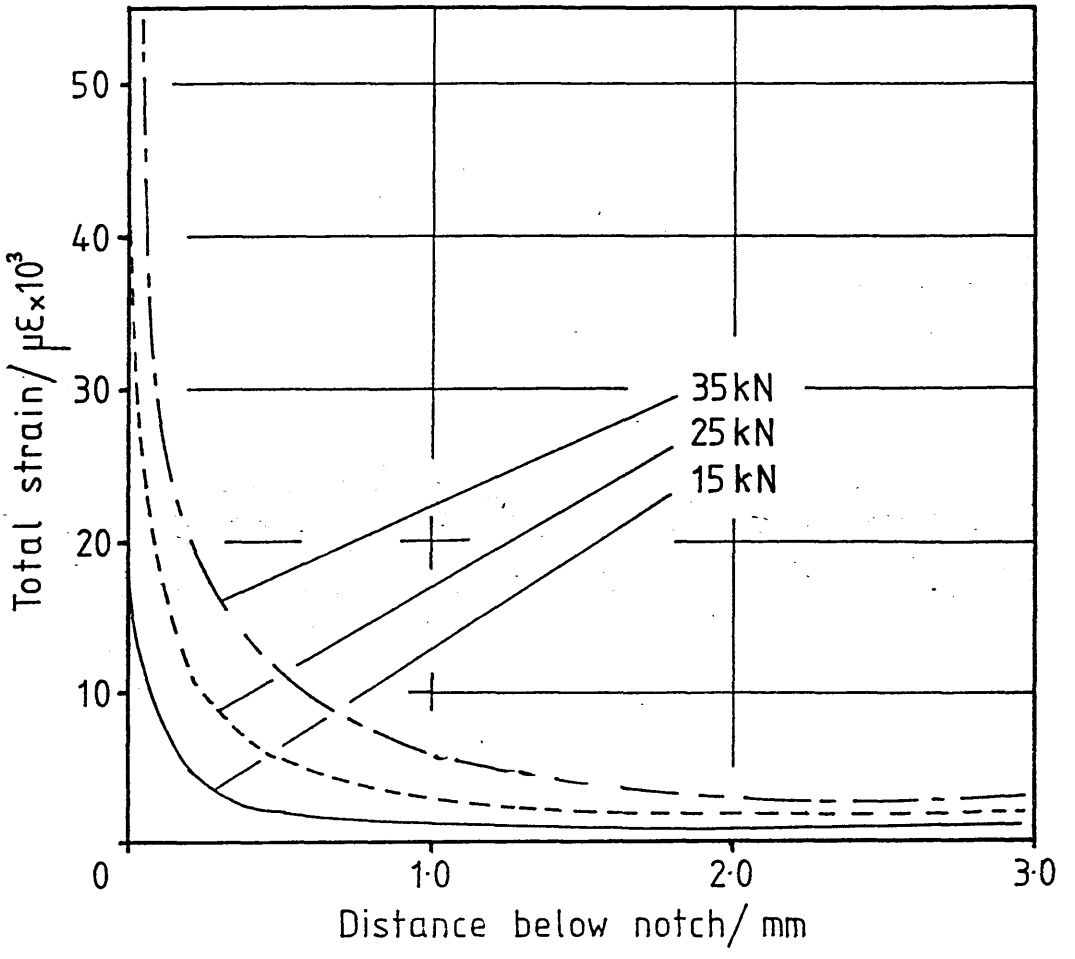

Fig. 5.64
V Notch NE8

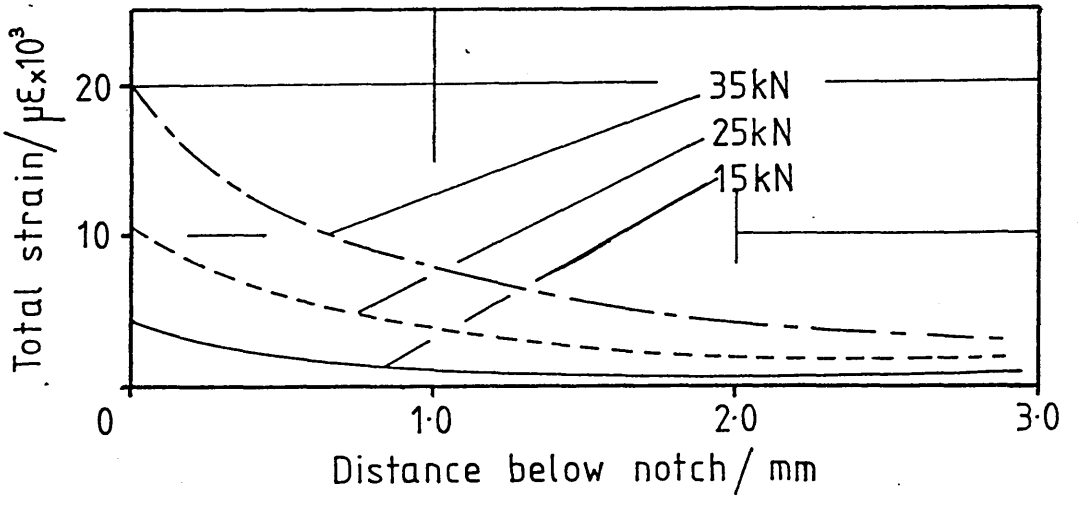

Fig. 5.65
U Notch NE8

Total Strain Gradient Below Notch - Plane Stress

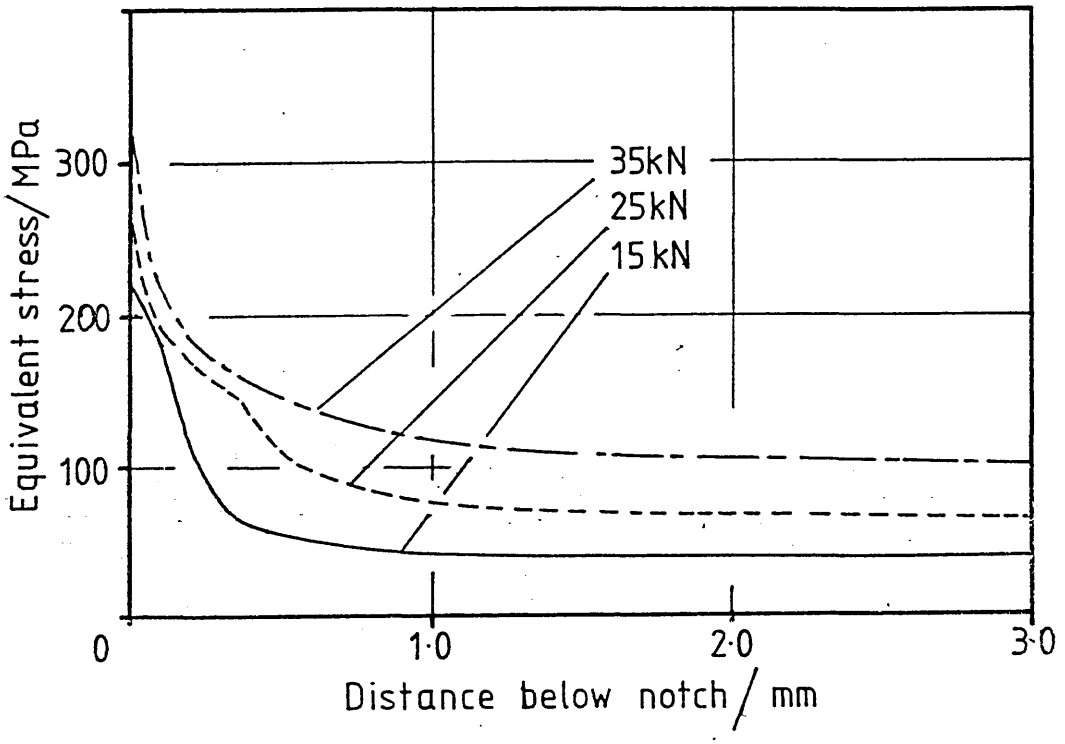

Fig. 5.66
V Notch NE8

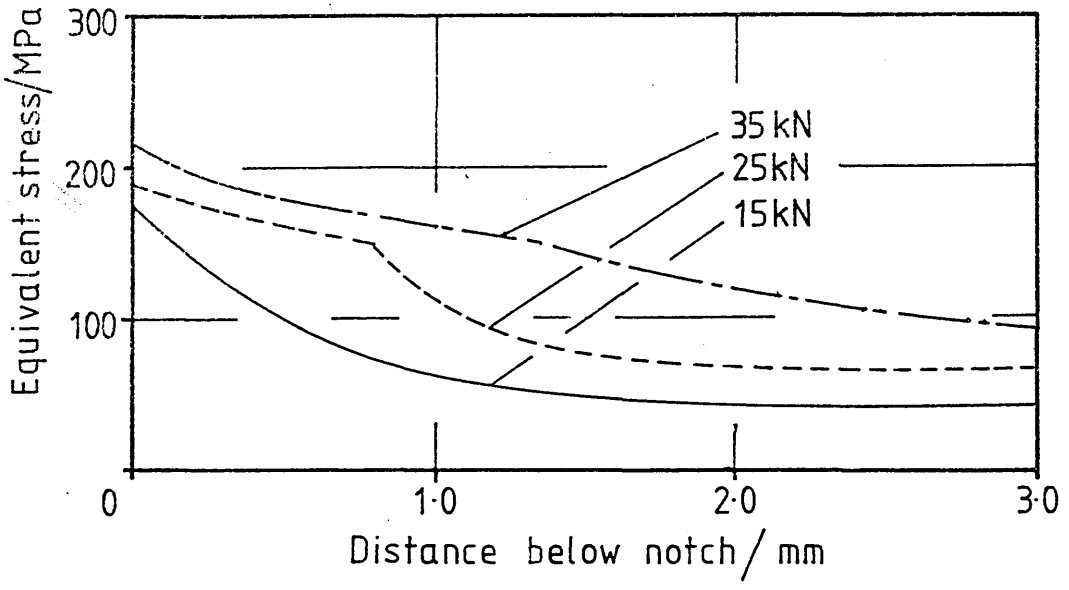

Fig. 5.67
U Notch NE8

Stress Gradient Below Notch - Plane Strain

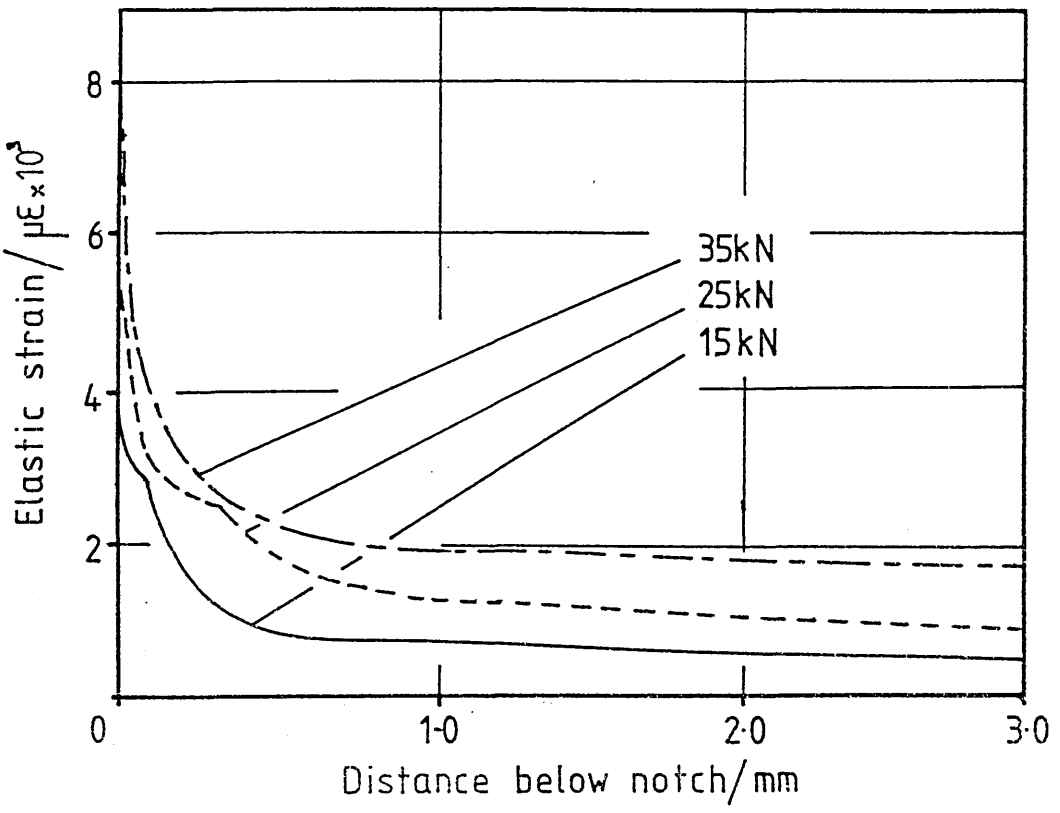

Fig. 5.68
V Notch NE8

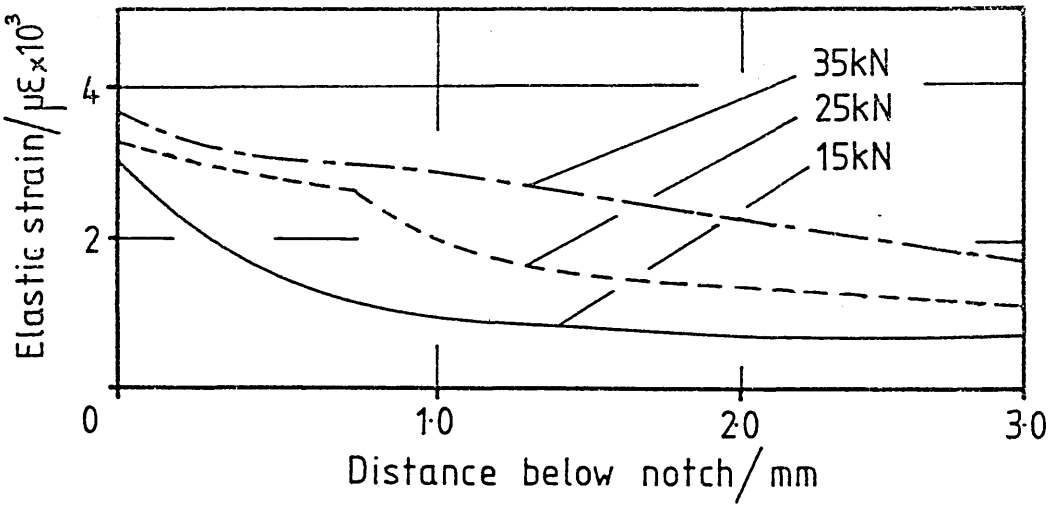

Fig. 5.69
U Notch NE8

Elastic Strain Gradient Below Notch - Plane Strain

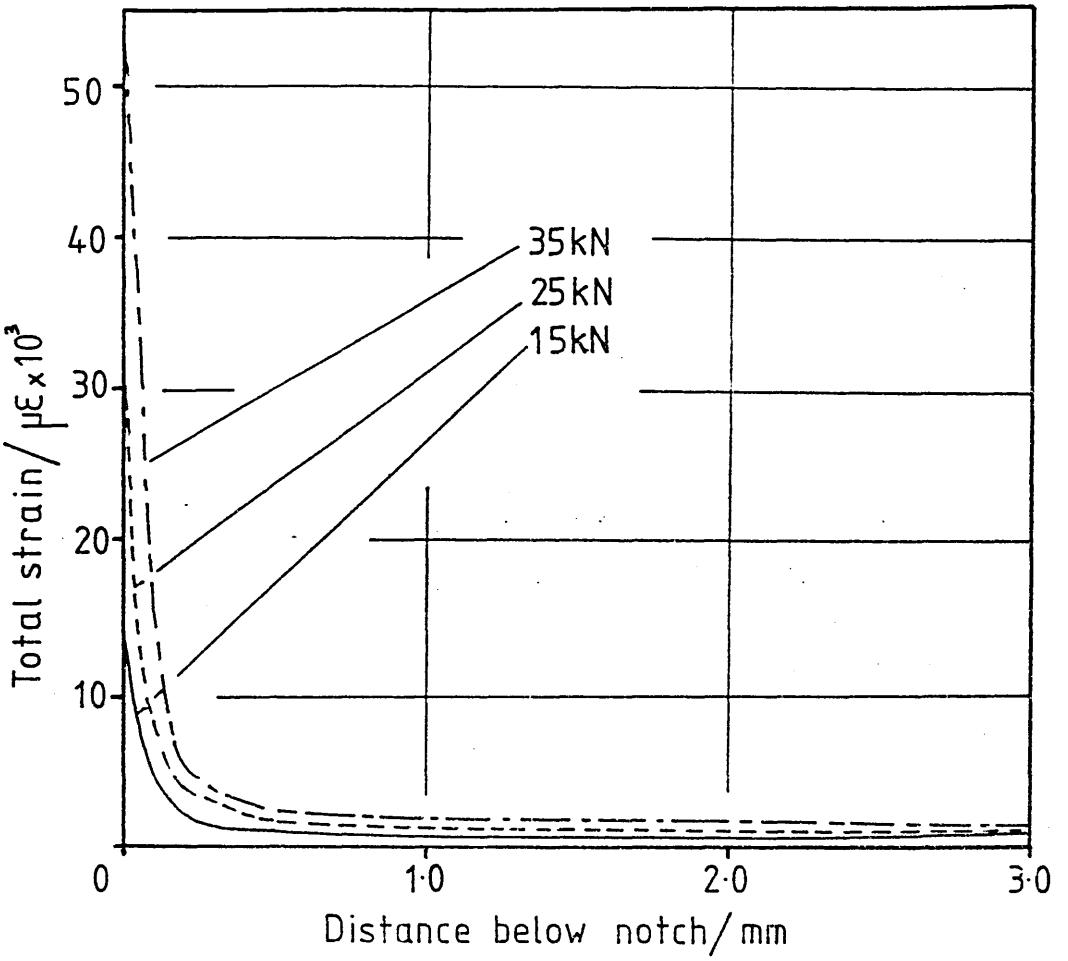

Fig. 5.70
V Notch NE8

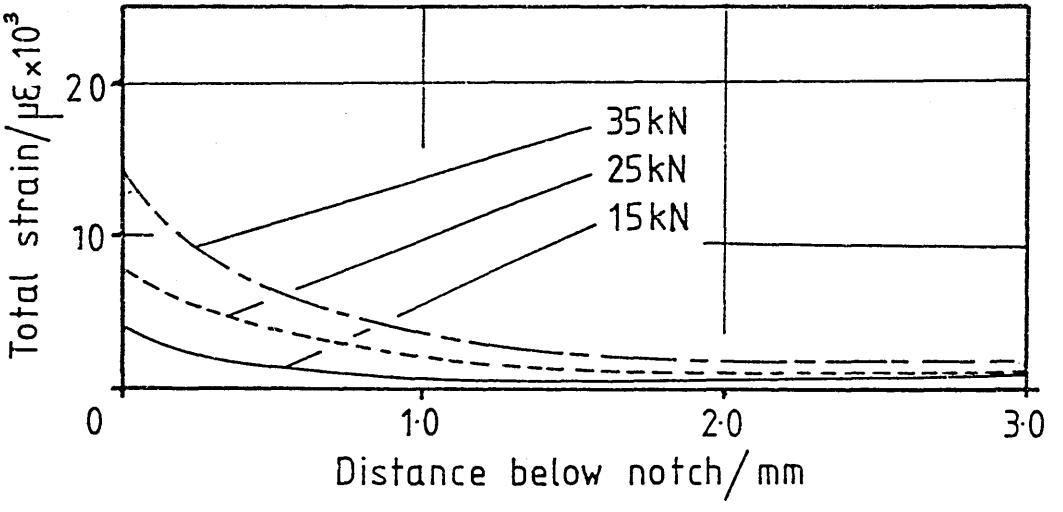

Fig. 5.71
U Notch NE8

Total Strain Gradient Below Notch Plane Strain

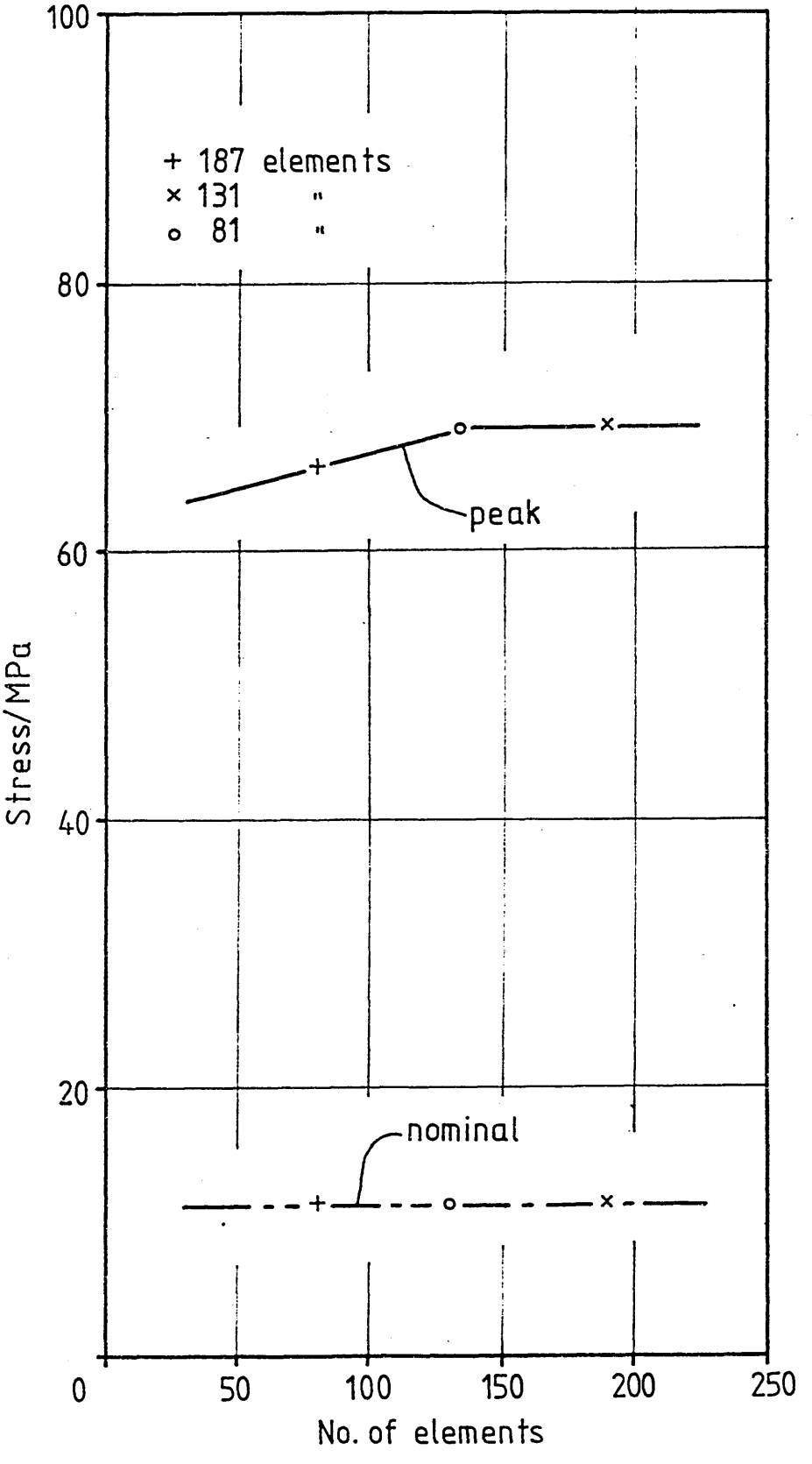

Fig. 5.72 V Notch EN1A : Plane Stress : Convergence of Elastic FE Solution

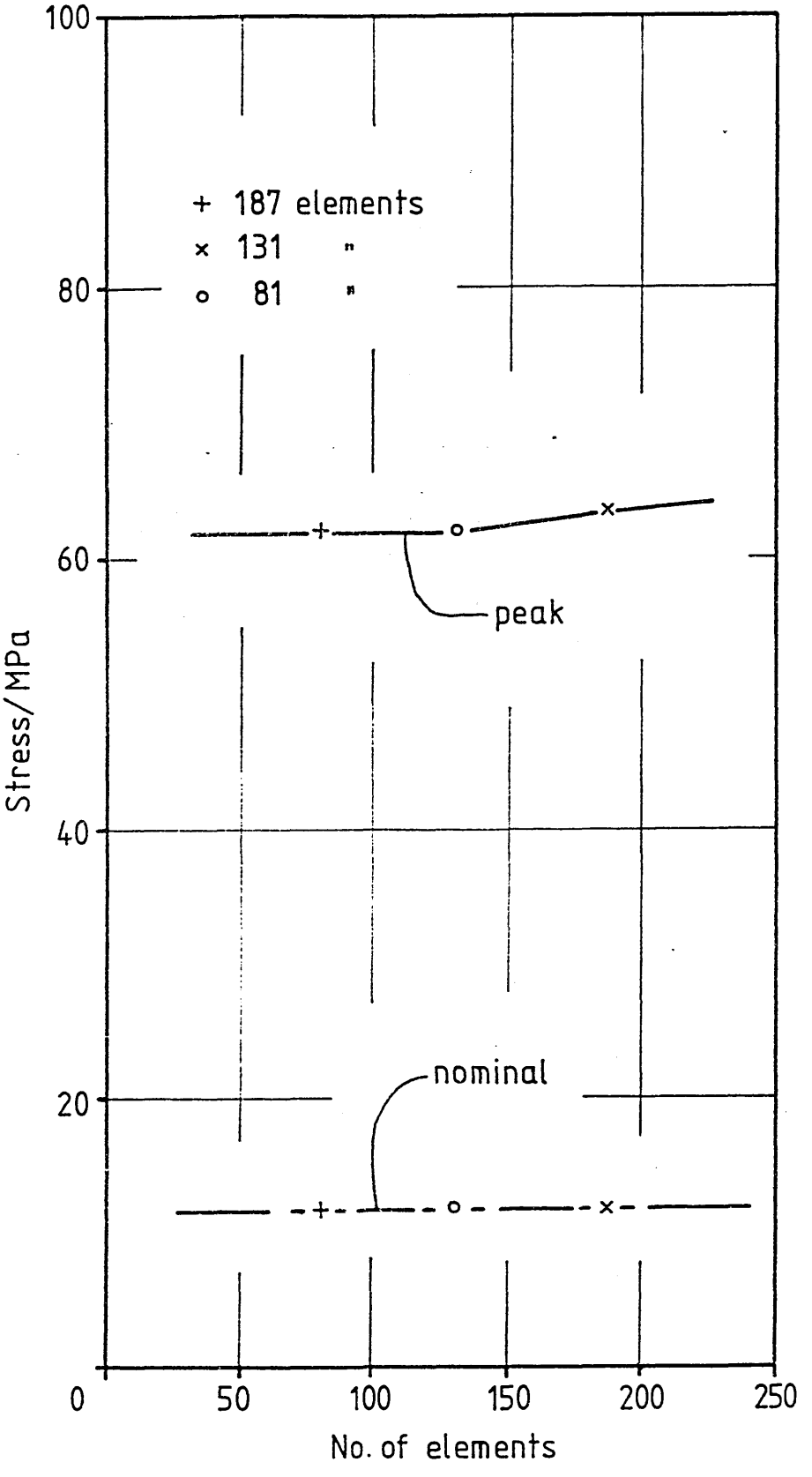

Fig. 5.73 V Notch EN1A : Plane Strain : Convergence of Elastic FE Solution

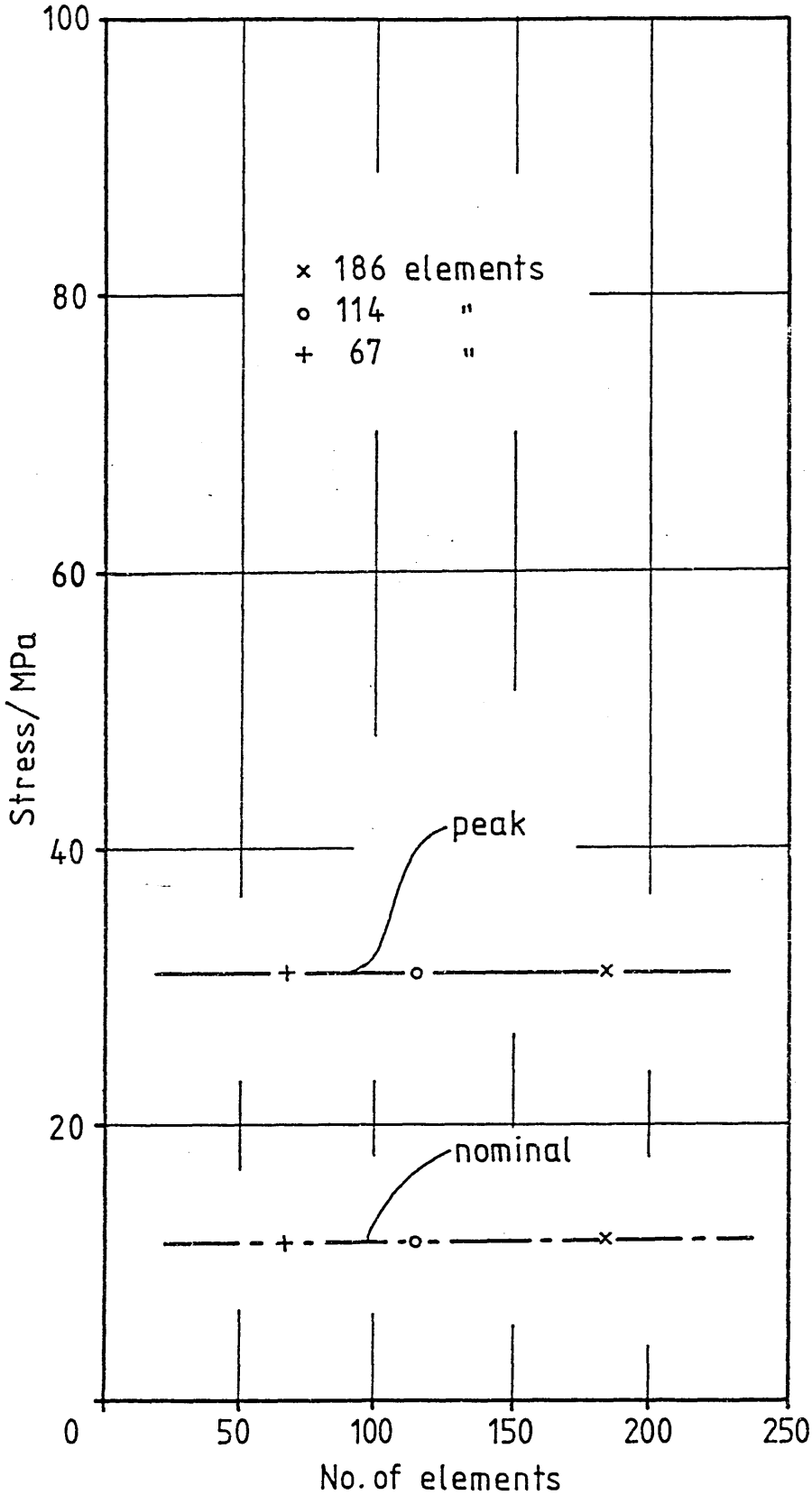

Fig. 5.74 U Notch EN1A : Plane Stress : Convergence of Elastic FE Solution

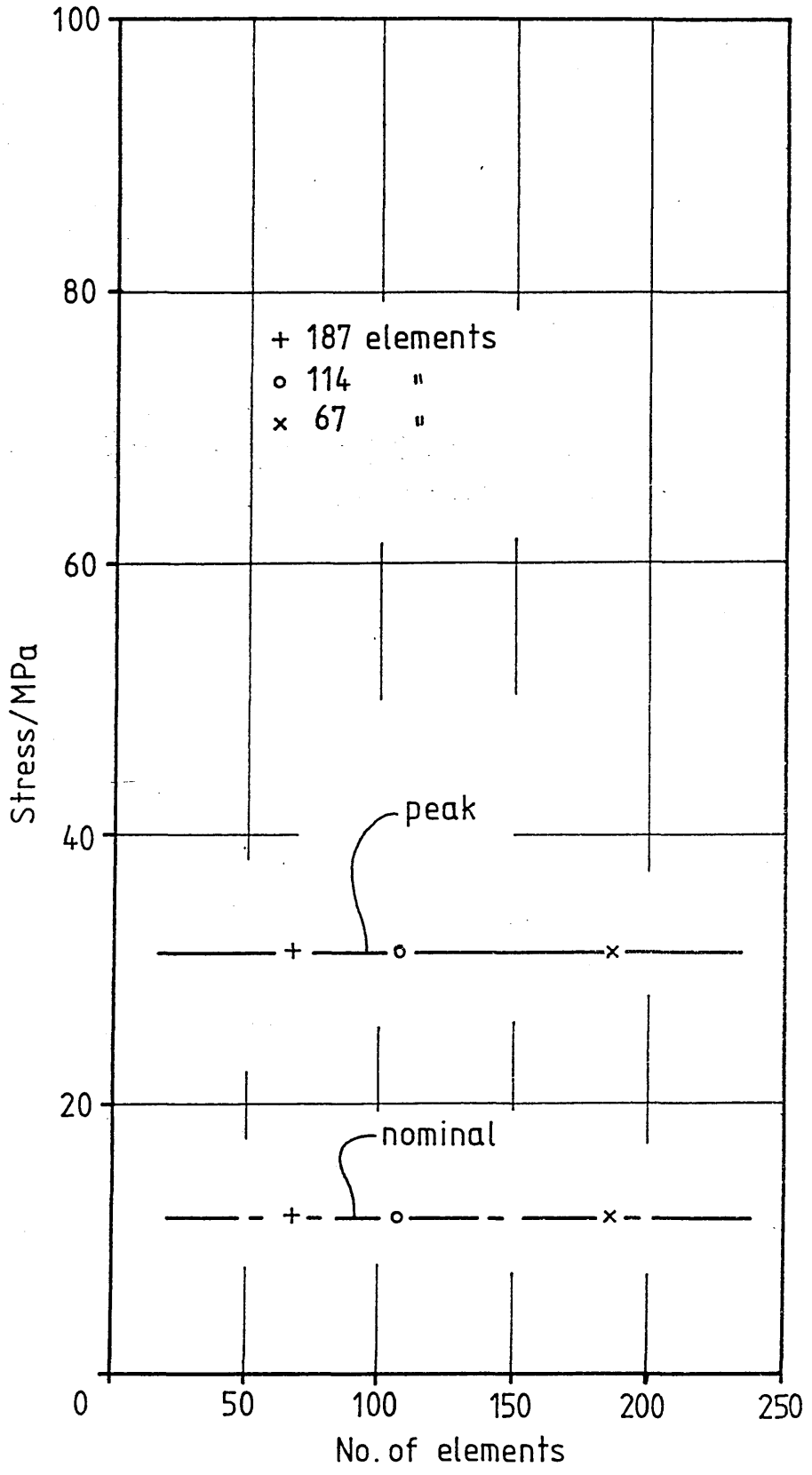

Fig. 5.75 U Notch EN1A : Plane Strain :
Convergence of Elastic FE Solution

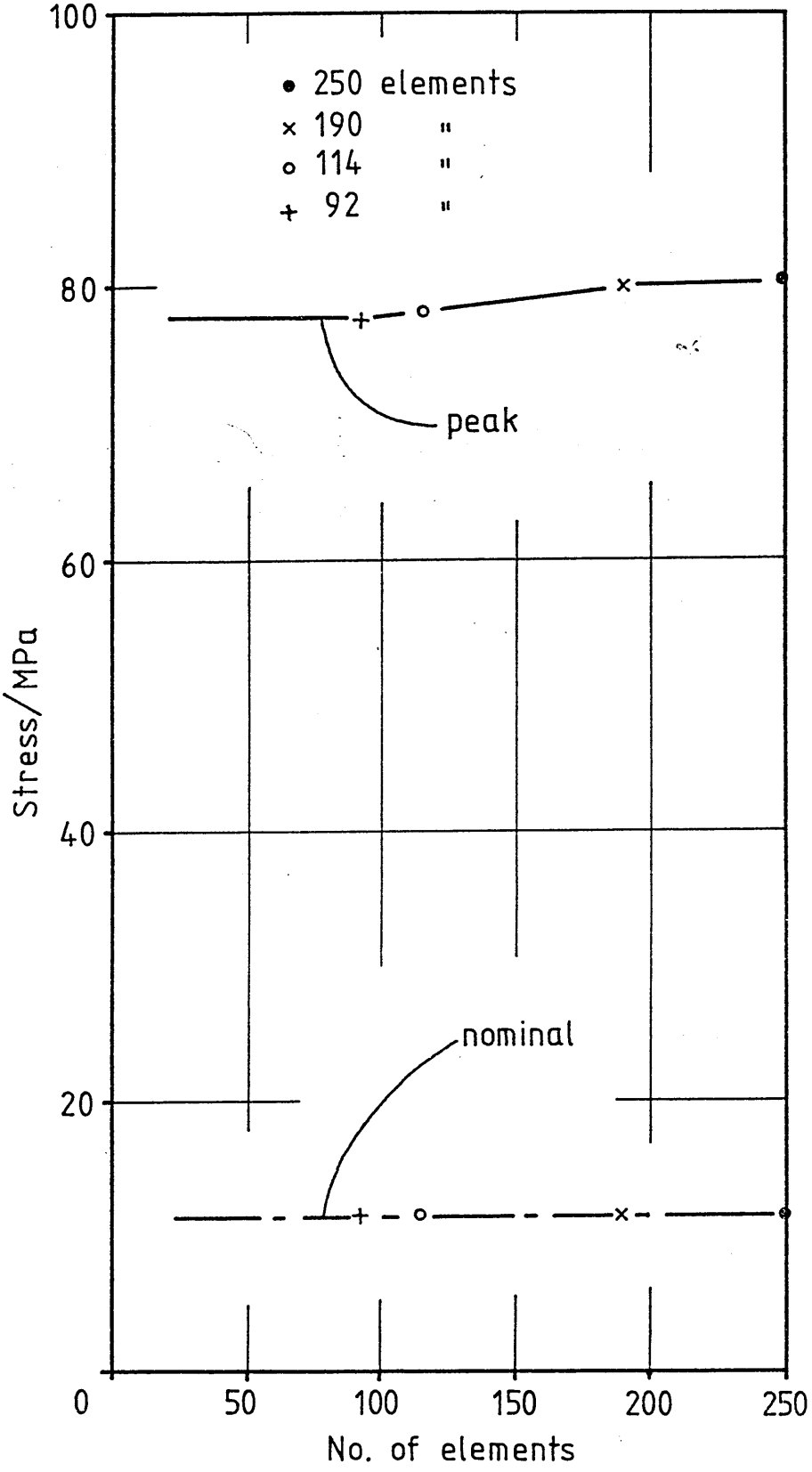

Fig. 5.76 V Notch NE8 : Plane Stress : Convergence of Elastic FE Solution

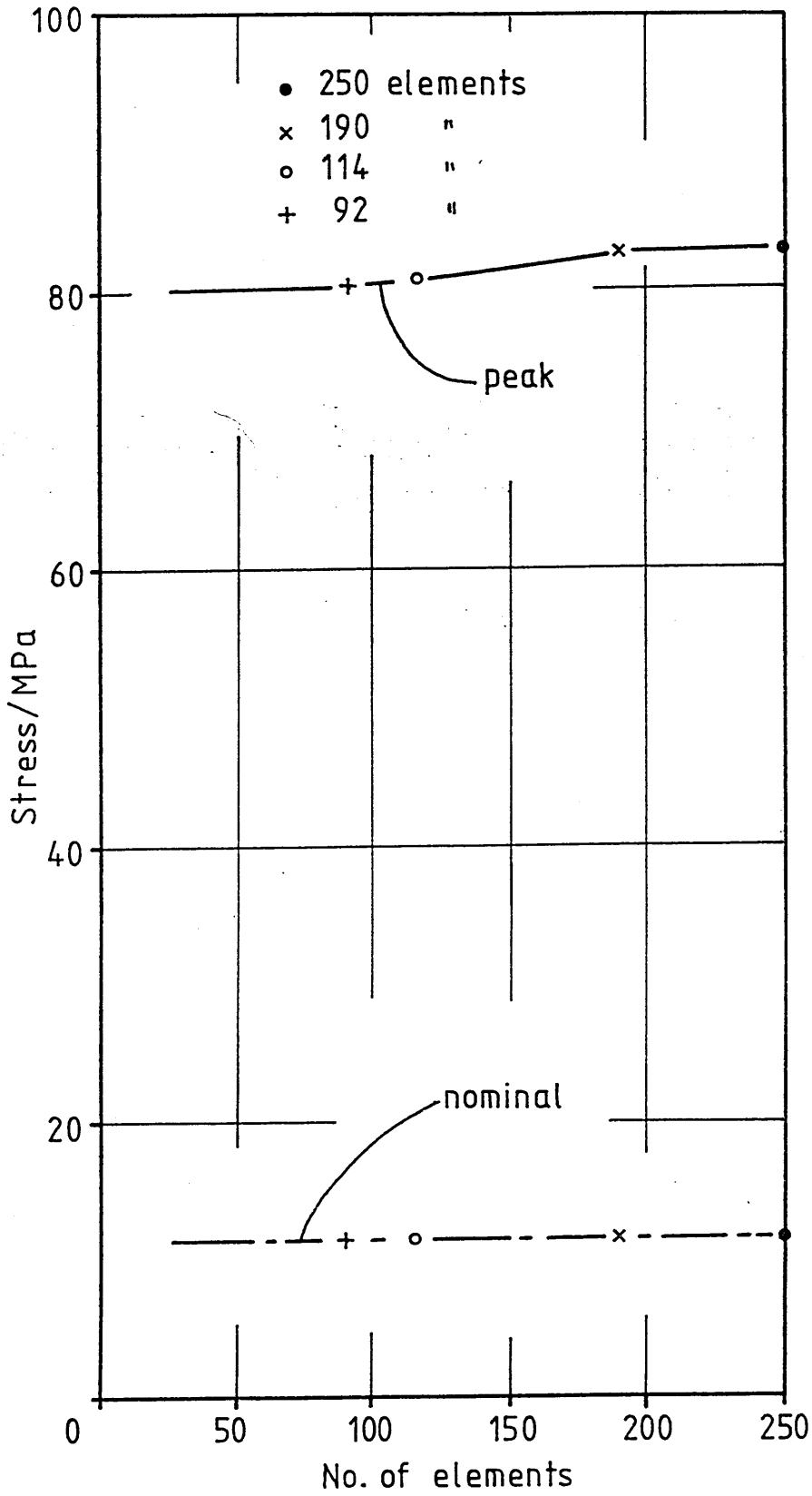

Fig. 5.77 V Notch NE8 : Plane Strain :
Convergence of Elastic FE Solution

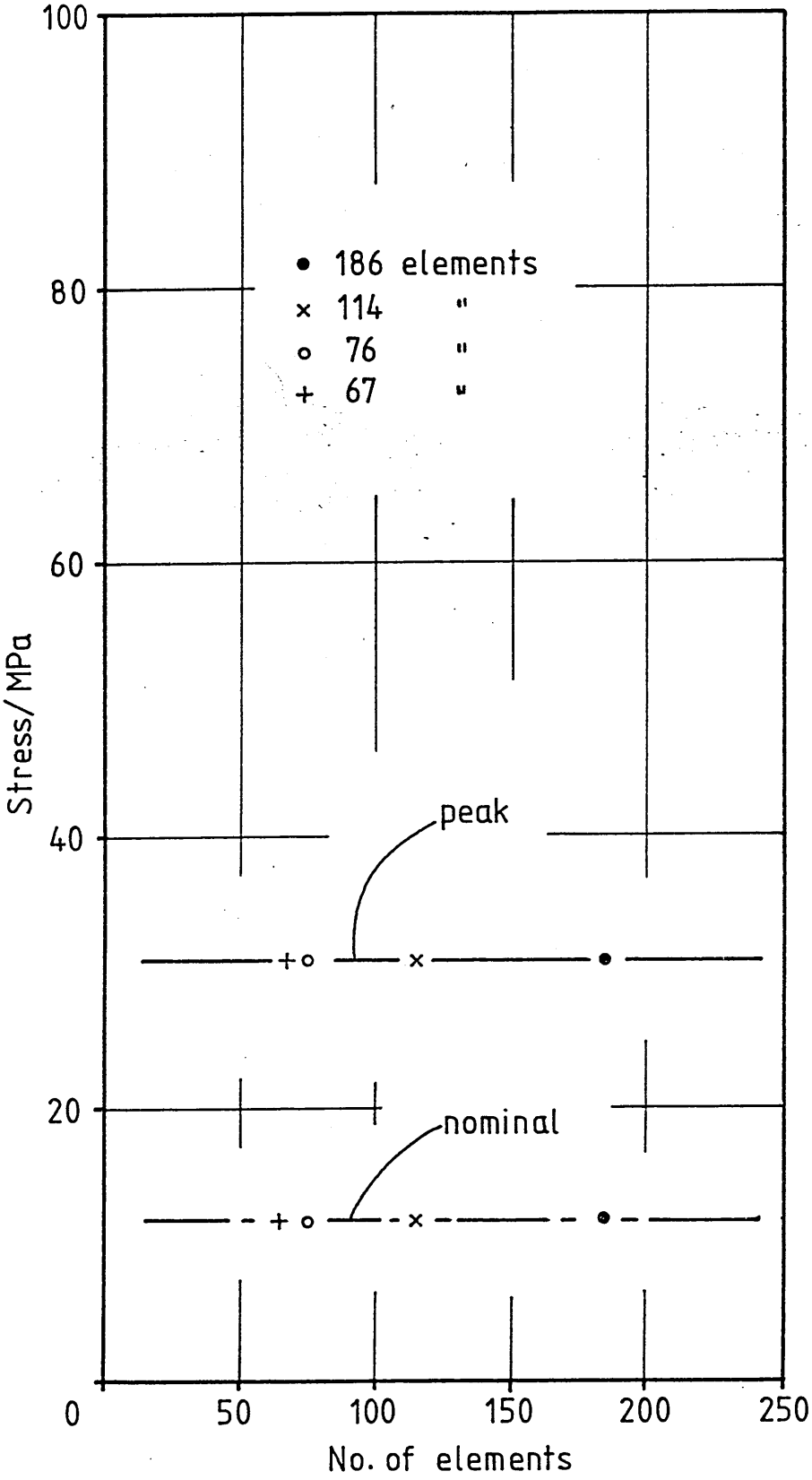

Fig. 5.78 U Notch NE8 : Plane Stress :
Convergence of Elastic FE Solution

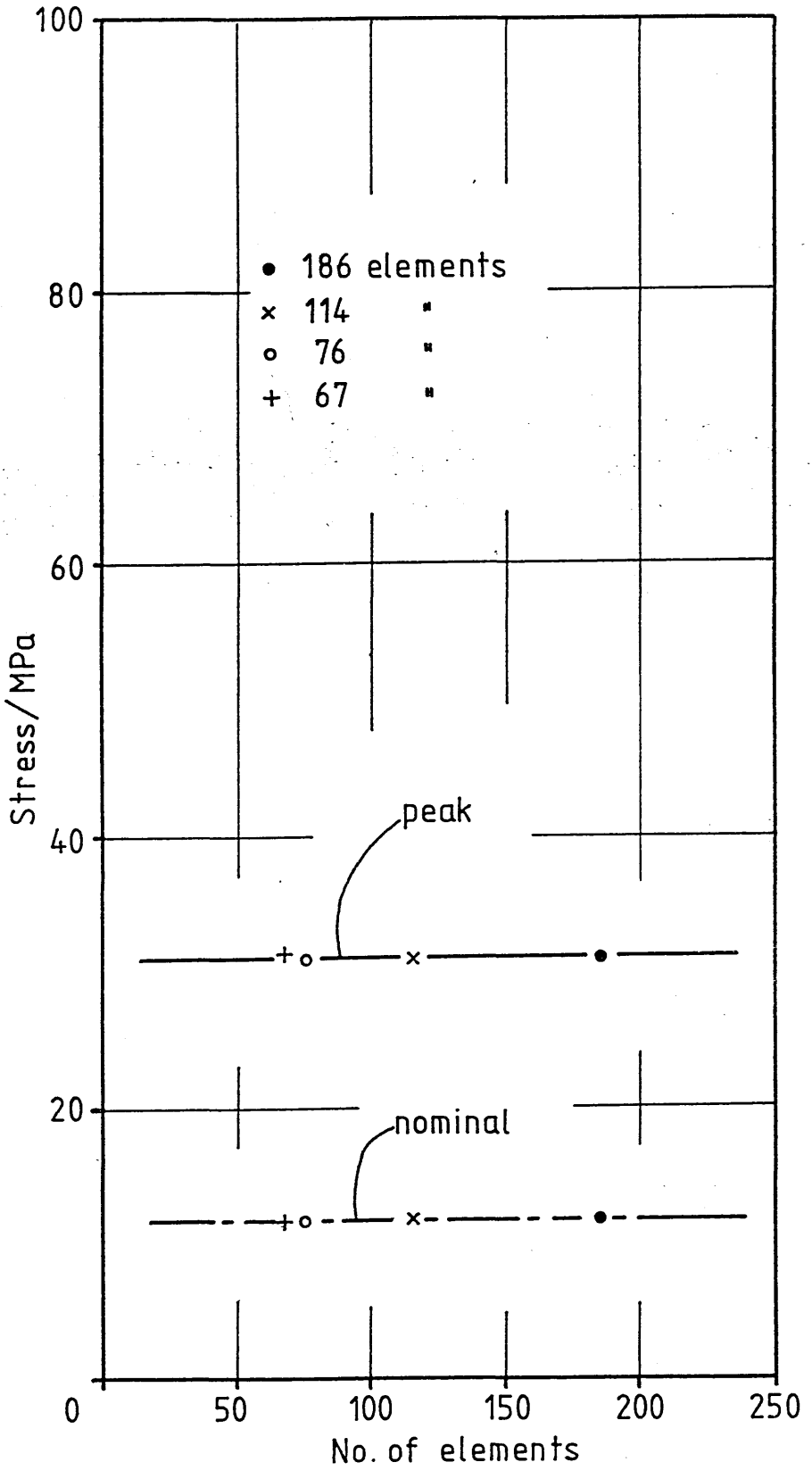

Fig. 5.79 U Notch NE8 : Plane Strain :
Convergence of Elastic FE Solution,

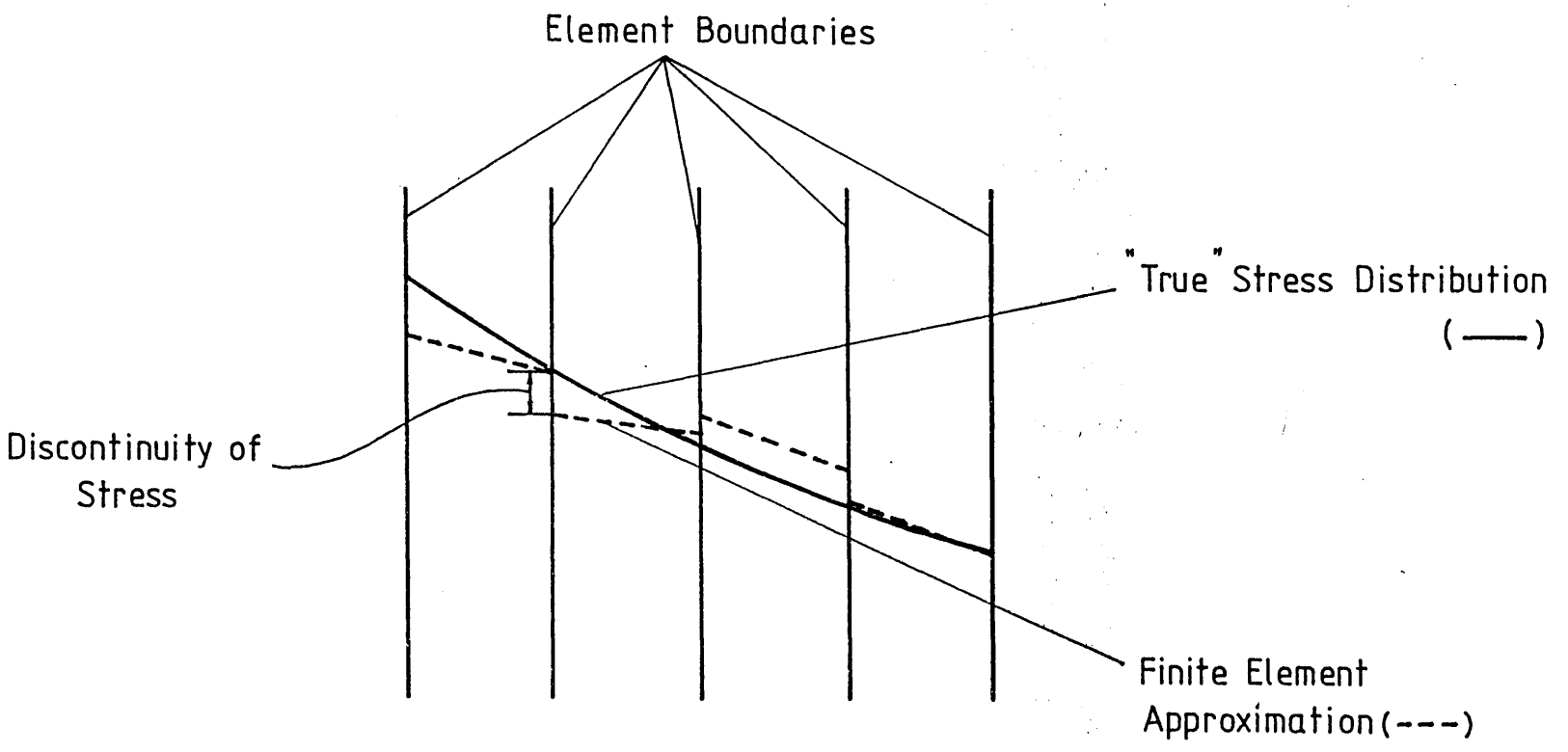

Fig. 5.80 Cöntinuity of Stress Across Adjacent Element Boundaries in FE Solution

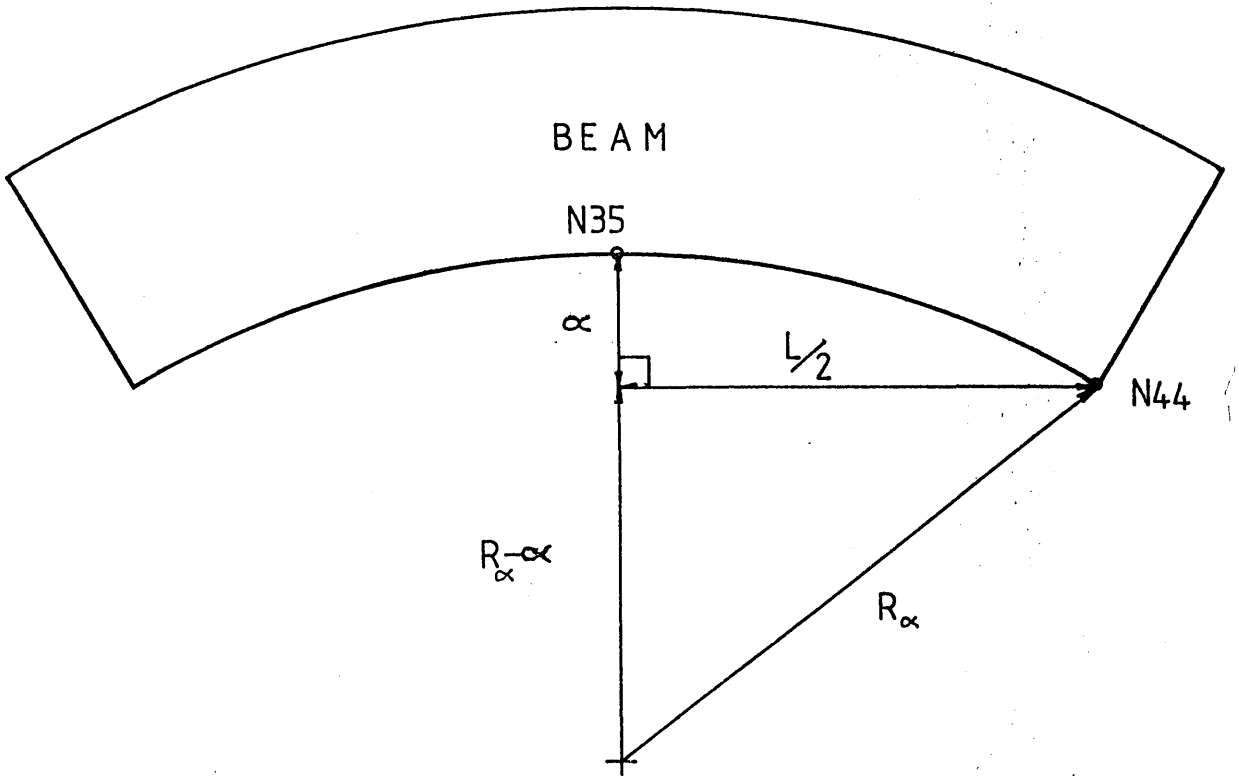

Fig. 5.81 Notation in Calculation of Elastic Displacement of Stressed Beam

CHAPTER 6 - DETERMINATION OF THE VARIATION OF THE ELECTRICAL RESISTIVITY WITH STRAIN

6.1 INTRODUCTION

Inspection of eqn 6.1 for the AC skin depth, δ, reveals a number of important points.

$$\delta = \left(\frac{\rho}{\pi\mu f}\right)^{\frac{1}{2}} \qquad 6.1$$

In most practical situations the frequency of the energising AC signal, f, is kept constant and therefore the skin depth is governed solely by the electrical resistivity (ρ) and the magnetic permeability ($\mu = \mu_r\mu_o$).

(NB It should be noted that when discussing variations in the magnetic properties of materials reference can either be made to μ or the relative magnetic permeability (μ_r) with equal validity. The two parameters are proportional to each other with the constant of proportionality being the permeability of free space (μ_o). Therefore any variation of magnetic properties reflected by changes in μ is shown equally in μ_r, and vice versa).

Changes in both these parameters are caused through alterations to the basic microstructure of the material under consideration. ρ is affected by the ease with which the conduction electrons may pass through the surrounding lattice structure, μ_r by the mobility and directional alignment of the magnetic domains, see Appendix I. Since strain and deformation result in disruption of the basic lattice structure it could be expected that strain effects would also manifest themselves in the observed ACPD response.

To successfully explain the complex response seen in the EN1A specimens and the contrastingly null response in the case of NE8 it would be useful to know how each of these two parameters vary independently with increasing strain. If possible the measurements should be of a quantitative nature giving reliable absolute values.

Neither of these two parameters is particularly straightforward to measure accurately, and it was not known beforehand if independent measurement of each as they varied with increasing strain was indeed practical or possible.

μ_r is by far the more complex of the two parameters. It is not single valued, being dependent upon the absolute level of magnetic flux density established in the material and the excitation history. Details of the measurement of this parameter are given in the following section, chapter 7.

ρ is marginally the easier of the two to measure, the additional complexity of measuring strain concurrently needing to be taken into account.

6.2 CONSIDERATIONS IN THE MEASUREMENT OF THE ELECTRICAL RESISTIVITY

ρ, or equivalently the electrical conductivity, $\sigma = 1/\rho$, is determined by the ease of passage of the conduction electrons through the surrounding ionic lattice. Essentially ρ can be thought of as a DC property of the material and this provided the necessary first step toward the development of a successful measuring technique. By passing a constant DC signal through a tensile specimen and measuring the change in voltage between two suitable points on the surface it should be possible to record the strain/resistivity history of the material. There were, however, a number of further considerations in such an apparently simple procedure.

The value of ρ for most metals and alloys is very small. Hence to produce a measurable potential drop a large DC signal (20-30A) would be required. With such a large DC signal there was likely to be appreciable heating of the specimen leading to thermal effects influencing the measured potential across the specimen. To circumvent this problem a "dummy" specimen in series with the "active" strained specimen was used. Any fluctuations in the active voltage signal through heating effects would then be reflected in the "dummy" signal and could be compensated for.

Additionally, since the observed voltage changes were likely to be in the μV range, a high quality DC amplifier was required together with a very stable DC power supply.

6.3 TESTPIECE SPECIFICATION AND PREPARATION

The aim of the experimental program was to quantitatively assess the effect of strain on the value of ρ for both the materials, EN1A and NE8. To ease the experimental measurement and subsequent calculation of strain and resistivity a simple tensile geometry was used, see figure 6.1.

The specimen was purposely designed to be sufficiently long (400mm) so as to provide a suitable gauge length of uniform tensile strain over which the voltage pickups and extensometer could be attached and measurements conducted.

The geometry of the specimen was nominally circular (Ø20mm) with two symmetrical flats machined on either side to give a uniform central region of cross-sectional area 281.46mm^2.

Onto the ends of the specimen a standard large metric thread was machined. Between the thread and the central flats a distance of 70mm was left to allow for the attachment of the current inputs. This allowed the inputs to be attached 65mm from the voltage pick-ups. (As a rule of thumb, attachment >3Øs from pick-ups was sufficient to produce a uniform DC electric field across the central portion of the specimen).

The load was applied via two large metric nuts attached to the ends of the specimen. The nuts bore onto a steel spacing washer and specially designed Tuffnell collar ensuring electrical insulation of the specimen, see fig 6.2.

To ensure uniform material properties consistent with the earlier bend specimens both sets of tensile specimens were given identical heat treatments following machining.

Following heat treatment the diameter of the bar and distance across the flats were measured and a note made of the dimensions.

The current inputs and voltage pick-up wires were attached in the relative positions shown in fig 6 .3.

The current inputs consisted of multi-strand plastic-coated copper wire. These were clamped tightly to the specimen via hose clips, any surface scale or tarnish being removed beforehand using fine emery cloth.

The voltage pick-ups were of single strand 27SWG plastic coated copper wire and were spot-welded directly onto the surface of the specimen at the required locations. The central flats of the specimen were prepared beforehand with fine emery paper and a degreasing agent.

The voltage pick-up wires were then reinforced using an adhesive cement which was allowed to harden totally prior to any mechanical testing.

6.4 EXPERIMENTAL PROCEDURE

(i) The specimens were prepared in advance as detailed in section 6.3.

(ii) The active specimen was then placed in the loading rig ensuring correct seating of the load bearing washers and insulating collars. The dummy specimen was then placed alongside and all the electrical connections made (see plate 6.1). To reduce the levels of induced noise, the pick-up wires on each specimens were twisted closely together.

At this stage DVM1, see figure 6.4, was connected into the measurement system.

The current supply was switched "ON" and a DC signal of 2-3A injected into the specimen.

(NB With DVM1 connected the current must NOT exceed 10A as this may harm the meter).

(iii) The extensometer was attached centrally between the voltage pick-ups ensuring the probe was fully retracted and zero strain indicated on the digital readout. The feet of the extensometer were insulated from the specimen via a thin sheet of melamine paper to minimise disturbance of the electric field.

(iv) At this stage the active specimen insulation was checked using a DVM and hand held probes. If the active specimen was successfully insulated it was then left to soak at the 2-3A current level for 20 minutes. If not insulated completely the specimen was then reseated in the grips and rechecked.

(v) After 20 minutes soaking a voltage/current calibration curve was determined for the system.

The current into (DVM1) together with the voltage drop across the active specimen (DVM2) was then recorded and a note made of the values. The switch was then thrown across the dummy and a similar set of readings taken.

The current was then increased slightly and the readings repeated.

(vi) DVM1 was then removed from the measurement system and the current increased to approximately 30A. The specimens were then left to soak at this level for 45 minutes.

(vii) After soaking the current was then checked. The voltage back-off was also adjusted to give a readout on DVM2 in the 0-2V range for both the "active" and "dummy" specimens.

(NB If necessary the choice of range was altered, as required, as the test progressed).

(viii) The plotter was connected to the load cell and extensometer to provide a continuous record of load and strain during testing. A note of the plotting scales was then made. The hose clips were tightened and initial (zero load) values of potential, across the "active" and "dummy" specimens, taken together with the test back-off voltage.

(ix) The loading sequence was then ready to commence.

The load was increased in 1.4/1.75kN steps. (1% and 2% of the 70kN and 175kN loadranges respectively).

At each load step the voltage across the active specimen was recorded manually and then the diagonal switch thrown and the dummy voltage recorded also.

The load was increased until the required maximum was reached or the specimen failed. The hose clips were checked frequently during testing and tightened if necessary.

Instrumentation details and the complete loading/measurement system can be seen in plates 6.2 and 6.3 respectively.

6.5 RESULTS

The data collected during the experimental work did not correspond directly to the value of ρ for either material. Hence some processing of the results was required before a true picture of the variation of ρ with strain could be obtained.

Representative examples of the raw data from the experimental work can be seen in figures 6.5 and 6.6. Here the change in active voltage has been plotted against load for EN1A and NE8 respectively. The active voltage was converted to μV allowing for the backoff voltage and gain of the amplifier. The difference plotted was the change of voltage from the unloaded (initial) value. It should be noted that the sharp increasein voltage evident in both cases correlated exactly with the yield point of each material and would seem to indicate that plastic deformation has a significant effect on ρ. However this plot could be misleading since no account has been taken of voltage drift due to heating of changes in specimen cross-section due to strain.

To convert figures 6.5 and 6.6 into plots of resistivity against strain a number of steps to account for the aforementioned effects had to be taken and these are outlined below.

Consider the expression for the DC resistance of a conductor:

$$R = \frac{\rho l}{A} \qquad 6.2$$

Now from Ohms's law,

$$V = IR \qquad 6.3$$

Hence,

$$\frac{\rho l}{A} = \frac{V}{I} \qquad 6.4$$

Rearranging,

$$\rho = \frac{V}{I} \cdot \frac{A}{l} \qquad 6.5$$

In expression 6.5 all the terms on the right hand side were calculable from readings taken during experimentation. However allowance for the factors detailed previously had to be made.

The test current was calculated from the calibration values of current and voltage. Plotting voltage against measured current a calibration curve as in figure 6.7 was obtained. The intercept on the voltage axis gave the zero load voltage offset, V_o, and by extrapolation the test current could be found knowing the zero load active voltage. Strictly speaking there were two calibrations (active and dummy). The offsets in each case were almost identical, the test current having been obtained from the "active" calibration curve.

Now consider the thermal variations in voltage.

At each load step a value of "active" and "dummy" voltages were taken, V_a and V_d, say, with any thermal variations reflected equally in each. To reduce this influence a new value of active voltage was considerd, V_a', where

$$V_a' = V_a x\ Vref/V_d \qquad 6.6$$

and Vref was the average of all the recorded dummy voltages. V was then replaced by V_a' in eqn 6.5 as a more representative value.

Consider also the dimensional changes due to straining of the specimen.

The quotient (A/l) is the ratio of the instantaneous values of cross-sectional area and distance between the pick-ups.

Now,

$$l = l_o\ (1 + E_{long}) \qquad 6.7$$

Also,

$$A = A_o\ (1 + E_{lat})^2 \qquad 6.8$$

But,

$$\nu = \frac{-E_{lat}}{E_{long}} \qquad 6.9$$

$$E_{lat} = -\nu E_{long} \qquad 6.10$$

$$A = A_o(1 - \nu E_{long})^2 \qquad 6.11$$

Combining the above,

$$\rho = \frac{V_a'}{I}\ \frac{A_o(1 - \nu E_{long})^2}{l_o(1 + E_{long})} \qquad 6.12$$

Clearly calculation of equation 6.12 at every value of load would have been a lengthy and time consuming procedure with typically 60 pairs of values from each test. To provide a means of data storage and ease the computational effort use was made of an APPLEIIE microcomputer.

Two programes "DATA CREATOR" AND "TESTWELL" were written in Applesoft Basic. "DATA CREATOR" was written to provide an efficient means of storing, handling and editing the raw results from each test in suitably formatted data files which could be processed later by "TESTWELL".

Details of these programs are given in Appendices II and III.

The results following processing by "TESTWELL" can be seen in figure 6.8. Here the true value of ρ has been plotted against increasing strain up to a strain level of 6%.

This plot clearly shows that correcting for changes in dimensions during loading negated any change in active voltage. The maximum change in ρ from its initial value was betwen 1% and 2% and so could be considered not to change to any significant degree.

Although the change observed was negligible up to 6% strain there was experimental evidence to suggest that ρ could not be taken as an absolute constant over all possible values. Levels of 10% strain were reached during the EN1A testing and at such levels a change of 5.3% in ρ was observed with a marked increase from 8% onwards.

ρ may therefore be taken as a material constant up to strain levels of 6% in both materials.

Hence over the range 0-6% strain,

(EN1A) = 170 $\mu\Omega$mm

(NE8) = 69 $\mu\Omega$mm

From these values it is possible to estimate the skin depth for both materials at the energising frequency of 8kHz used in the CPD3.

The skin depth δ is given by equation 6.1 as,

$$\delta = \left(\frac{\rho}{\pi\mu f}\right)^{\frac{1}{2}}$$

where $\mu = \mu_r\mu_o$

The permeability is also a function of strain in ferromagnetic materials. An estimate of its value has been given by Okumura (24) as 1.5×10^{-4} Hm^{-1} in the annealed condition for mild steel. The relative permeability of NE8 is assumed constant and equal to unity, hence $\mu = 4\pi \times 10 - 7\ Hm^{-1}$

Thus for EN1A,

$$\delta = \left(\frac{170 \times 10^{-9}}{\pi \times 1.5 \times 10^{-4} \times 8 \times 10^{3}} \right)^{\frac{1}{2}}$$

$$= 2.1235 \times 10^{-4} m$$

$$= 0.21235 \text{ mm}$$

and for NE8,

$$\delta = \left(\frac{69 \times 10^{-9}}{\pi \times 4\pi \times 10^{-7} \times 8 \times 10^{3}} \right)^{\frac{1}{2}}$$

$$= 1.4781 \times 10^{-3} m$$

$$= 1.4781 \text{ mm}$$

These figures clearly highlight the very much more pronounced skin effect in the strongly ferromagnetic EN1A than in the non-ferrous NE8.

6.6 DISCUSSION

From the results of the experimental work it has been clearly demonstrated that within the range of interest (0-6% strain) the value of ρ was not significantly affected by either elastic or plastic strain. There was at most a change of only 1.5% from the value in the unloaded annealed condition of both materials.

Such changes in resistivity would therefore produce a change in PD of only 1%.

This clearly demonstrates that resitivity was not a crucial factor in determining the changes in ACPD response observed across the notches of either the EN1A or NE8 bend specimens.

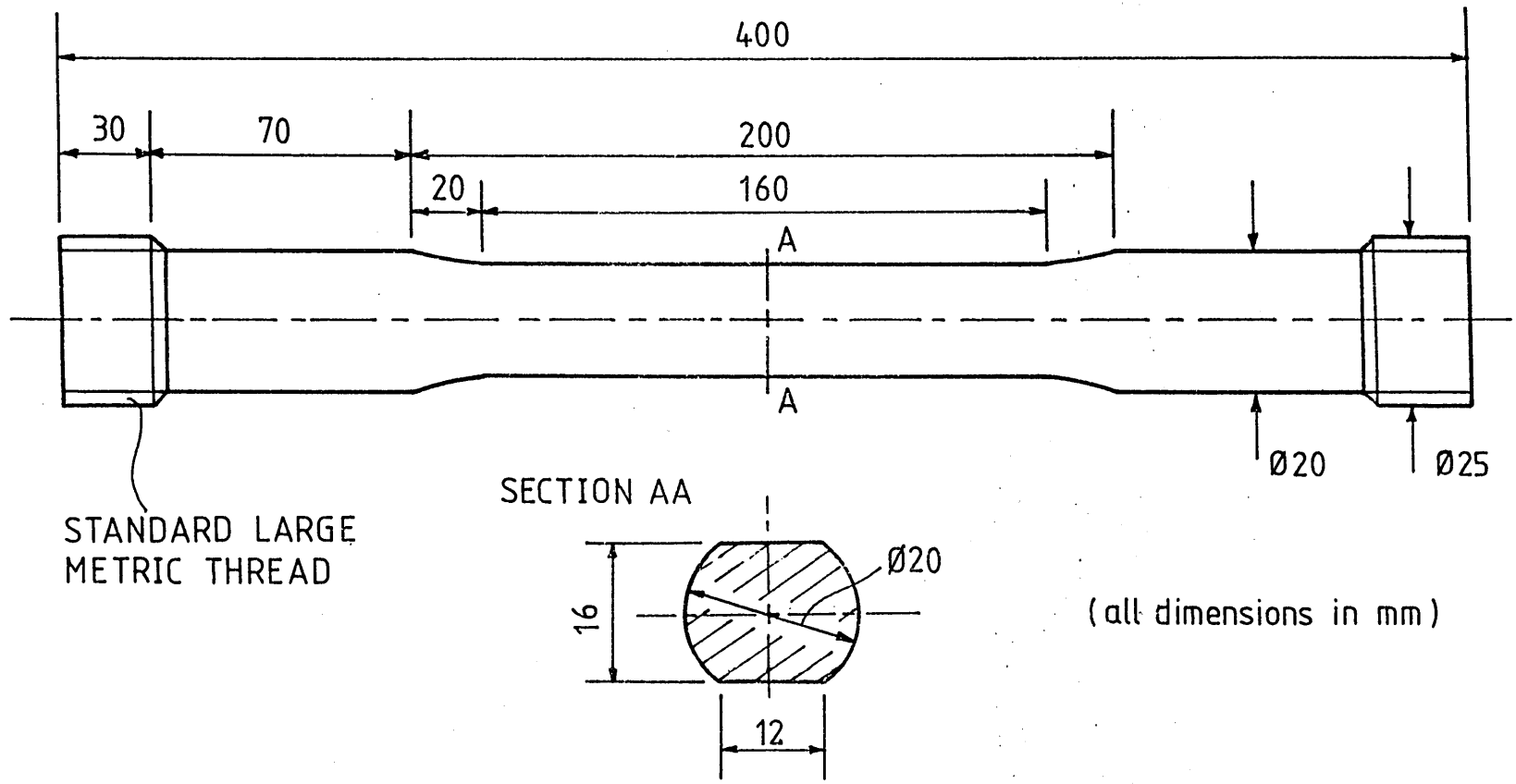

Figure 6.1 Geometry of specimen for determination of material resistivity

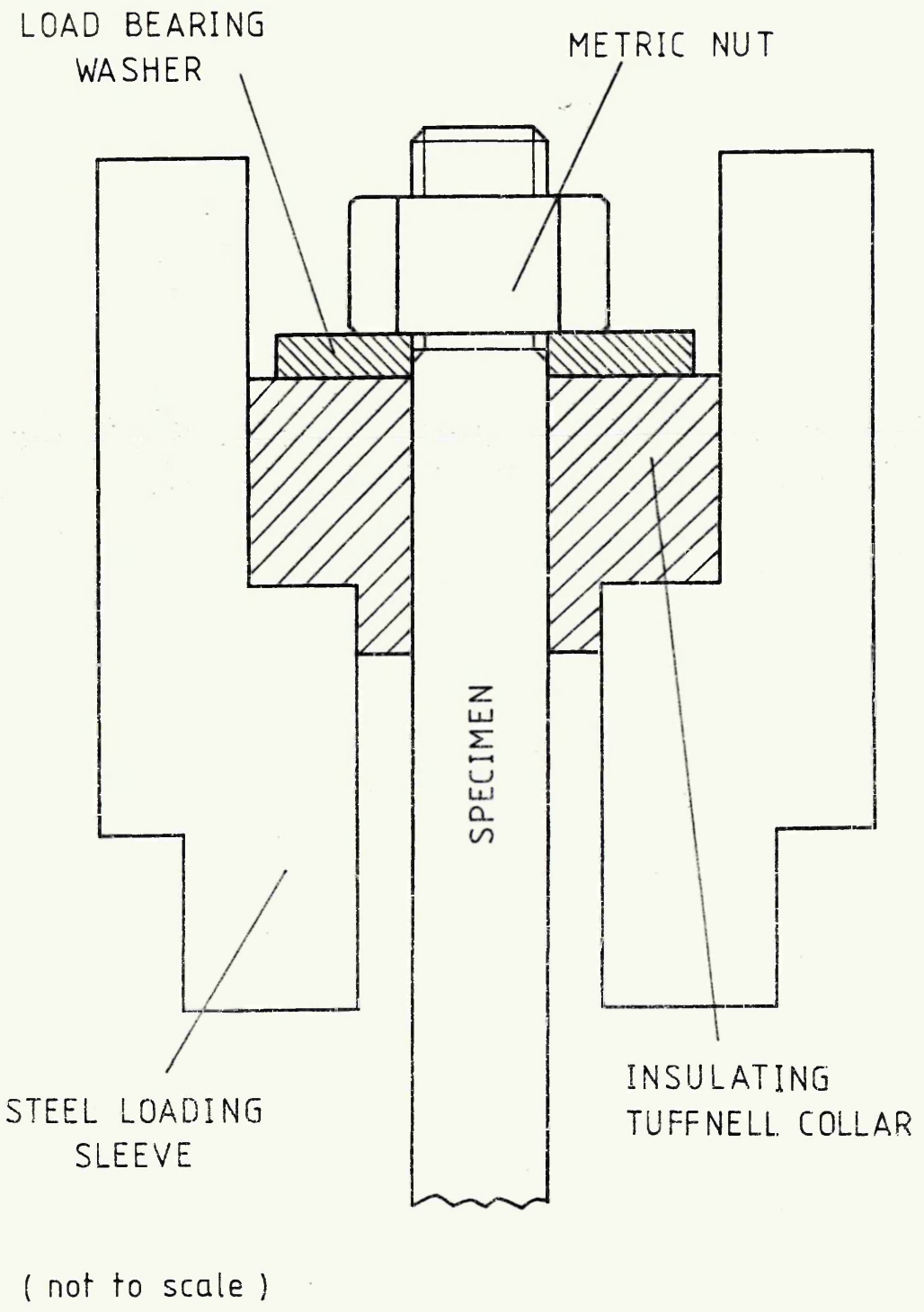

Figure 6.2 Insulation of specimen from loading apparatus via Tuffnell collar

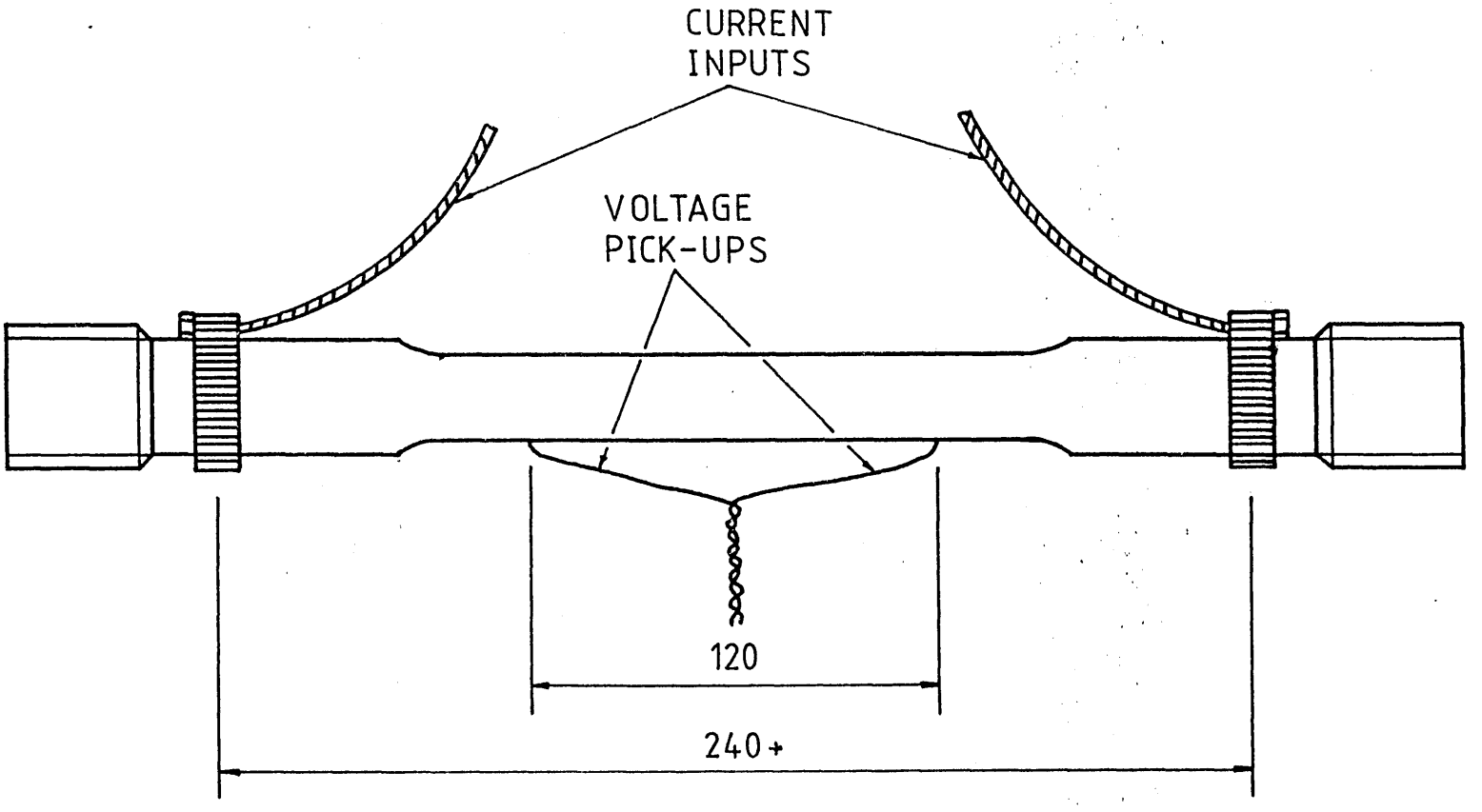

Figure 6.3 Positioning of current input and voltage pick-up leads

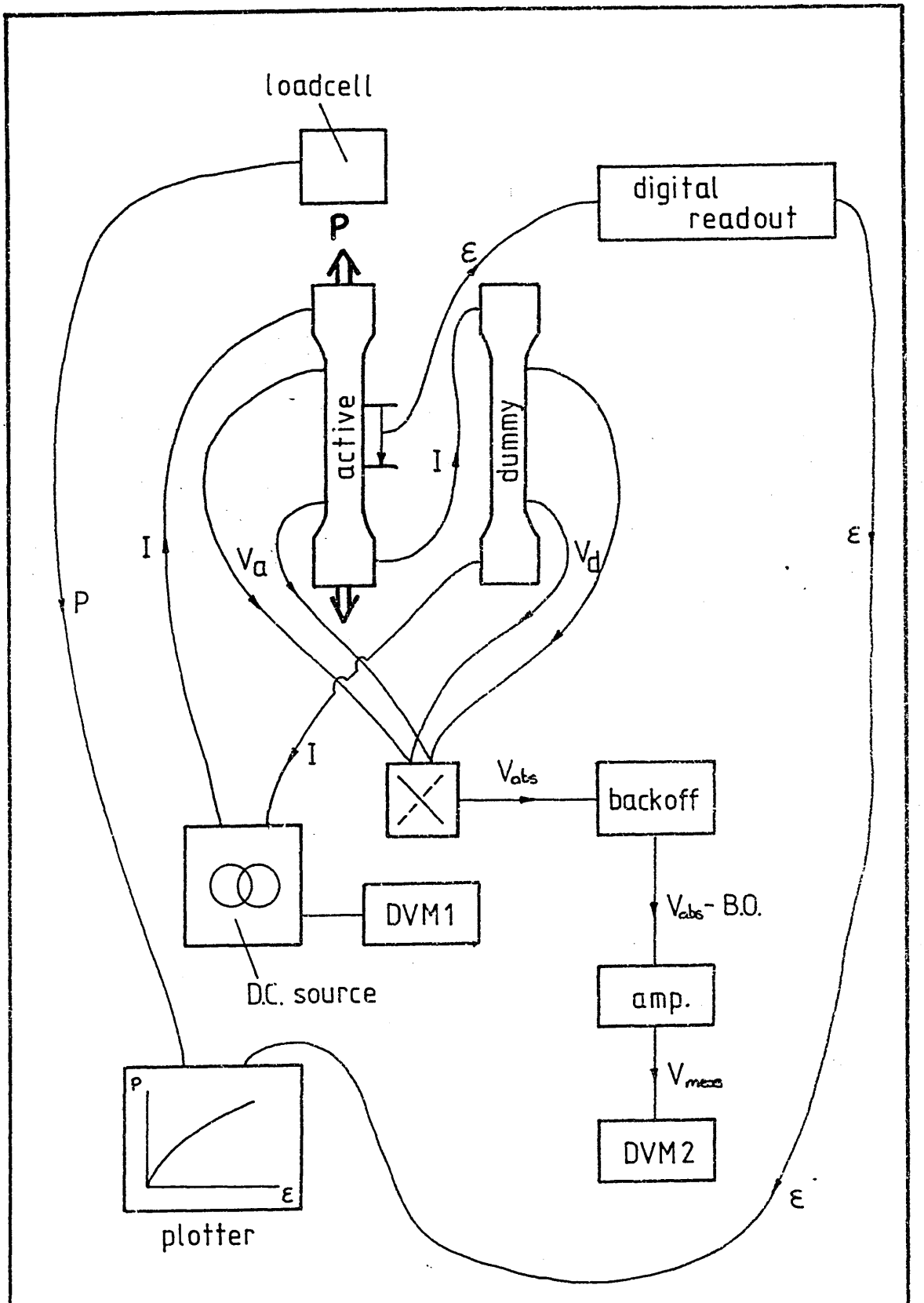

Figure 6.4 Schematic representation of measurement system

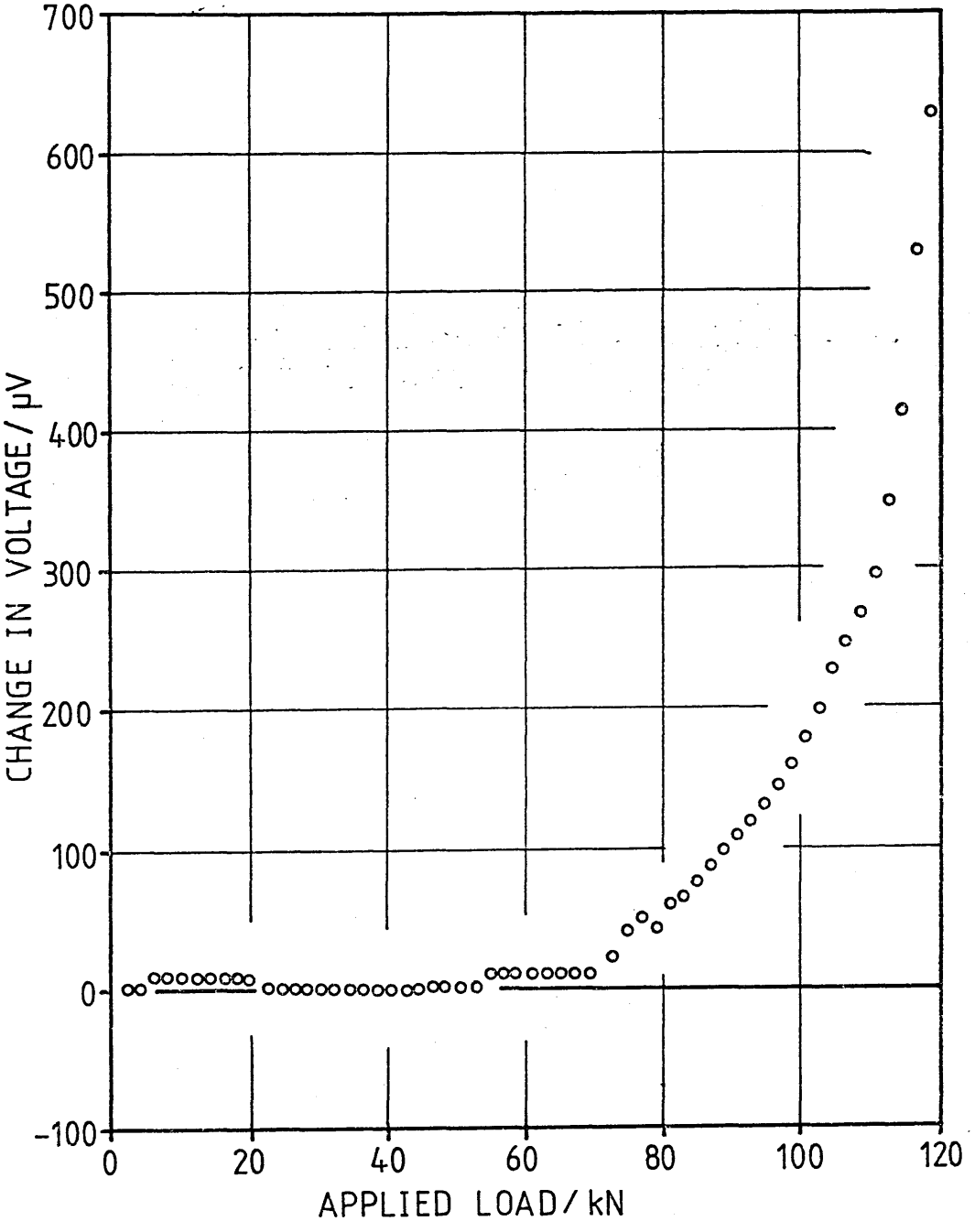

Figure 6.5 Change in active voltage vs applied load -EN1A

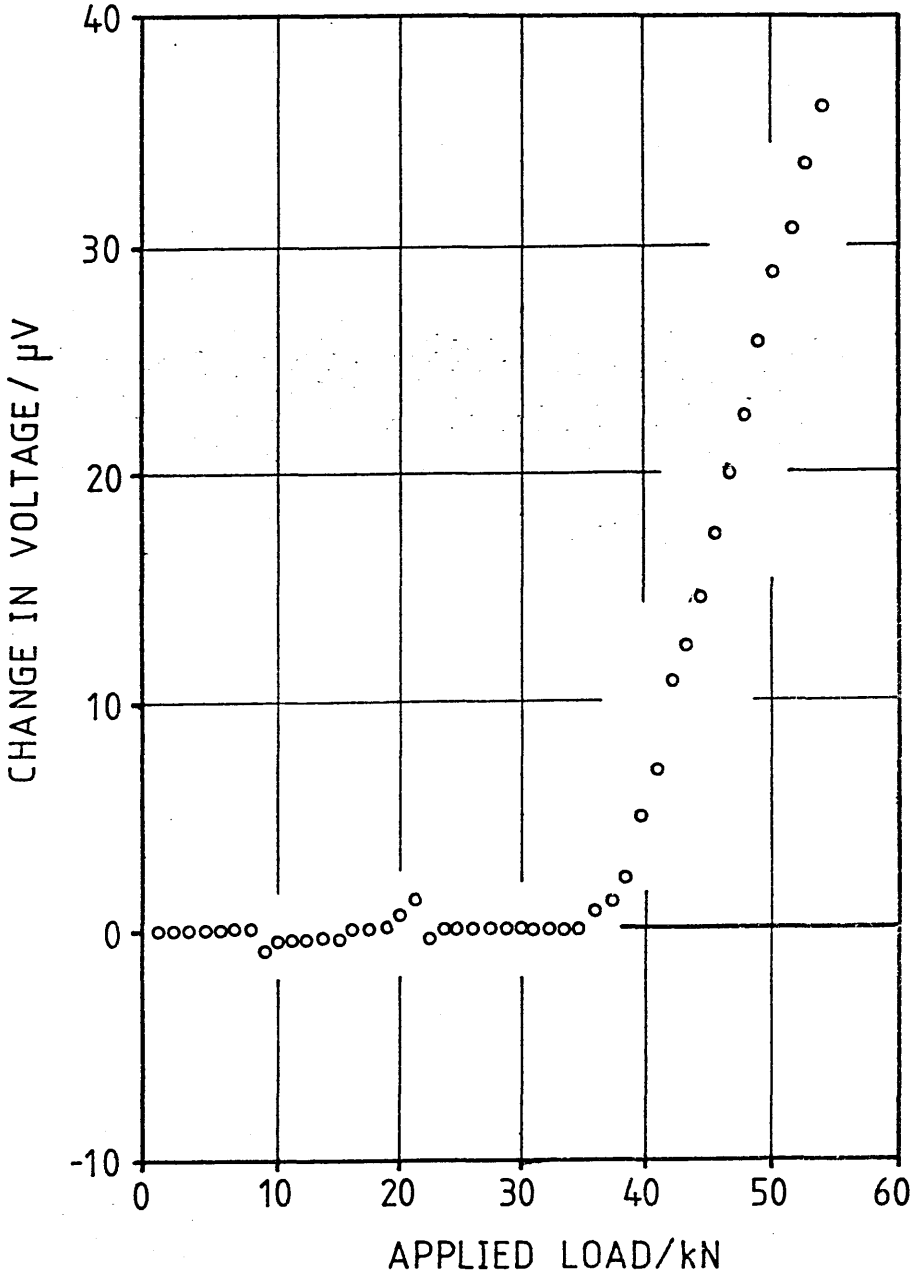

Figure 6.6 Change in active voltage vs applied load -NE8

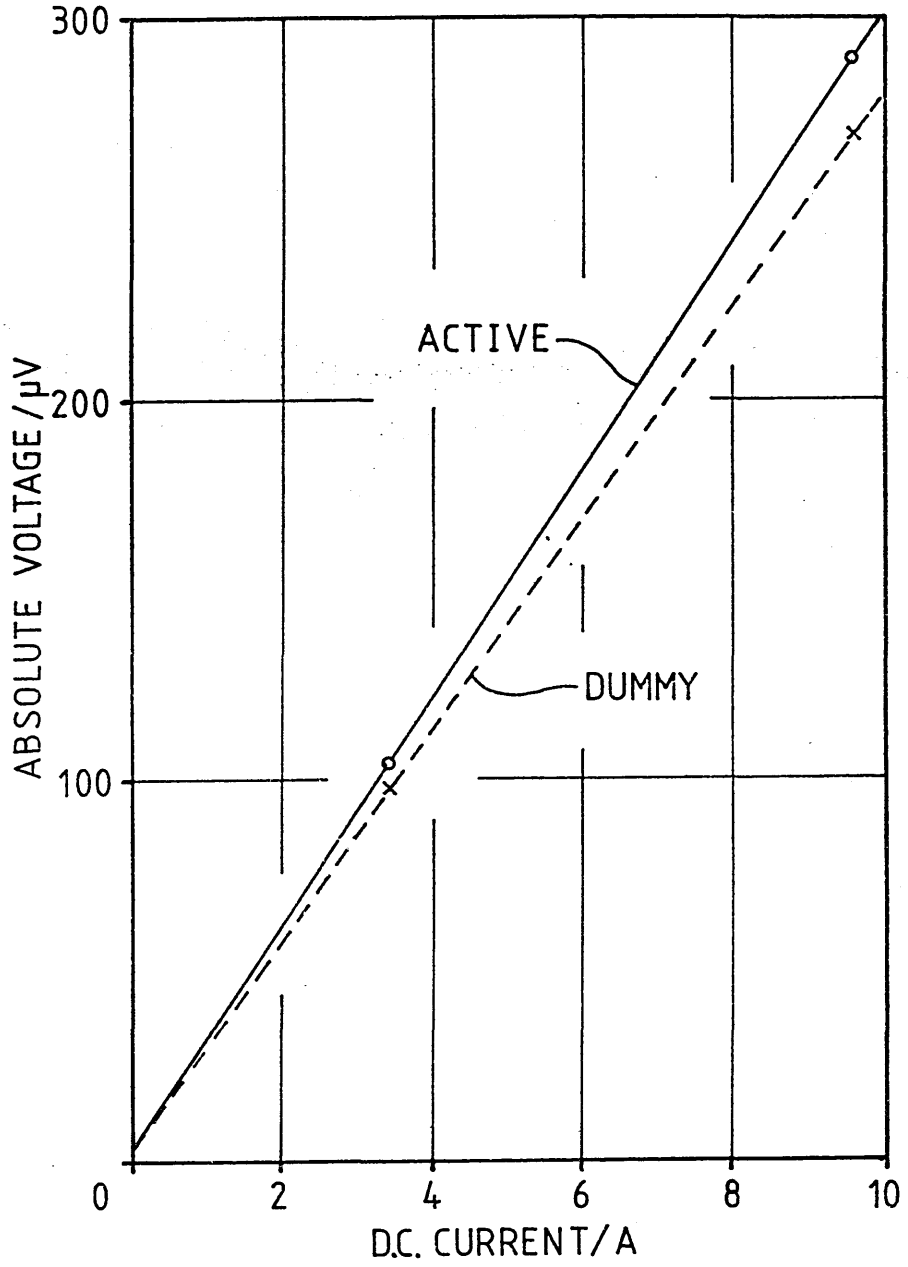

Figure 6.7 Typical current/voltage calibration curves for active and dummy specimens

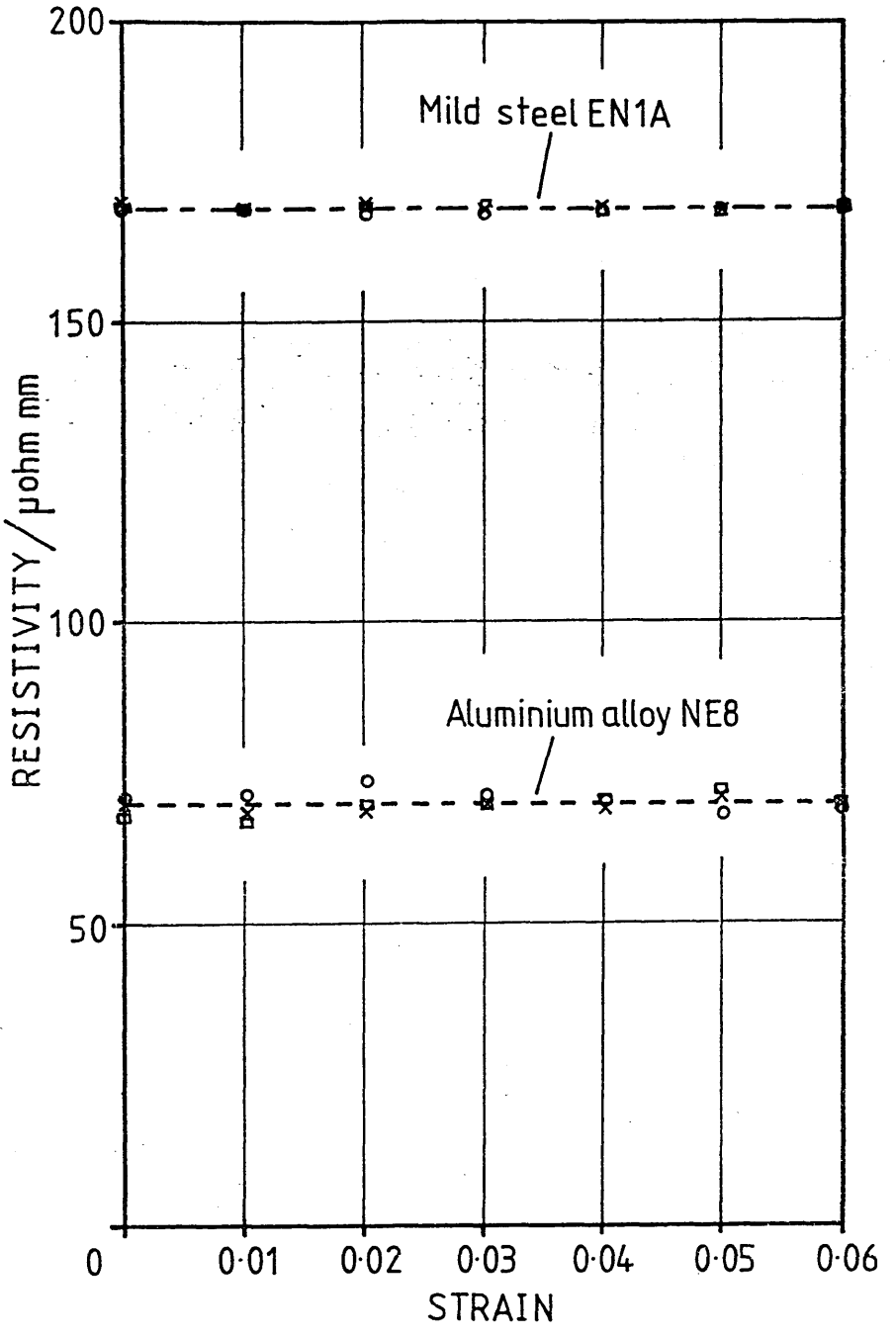

Figure 6.8 Change in electrical resistivity with increasing strain following correction for specimen dimensional changes and voltage drift due to heating

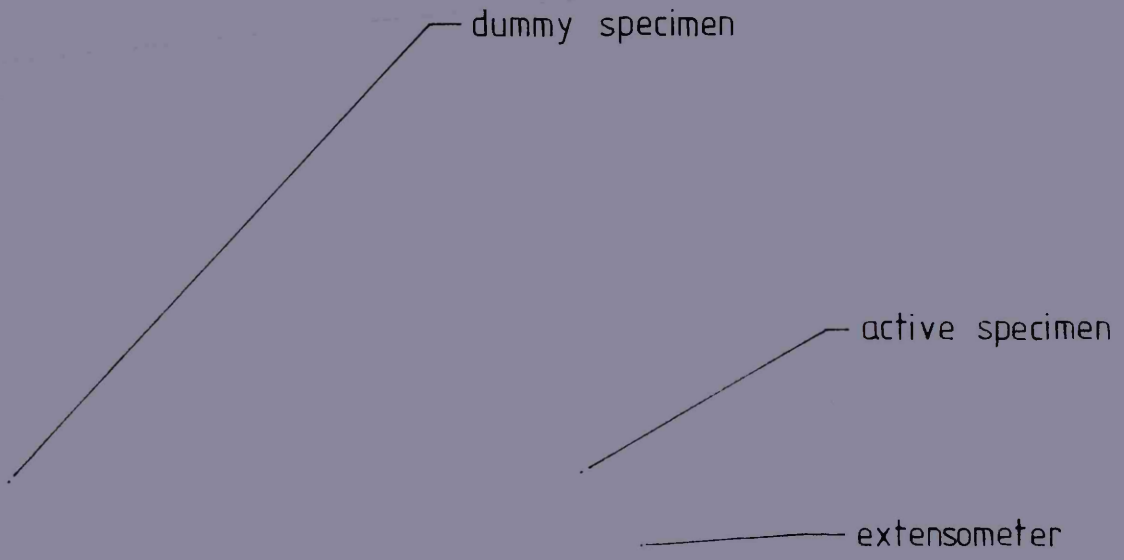

Plate 6.1
Active and dummy specimens in situ in loading rig

Plate 6.1
Active and dummy specimens in situ in loading rig

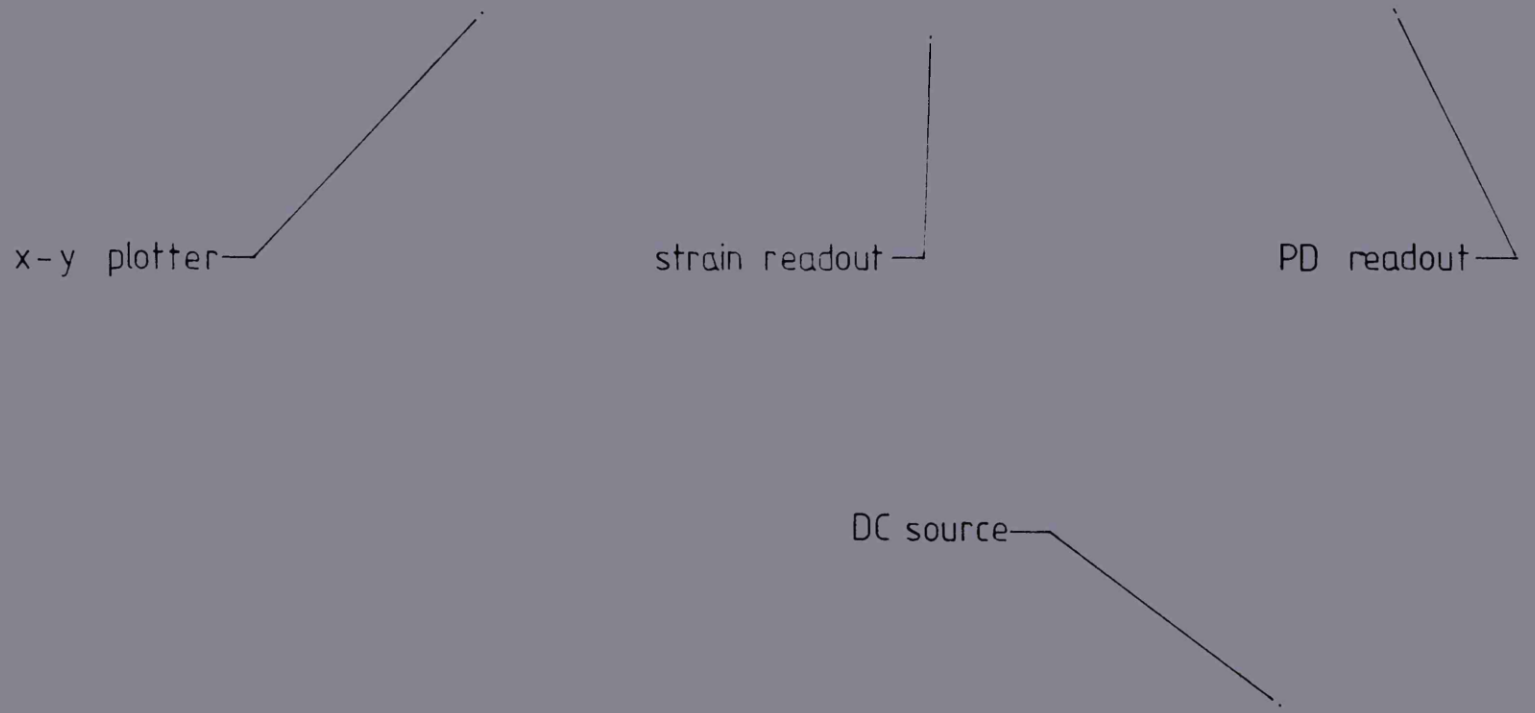

Plate 6.2
Instrumentation details

Plate 6.2
Instrumentation details

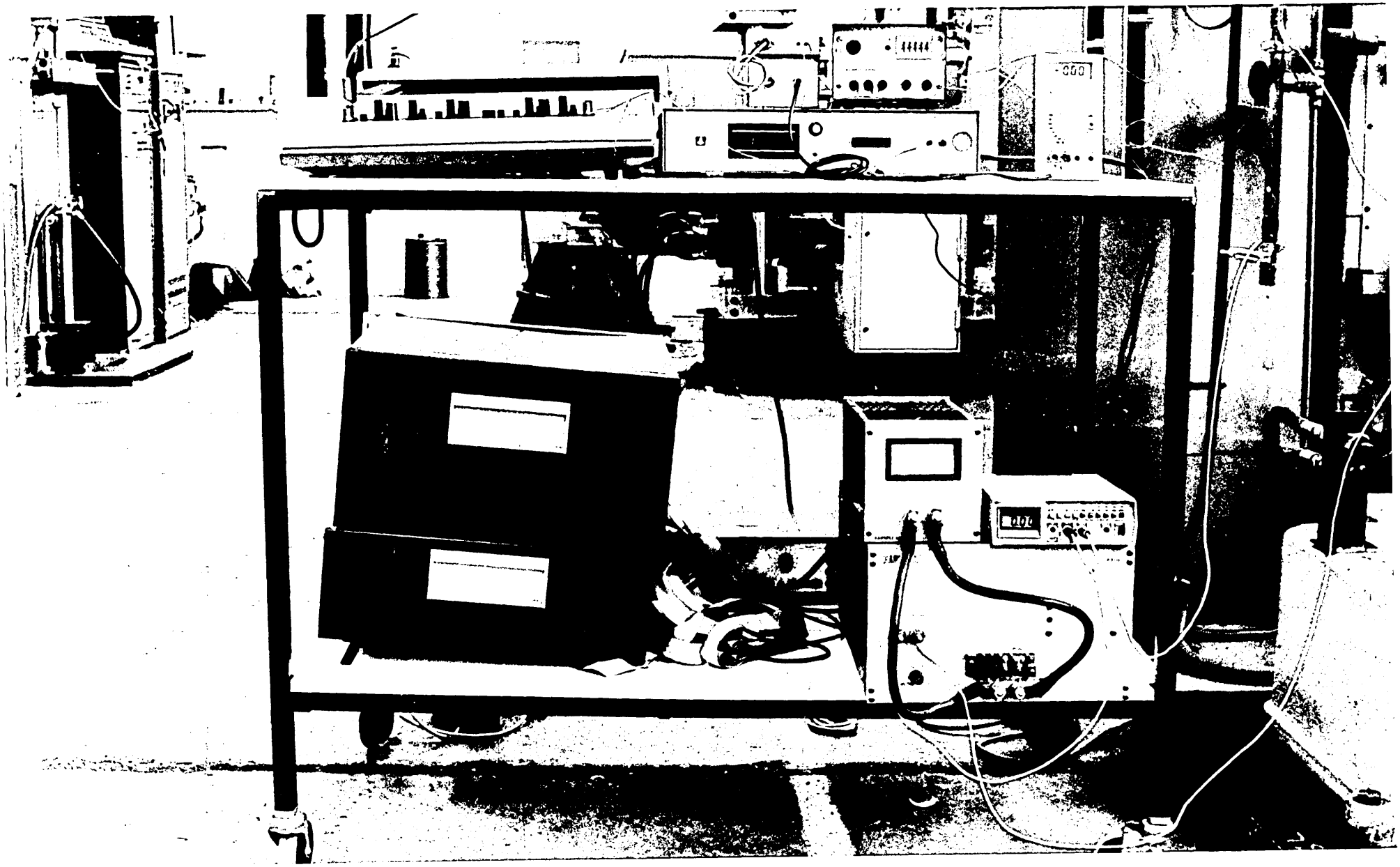

Plate 6.3
Complete loading and PD monitoring system

Complete logging and PD monitoring system

Plate 8.3

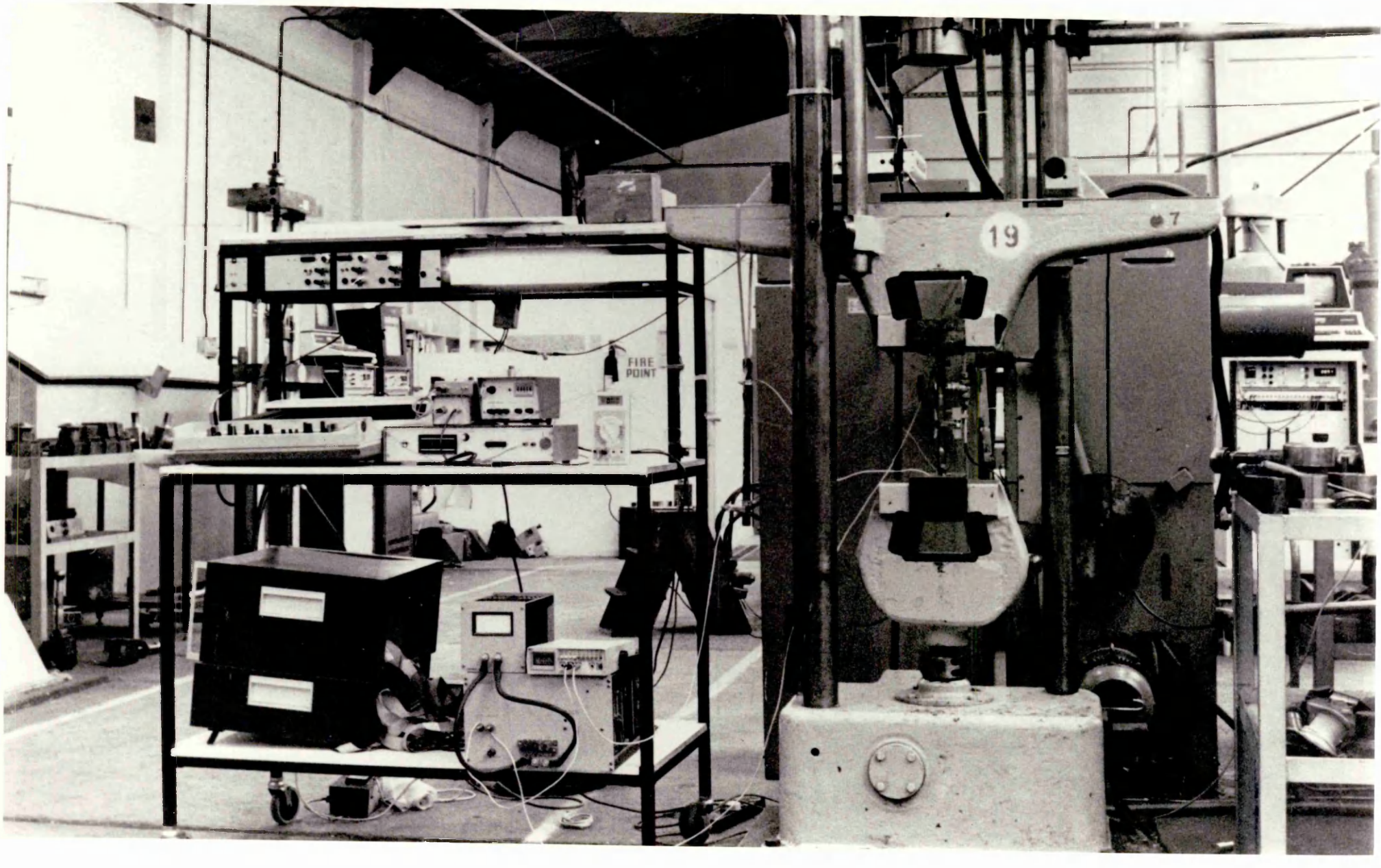
19
FIRE
POINT

CHAPTER 7 - DETERMINATION OF THE VARIATION OF THE RELATIVE MAGNETIC PERMEABILITY WITH STRAIN

7.1 INTRODUCTION

In the preceding chapter the influence of strain upon the electrical resitivity (ρ) was considered and details were given of the experimental procedure together with the results obtained during the investigation up to strain levels of 6-7%.

Following completion of the electrical resistivity measurements a similar programme of experimental work was initiated to investigate the influence of strain on the only other material parameter governing the skin depth and ACPD response, the relative magnetic permeability, μ_r.

There were several major differences in the characteristics of both these parameters with μ_r being a far more complex property than ρ (see Apendix I) and correspondingly more difficult to measure accurately. Unlike ρ, μ_r was not single valued but depended upon the size of the applied magnetizing force (H) which varied continuously throughout each cycle of the AC energising signal. The magnitude of H increasing in proportion to the instantaneous current amplitude up to a positive maximum then decreasing, passing through zero, to a negative minimum before returning to zero. This process repeated during each and every energising cycle causing a constant change in magnetic flux density (B) within the specimen, ratio of $B/\mu_o H$ giving the value of μ_r at any particular instant. However the experimental difficulties were eased somewhat by the fact that there was no necessity to include the aluminium alloy NE8 in the magnetic experimental work since this was a non-ferrous alloy and displayed only weakly magnetic characteristics. During the investigation, the value of μ_r for

this material was therefore considered constant and equal to unity. (From this it followed that the magnetic permeability (μ) was then equal to the permeability of free space, μ_o).

From a consideration of possible methods of experimentally determining the variation of μ_r with increasing strain it was clear that direct measurement of μ_r at each level of strain would have produced a whole family of magnetic hysteresis curves mapping the complete magnetic history of the material (See Appendix I). This point highlighted one of the major difficulties in the direct measurement approach in that correct interpretation of the experimental data, hysteresis curves, was required to extract a single value of μ_r that could be used later in the skin depth calculations. The actual measurement of μ_r was also subject to severe practical difficulties. The most satisfactory testpiece geometry on which to carry out any magnetic measurements was that of a torus (a circular ring of circular cross-section). Such a toroidal geometry would have allowed all the magnetic flux to be contained within the specimen greatly simplifying the calculation of the relevant magnetic parameters. However, such a ring geometry would also have been very difficult to load evenly and undertake strain calculations upon. Equally, if a typical tensile geometry was used to ease the strain calculations then the leakage of magnetic flux would have become a major problem.

From these considerations, the problems associated with directly measuring the variation of permeability with strain appeared almost insurmountable, however results from the electrical resistivity measurements suggested an alternative to the direct measurement approach and hence a means of avoiding these difficulties.

It was clearly demonstrated that up to the strain levels of interest, (6-7%) ρ could be considered a material constant and did not contribute to any observed changes in ACPD response. This implied that the response was governed solely by variations in the value of μ_r and by measuring the changes of ACPD response against strain in a tensile specimen the variation of μ_r could be inferred directly. Another advantage of this approach was that it also gave, directly, a single representative value of μ_r that could be used to determine the skin depth at each strain level.

7.2 CONSIDERATIONS IN THE MEASUREMENT OF THE RELATIVE MAGNETIC PERMEABILITY

Prior to the measurement of the variation of μ_r with strain using a method based on the ACPD crack monitoring technique, a preliminary series of direct measurements was undertaken to produce a series of hysteresis curves for the mild steel EN1A. The aim was to determine the magnetic characteristics of the material in an undeformed and annealed condition.

Several small ring specimens of rectangular cross-section were produced for the experimental work (see figure 7.1). This rectangular geometry was chosen as a compromise to ease manufacture of the specimens since machining of the preferred toroidal shape would have been unjustifiably costly. The test method developed was based closely on an AC technique suggested by Bozorth [6]. The fundamental basis of this technique was to establish a magnetic field in the EN1A ring by cyclically changing the applied magnetizing force (H), for a series of different maximum values, and evaluating the corresponding change of magnetic flux density (B).

The magnetizing field was created by passing an AC signal through an energising coil of enamelled copper wire wound around the ring. To detect the change in magnetic flux (B) produced in the ring by the changing magnetic field a search coil was similarly wound around the specimen. As the flux changed in the ring an EMF was induced in the search coil, the magnitude of which was a measure of the flux change.

A circuit diagram of the experimental measuring system can be seen in figure 7.2.

The energising circuit consisted of an AC source and a rheostat for varying the level of current injected into the energising coil and hence control the strength of the magnetic field (H) applied to the ring. The coil was energised using AC to produce a state of cyclic magnetisation in the ring at each level of H. (The signal and electrical component notation used throughout this section can be seen in figure 7.3).

The resistor R_1 was used as a monitoring resistor to measure the current level, I_m, in the energising coil. The size of the magnetising force produced (H) is then given by,

$$H = \frac{I_m . N_1}{s} \qquad 7.1$$

and, $$I_m = \frac{V_m}{R_1} \qquad 7.2$$

where, I_m = magnetizing current produced in the energising coil

V_m = voltage measured across resistor R_1

N_1 = number of energising coils

s = mean circumference of EN1A ring.

The search coil circuit was slightly more complicated than the energising circuit and was in effect a simple integrating circuit. This was necessary since the EMF induced in the search coil (E_s) was actually proportional to the rate of change of flux therefore it was necessary to integrate this signal to obtain V_ϕ representing the actual flux changes ($E_s = N_2 \frac{d\phi}{dt}$, where N_2 corresponds to the number of search coil turns). Using an oscilloscope with X-Y plotting capabilities it was then possible to display the integrated EMF (V_ϕ) coil against V_m at each level of energising current and record a series of approximate hysteresis curves for the material. Precise measurements of these parameters are difficult to make because the inherently non-linear relationships give rise to waveform problems. In order to minimise these undesirable effects the flux waveform was made as near sinusoidal as possible.

The number of copper coils applied to the ring and values for the circuit components were varied during the experimental work in an attempt to improve the performance of the circuit and the final optimal values can be seen in figure 7.2. With this circuit it was possible to undertake a series of measurements using the EN1A ring and produce a series of hysteresis curves for this material. Once suitable values had been determined for the circuit components the experimental procedure was fairly straightforward:

(i) The specimen was demagnetized by injecting a large AC signal into the specimen and gradually reducing it to zero using the rheostat. The value of the initial current level was chosen as high as possible (3.5A) to ensure effective demagnetization.

(ii) The AC energising current was then incremented in steps of 50/100 mV up to 0.8A and all the measurements were conducted at an input frequency of 50Hz. At each increment the hysteresis curve for that particuar level of energising current was recorded on the X-Y plotter. A note was also made of the values of V_ϕ and V_m on the plots.

Additionally similar tests were conducted on specimens of the non-ferrous aluminium alloy NE8, the results confirming the invariance of μ_r for this material.

7.2.1 Calculations

The voltage values and hysteresis curves recorded during the test were only representative of the relevant magnetic parameters and therefore some processing of the results was necessary to obtain true estimates of the absolute values and a representative calculation is given below.

Consider the instantaneous value of current in the magnetizing coil, i_m, and the associated magnetizing force, H.

From equation 7.1,

$$H = \frac{N_1 i_m}{s} \qquad 7.3$$

(NB Throughout the analysis small letters denote the instantaneous values of variables and capital letters the RMS and peak values of the same quantities).

The peak value of H, $\hat{H}$, during each magnetizing cycle is then given by,

$$\hat{H} = \frac{N_1 I_m}{s} \qquad 7.4$$

Assuming the flux, $\phi(t)$, created in the EN1A ring specimen varies sinusoidally then,

$$\phi(t) = \hat{\phi} \sin \omega t \qquad 7.5$$

where $\hat{\phi}$ is the peak value of flux created in the energising coil during each magnetizing cycle.

The EMF induced in the search coil is given by,

$$e_S = N_2 \frac{d\phi}{dt} \qquad 7.6$$

Hence from 7.4,

$$e_S = N_2 \hat{\phi}\ \omega \cos \omega t \qquad 7.7$$

In the steady state, and assuming sinusoidal conditions, the search coil circuit gives rise to,

$$E_\phi = \frac{1/j\omega C}{1/j\omega C + R_2} \cdot E_S \qquad 7.8$$

$$= \frac{E_S}{\sqrt{1 + \omega^2 C^2 R_2^{\,2}}} \cdot \angle -\tan^{-1}(\omega C R_2)$$

where E_S and E_ϕ are the RMS values of the EMF induced in the search coil and the potential drop created across the capacitor, respectively.

From 7.6 and 7.7 the magnitude of the peak value of E_ϕ is then given by,

$$E_\phi = \frac{1}{\sqrt{1 + \omega^2 C^2 R_2^{\,2}}} \cdot N_2 \hat{\phi}\ \omega \qquad 7.9$$

Rearranging,

$$\hat{\phi} = \frac{\sqrt{1 + \omega^2 C^2 R2^2}}{N_2\ \omega} \cdot E_\phi \qquad 7.10$$

The peak flux density, $\hat{B}$, can then be written as,

$$\hat{B} = \frac{\hat{\phi}}{a} \qquad 7.11$$

where a is the cross-sectional area of the EN1A ring. Equations 7.4, 7.10 and 7.11 present a means of estimating the magnetizing force and flux density from the parameters measured during the magnetic testing. Re-expressing these equations in terms of the actually measured variables, V_m and V_ϕ,

$$\hat{H} = \frac{N_1}{s.R_1} \cdot \hat{V}_m \qquad 7.12$$

and,

$$\hat{B} = \frac{\sqrt{1 + \omega^2 C^2 R_2^2}}{N_2 \omega a} \cdot \hat{V}_\phi \qquad 7.13$$

Equations 7.12 and 7.13 could then be evaluated for each of the experimental hysteresis curves and the results plotted on the same absolute scales of B and H. A representative selection of these results is given in figures 7.4 showing the hysteresis curves obtained for several different levels of the magnetising force. This also allowed quantitative estimates of μ_r to be made for each set of results. As an example of the calculations consider the case of $\hat{V}_m$ = 800mV and $\hat{V}_\phi$ = 450mV.

From 7.12,

$$\hat{H} = \frac{500 \times 800 \times 10^{-3}}{103.7 \times 10^{-3} \times 0.25}$$

$$= 15\,432 \text{ Atm}^{-1}$$

Similarly from 7.13,

$$\hat{B} = \frac{[1 + (314 \times 2.2 \times 10^{-6} \times 22)^2]^{\frac{1}{2}} \times 450 \times 10^{-3}}{33 \times 314 \times 30 \times 10^{-6}}$$

$$= 1.45 \text{ T}$$

Also to estimate the value of μ_r,

$$\hat{B} = \mu_r \mu_o \hat{H}$$

$$\mu_r = \frac{\hat{B}}{\mu_o \hat{H}}$$

$$\mu_r = \frac{1.45}{4\pi \times 10^{-7} \times 15432}$$

$$= 74.8$$

It was therefore possible to plot $\hat{B}$ against $\hat{H}$ for all the hysteresis curves to obtain an approximate initial magnetization curve for EN1A, figure 7.5, and also to show the variation of μ_r with H, figure 7.6.

Although these results provided useful data about the magnetic properties of EN1A, the direct measurement technique using ring specimens did not represent a totally satisfactory approach for several important reasons. Even after considerable effort it was found impossible to drive a current greater than 3.2A at a frequency of only 50Hz into the specimen because of the large inductive impedance of the wire wound ring. These levels were much less than the required 5A at 8kHz used during the ACPD measurements of the strained notches and therefore did not produce any directly applicable results. However, they did give some initial insight into the magnetic behaviour of EN1A and also helped to confirm the validity of the later magnetic measurements using the ACPD technique. (Both experimental approaches gave very similar estimates for μ_r: Ring tests, $\mu_r = 299 \rightarrow 75$; Tensile tests, $\mu_r = 284 \rightarrow 164$).

The ring testing also highlighted the practical difficulties associated with the direct measurement technique. Since the conditions of these experiments and the geometry of the EN1A specimen could be considered close to the ideal it was clear that production of accurate hysteresis curves with the specimen in a testrig and subject to high levels of strain would have been extremely difficult. These conclusions together with the results from the

electrical resistivity measurements suggested the possibility of adopting an alternative approach to the problem derived from the ACPD crack monitoring technique detailed in sections 7.1 and 7.4. Adoption of this alternative approach allowed the use of a tensile geometry for the specimen and greatly simplified the complexity of the magnetic measurements. Additionally the CPD3 crack detection system could be used as the source of the AC energising signal allowing easy generation of a readily variable magnetizing current at the required 8kHz frequency.

7.3 TESTPIECE SPECIFICATION AND PREPARATION

As mentioned in the previous section it was found possible to use a testpiece with a simple tensile geometry considerably easing the possible complexities of both the strain and magnetic measurements.

The testpiece geometry and material condition were identical to those used during the resistivity measurements details of which have been given in section 6.3 of the previous chapter. The load was also applied in similar manner via two large metric nuts attached to the ends of the specimen. Electrical insulation was ensured by using specially designed Tuffnell collars together with a steel spacing washer, although insulation was not as critical as in the previous measurements using a DC energising source.

The location of the current input and voltage pick-up leads differed substantially from the previous resistivity measurements. The current inputs consisted of multi-strand plastic coated copper wire positioned 240mm apart. At this spacing the electric field in the region of the voltage pick-ups could be assumed fairly

uniform. Unlike the resistivity measurements the leads were not clamped onto the specimen using hose clips but were soldered onto a flange of thin steel spot welded onto the specimen at the correct locations beforehand, see figure 7.7. The voltage pick-ups were positioned closer together than in the previous resistivity measurements with a spacing of only 60mm. The smaller spacing was chosen to reduce the size of the standing voltage on the surface of the specimen which if too large would give rise to problems of clipping of the voltage signal at high levels of instrument gain. This occurs if the amplifiers of the CPD3 receive a very large input signal outside of their operating range and so cannot function properly.

The variation of μ_r was to be deduced from measurements of the voltage across the specimen as it was strained and it was therefore unnecessary to use a pair of compensating leads across an undeformed section of material but vital to keep any voltage pick-up to minimum since with this technique no account could be made for these effects and obtaining a true voltage, reflecting only strain effects, was very important.

The voltage pick-ups comprised two single strand 27SWG plastic coated copper wires spotwelded directly onto the surface of the specimen further secured with a small dab of cement which was allowed to harden completely prior to any mechanical testing. To reduce the risk of induced EMF's in the pick-ups they were run flush along the surface of the specimen, taped in position and then twisted tightly together as they left the specimen. Since the pick-ups were so tightly coiled there was a risk they might be pulled off as the specimen stretched during loading. To prevent this the

leads were zig-zagged across the width of the specimen allowing some leadwire movement without unnecessarily increasing the size of any likely induced EMF's.

7.4 EXPERIMENTAL PROCEDURE

(i) The specimens were prepared in advance as detailed in section 7.3.

(ii) The specimen was placed in the loading rig ensuring correct seating of the load bearing washers and the insulating collars. To reduce the risk of any induced noise, the pick-up wires were twisted tightly together as they left the specimen and taken off on the opposite side to the current inputs.

(iii) The extensometer was attached centrally between the voltage pick-ups ensuring the probe was fully retracted and zero strain indicated on the digital readout. The feet of the extensometer were insulated from the specimen via a thin sheet of melamine paper to minimise any disturbance of the electrical field.

(iv) The CPD3 was then switched on and the current level adjusted to supply 5.0A at a constant 8kHz frequency to the specimen. To provide an accurate check on the current level supplied to the specimen a portable Fluke DVM was connected in series between the current output of the CPD3 and the specimen itself. This step allowed the current to be observed continuously throughout the testing whilst at the same time monitoring the specimen voltage via the DVM of the CPD3. The current input level to the specimen was adjusted to the 5.0A level and left to soak for approximately 20 minutes.

see figure 7.8 for a schematic representation of the complete monitoring system.

(v) After the soaking period the current level was rechecked and any necessary adjustments made. The levels of system gain and voltage offset applied to the rectified and amplified PD signal were then adjusted to the required levels. Throughout the testing a gain of 3000 together with a 10V offset was used. These settings produced a voltage output of a reasonable level giving an indicated 5-7V that corresponded to an absolute value of between 5000-5700 μV on the specimen surface. The level of gain was not set too high because of possible problems with signal clipping at the 5A input current level which created an appreciable standing voltage on the surface of the specimen.

(vi) All the instrument settings were again rechecked and any necessary final adjustments to the measurement system made. To provide a continuous record of the stress/strain behaviour of the specimen during loading an X-Y plotter was used to record the output from the load cell against the extensometer output. A note of the plotting scales was made onto the plotting paper for later reference.

(vii) The loading sequence was then ready to commence. The load was increased in steps of 1.75/3.50 kN which corresponded to 1/2% of the 175kN load range of the Losenhausen testing machine. At each of these load levels a note was made of the load level itself and the PD measured across the specimen. This process was repeated until the required miximum load level was attained. The load on the specimen was then reduced in a series of load decrements back down to the zero

load level with a note being made of load and PD response at each decrement and a continuous record of load against strain provided by the plotter.

In addition to these simple tensile tests a series of experiments was conducted to investigate the effect of unloading the specimen from different levels of strain both above and below the yield point of the mateial. The loading/unloading sequence adopted for the testing is illustrated in figure 7. 9 where each of the separate load cycles is clearly shown. Throughout each of these cycles the PD, load and strain were recorded as in the tensile test.

The specimen was first cycled below the yield point of the material, C1, to investigate whether there was any permanent change in the value of when the strain was purely elastic and therefore reversible. Subsequently the specimen was loaded into the plastic region up to 1.25% strain and the unloaded, C2. This was repeated up to 6.8% strain, C3, and finally 6.9% strain, C4.

7.5 RESULTS

The information collected during the experimental work did not correspond directly to the variation of μ_r with strain and hence some processing of the raw results was required before a clear picture of any variation could be obtained. Although the voltage was indicative of any variations in μ_r due to strain there was no precise one to one correspondence. Therefore the voltage values needed to be converted using the skin depth formula and the expression for the AC impedance of a conductor into true values of μ_r. The steps taken during the conversion are outlined below.

Consider the expression for the Ac impedance, Z, of a cylindrical conductor, length l and radius r.

$$Z = \frac{\rho l}{2\pi r\delta} \quad , \delta << r \qquad 7.14$$

where

$$\delta = \left(\frac{\rho}{\pi\mu_r\mu_o f}\right)^{\frac{1}{2}} \qquad 7.15$$

The condition $\delta << r$ was satisfied since r = 10.0mm and δ, at a supply frequency of 8kHz, was of the order of 0.1mm.

Thus combining 7.14 and 7.15,

$$Z = \frac{1}{2\pi r} \times (\pi\mu_r\mu_o f\rho)^{\frac{1}{2}} \qquad 7.16$$

But Z may be written as,

$$Z = \frac{V}{I} \qquad 7.17$$

where V is the voltage drop across the conductor and I is the value of current flowing through the conductor.

Hence,

$$Z = \frac{V}{I} = \frac{1}{2\pi r} \times (\pi\mu_r\mu_o f\rho)^{\frac{1}{2}} \qquad 7.18$$

The variable of interest is μ_r.

Rearranging,

$$\frac{V}{I}^2 = \frac{1}{2\pi r}^2 \times (\pi\mu_r\mu_o f\rho)$$

$$\mu_r = \frac{1}{(\pi\mu_o f\rho)} \times \frac{(V \times 2\pi r)^2}{Il} \qquad 7.19$$

All the quantities on the RHS of expression 7.18 were known or calculable from the experimental work except for r and l which altered as the specimen stretched and deformed during loading.

From a consideration of the dimensional changes during the tensile loading of the bar it is possible to say,

$$l = l_o\ (1 + E_{long}) \qquad 7.20$$

$$r = r_o\ (1 + E_{lat}) \qquad 7.21$$

where, r = initial radius of the specimen

l = initial distance between voltage pick-ups

E_{long} = longitudinal strain measured by extensometer

E_{lat} = lateral strain

It is also known from Poisson's Ratio, ν, that

$$\nu = \frac{-E_{lat}}{E_{long}} \qquad 7.22$$

Therefore 7.21 can be rewritten as,

$$r = r_o(1 - \nu E_{long}) \qquad 7.23$$

Combining 7.18, 7.20 and 7.23,

$$\mu_r = \left(\frac{V}{I}\right)^2 \times \frac{4\pi}{\rho\mu_o f} \times \left[\frac{r_o\ (1 - \nu E_{long})}{l_o\ (1 + E_{long})}\right]^2 \qquad 7.24$$

Thus the expression for μ_r could be written in terms of quantities that were readily measured during the test and so 7.24 could be evaluated at various levels of strain to reveal how the relative premeability varied with increasing tensile strain.

The data from each of the tests was calculated as a series of load and voltage readings across the specimen with up to 90 readings being typical. Before equation 7.24 could be evaluated the load reading had to be converted to a strain value via the load/strain curve recorded automatically during the test and the measured potential converted to an absolute value knowing the gain and offset of the CPD3. These values could then be inserted into 7.24 and the relative magnetic permeability calculated at a given load (strain) level. The number and repetition of the calculations suggested some automation of this numerical process to calculate the

relative permeability at each strain level. To perform this task the APPLESOFT BASIC program "CONVERSION" was written for the APPLEIIE microcomputer and a full program listing is given in Appendix IV.

The processed results for the simple tensile tests are presented in figures 7.10 and 7.11 where the values of relative magnetic permeability, μ_r, have been plotted against increasing tensile strain with figure 7.10 showing the effect of purely elastic strain and figure 7.11 showing the effect of combined elastic and plastic on μ_r strain up to levels of 12% strain.

The results shown are from two separate tests and the consistency was obviously very good with both tests giving very similar results.

The results from the loading/unloading cycles C1-C4 shown in figure 7.9 are given in figures 7.12-7.18. The response when the material was cycled elastically below the yield point of the material was given in figure 7.12 and in this case strain was proportional to the applied load. For the remaining load cycles C2, C3 and C4 the material was taken above yield and there was some degree of permanent set after each cycle. In these cases strain was no longer proportional to load and each cycle is therefore illustrated with two plots, the first giving the variation of μ_r with strain and the other the variation of μ_r with applied load.

7.6 DISCUSSION

The results presented in the previous section reveal the dependence of the relative magnetic permeability of the mild steel EN1A upon the levels of strain experienced by the material. Further since

the material was not chosen specifically for its favourable magnetic properties, and as such could be considered a typical ferromagnetic material, it seems reasonable to expect that other similar alloys would show a marked strain dependence. However it would be unwise to extrapolate further and state all ferromagnetic alloys will behave in exactly the same manner as the magnetic behaviour of materials is affected by a great many other factors such as the alloying elements etc.

The results presented for the EN1A represent changes in the value of μ_r due to increasing strain with a current level of 5A at an input frequency of 8kHz. Some deviation from these results could be expected if a different current level was used since this would affect the value of the magnetizing force. This was in fact confirmed during the experimental work when a current level of 3A was employed resulting in a noticeable deviation from the 5A results.

The results contrast strongly with the null response obtained from the electrical resistivity measurements clearly indicating that μ_r is the dominant material parameter governing changes in ACPD response.

It can be seen from figures 7.10 and 7.11 that the variation of μ_r with strain is monotonically decreasing showing several distinct changes in gradient which divide the response up into three separate sections:

(i) 0-0.12% This region represents the variation of magnetic permeability with increasing purely elastic strain. The drop in the value of μ_r is very sharp

representing a decrease of 15% from its initial value of 284 down to 243 suggesting that μ_r is very sensitive to elastic strain. The decrease is also fairly linear up to the yield point of the material at 0.12% strain.

(ii) 0.12-3.0% Above the yield point of the material the value of μ_r continues to decrease linearly with increasing plastic strain but at a much reduced rate up to a value of 190 at 3.0% strain.

(iii) 3.0-12.0% As the strain increases above 3.0% the rate of decrease of μ_r lessens considerably and approaches a steady state value μ_r = 164 at a strain level of around 8.0%. Above this level there is no further decrease from this steady value. This agrees with Bozorth [6] and Venkatasubramanian [9] who also observed a decrease in the value of μ_r with increasing plastic strain, reaching a similar steady value at high levels of strain.

Consideration of the loading/unloading responses given in figures 7.12-7.18 gives a further insight into the effects of both elastic and plastic strain on the magnetic permeability of EN1A. From figure 7.12 it can be seen quite clearly that purely elastic strain had no lasting effect on the value of μ_r and that once the load was removed μ_r returns to its initial unloaded value.

The effects of increasing degrees of plastic deformation can be seen in figures 7.13-7.18.

In figures 7.13 and 7.14 the results for load cycle C2 are given. In this cycle the specimen was strained above yield (0.13% strain) up to 1.30% strain and after the load was removed there was a permanent set of 1.04% strain. On unloading the value of μ_r did increase back towards its initial unloaded value but at zero load there was a slight permanent change in the value of μ_r from 278 to 273 corresponding to approximately 1.0% permanent set. The influence of permanent plastic deformation on μ_r is further illustrated by the results from cycle C3 where the specimen was taken up to 6.9% strain and then unloaded giving a permanent set of 6.6% strain an increase of some 5.54% strain from the 1.0% strain of cycle C2. This increase in permanent strain at zero load gave a correspondingly large decrease in the unloaded value of μ_r from 273 down to 227. This correlation between the degree of permanent set and the decrease in the unloaded value of μ_r was reinforced by examining the unloaded value of μ_r from the specimens used to produce figure 7.11. Here the specimens were strained up to 16% and on unloading the permanent set was 15.7%. Initially the value of μ_r was 282 but after loading/unloading and the introduction of a large permanent set into the specimen the unloaded value fell to 189.

A further interesting result confirming the reversible elastic effect was the variation of μ_r over cycle C4 when the specimen had already undergone a large degree of plastic deformation and starts at zero load with a permanent set of 6.6%. The specimen was loaded up close to the new increased yield point of the material so there was little or no increased plastic strain and the deformation was almost purely elastic. On unloading the permanent

set returned very close to its initial value unloaded value of 6.6% strain and approximately the same initial value of μ_r.

N.B. There was some slight discrepancy since it was impossible to just attain yield exactly and some slight increase in plasticity was unavoidable.

In conclusion these results clearly indicate the considerable effect both elastic and plastic strain have on the value of μ_r with a 14% decrease from its initial value up to the yield point of the material and overall a decrease of 42% as μ_r approaches a steady state value at around the 8.0% strain level.. It has also been shown that elastic deformation has no permanent effect on the value of μ_r and once the load was removed the value of μ_r returned to its initial value. However when the material was deformed plastically there was a very marked permanent change in μ_r. As the specimen was strained the value of μ_r fell rapidly with increasing elastic strain and above yield the decrease was still steady but less rapid reaching a constant minimum value at 8% strain. On unloading the value of μ_r recovered slightly, increasing as the elastic component of strain was reduced towards zero. However μ_r never again attained its initial unloaded maximum value with the discrepancy in the two unloaded values being dependent on the increase of permanent set.

The complete set of results from this testing programme clearly confirmed μ_r as the dominant material parameter governing any observed changes in ACPD response.

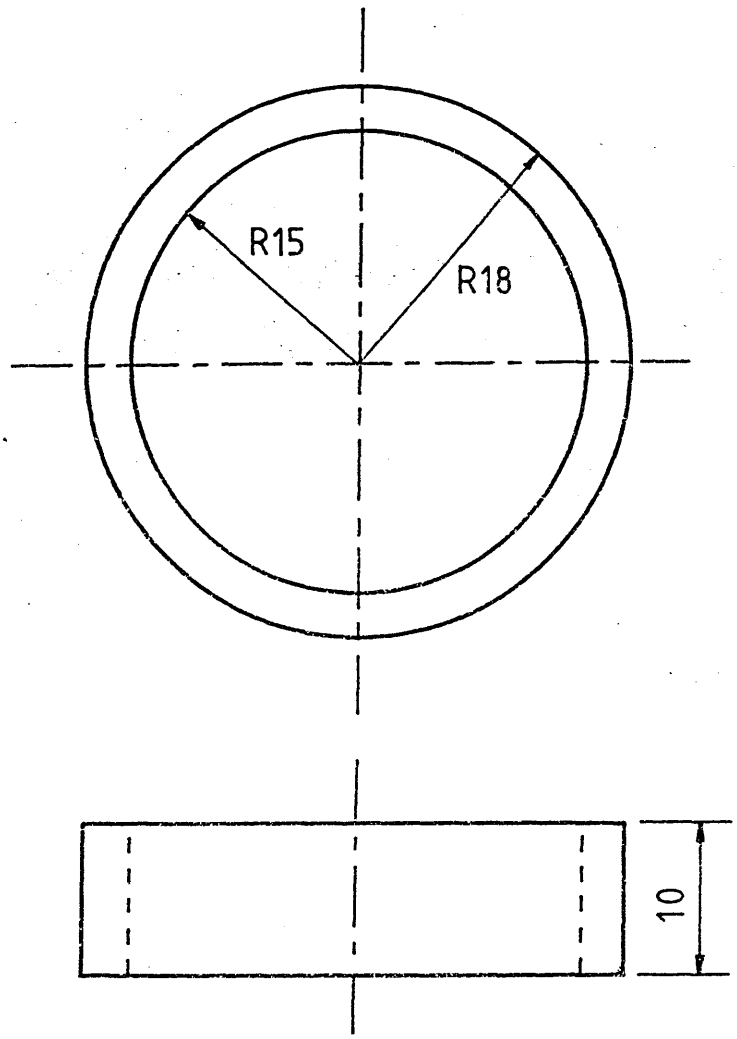

(all dimensions in millimetres)

Mean Circumference of Ring, s = 103·7 mm

Figure 7.1 Specimen Geometry for Magnetic Ring Specimens

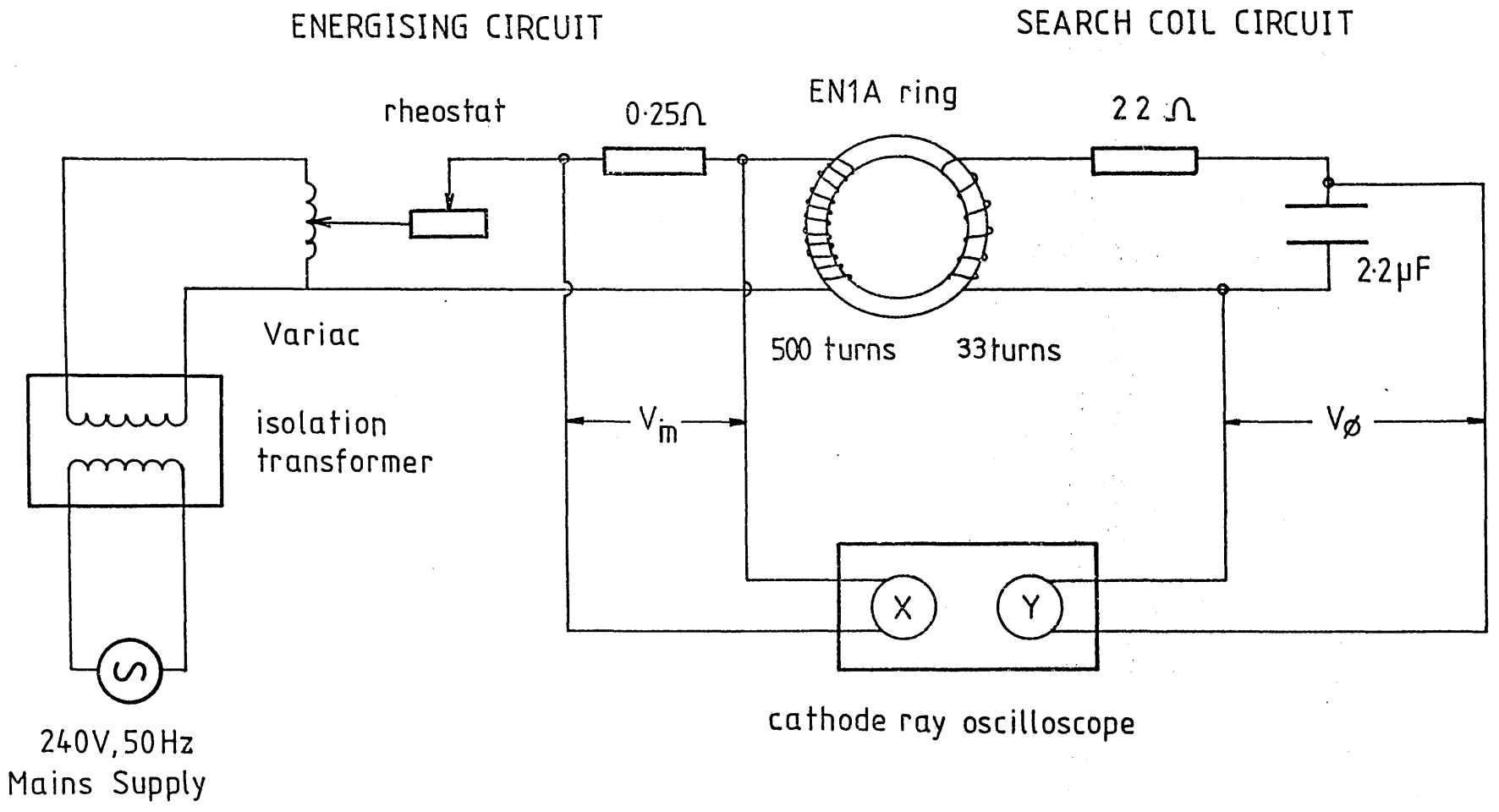

Figure 7.2 Circuit for Measuring Cyclic Magnetization Characteristics of EN1A Ring Specimens

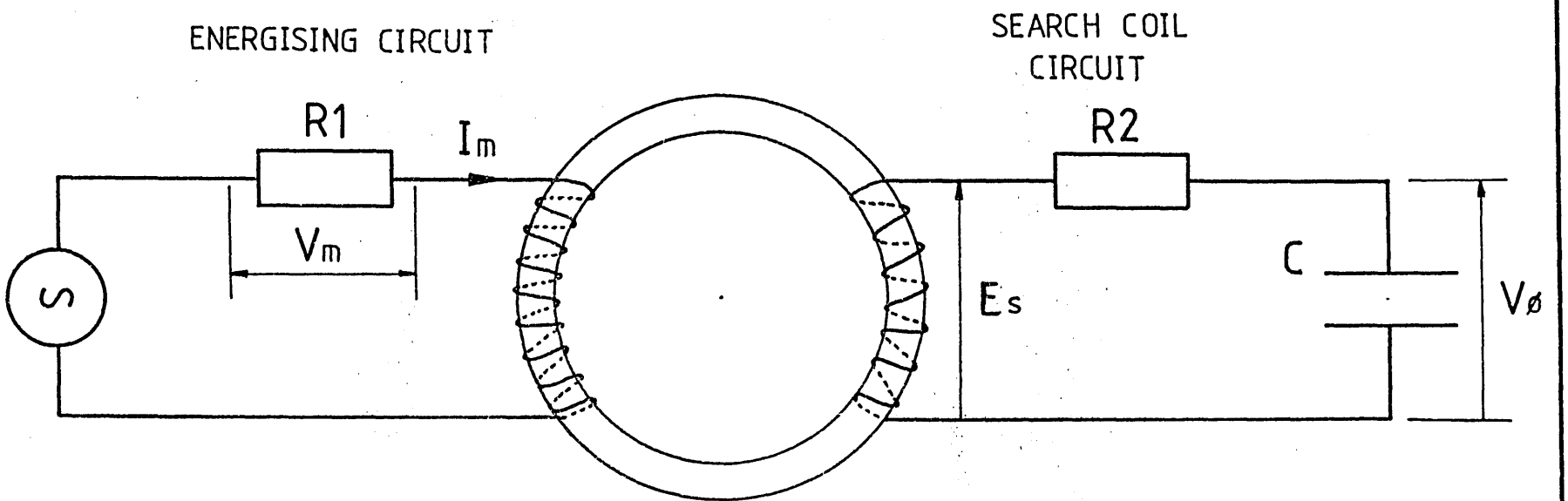

Figure 7.3 Signal and Electrical Component Notation

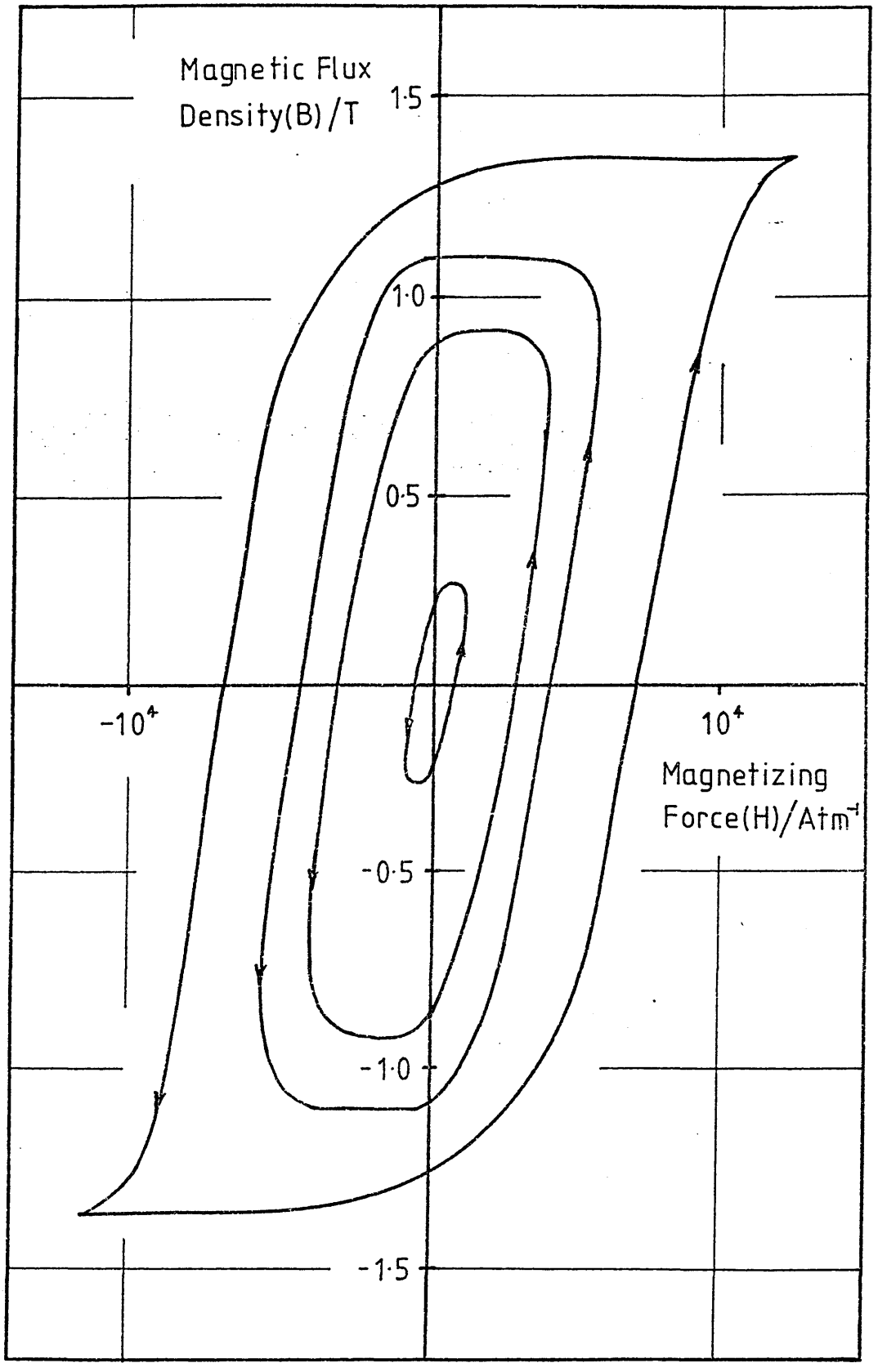

Figure 7.4 Magnetic Hysteresis Curves produced from EN1A Ring Specimens

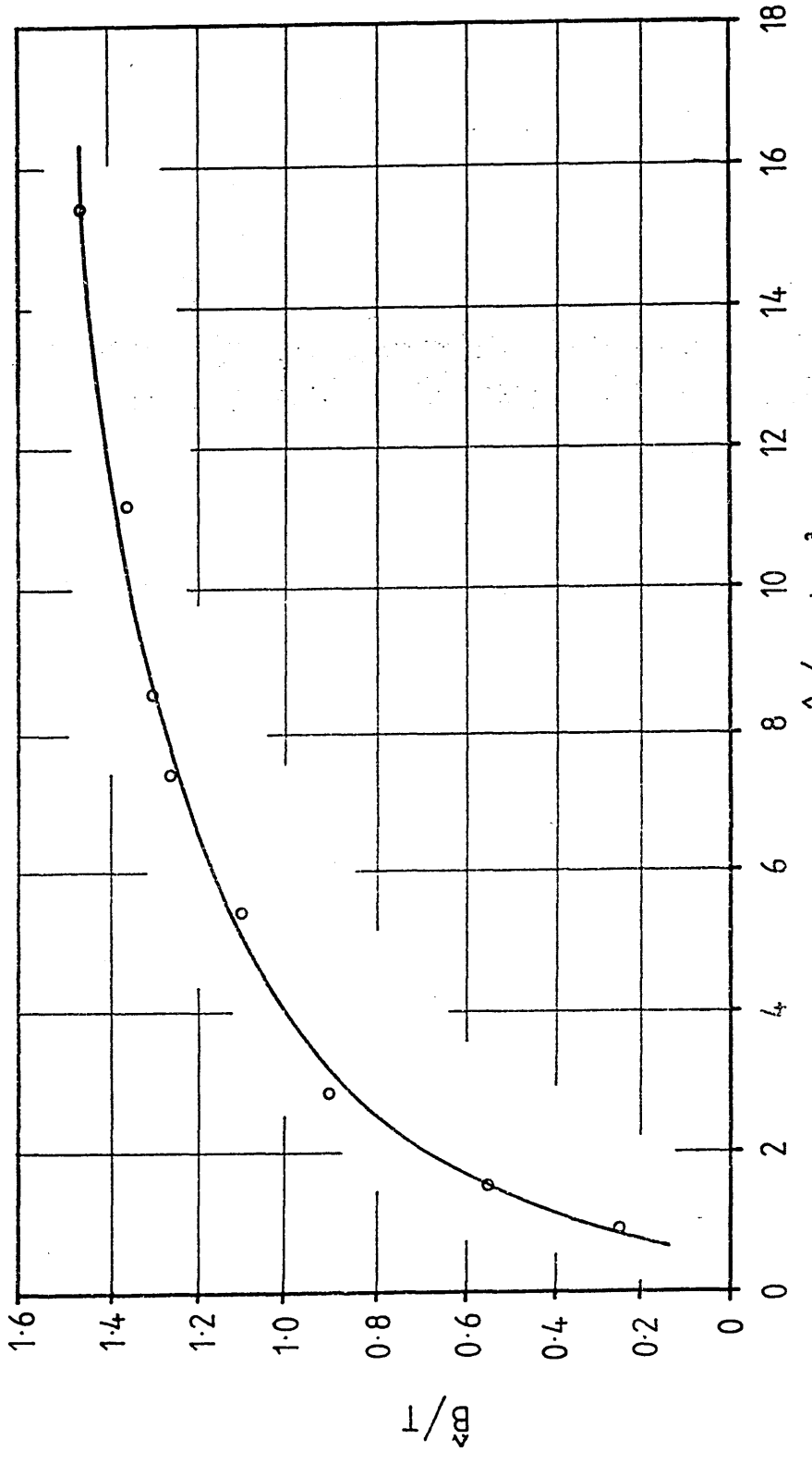

Figure 7.5 Approximate Initial Magnetization Curve for EN1A

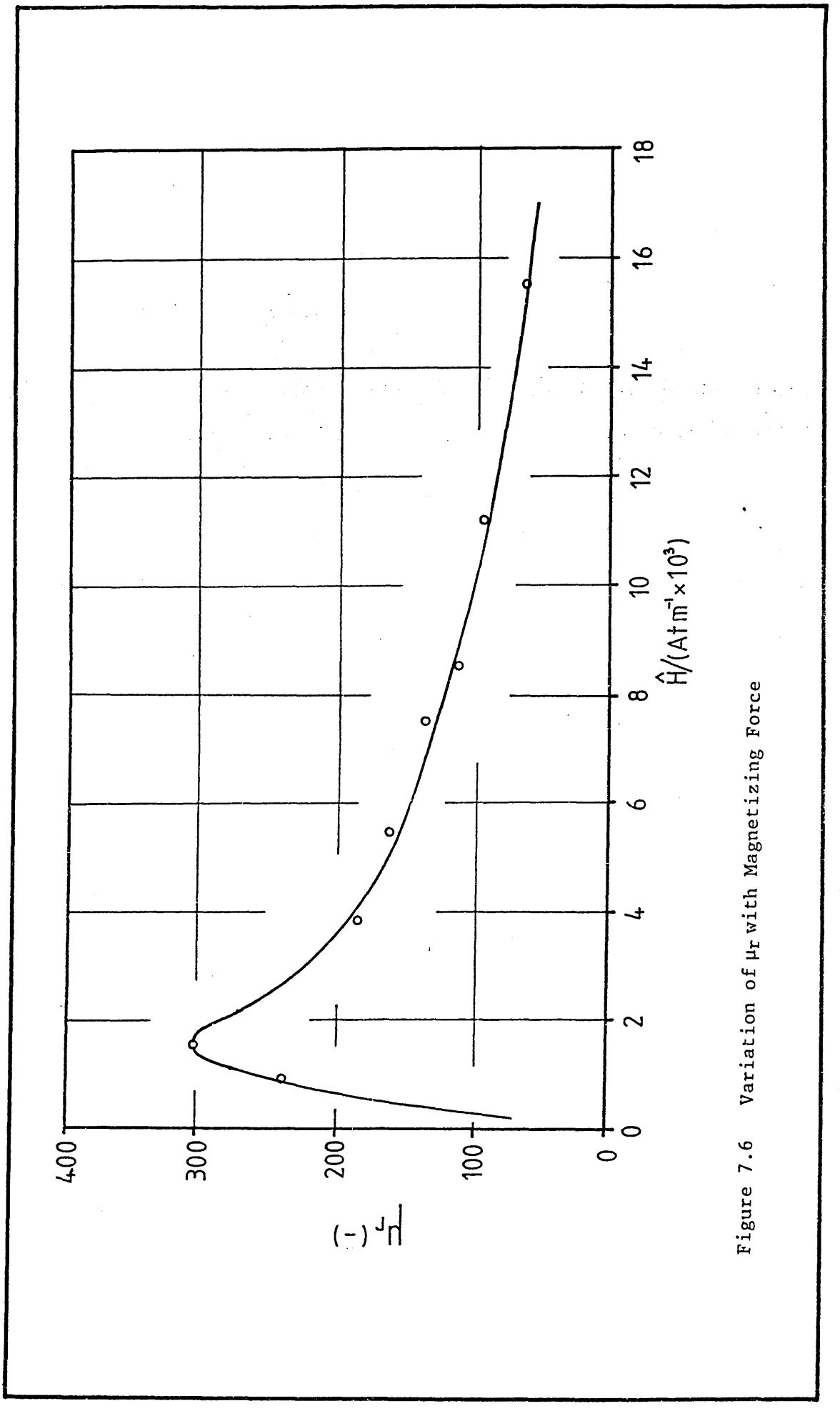

Figure 7.6 Variation of μ_r with Magnetizing Force

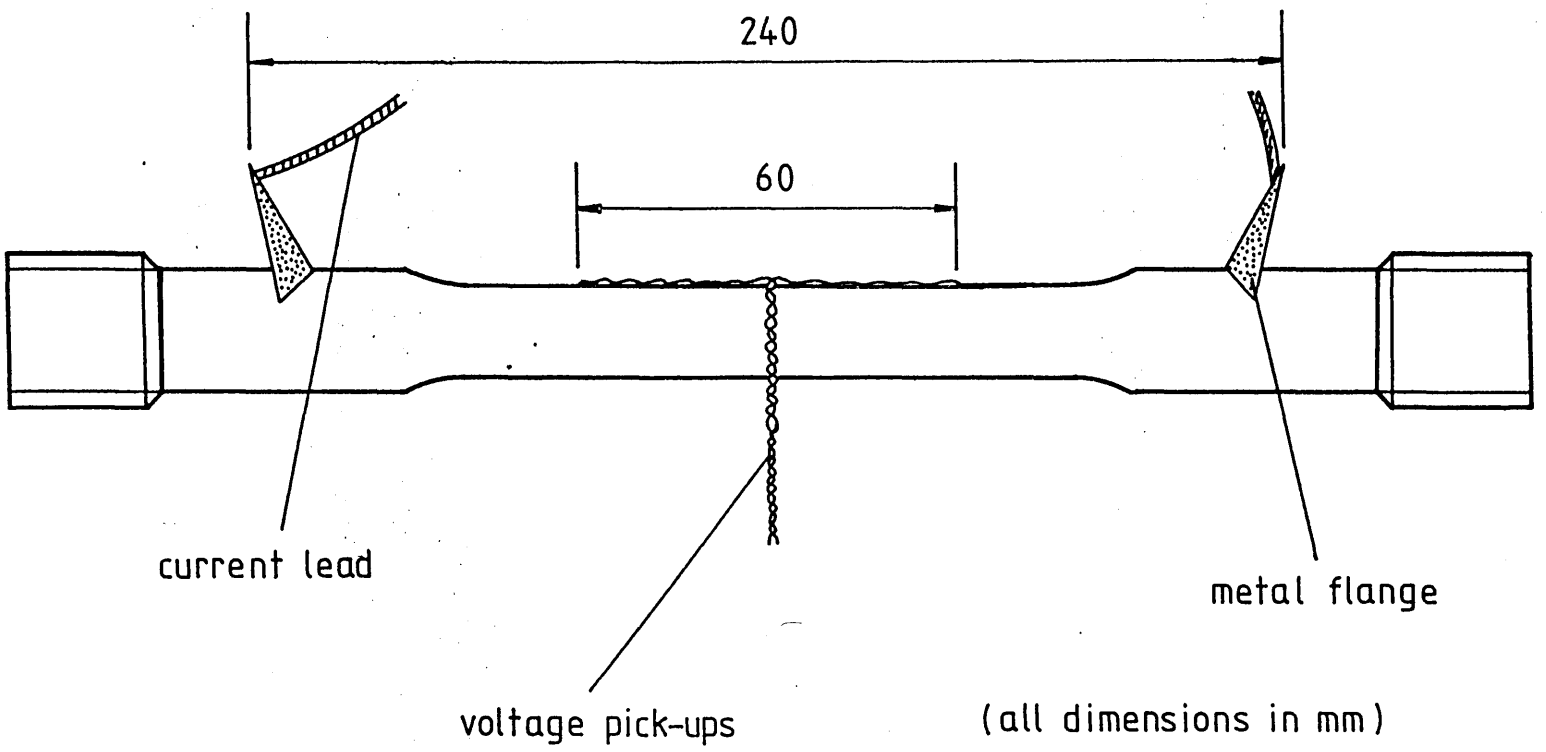

Figure 7.7 Geometry of Magnetic Tensile Specimens and Location of Current Input Leads and Voltage Pick-ups

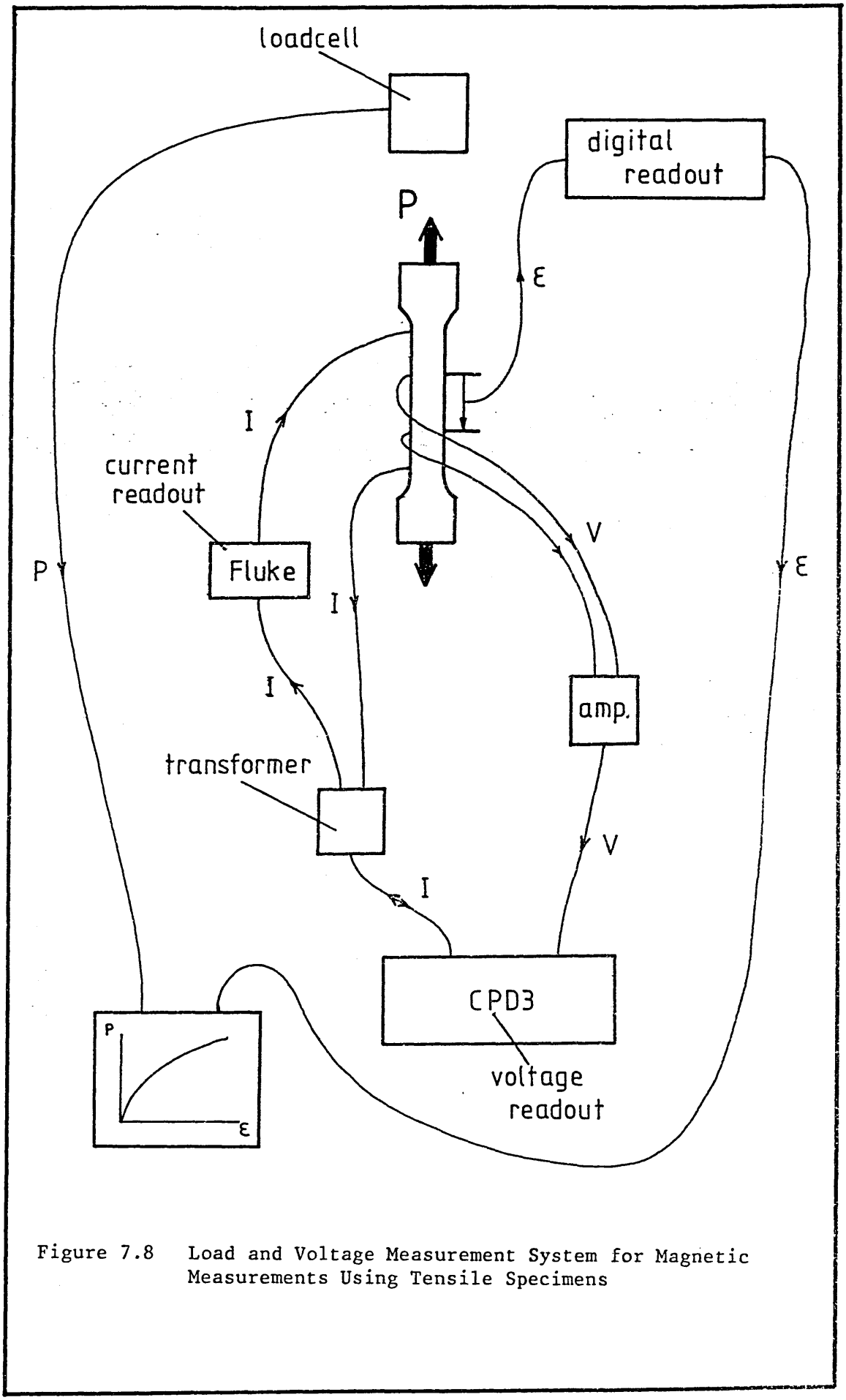

Figure 7.8 Load and Voltage Measurement System for Magnetic Measurements Using Tensile Specimens

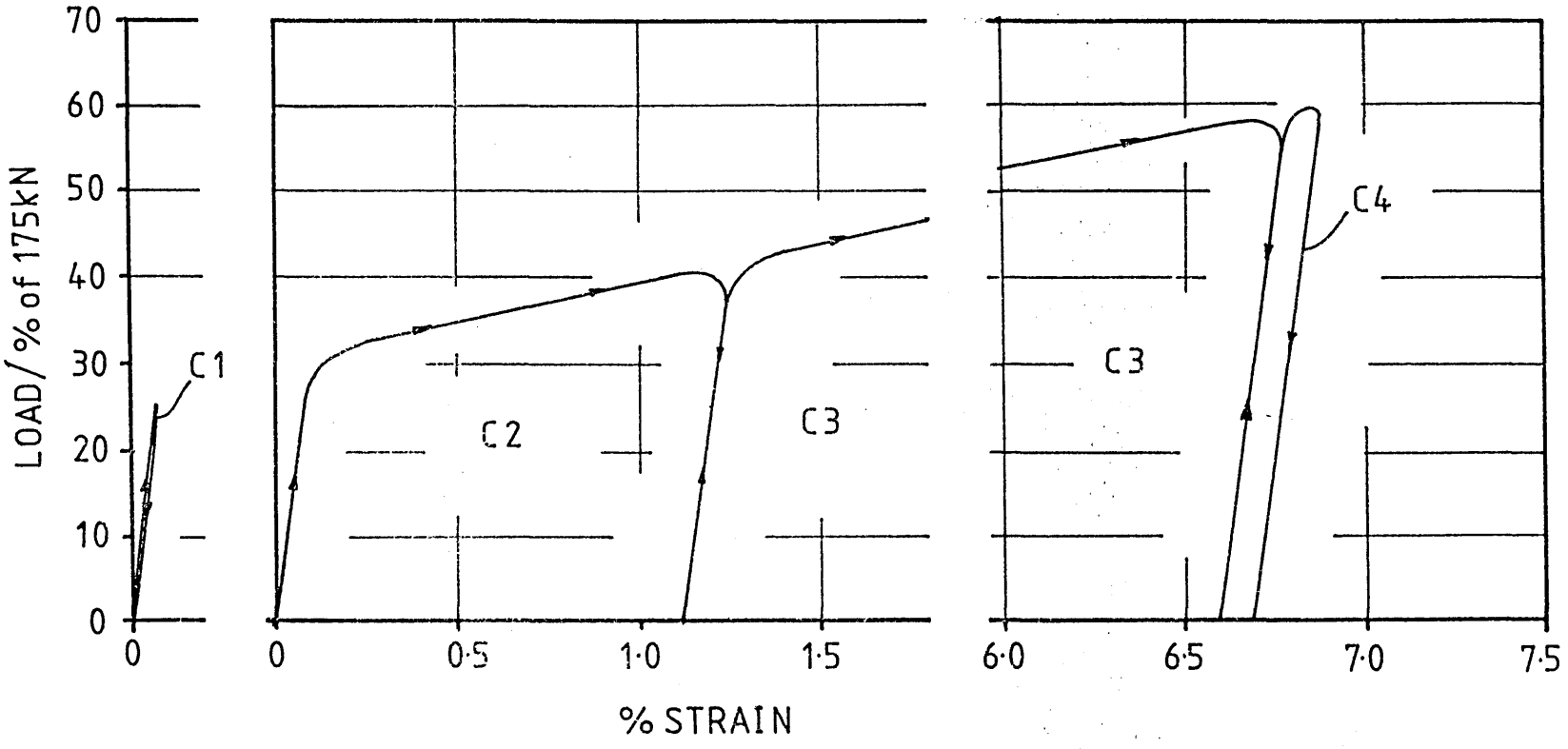

Figure 7.9 Loading/Unloading Sequence for Tensile Specimens

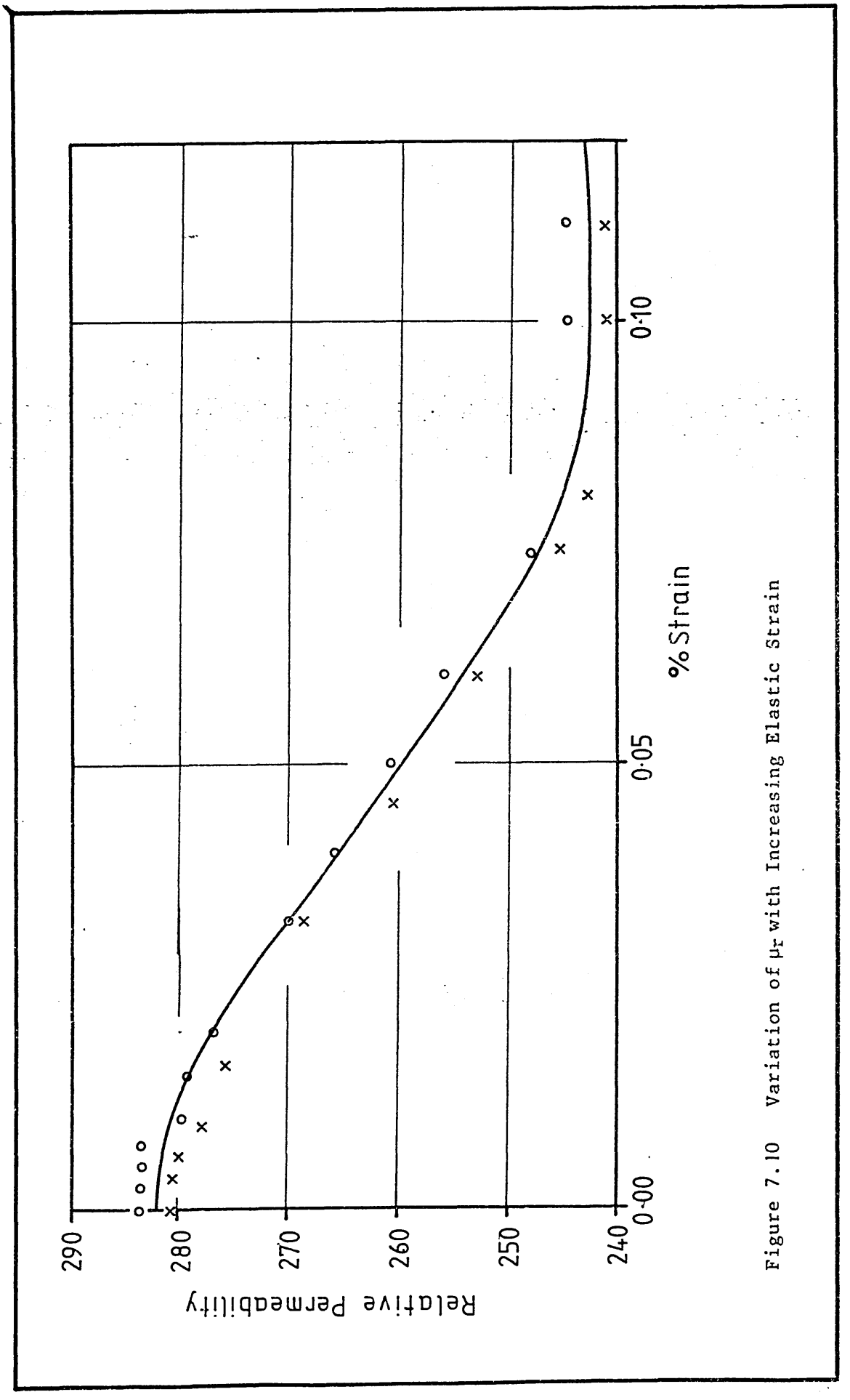

Figure 7.10 Variation of μ_r with Increasing Elastic Strain

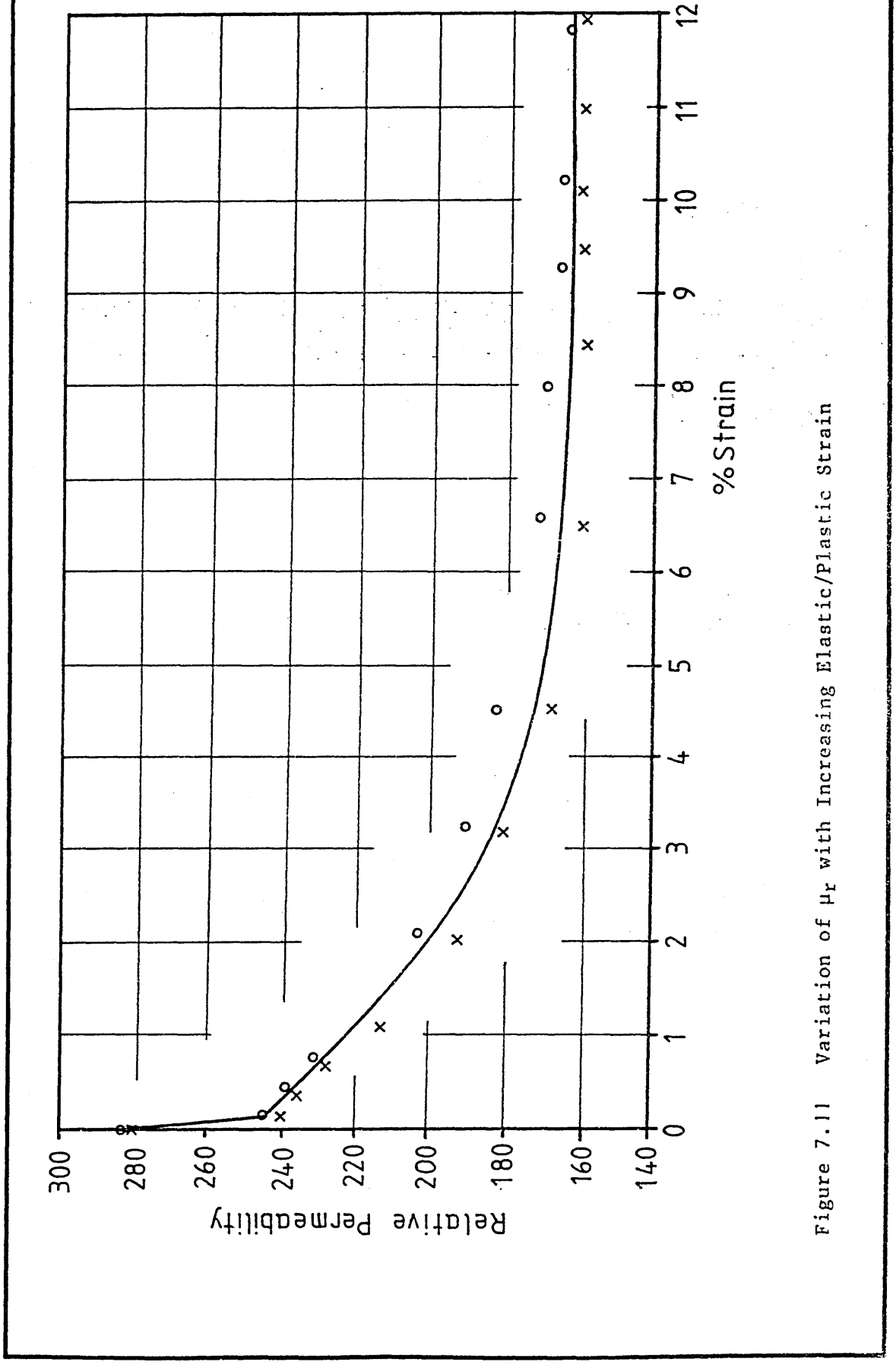

Figure 7.11 Variation of μ_r with Increasing Elastic/Plastic Strain

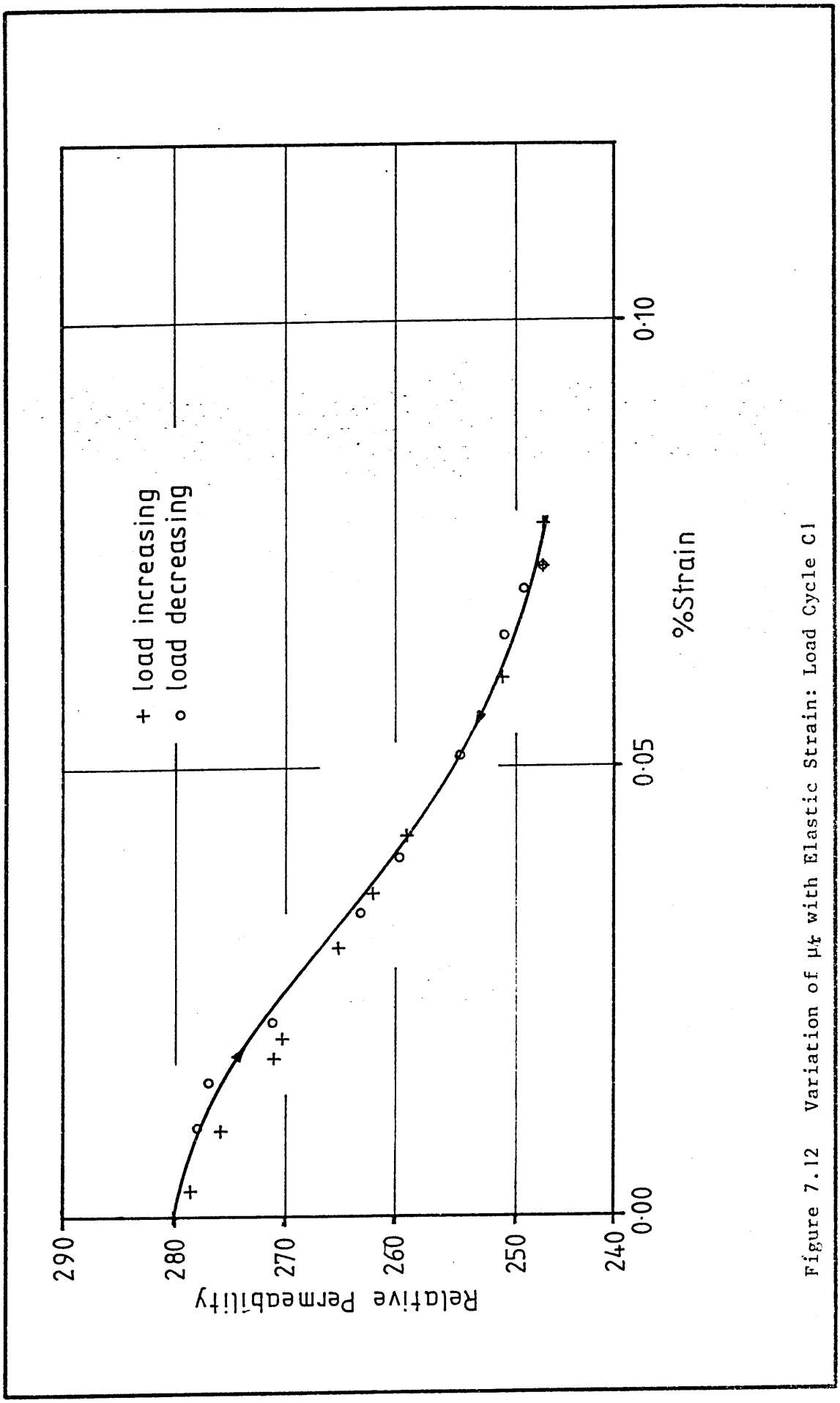

Figure 7.12 Variation of μ_r with Elastic Strain: Load Cycle C1

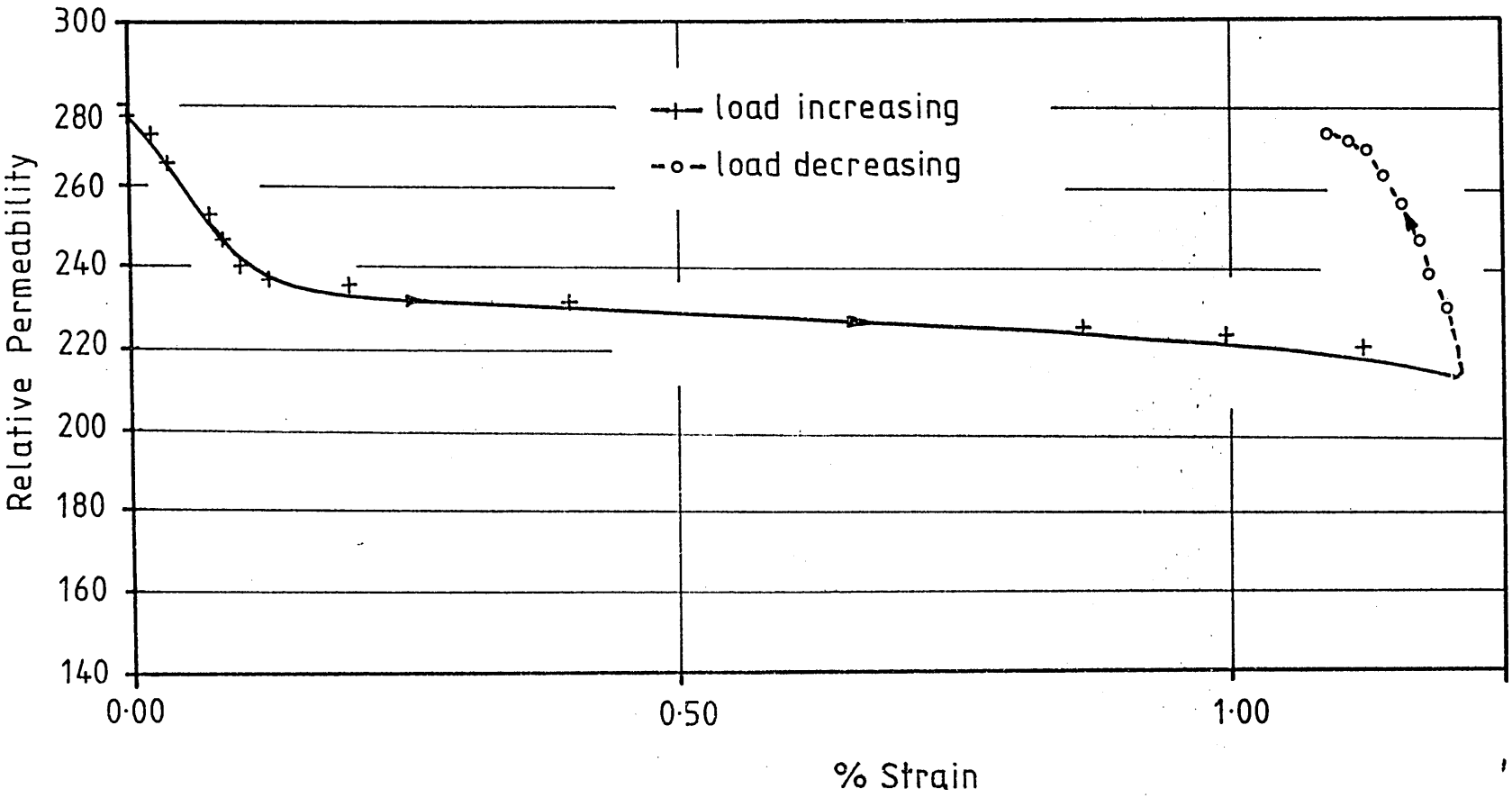

Figure 7.13 Variation of μ_r with Elastic/Plastic Strain: Load Cycle C2

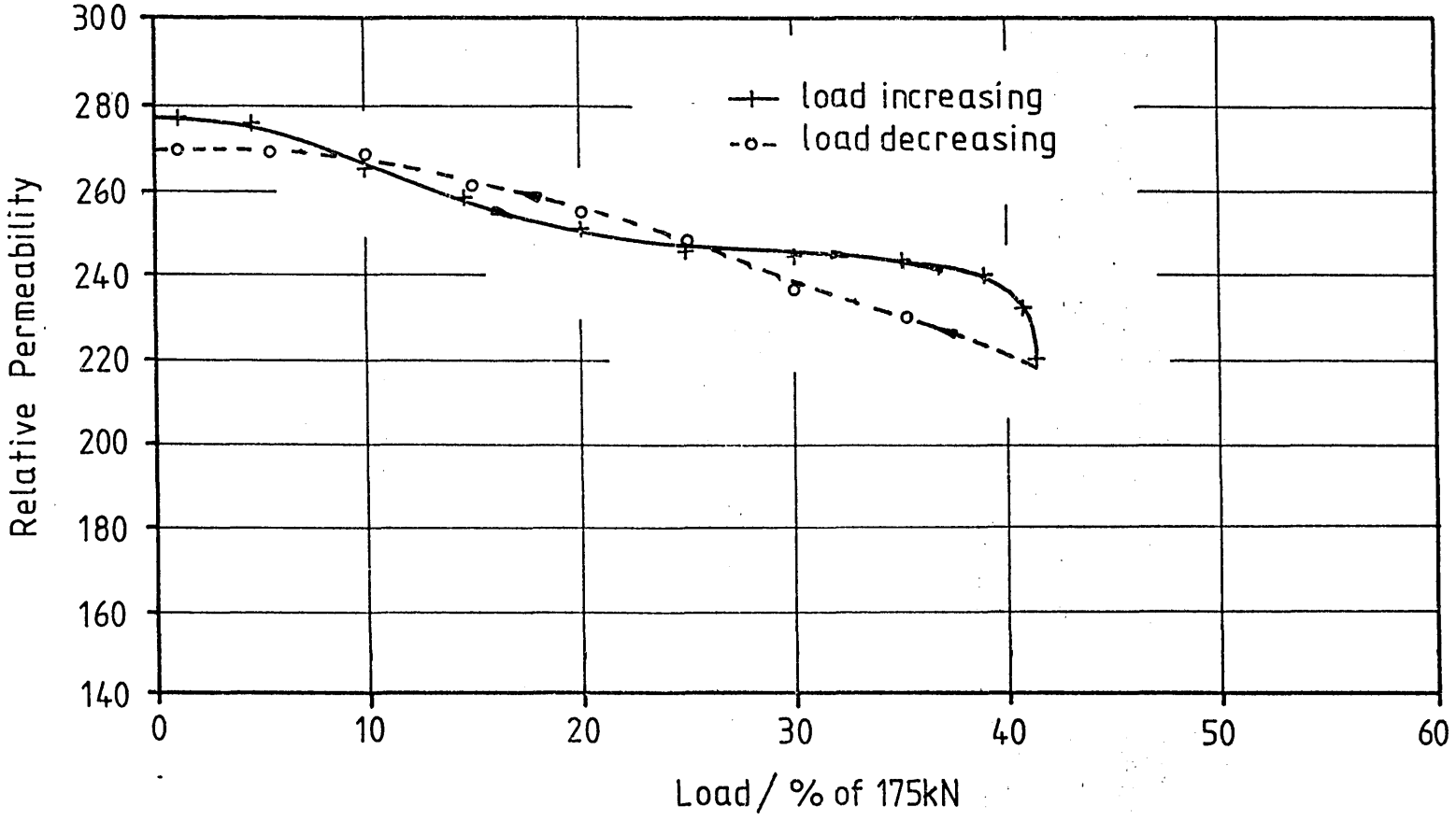

Figure 7.14 Variation of μ_r with Load: Load Cycle C2

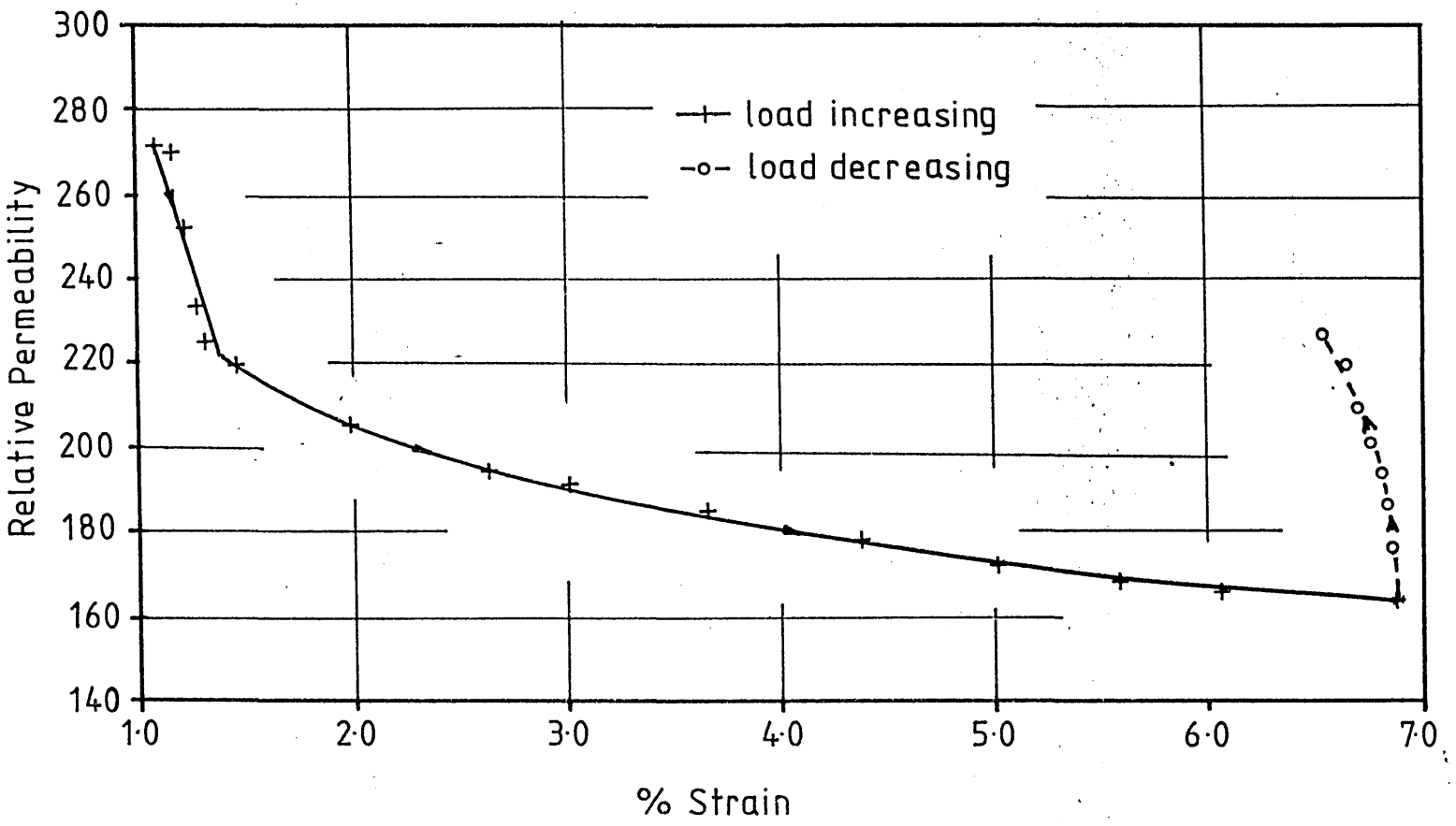

Figure 7.15 Variation of μ_r with Elastic/Plastic Strain: Load Cycle C3

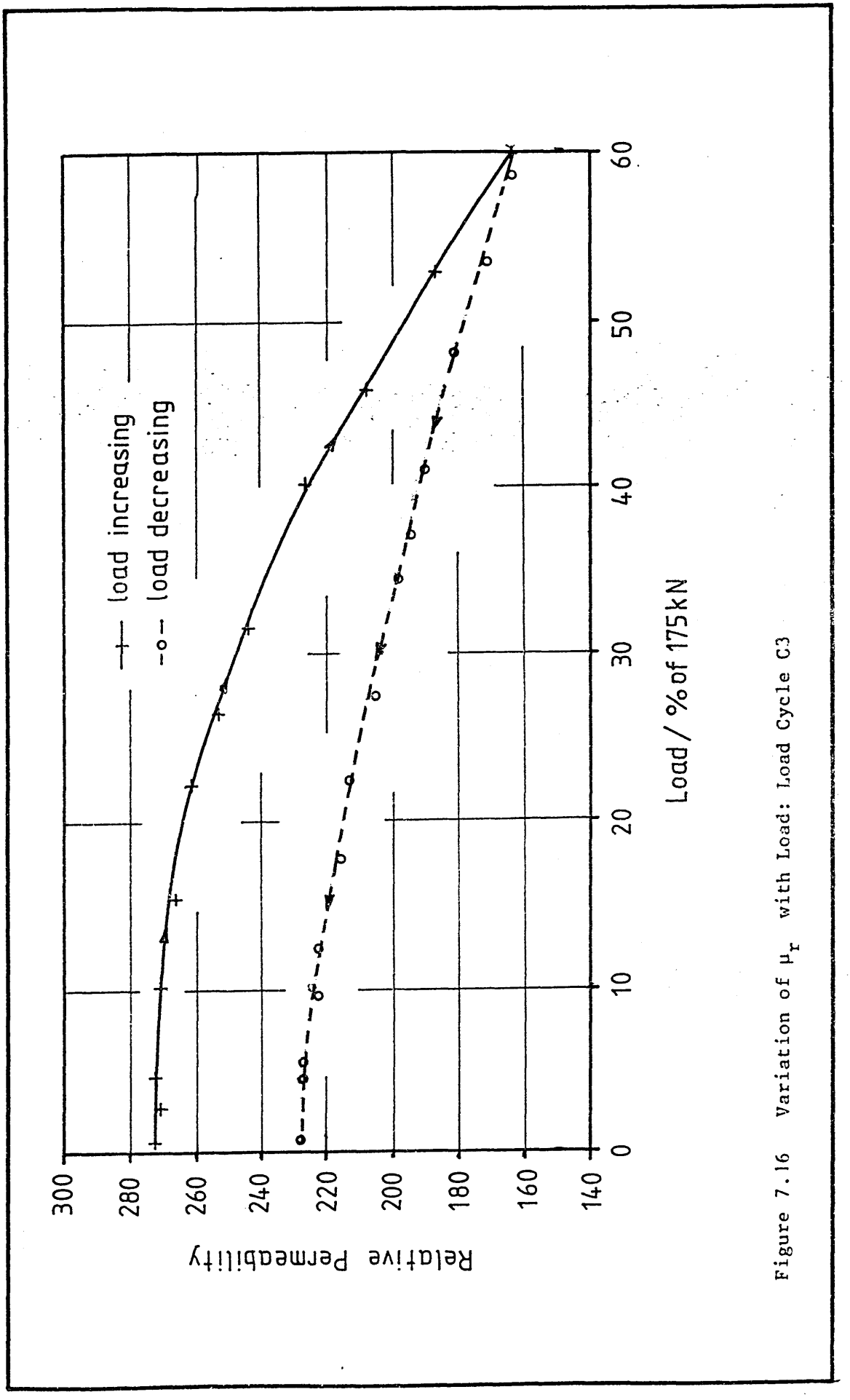

Figure 7.16 Variation of μ_r with Load: Load Cycle C3

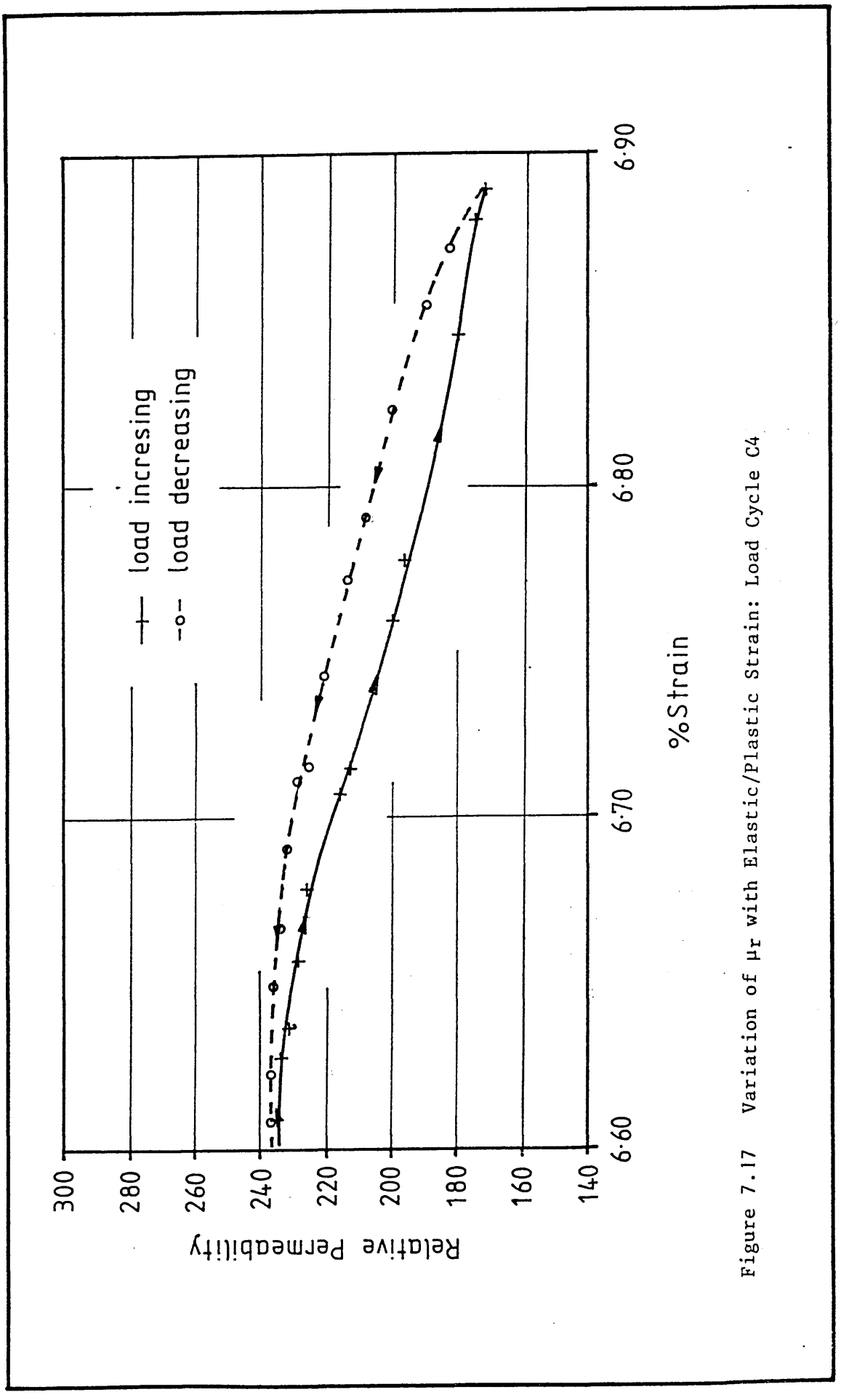

Figure 7.17 Variation of μ_r with Elastic/Plastic Strain: Load Cycle C4

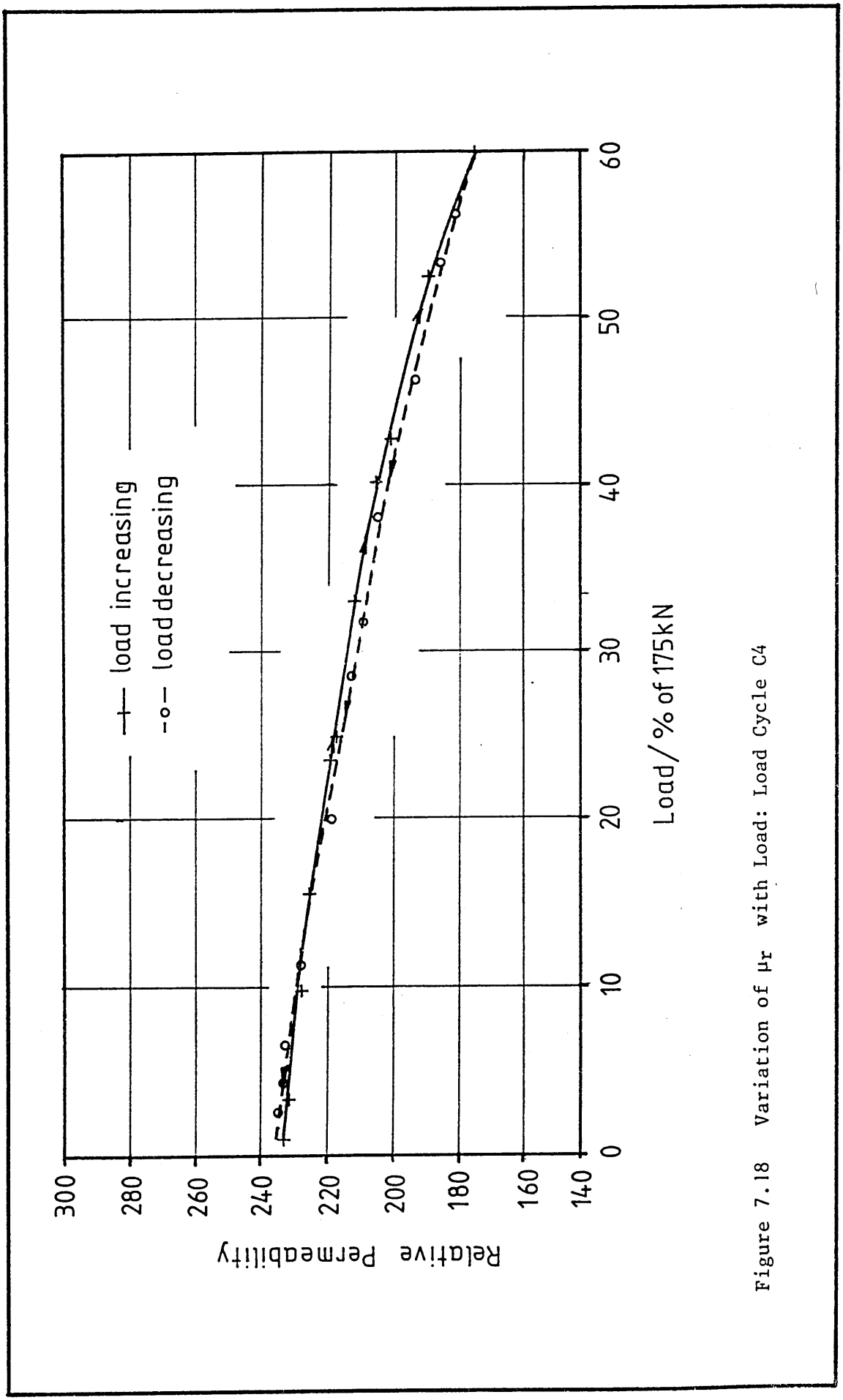

Figure 7.18 Variation of μ_r with Load: Load Cycle C4

CHAPTER 8 - A SIMPLE AC ELECTRIC FIELD MODEL

8.1 INTRODUCTION

During the experimental work detailed in previous chapters a great deal of data was collected about the parameters influencing the observed changes in ACPD response measured across the notch due to elastic/plastic deformation at the notchroot. At this stage of the project it was thought perhaps possible to predict the observed ACPD response via a simple electric field model of the AC distribution around the notch and details of the development of such a model are given in this chapter.

It had been successfully demonstrated, up to the 6-7% strain level, that the electrical resistivity (ρ) had an insignificant role in determining any variations in ACPD response and it was the magnetic permeability (μ), or equivalently the relative magnetic permeability (μ_r), which governed any observed changes. Following the successful completion of the experimental work to quantitatively determine the variation μ_r with strain and the finite element (FE) analysis to determine the local strain fields around the different notches, all the necessary parameters and conditions were known to allow some predictions to be made of the ACPD response observed across the EN1A notch profiles. No further consideration of the NE8 notches was necessary since the null ACPD response observed could be fully explained by the invariance of both μ_r and ρ.

8.2 DEVELOPMENT OF THE AC ELECTRIC FIELD MODEL

8.2.1 Introduction

As stated in the previous section it was discovered from

the experimental results that μ_r was the only material parameter affected by strain and therefore the only parameter determining the changes in ACPD response observed across the different notches. It was also found that μ_r varied non-linearly with strain, being particularly sensitive to elastic strain with a continual decrease from its initial value of 284 to reach a steady value of 164 at high levels of plastic strain (>5%).

From the results of the FE analysis it could be seen there was a very marked strain gradient along the surface of the specimen and notch sides and also going inwards from the surface of the specimen. Clearly then μ_r and hence the AC impedance varied continuously from "point" to "point" of the material and the potential drop observed would have been the resultant of all these infinitesimal impedances acting collectively together.

A rigorous mathematical determination of the resultant impedance would have required the integration of a function describing the variation of μ_r with position (strain) in the neighbourhood of the notch over an appropriate region of the specimen. Given the non-linear nature of the strain/permeability response and the complexity of the strain field this would have been a very difficult task almost certainly requiring numerical integration techniques and far beyond the scope of the present study. In an attempt to reduce the complexity of the calculation several simplifying assumptions were incorporated into the basic electromagnetic field model.

The strain data from the FE analysis was in the form of discrete values given at every element node in the structure with

each nodal strain value corresponding to a particular value of μ_r, see figure 8.1. This suggested strongly the possibility of considering a single element of the FE mesh as a discrete block of material with a characteristic AC impedance determined by the level of strain within the element. Further since the skin effect was very strong in EN1A and the skin depth of the order of 0.1 mm it was assumed that only the element nodes along the surface of the material and faces of the notch need be considered in calculating the overall AC impedance. For every node the equivalent strain was considered rather than the individual strain components since this gave a single value representative of the overall state of deformation at a particular node. These nodal values were then averaged to produce a representative value of strain for each element, see figure 8.1. Once the characteristic level of element surface strain was known μ_r and the element impedance could then be determined. The electric field was then modelled as a simple electrical circuit with every elemental impedance being in series with the next and each experiencing the same input current, I, see figure 8.2.

(This latter assumption may not have been strictly correct since if the skin depth was greater than the depth of an element the current would in fact have been distributed between two or more elements. However this was only likely to occur around the notch root where the element size was small and otherwise forms a reasonable assumption.)

8.2.2 Analysis

The basic assumptions incorporated into the electromagnetic

field model have been outlined above and a detailed description of their application to produce estimates of the ACPD response expected across each of the notch profiles is given below.

Consider the expression for the AC impedance, Z, of a cylindrical conductor, length 1 and radius r.

$$Z = \frac{\rho l}{2\pi r\delta} \quad , \quad \delta << r \qquad 8.1$$

where,

$$\delta = \left\{\frac{\rho}{\mu_r \mu_o \pi f}\right\}^{\frac{1}{2}} \qquad 8.2$$

Z may also be written as,

$$Z = \frac{V}{I} \qquad 8.3$$

where V is the potential drop across length 1 of the conductor and I is the input current.

Equation 8.1 represents the AC impedance of a conductor of circular section and does not strictly apply to other geometries. However, in the development of the electric field model, it was assumed that the rectangular section of the bend specimen could be represented by an equivalent cylindrical conductor, with a radius such that the impedance of each was the same.

The equivalent radius was not known beforehand but was assumed constant throughout.

Combining 8.1 and 8.2,

$$Z = \frac{V}{I} = \frac{\rho l}{2\pi r\delta} \qquad 8.4$$

Substituting into 8.4 the expression for the skin depth, equation 8.2,

$$\frac{V}{I} = \frac{1}{2\pi r} \cdot \left(\frac{\mu_r \mu_o f}{\rho}\right)^{\frac{1}{2}}$$

Rearranging,

$$V = \frac{I}{2\pi r} \cdot (\rho \mu_o \pi f)^{\frac{1}{2}} . l\mu_r^{\frac{1}{2}} \qquad 8.5$$

Equation 8.5 can be written as,

$$V = K . l\mu_r^{\frac{1}{2}} \qquad 8.6$$

where,

$$K = \frac{I}{2\pi r} . (\rho \mu_o \pi f)^{\frac{1}{2}} \qquad 8.7$$

(K is a constant multiplying factor, independent of load and element length, converting the product $l\mu_r^{\frac{1}{2}}$ to a potential drop in μV.)

It can be seen from equation 8.6 that the potential drop across each of the finite elements was proportional to both the length of the element surface and the square root of μ_r for the element, this being determined by the level of elemental strain. Hence it was possible to evaluate 8.6 for every element and since each was in series with the next the results could simply be summed to give the resultant total potential drop across the notch.

It should be noted that the technique of potential drop monitoring used throughout the experimental work was that of material compensation with an additional pick-up loop across a plain

section of material adjacent to the notch, see section 2.2. Therefore the resultant signal was the difference between the notch voltage, Vn, and the compensating voltage, Vc. This was taken into account in the calculations by considering the elements spanned by the compensating loop which were themselves subject to appreciable levels of strain.

Let the active loop span m elements and the compensating loop n elements, say.

Hence,

$$Vn = Kl_1\mu_{r1}^{\frac{1}{2}} + Kl_2\mu_{r2}^{\frac{1}{2}} + \ldots\ldots + Kl_m\mu_{rm}^{\frac{1}{2}}$$

$$= K\sum_{i=1}^{m} l_i\mu_{ri}^{\frac{1}{2}} \qquad 8.8$$

Similarly for the compensating loop,

$$Vc = Kl_{m+1}\mu_{rm+1}^{\frac{1}{2}} + Kl_{m+2}\mu_{rm+2}^{\frac{1}{2}} + \ldots\ldots + Kl_n\mu_{rn}^{\frac{1}{2}}$$

$$= K\sum_{i=m+1}^{n} l_j\mu_{ri}^{\frac{1}{2}} \qquad 8.9$$

Therefore the overall potential drop registered, V, is given by,

$$V = Vn - Vc = K.\left\{\sum_{i=1}^{m} l_i\,\mu_{ri}^{\frac{1}{2}} - \sum_{i=m+1}^{n} l_i\mu_{ri}^{\frac{1}{2}}\right\} \qquad 8.10$$

The evaluation of equation 8.10 at every load level for all the necessary elements would have been a very time consuming procedure. To speed the evaluation of this equation a program was written in APPLESOFT Basic and run on an APPLEIIE microcomputer to process the element strains and dimensions and automatically

produce estimates of potential drop. A complete listing of the "DRAGON" program is given in Appendix V.

All the necessary information was input at the beginning of the program using a series of data statements. The information was presented as a series of strain values preceded by the element number and surface length with each strain value corresponding to the average strain over the three nodes at the element surface for each load level. The strains were taken from the results of the PAFEC elastic/plastic FE analysis of the U and V notches assuming conditions of plane strain.

Plane strain conditions were chosen since the potential drop was measured along the centreline of the specimen where this particular stress state was likely to prevail over that of plane stress. However the use of the plane stress results would make no appreciable difference to the results.

8.3 RESULTS AND DISCUSSION

The computer predictions of the ACPD response across the U and V notches for the mild steel EN1A can be seen in figures 8.3 and 8.4. In both cases the potential drop across the notch using the compensation method has been plotted against increasing load allowing a direct comparison with the experimental results given in Chapter 3. It should be noted that the choice of PD scale is somewhat arbitrary and depends on the values assigned to the constant K in equation 8.7, which in turn depends on the choice of circumference, $2\pi r$, for the circular conductor equivalent to the rectangular section

of the bend specimen. The circumferential distance was chosen as 60 mm to give potential drop values in the same range (100 - 200 μV) as the experimental values. The choice of 60 mm was also quite acceptable from an intuitive point of view. The rectangular section of the bend specimen has a cross-sectional area of 450 mm^2 and the circular section with the same area has a circumference of 75 mm, a slightly greater value than required. However, current was only injected into the top surface of the bend specimen and so would have tended to be concentrated in this region and therefore behave as a circular conductor of somewhat lesser cross-section.

Contrasting the predicted results given in figures 8.3 and 8.4 with the experimental first cycle responses given in chapter 3 several points are immediately obvious.

Firstly, the similarity between the shapes of the predicted and experimental curves with the same turning points seen on each. The results shown in figures 8.3 and 8.4 predict an initial fall in ACPD response with a minimum value occurring at around 10 kN, with the V notch falling 15 μV and the U notch 7 μV. This is in excellent agreement with the experimental values of 10-20 μV for the V notches and the slightly lesser value of 5-15 μV for the U notches. After this minimum value there is then a predicted uniform increase of around 32 μV to a maximum at 40 kN for both notch profiles. This increase was seen in the experimental results but was not quite as large with 15-20 μV being typical.

However, the predicted turning point at 40 kN is in good

agreement with the experimental values.

In all the simple electric field model gave a good quantitative prediction of the experimentally observed ACPD response. Unfortunately it was not possible to model the unloading response since no detailed strain information during unloading was available from the FE analysis once the material around the notch root had yielded.

The electric field model was also applied to the results seen with the NE8 specimens to see if it predicted an ACPD response in the range observed during the experimental work. Using the same value of equivalent section as before, the field model predicted responses of 6.5 μV and 7.1 μV for the V and U notches respectively, much less than the experimental values of 20-50 μV. The reason for the large discrepancy was due to the inherent limitations of the field model. The model assumes a surface distribution of current when in fact the skin depth for NE8 is of the order of 1.5 mm with an energising frequency at 8 kHz and the current is therefore carried in a layer of appreciable depth below the surface of the material. Hence additional finite elements, some distance below the surface of the specimen, need to be considered when the skin depth is large and the simple series impedance model no longer suffices.

During the development of the simple field model it became apparent that the compensation loop played a major role in determining the observed ACPD response. During the experimental work the compensation method was used to minimise the effect

of static and current fluctuation on the measured ACPD response. In effect the compensating voltage was assumed an invariant base voltage against which the notch signal could be compared and used to eliminate the effects of static and current fluctuation on the notch signal. However from the electric field model it became apparent that the compensating voltage was not constant and like the notch signal was subject to the effects of strain. Therefore the experimentally recorded ACPD response was the result of the interaction of these two variable signals and not directly indicative of any notch effects. The predicted ACPD response without the compensating loop can be seen in figures 8.5 and 8.6. There is a great difference between these results and the compensation results, most noticeably the disappearance of the two turning points. These results imply that the observed maxima and minima are not material effects but merely characteristics of the compensation measurement technique. Further from a consideration of the simple electric field model it is possible to explainfully the shape of the experimentally observed ACPD response in terms of the interaction of the two voltage signals as follows.

Using the compensation method the ACPD response recorded is the difference, (Vn-Vc), of the voltage across the notch, Vn, and the compensating voltage, Vc.

Consider the first portion of the ACPD response in either figure 8.3 or 8.4 where the PD initially falls up to 8-10 kN corresponding to the onset of yield at the notch root. Up to this level both the material around the notch and that spanned by the compensating loop is deforming elastically and, as seen in

figure 7.4, μ_r falls linearly with increasing elastic strain. Because of the very high elastic strains at the notch root the notch signal dominates the response with Vn falling more rapidly than Vc giving a resultant drop in (Vn - Vc).

Above 8 - 10 kN the ACPD response increases steadily up to 40 kN. In this region the notch is deforming plastically and consequently the decrease in μ_r becomes far less rapid, see figure 7.5. However the compensation loop is still deforming elastically and so μ_r, and therefore Vc, in this region falls at a much higher rate than across the notch. Hence the recorded difference (Vn - Vc) increases as Vc falls more rapidly than Vn.

Above 40 kN yielding takes place along the top surface of the specimen spanned by the compensating loop. The rate of decrease of μ_r is now very similar in both loops and once again the notch begins to dominate the ACPD response. As a result of the very high notch root plastic strains Vn decreases faster than Vc producing the observed fall in (Vn - Vc) above 40 kN.

Now consider the predicted results without the compensating loop shown in figures 8.5 and 8.6. These reveal that the AC impedance across the notch actually decreases nearly linearly with increasing strain exhibiting no maxima or minima. This points strongly to the possibility of detecting crack initiation from the root of a notch even when appreciable levels of plastic ity are present provided the compensation loop is omitted. The growth of a crack results in an increase in

ACPD response, and provided it grows sufficiently quickly, crack initiation would correspond to a turning point on the PD load curve and a subsequent increase in ACPD response as the crack propagated further.

Although it has proven possible to understand and predict the ACPD response during the initial loading the problem of explaining the unloading response is more difficult and outside the scope of the present work. The variation of μ_r with a decreasing load from various levels of plastic strain has been determined in the previous chapter. However it is not possible to explain fully the observed ACPD response with the notched specimens from this data. On unloading the plastic zone at the notch root is likely to be under compression from the surrounding bulk of elastic material and the effect of compressive stresses on μ_r is unknown. Further investigation of these effects may form the basis of future work.

In conclusion the simple electric field model allows a reasonably accurate predictionof ACPD response to increasing strain in materials where the skin depth is small. Additionally the compensation method of crack monitoring can lead to confusing results when appreciable levels of plasticity are present and the omission of the compensating loop would provide a clearer indication of crack initiation and subsequent propagation.

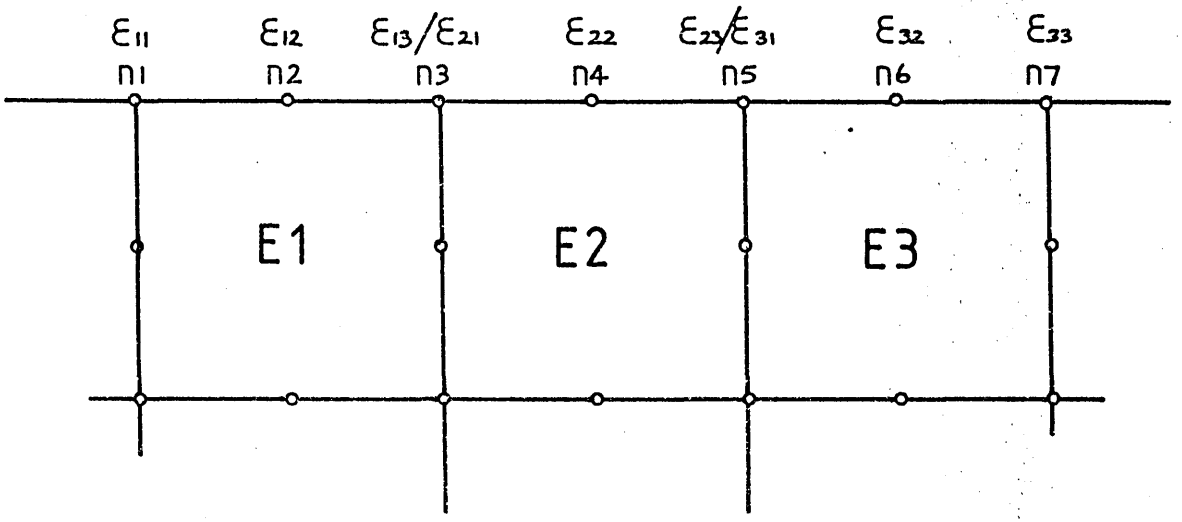

Element E2

Characteristic Strain Value = $\frac{\varepsilon_{2i}+\varepsilon_{22}+\varepsilon_{23}}{3}$

Fig. 8.1 Finite Element mesh and characteristic strain value

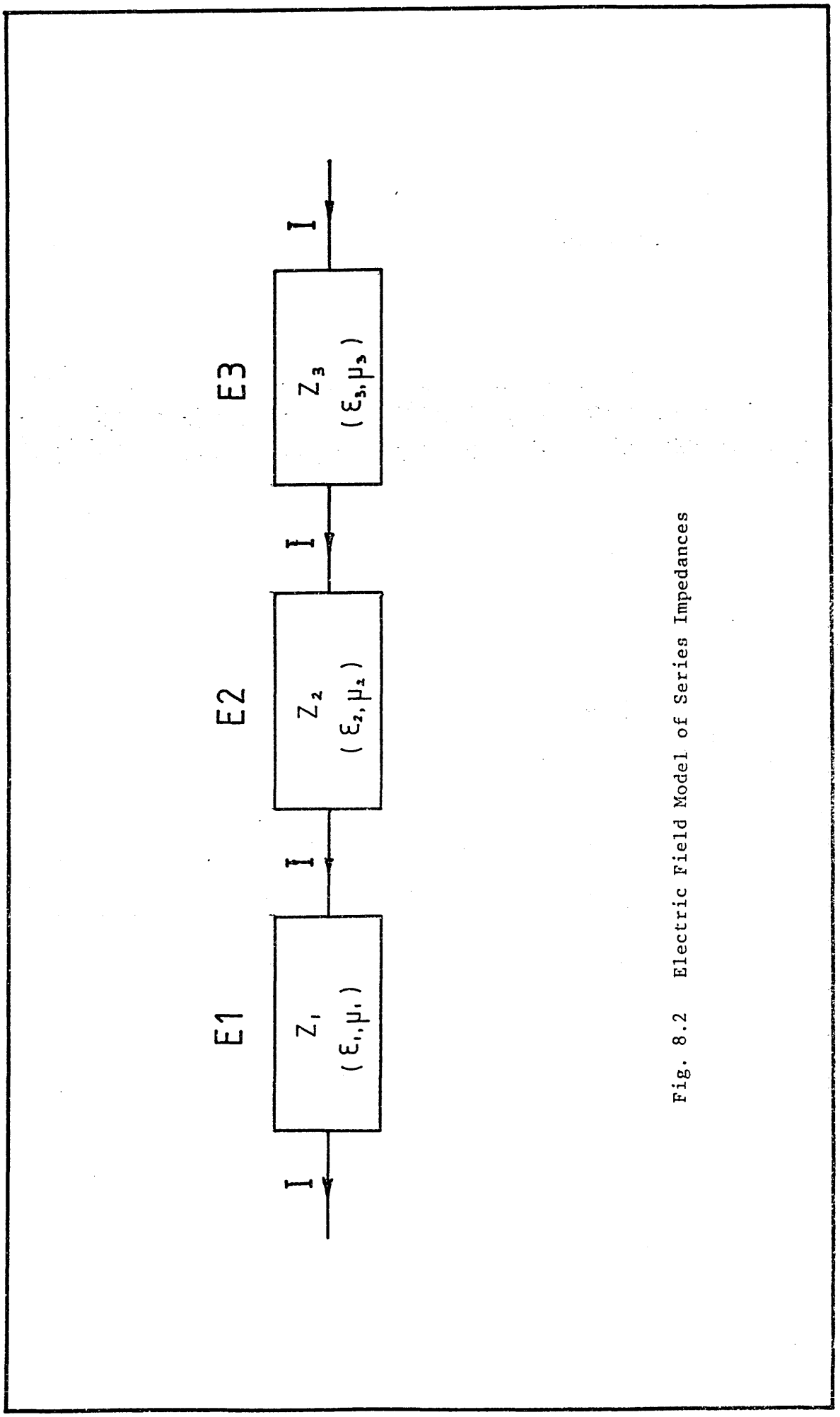

Fig. 8.2 Electric Field Model of Series Impedances

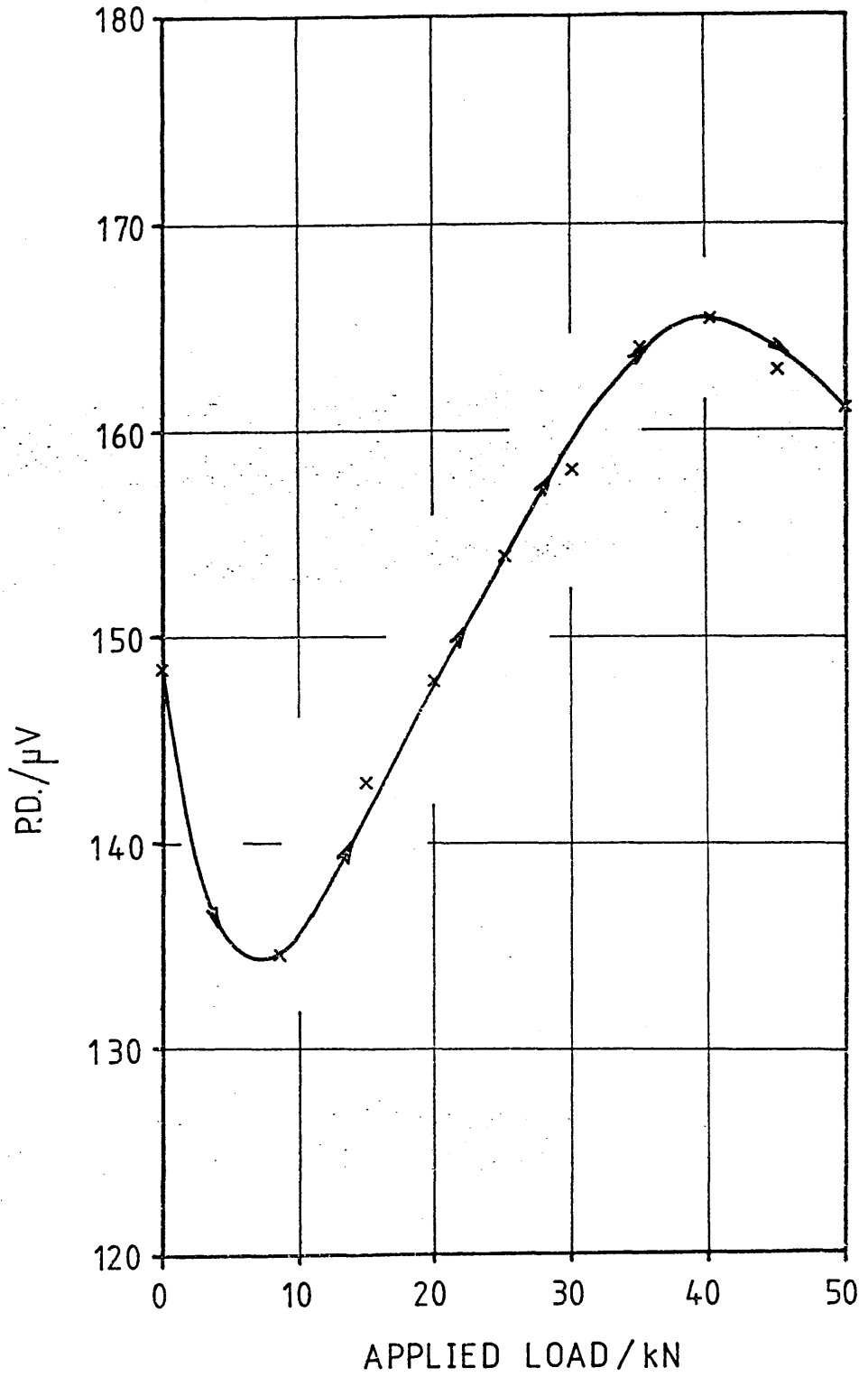

Fig. 8.3 Prediction of ACPD response across EN1A V Notch using compensation method.

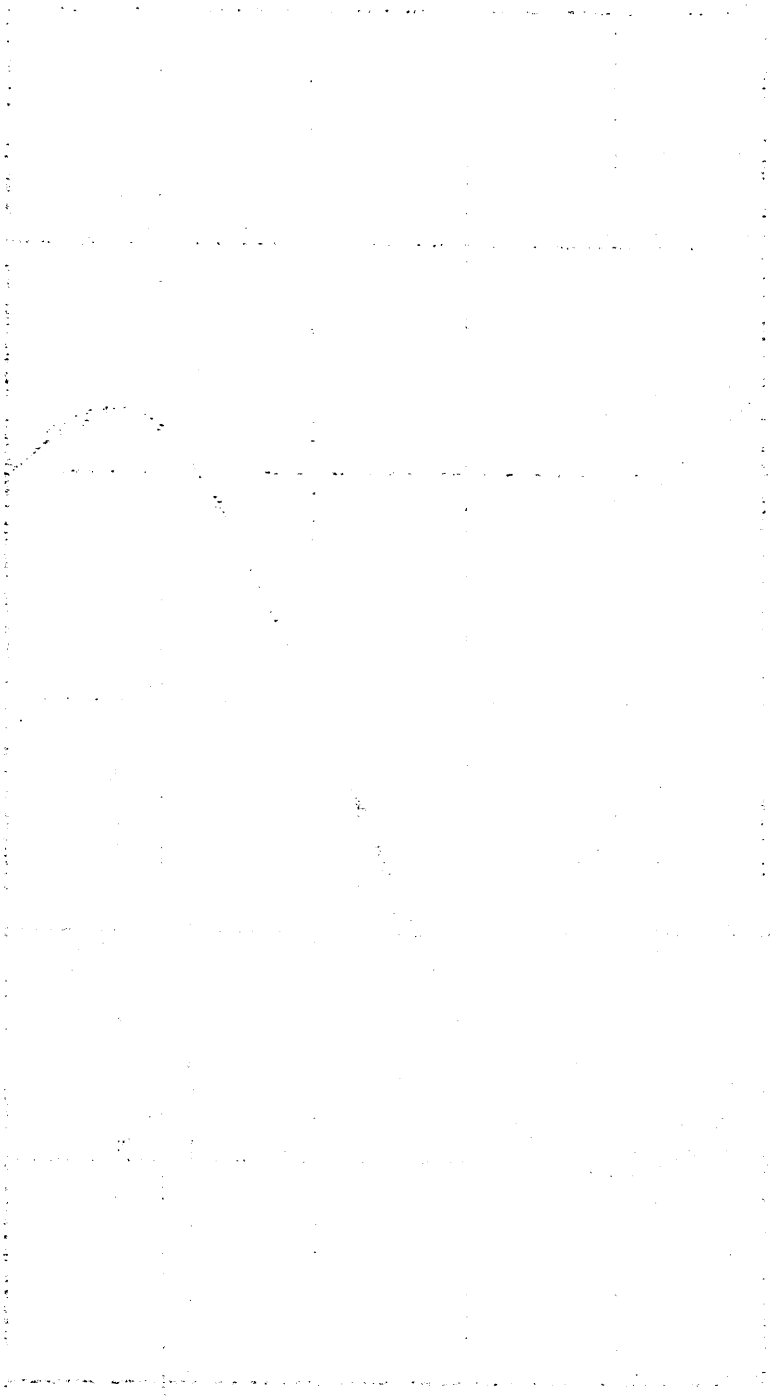

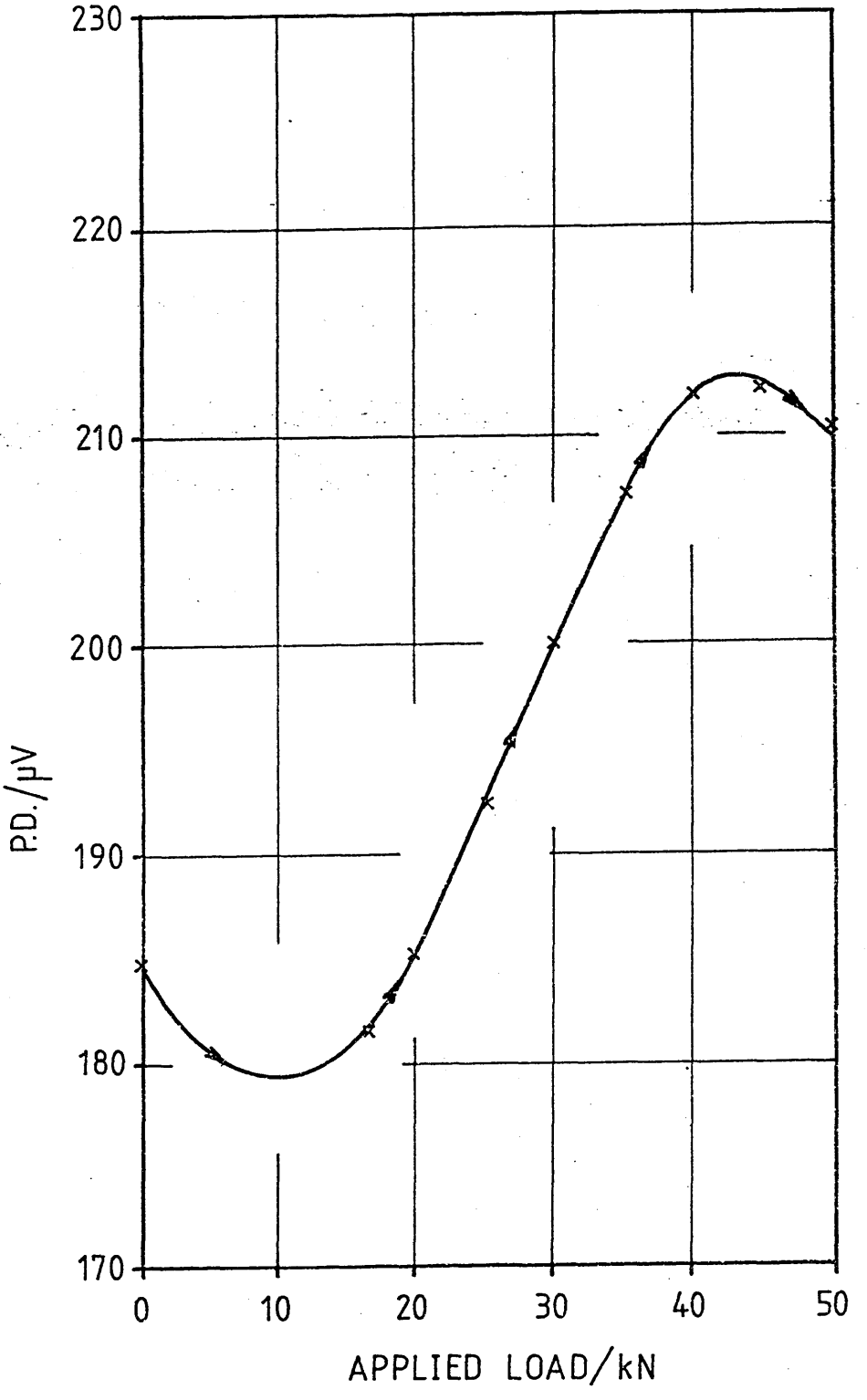

Fig. 8.4 Prediction of ACPD response across EN1A U Notch using compensation method

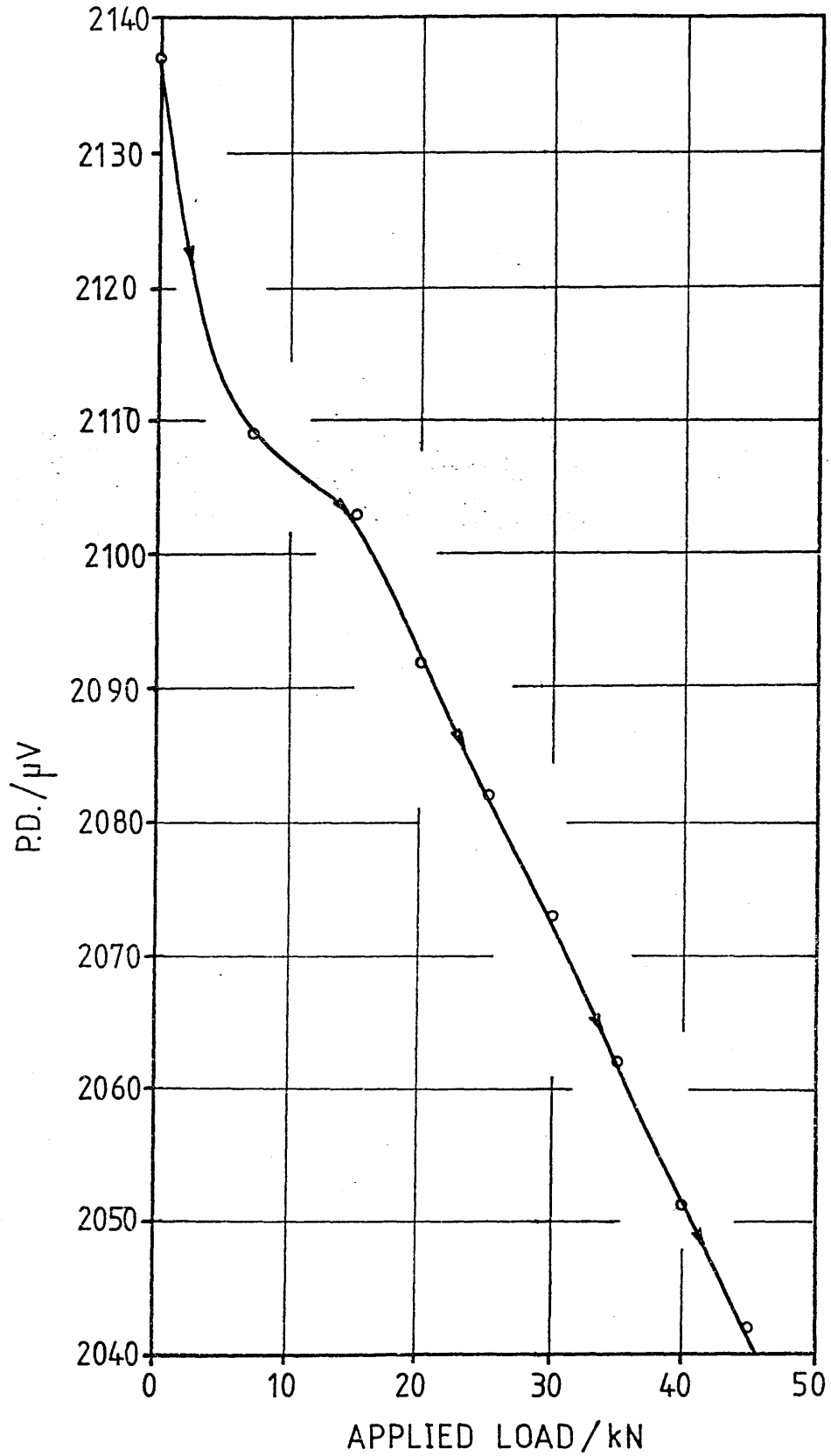

Fig. 8.5 Prediction of ACPD Response Across EN1A V Notch omitting compensation loop

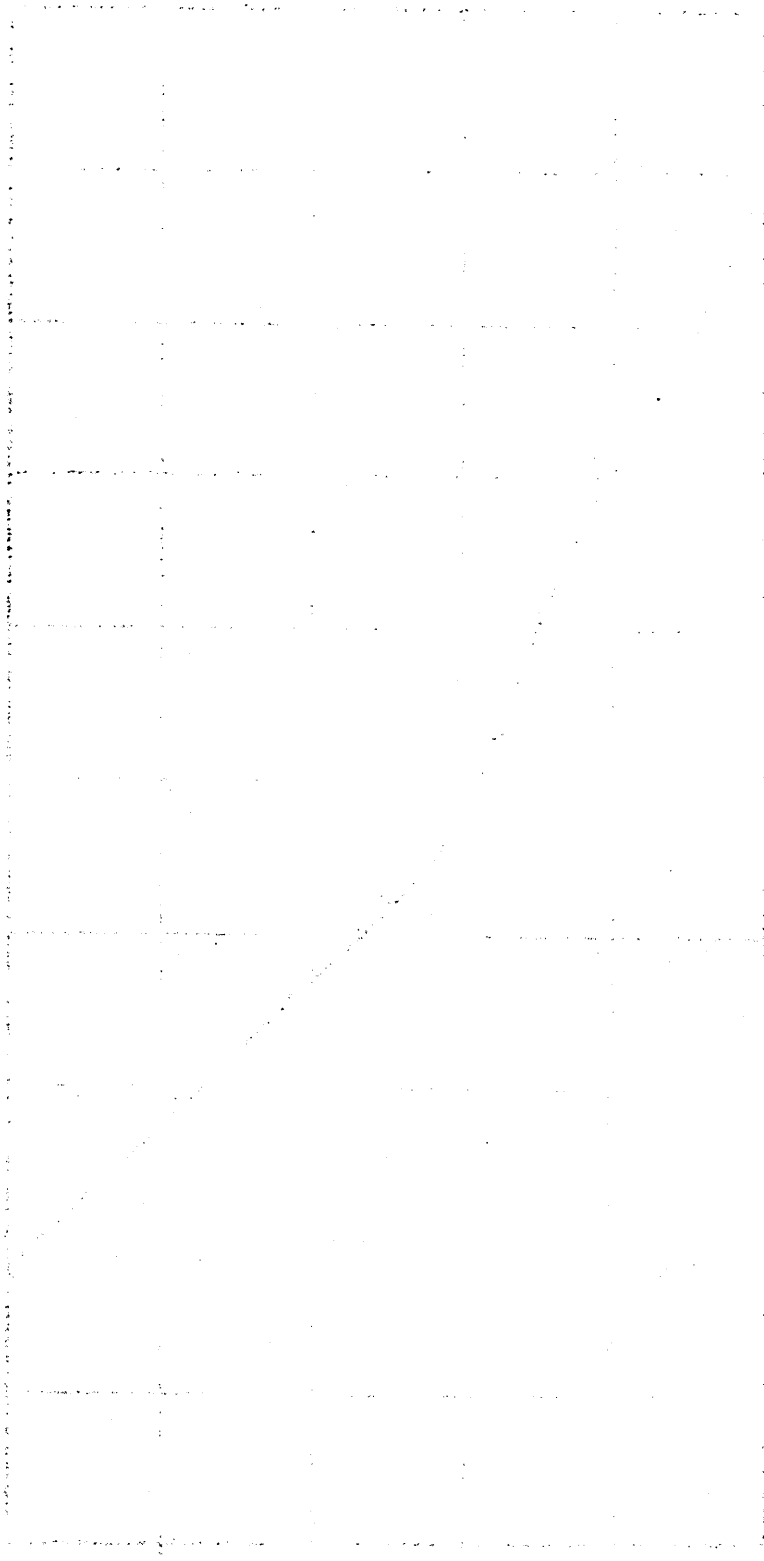

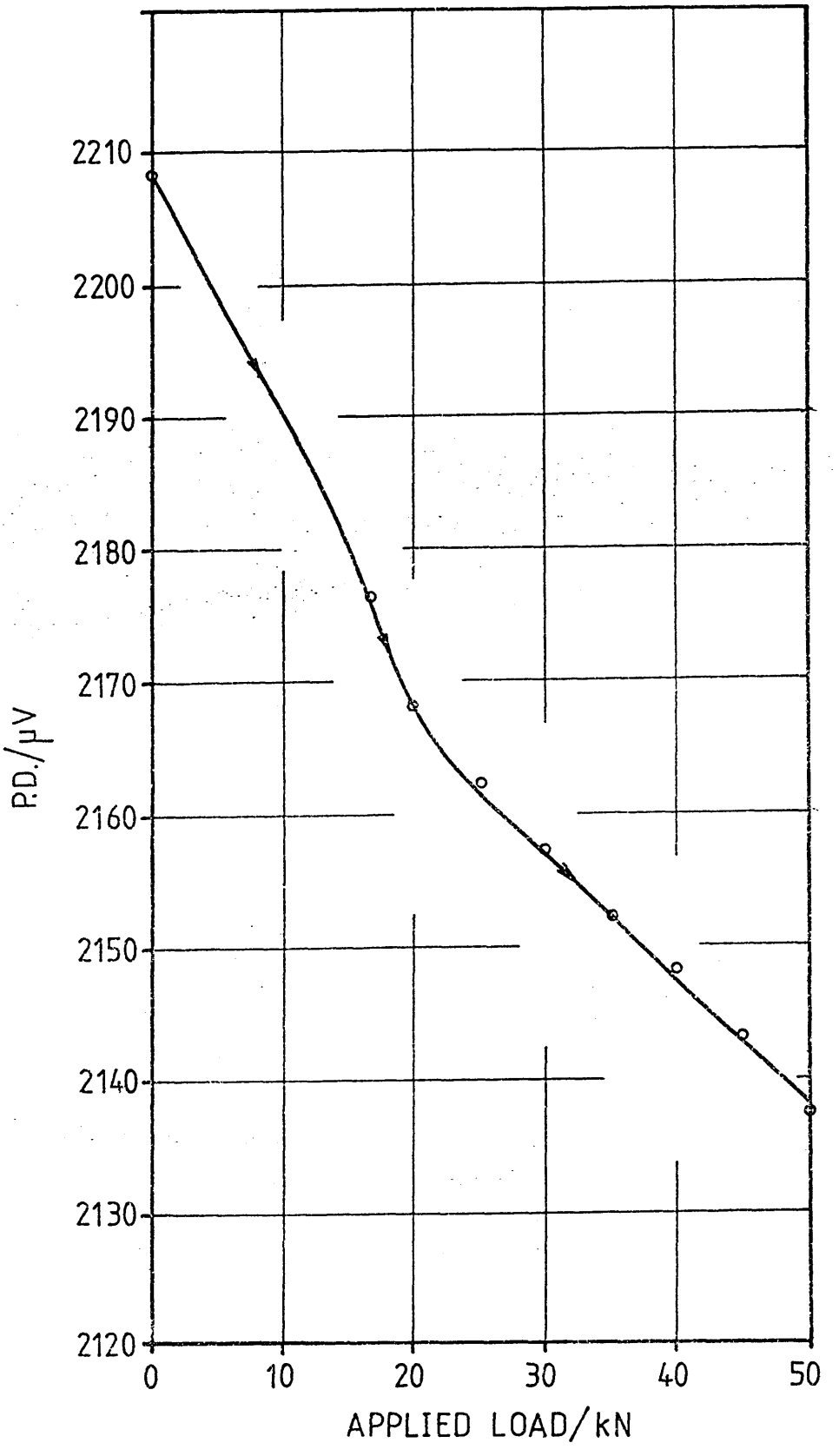

Fig. 8.6 Prediction of ACPD response across EN1A U Notch omitting compensation loop

9.1 CONCLUSIONS

In the present study an investigation has been undertaken into the effect of elastic/plastic deformation on the response of ACPD crack monitoring systems.

Data has been collected on the ACPD response in both the strongly ferromagnetic mild steel EN1A and the weakly magnetic non-ferrous aluminium alloy NE8. Such contrasting materials were selected in order to give an insight into how variations in the relative magnetic permeability (μ_r) and the electrical resistivity (ρ) affect the ACPD response. A more fundamental study was also undertaken into the effect of elastic/plastic strain on each of these two parameters separately.

Results from the investigation have given a valuable insight into the physical nature of both these parameters allowing several important conclusions to be drawn about the influence of strain upon ACPD response.

It has been demonstrated from the results of the NE8 testing, and more specifically through the DC resistance measurements in both materials, that ρ was not a significant parameter in governing any observed changes in ACPD response. This lack of strain dependence accounts for the null ACPD response observed in the NE8 bend specimens and may be explained as follows: The values of ρ has been shown to be constant in both materials up to strain levels of 6 - 7 % and μ_r, by the nature of all non-ferrous materials, constant and equal to unity. This invariance of properties giving no variation in the ACPD response. From this it was concluded that even substantial levels of plasticity have no effect on the response

seen during ACPD crack monitoring in non-ferrous alloys and in such cases the effects of plasticity may be ignored. Any observed changes in response may be attributed directly to the size and geometry of the defect under examination and not its associated local strain field.

Contrastingly the ACPD response seen during the EN1A testing showed a marked dependence on the levels of strain around the notch. Similarly for this material the electrical resistivity has been shown to be constant up to strain levels well above the notch root maximum. This, together with the results from the magnetic permeability testing, clearly demonstrated that it was the strain dependence of μ_r that determined any observed changes in ACPD response and again ρ did not play a significant role.

From measurements of μ_r it has been seen that its value falls quite dramatically with increasing strain. Such a decrease should also have produced a corresponding decrease in the PD measured across the notch. However the ACPD response across both the V and U notch profiles was observed to be rather different than would have been expected.

Following a critical reappraisal of all the available data it was concluded that the rather complex response seen was due in part to the ACPD measurement technique used during the testing and not solely attributable to the levels of strain around the notch. The technique used was the standard compensation method with two pairs of pick-ups attached across the notch and across an adjacent section of plain material. However with this pick-up configuration it was realised that strain would affect both signals and the compensation signal could no longer be considered an invariant base signal

against which to gauge changes in notch PD. The observed ACPD response was then the result of the interaction of the two strain dependent signals accounting for its rather complex appearance.

This conclusion was further reinforced by the development of a simple electric field model to predict the potential drop across the notch. Results from the model, based on a series impedance principle, confirmed the ACPD response as the interaction of the notch and compensation signals. The model also allowed the prediction of the response omitting the compensation leads revealing a much simpler, linearly decreasing response as initially expected. The model was also applied to the NE8 specimens to predict the standing voltage across the specimen surface but was unsuccessful. The large skin depth generated in this material meant that the distribution of current could no longer be considered a surface phenomena resulting in a breakdown of the series impendance model.

These results suggested that, at best, the compensation method produces very misleading results when appreciable levels of plasticity are present. However, by simply omitting the compensation loop, an ACPD signal indicative of the levels of strain around the notch could be obtained. Further, since plasticity results in a decrease, it should be possible to identify initiation and subsequent crack growth as appropriate turning points in the ACPD response.

The project has successfully demonstrated that the ACPD response is only significantly affected by strain in strongly ferro-magnetic materials ($\mu_r >> 1$). The response in non-ferrous materials is not affected by strain due to the invariance of the electrical resistivity. Therefore the levels of plasticity need only be taken

into account when applying the ACPD technique to ferro-magnetic alloys. In such cases the adoption of the standard compensation technique makes correct interpretation of the results very difficult and a single pair of pick-ups spanning the notch is recommended when appreciable levels of plasticity are to be expected.

Finally the investigation has satisfied all the initial aims of the project which were to quantify and understand the influence of strain on ACPD response. It is anticipated that these results will improve the accuracy and reliability with which ACPD systems are used to size cracks in ductile engineering alloys where appreciable levels of plasticity are present. Consequently this will increase the applicability of the technique to a much wider class of engineering metals and alloys.

9.2 SCOPE FOR FURTHER WORK

The present study has been concerned with studying and explaining the ACPD response to increasing notch tip strain and has successfully fulfilled all its initial aims.

However further useful work could be undertaken with regard to explaining the unloading and cyclic loading ACPD response and a number of other points.

(i) Unloading and Cyclic Response

The effect of compressive strains on μ_r and ρ could be considered in an attempt to explain the unloading and cyclic responses. This is necessary since under these circumstances the notch tip plastic zone is under compression at zero load from the surrounding bulk of elastic material.

(ii) Electric Field Model

Further theoretical development of the simple field model could be undertaken to predict the ACPD response in materials such as NE8 where the skin depth is large and also the response on unloading and under cyclic loading conditions.

(iii) Frequency Variation

The recent introduction of variable frequency ACPD systems has introduced another variable into the analysis. The effect of varying frequency and altering the skin depth could be usefully investigated to quantify the usefulness of this new facility and its implications to ACPD monitoring in general.

REFERENCES

1. Verpoest I, Aernoudt E, Derruyterre A. 'Crack propagation and measurement', GKN Translation No 11 480.

2. Wei R P, Brazill R L. 'An assessment of AC and DC potential systems for monitoring fatigue crackgrowth', ASTM STP 738, 1981, pp 103-119.

3. Aboutarabi A A, Cowling M J. 'Measurement of crack profile of semi-elliptical surface cracks using the AC potential technique', NDT International, June 1983, pp 139-145.

4. - 'The use of AC field measurements to determine the shape and size of a crack in a metal', Unit Inspection Company.

5. Michael D H, Waechter R T, Collins R. 'The measurement of surface cracks in metals by AC electric fields', Proc R S, A381, pp 139-157, 1982.

6. Bozorth R M, Williams H J. 'The effects of small stresses on magnetic properties', Rev Mod Phys, 17, pp 72-80, 1945.

7. Rossiter P L. 'Application of electrical resistivity to investigation of atomic and magnetic microstructures', Metals Forum, Vol 8, no 4, pp 204-217, 1985.

8. Esin A, Jones W J D. 'The effect of strain on the AC resistance of metal: a method of studying micro-plasticity'. B J of Appl P, vol 18, pp 1251-1256, 1967.

9. Venkatasubramanian T V, Okumura N, Unvala B A, Baker T J. 'Application of the ACPD techniques to the determination of R-curves of tough ferritic steels', Eng Fract Mech, vol 14, pp 617-625, 1981.

10. Ryman R J, Mann D L, Blackwell M P. 'The use of an ACPD system for crack detection and measurement', Paper presented at Brit Inst NDT, 1979.

11. Truchon M. 'Application of low cycle fatigue test results to crack initiation from notches', Low Cycle Fatigue and Life Protection, ASTM STP 777, pp 254-268, 1982.

12. Knott J F. 'Fundamentals of Fracture Mechanics', Butterworths.

13. Ritchie R O, Garrett G G, Knott J F. 'Crackgrowth monitoring: optimization of the electrical potential technique using an analogue method', Int J Fract, (7), pp 462-467, 1971.

14. Clark G, Knott J F. 'Measurement of fatigue cracks in notched specimens by means of theoretical electrical potential calibrations', J Mech Phys S, vol 23, pp 265-276, 1975.

15. Klintworth G C, Webster G A. 'Optimization of electrical potential methods of measuring crackgrowth', JSA, vol 14, no 4, 1979, pp 187-192.

16. Carlsson J. 'Experimental studies of brittle fracture propagation' Trans R Inst Tech, Stockholm, no 189, pp 1-55.

17. Marandet B, Sanz G. 'Experimental verification of the JIC and equivalent energy methods for the evaluation of the fracture toughness of steel', ASTM STP 631, 462.

18. de Roo P, Marandet B. 'Application of the ACPD method to the detection of initiation in static and dynamic testing'. Proc of French Conf on Ductile Fracture Test Methods.

19. Verpoest I, Aernoudt A, Deruyterre A, Neyrinck M. 'An improved ACPD method for detecting surface micro-cracks during fatigue tests of unnotched specimens', F Eng Mat Struct, vol 3, pp 203-217, 1981.

20. Testwell Ltd. 'CPD3 crack detector - principles and operation', Tech Memo 127, Testwell Ltd, Daventry.

21. - 'Crack Growth Monitor, CGMS', Datasheet, Matelect Ltd, London W8 7EF, 1986.

22. Erbe H H. 'Three-dimensional elastic/plastic finite element analysis of throughcracked panels and notched bend bars', Int J Press Vess and Piping, vol 14, pp 67-93, 1983.

23. Wang Tzu Chiang, Miller K J. 'Elastic/plastic finite element analysis of short cracks', F Eng Mat Struct, Vol 15, No 3, pp 249-263, 1982.

24. Griffiths J R, Owen D R J. 'An elastic-plastic stress analysis for a notched bar in plane strain bending', J Mech Phys Solids, vol 19, pp 419-431, 1971.

25. - 'PAFEC 75 system manual', Pafec Ltd (1977).

26. - 'PAFEC 75 theory and results manual', Pafec Ltd, (1977).

27. - 'PAFEC data preparation user manual - supplement for level 4', Pafec Ltd (1984).

28. - 'PAFEC PIGS user manual', Pafec Ltd, (1985).

29. Brown M. Private communication.

BIBLIOGRAPHY

1. Mirshekar-Syahkai D, Michael D H, Collins R. Parasitic voltages induced by artificial flaws when measured using AC field technique', J NDT E, vol 2, no 3/4, pp 195-202, 1981.

2. Taylor H, Kilpatrick I M, Jolley G. 'Developments in ACPD crack sizing'. B J NDT, pp 88-90, 1984.

3. Uemura T, Kimura T, Nakamura Y, Sakai K, Uchiro K. 'An improved AC electrical potential method and its application to detection of micro-fatigue cracks in fillet welded joints', submitted to Int J of F (1980).

5. Wilson W K. 'On the electrical potential analysis of a cracked fracture mechanics test specimen using the finite element method', Eng F M, vol 18, no 2, pp 349-358, 1983.

6. Bachmann W, Munz D. 'Unusual potential drop during the application of the electrical potential method in a fracture mechanics test', JTE, vol 4, no 4, pp 252-260, 1976.

7. Venkatasubramanian T V, unvala B A, 'An ACPD system for monitoring cracklength', J Phys E, vol 17, pp 765-771, 1984.

8. Bauschke H M, Schwalbe A H. 'Anwendung der Gleichstrompotential-methode auf oberflachenriss', Deutscher Verband fur Materialprufung eV, pp 181-188.

9. Gangloff R P. 'Electrical potential monitoring of crack formation and subcritical growth from small defects', F Eng Mat Struct, vol 4, no 1, pp 15-33, 1981.

10. Green G, Knott J F. 'The initiation and propagation of ductile fracture in low strength steels', J Eng Mat Tech, pp 37-45, 1976.

11. Hammouda M M, Smith R A, Miller K J. 'Elastic-plastic fracture mechanics for initiation and propagation of notched fatigue cracks', F Eng Mat Struct, vol 2, pp 139-154.

12. Davidson D L, Lankford J. 'Plastic straindistribution at the tips of propagating fatigue cracks', Trans ASME, pp 24-29, 1976.

13. Hahn G Tm Hoagland R G, Rosenfield A D. 'Local yielding attending fatigue crackgrowth', Met Trans, vol 3, pp 1189-1202, 1972.

14. Nair P K, 'Fatigue crackgrowth model for part through flaws in plates and pipes', J Eng M T, vol 101, pp 53-58, 1979.

15. Roman I, Kanyi O. 'Model for fracture toughness alteration due to cycle loading', Int J of Fract, pp 67-80, 1982.

16. Vecchio R S, Hertzberg R W, Jaccard R. 'On the overload induced fatigue crack propagation behaviour in aluminium and steel alloys', F Eng Mat Struct, vol 7, no 3, pp 181-194, 1984.

17. Wilkins M A, Smith G C. 'Dislocation structures near a propagating fatigue crack in an Al (0.5% Mg) alloy', Acta Met, vol 18, pp 1035-1043, 1975.

18. Schutz W. 'The predictionof fatigue life in the crack initiation and propagation stages - a state of the art survey', Eng Fract Mech, vol 11, pp 405-421, 1979.

19. Pook L P, Greenan A F. 'Fatigue crack arrest in mild steel specimens under constant amplitude loading', F Eng Mat Struct, vol 7, no 1, pp 65-73, 1984.

20. Sherratt F. 'Fatigue life estimation using simple fracture mechanics', J of Soc Eng Engrs, pp 23-28, 1983.

21. Sneddon I N. 'The distribution of stress in the neighbourhood of a crack in an elastic solid', Proc R S, pp 229-259, 1945.

22. Griffith A A. 'The phenomena of rupture and floe in solids', Proc R S, vol CCXXI A.

23. Hutchinson J W. 'Fundamentals of the phenomenological theory of fracture mechanics', J of App Mech, vol 50, pp 1045-1051, 1983.

24. Chang S J, Ohr S M. 'Effect of thickness on plastic zone size in BCS theory of fracture', Int J Fract, pp 3-13, 21, 1983.

25. Smith E. 'The theory of linear elastic fracture mechanics procedures for predicting crack growth rates when plasticity is extensive', Mat Sci Eng, 70, pp 197-204.

26. Erdogan F. 'Stress intensity factors', J of App Mech, vol 50, pp 992-1002, 1983.

27. Shah R C, Kobayashi A S. 'Stress intensity factors for an elliptical crack approaching the surface of a semi-infinite solid', Int J Fract, 9, pp 133-146, 1973.

28. Shih C F, Hutchinson J W. 'Fully plastic solutions and large scale yielding estimates for plane stress crack problems', J Eng Mat Tech, pp 289-295, 1976.

29. Pratap C R, Pandey R K. 'Effect of geometry and finite root radius on plastic zone and tip opening displacement', Eng Fract Mech, vol 19, pp 849-861, 1984.

30. Schijve J. 'Stress gradients around notches', Fat Eng Mat Struct, vol 3, no 4, pp 325-330, 1980.

31. Hutchinson J W, Needleman A, Shih C F. 'Fully plastic crack problems in tension and bending', Fract Mech, pp 515-527.

32. Berezin A V, Koshelev P F. 'Plastic yield of notched bars in tension and bending', Izv ANUSSR Meckhanika tverdogo Tela, vol 11, no 5, pp 82-90, 1976.

33. Molski K, Glinka G. 'A method of elastic-plastic stress and strain calculation at a notch root', Mat Sci Eng, 50, pp 93-100, 1981.

34. Glinka G. 'Energy density approach to calculation of inelastic strain-stress near notches and cracks', Eng Fract Mech, vol 22, no 3, pp 485-508, 1985.

35. Dorn J E, Pietrowsky P, Tietz T E. 'The effect of alloying elements on the plastic properties of aluminium alloys', Trans AIME, vol 188, pp 933-943, 1950.

36. - 'Methods of test for Plane Strain fracture testing (K1C) of metallic materials', BSI 5447: 1977.

37. Driels M R. 'A general purpose micro-computer I/O interface for educational use', Int J of Mech Eng Educ, vol 11, no 3, pp 189-198.

APPENDIX I

BASIC ELECTRICAL AND MAGNETIC PARAMETERS

The Electrical Resistivity

The Electrical Resistivity is denoted by the Greek letter ρ. ρ is a measure of the difficulty with which the charge carrying conduction electrons may pass through a particular material and as such ρ may be thought of as a DC property of the material.

ρ is a material property independent of specimen dimensions and for homogeneous materials the value of ρ is a constant. If however the temperature of the material is increased it is found that the value of ρ will increase and for many pure metals this increase is almost proportional to the absolute value of temperature. The fractional increase of ρ with temperature is known as the temperature coefficient of resistance. The overall resistance of a conductor to the flow of electrons not only depends on the material but also on its physical size and shape. The Electrical Resistance, R, of a circular conductor, length l and cross-sectional area A, being related to ρ by the formula given below,

$$R = \frac{\rho l}{A}$$

The Magnetic Permeability

The Magnetic Permeability is denoted by the Greek letter μ and is often expressed in terms of the product of the Relative Magnetic Permeability (μ_r) and the Permeability of Free Space (μ_o), a constant, as given below.

$$\mu = \mu_r \times \mu_o$$

In the following section a brief description of the physical nature of μ, illustrating the complexity of this parameter, is given.

Consider a source of magnetism in a region of empty space (in vacuo). The magnetic field produced by the source will have a certain magnetic flux density associated with it dependent solely on the strength of the source. In this case $\mu = \mu_o$ and $\mu_r = 1$ since no other medium is present in the magnetic field. Now, if a piece of any material is placed in the field it is found that the magnetic flux density within this material is different from thevalue in free space. The ratio of the flux density produced in the material to the flux density produced in vacuo by the same magnetic source is termed the Relative Magnetic Permeability (μ_r).

For most materials μ_r is close to unity and is independent of the strength of the magnetizing field. For other, ferromagnetic, materials μ_r varies with the strength of the applied field and is often considerably greater than unity.

The magnetic properties of ferromagnetic materials are very complex and often displayed as curves of magnetic flux density (B) against magnetizing force (H), where,

$$B = \mu H = \mu_r \mu_o H$$

Consider the curve given in figure AI.1 representing the magnetisation curve of a typical ferromagnetic material.

The material, initially unmagnetized, is placed in a gradually increasing magnetic field (increasing H) and the value of B in the material increases non-uniformly to a maximum or saturation value (curve OA). As the field strength is decreased to zero B does not return to zero but some value given by OB, which is termed the Remanence or Remanent Magnetism (curve AB). To reduce B to zero it is necessary to reverse the applied field and the size of the reversal in H is termed the Coercive Force, represented by OC (curve BC). As the force is reversed still further saturation occurs in the opposite direction (curve CD). Taking H back to its original positive value a similar curve DEFA is obtained.

The closed loop ABCDEFA represents a complete cycle of magnetisation for the material and is termed a Hysteresis Loop, the area of the loop being a measure of the energy lost during the magnetisation cycle. The value of μ_r ($\mu_r = B/\mu_o H$) is constantly changing over an infinite range of values during each cycle of magnetization.

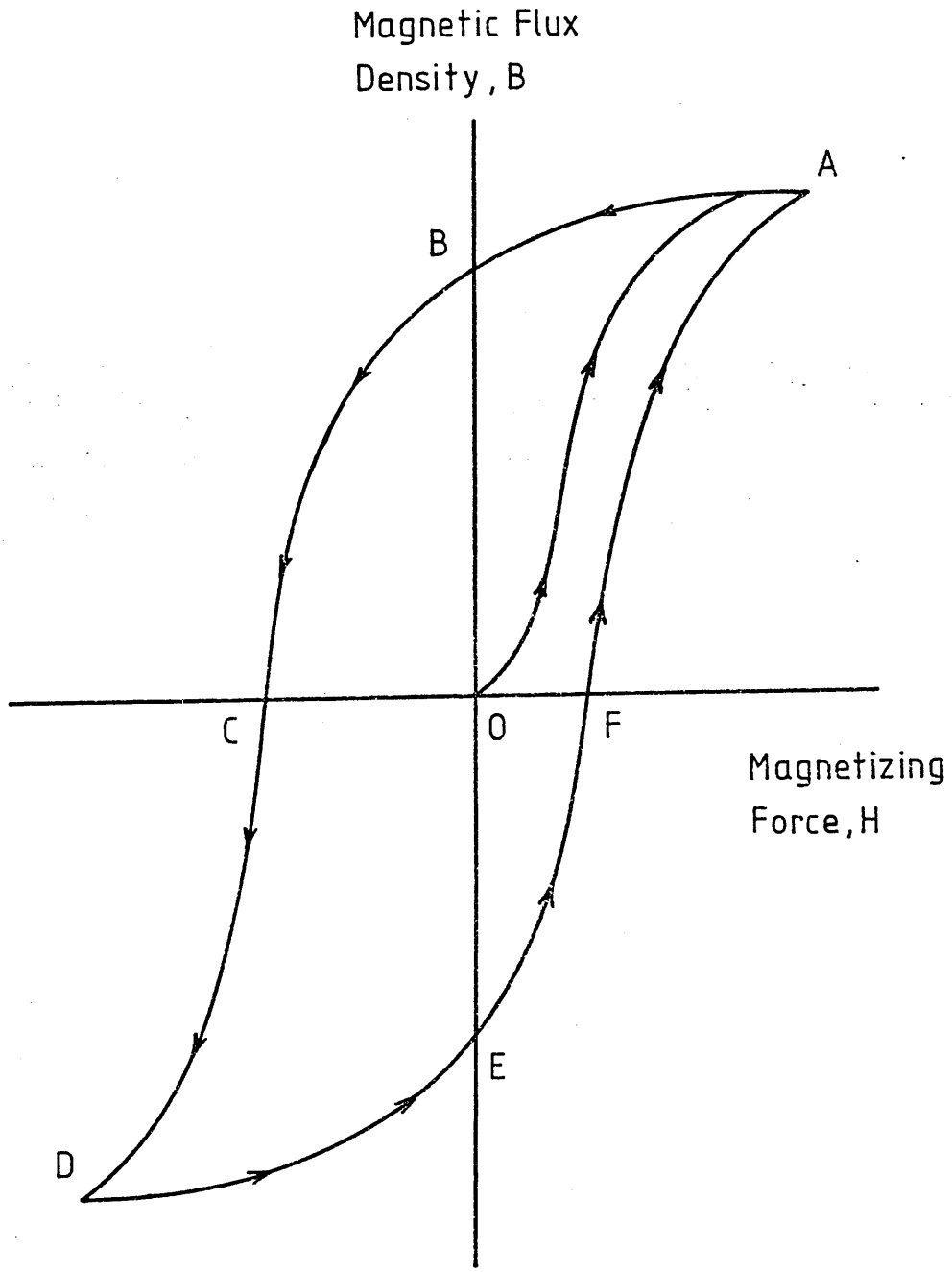

Fig. AI.1 Cyclic Magnetization Curve

APPENDIX II

LISTING OF PROGRAM "DATA CREATOR"

In the following section a listing is givenof the "DATA CREATOR" program designed to store and edit the raw data obtained from the resistivity experiments on suitably formatted datafiles. These can then be processed by running "TESTWELL" as required.

```
100  REM
110  REM  PROGRAM "DATA CREATOR"
120  REM
130  REM  CURRENT VERSION BY A.E.WALKER 20/12/86
140  REM
150  REM
160  REM  *** PROGRAM NOTATION ***
170  REM
180  REM  LD(100),STR(100) : COORDS DEFINING LOAD/STRAIN CURVE
190  REM                      OF THE MATERIAL
200  REM  IC(10),VC(10),BO(10) : CALIBRATION VALUES OF CURRENT ,
210  REM                 VOLTAGE AND BACKOFF
220  REM  VA(100)    : ACTIVE VOLTAGE
230  REM  VD(100)    : DUMMY VOLTAGE
240  REM  PLR(100)   : % OF LOAD RANGE
250  REM  B$(20)     : ARRAY DEFINED TO AID FORMATTING OF OUTPUT
260  REM  DF$        : NAME OF DATAFILE TO BE READ
270  REM  AO         : INITIAL CROSS-SECTIONAL AREA OF SPECIMEN
280  REM  LO         : INITIAL SPAN BETWEEN VOLTAGE PICK-UPS
290  REM  PE         : ELASTIC VALUE OF POISSONS RATIO
300  REM  PP         : PLASTIC VALUE OF POISSONS RATIO
310  REM  LR         : LOAD RANGE
320  REM  BO         : BACKOFF VOLTAGE
330  REM  GN         : DC AMPLIFIER GAIN
340  REM  NP         : NUMBER OF COORD PAIRS DEFINING LOAD /STRAIN
350  REM                CURVE OF THE MATERIAL
360  REM  NN         : NUMBER OF DATA READINGS TAKEN DURING TEST
370  REM
380  REM
390  REM  ************************************
400  REM  ***       CREATE DATAFILES       ***
410  REM  ************************************
420  REM
```

```
430  REM
440  HOME
450  DIM STR(100),LD(100),PLR(100),VA(100),VD(100),B$(20)
460  CLEAR
470 D$ =  CHR$ (4): REM  CTRL-D
480  FOR I = 0 TO 19:B$(I + 1) = B$(I) + " ": NEXT
490  PRINT "PLEASE CHOOSE FROM THE FOLLOWING MENU": PRINT : HTAB 5: PRINT
     "(1) USE EXISTING DATAFILE": PRINT
500  HTAB 5: PRINT "(2) CREATE A NEW DATAFILE": PRINT
510  INPUT "PLEASE ENTER (1) OR (2) > ";PP
520  IF PP = 2 THEN  GOTO 670
530  REM  READING EXISTING DATAFILE
540  HOME : VTAB 3: INPUT "ENTER DATAFILE TO BE READ > ";DF$
550  PRINT : PRINT : PRINT D$;"OPEN";DF$: PRINT D$;"READ";DF$
560  INPUT AO: INPUT LO: INPUT PE: INPUT PP: INPUT LR
570  REM  STRAIN VS LOAD CURVE
580  INPUT NP: FOR I = 1 TO NP: INPUT STR(I): INPUT LD(I): NEXT
590  INPUT BO: INPUT GN
600 I = 0: FOR I = 1 TO 2: INPUT IC(I): INPUT VC(I): INPUT BO(I): NEXT I
610  INPUT NN:I = 0:VOA = 0
620  FOR I = 1 TO NN
630  INPUT PLR(I): INPUT VA(I): INPUT VD(I)
640  NEXT I
650  PRINT D$;"CLOSE";DF$
660  GOTO 900
670  REM  CREATING NEW DATAFILE
680  HOME : VTAB 3
690  INPUT "ENTER A SUITABLE NAME FOR DATAFILE > ";DF$: PRINT : PRINT : PRINT

700  PRINT "PLEASE ENTER DATA IN THE CORRECT FORMAT AFTER EACH PROMPT (>)
     ": PRINT
710  INPUT "AREA OF SPECIMEN (MM^2) > ";AO
720  INPUT "SPAN OF PICKUPS (MM) > ";LO: PRINT
```

```
730  INPUT "POISSON'S RATIO (ELASTIC) > ";PE: INPUT "POISSON'S RATIO (PLA
    STIC) > ";PP: PRINT
740  INPUT "LOADRANGE (KN) > ";LR: PRINT : PRINT
750  PRINT "ENTER LOAD STRAIN CURVE OF MATERIAL": PRINT "AS A SERIES OF C
    OORD.'S": PRINT
760  INPUT "NO. OF POINTS > ";NP: PRINT
770  FOR I = 1 TO NP: INPUT "STRAIN,LOAD > ";STR(I),LD(I): NEXT : PRINT
780  INPUT "VOLTAGE BACKOFF (MICRO-V) > ";BO: PRINT
790  INPUT "DC AMPLIFIER GAIN > ";GN: PRINT
800  PRINT "ENTER CALIBRATION VALUES OF VOLTAGE,CURRENT AND BACKOFF": PRINT

810  FOR I = 1 TO 2: INPUT "CURRENT,VOLTAGE,BACKOFF > ";IC(I),VC(I),BO(I)
    : NEXT : PRINT
820  PRINT "ENTER ACTUAL DATAPOINTS AS A TRIAD OF VALUES %,V,V": PRINT
830 I = 0
840  PRINT "ENTER 0,0,0 TO END DATA INPUT": PRINT
850 I = I + 1
860  INPUT "%LOAD,ACTIVE(V),DUMMY(V) > ";PLR(I),VA(I),VD(I)
870  IF (PLR(I) = 0) AND (VA(I) = 0) THEN  GOTO 890
880  GOTO 850
890 NN = I - 1
900  HOME : PRINT "DATA WILL NOW BE REPRINTED": PRINT : PRINT "EITHER ONT
    O THE": PRINT
910  HTAB 10: PRINT "(1) SCREEN": HTAB 10: PRINT "(2) PRINTER": PRINT
920  INPUT "ENTER (1) OR (2) > ";QQ
930  IF QQ = 1 THEN  GOTO 950
940  PRINT  CHR$ (4);"PR£1": POKE 1657,80
950  HOME
960  PRINT "AREA OF SPECIMEN (MM^2) : ";AO
970  PRINT "SPAN OF PICKUP'S (MM)    : ";LO: PRINT
980  PRINT "POISSON'S RATIO    ELASTIC : ";PE
990  PRINT  TAB( 20);"PLASTIC : ";PP: PRINT
1000  PRINT "LOADRANGE (KN) : ";LR: PRINT
```

```
1010  PRINT "STRAIN/LOAD COORDS"
1020  PRINT  TAB( 6);"STRAIN    LOAD"
1030  FOR I = 1 TO NP
1040  PRINT B$(5) +  STR$ (STR(I)) + B$(10 -  LEN ( STR$ (STR(I)))) +  STR$
    (LD(I))
1050  NEXT I: PRINT
1060  PRINT "BACKOFF : ";BO: PRINT "GAIN     : ";GN: PRINT
1070  PRINT "CALIBRATION VALUES": PRINT "VOLTAGE CURRENT BACKOFF"
1080  FOR I = 1 TO 2
1090  PRINT B$(1) +  STR$ (VC(I)) + B$(8 -  LEN ( STR$ (VC(I)))) +  STR$
    (IC(I)) + B$(9 -  LEN ( STR$ (IC(I)))) +  STR$ (BO(I))
1100  NEXT
1110  PRINT : PRINT "RAW DATA POINTS"
1120  PRINT  TAB( 10);"LOAD     ACTIVE     DUMMY"
1130  FOR I = 1 TO NN
1140  PRINT B$(1) +  STR$ (I) + B$(9 -  LEN ( STR$ (I))) +  STR$ (PLR(I))
     + B$(9 -  LEN ( STR$ (PLR(I)))) +  STR$ (VA(I)) + B$(11 -  LEN ( STR$
    (VA(I)))) +  STR$ (VD(I))
1150  NEXT I
1160  PRINT : PRINT
1170  IF QQ = 1 THEN  GOTO 1200
1180  PRINT  CHR$ (4);"PR£O"
1190  PRINT : PRINT
1200  INPUT "PRESS RETURN TO CONTINUE";G$
1210  HOME : VTAB 6: PRINT "DATA INPUT AND PRINTOUT COMPLETED": PRINT : PRINT

1220  VTAB 10: PRINT "PLEASE CHOOSE FROM OPTION MENU": PRINT
1230  HTAB 10: PRINT "(1) STORE DATA": HTAB 10: PRINT "(2) EDIT DATA": HTAB
    10: PRINT "(3) QUIT": PRINT : PRINT
1240  INPUT "ENTER (1),(2) OR (3) > ";SS
1250  IF SS = 3 GOTO 2090
1260  IF SS = 1 GOTO 1830
1270  REM  EDITING DATA
```

```
1280  HOME : VTAB 2: PRINT "MENU OPTION EDIT DATAFILE ";DF$: PRINT : PRINT

1290  PRINT "EDIT MENU OPTIONS :-": PRINT : PRINT "(1) DELETE DATA": PRINT
    "(2) ALTER DATA": PRINT "(3) ADD DATA": PRINT "(4) ALTER EXTRAS": PRINT
    "(5) END EDITING": PRINT : PRINT
1300  INPUT "ENTER (1),(2),(3),(4),(5) > ";MN
1310  ON MN GOTO 1330,1990,1730,1430,900
1320  GOTO 1210
1330  REM  DELETE DATA
1340  HOME : VTAB 2: PRINT "DELETE DATA": PRINT "___________": PRINT
1350 DP = 0
1360  INPUT "ENTER DATA PT. TO BE DELETED > ";DP
1370 PLR(DP) = 0:VA(DP) = 0:VD(DP) = 0
1380  FOR I = DP TO NN - 1
1390 PLR(I) = PLR(I + 1):VA(I) = VA(I + 1):VD(I) = VD(I + 1)
1400  NEXT
1410 NN = NN - 1
1420  HOME : VTAB 5: GOTO 1290
1430  REM  ALTER EXTRAS
1440  HOME : PRINT "DO YOU WISH TO ALTER": PRINT
1450  PRINT  TAB( 3);"(1)AO (2)LO (3)PE (4)PP": PRINT  TAB( 3);"(5)LR (6)
    BO (7)GN (8)OTHER/QUIT"
1460  PRINT : INPUT "ENTER 1,2,3 ETC > ";AN: PRINT
1470  ON AN GOTO 1480,1490,1500,1510,1520,1530,1540,1550
1480  INPUT "NEW AO > ";AO: GOTO 1440
1490  INPUT "NEW LO > ";LO: GOTO 1440
1500  INPUT "NEW PE > ";PE: GOTO 1440
1510  INPUT "NEW PP > ";PP: GOTO 1440
1520  INPUT "NEW LR > ";LR: GOTO 1440
1530  INPUT "NEW BO > ";BO: GOTO 1440
1540  INPUT "NEW GN > ";GN: GOTO 1440
1550  HOME : PRINT "DO YOU WISH TO": PRINT
```

```
1560  PRINT  TAB( 3);"(1)ALTER LOAD/STRAIN CURVE": PRINT  TAB( 3);"(2)ALT
    ER CALIBRATION": PRINT  TAB( 3);"(3)QUIT": PRINT
1570  INPUT "ENTER 1,2 OR 3 > ";NS
1580  ON NS GOTO 1590,1650,1280
1590  REM  LOAD/STRAIN CURVE
1600  VTAB 10
1610  INPUT "ENTER POINT TO ALTER > ";PN
1620  PRINT "STR= ";STR(PN): PRINT "LD= ";LD(PN): PRINT
1630  PRINT "ENTER NEW VALUES"
1640  INPUT "STR= ";STR(PN): INPUT "LD= ";LD(PN): GOTO 1550
1650  REM   ALTER VOLTAGE DATA
1660 PN = 0
1670  VTAB 10
1680  INPUT "ENTER POINT TO ALTER > ";PN
1690  PRINT "VC= ";VC(PN): PRINT "IC= ";IC(PN): PRINT "BO= ";BO(PN): PRINT

1700  PRINT "ENTER NEW VALUES"
1710  INPUT "VC= ";VC(PN): INPUT "IC= ";IC(PN)
1720  INPUT "BO= ";BO(PN): GOTO 1550
1730  REM  ADD DATA
1740  HOME : VTAB 2: PRINT "ADD DATA": PRINT "_________": PRINT
1750 I = NN
1760 I = I + 1
1770  INPUT "%LOAD= ";PLR(I): INPUT "ACTIVE VOLTAGE= ";VA(I)
1780  INPUT "DUMMY VOLTAGE= ";VD(I)
1790  INPUT "MORE DATA > ";P$
1800  IF P$ = "Y" THEN  GOTO 1760
1810 NN = I: HOME : VTAB 5: GOTO 1280
1820  END
1830  REM  SUBROUTINE TO STORE DATA
1840 D$ =  CHR$ (4)
1850  PRINT D$;"OPEN";DF$: PRINT D$;"DELETE";DF$
1860  PRINT D$;"OPEN";DF$
```

```
1870  PRINT D$;"WRITE";DF$
1880  PRINT AO: PRINT LO: PRINT PE: PRINT PP: PRINT LR
1890  PRINT NP: FOR I = 1 TO NP: PRINT STR(I): PRINT LD(I): NEXT
1900  PRINT BO: PRINT GN
1910  FOR I = 1 TO 2: PRINT IC(I): PRINT VC(I): PRINT BO(I): NEXT
1920  PRINT NN: FOR I = 1 TO NN: PRINT PLR(I): PRINT VA(I): PRINT VD(I): NEXT

1930  PRINT TL
1940  PRINT D$;"CLOSE";DF$
1950  HOME : VTAB 7
1960  HTAB 7: PRINT "DATA STORAGE COMPLETED": PRINT
1970  PRINT NN;" DATAPOINTS STORED IN DATAFILE ";DF$
1980  GOTO 1220
1990  REM  ALTER DATA LIST
2000  HOME : VTAB 5
2010 DP = 0
2020  INPUT "ENTER DATAPOINT TO BE ALTERED > ";DP: PRINT : PRINT
2030  PRINT "VALUES FOR DATAPT. ";DP: PRINT
2040  PRINT "%LOAD  : ";PLR(DP): PRINT "ACTIVE : ";VA(DP): PRINT "DUMMY :
     ";VD(DP): PRINT
2050  PRINT "ENTER NEW VALUES": PRINT : INPUT "%LOAD  > ";PLR(DP): INPUT
    "ACTIVE > ";VA(DP): INPUT "DUMMY > ";VD(DP): PRINT
2060  PRINT : INPUT "MORE ALTERATIONS > ";F$
2070  IF F$ = "Y" THEN  GOTO 2020
2080  GOTO 1280
2090  END
```

APPENDIX III

FLOWCHART AND LISTING OF PROGRAM "TESTWELL"

Computation of equations 6.5 to 6.12 for all recorded values of active and dummy voltage is a repetitive and time consuming procedure. To speed the calculation a computer program, "TESTWELL", was written in APPLESOFT BASIC and run on an APPLEIIE micro-computer.

TESTWELL processed data stored on suitably formatted datafiles created using the "DATA CREATOR" program listed in Appendix II.

As a guide to the computation algorithm a flow chart is given on pages A14 - A17.

A listing of "TESTWELL" is given on pages A18 - A23.

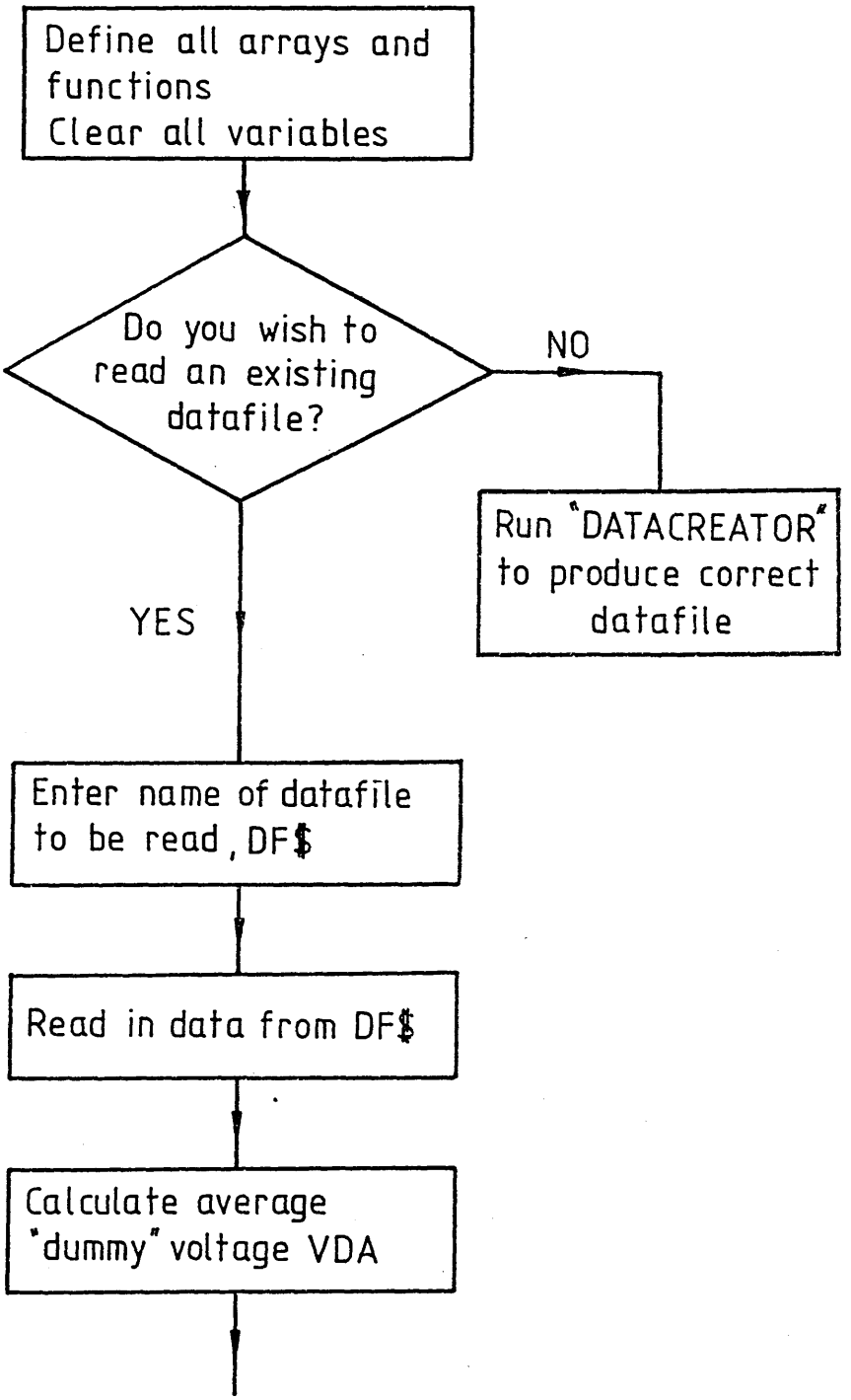
Define all arrays and functions
Clear all variables
Do you wish to read an existing datafile?
NO
Run "DATACREATOR" to produce correct datafile
YES
Enter name of datafile to be read, DF$
Read in data from DF$
Calculate average "dummy" voltage VDA

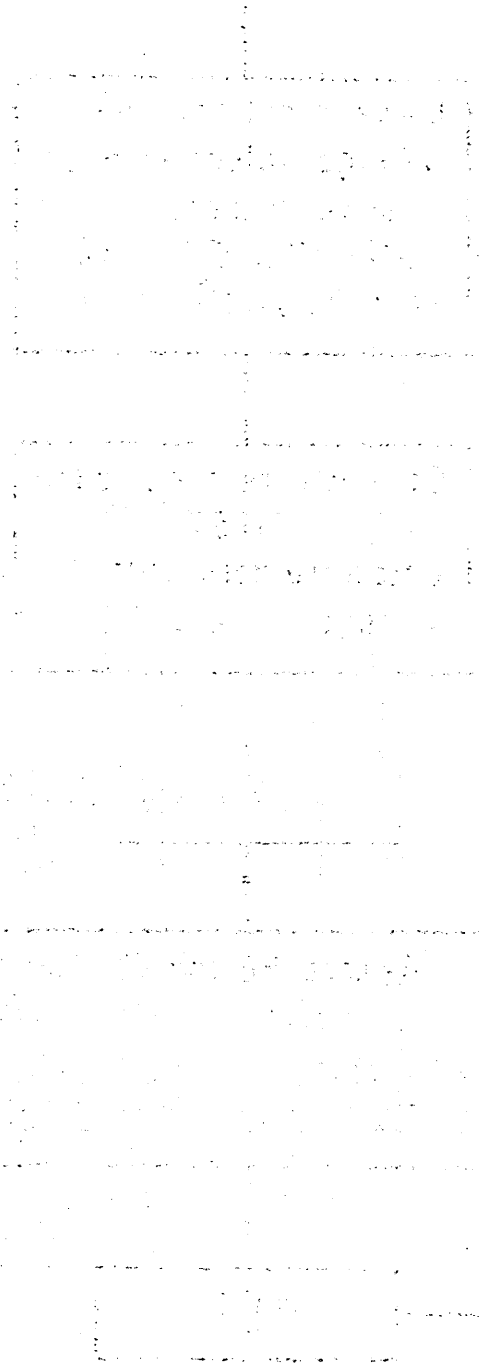

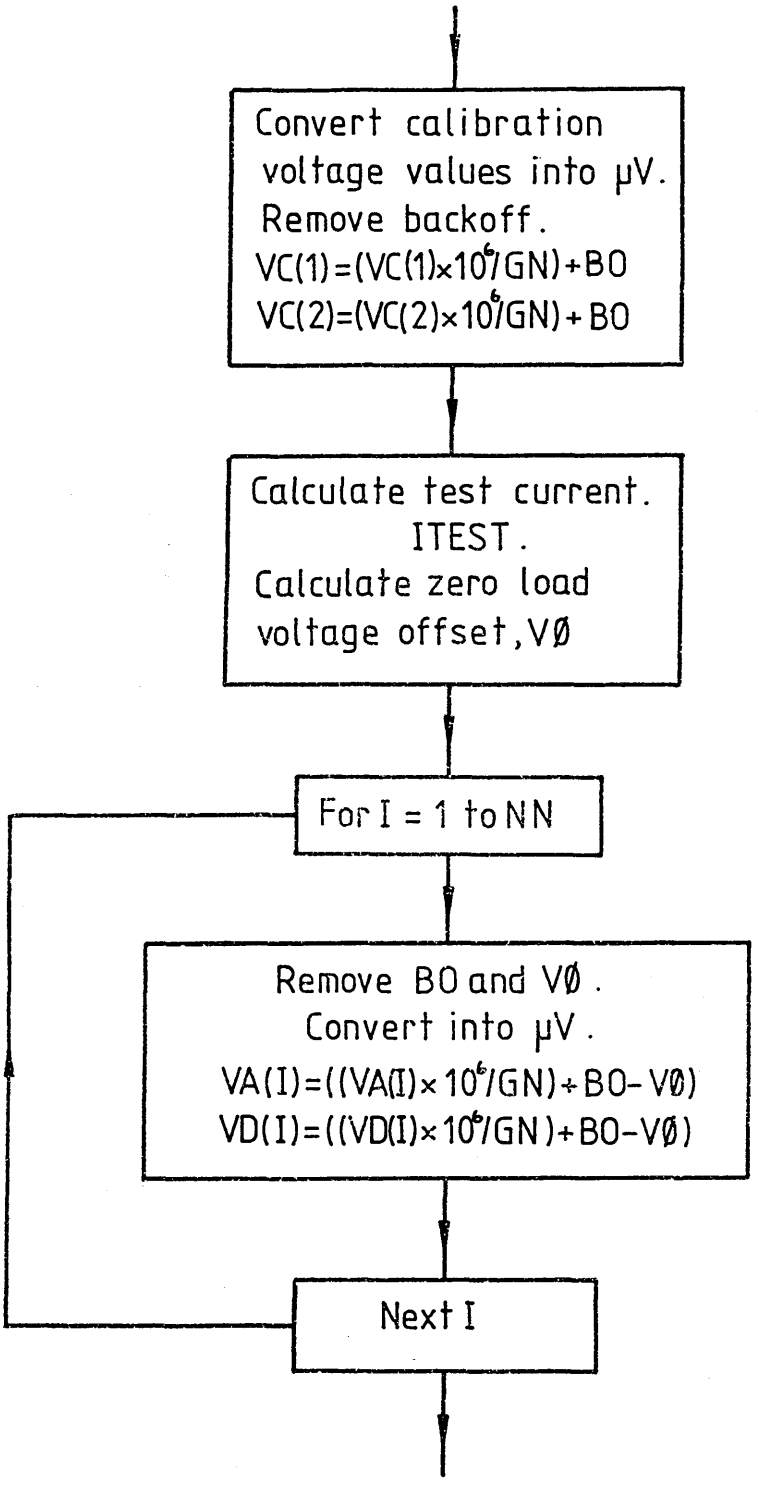
Convert calibration voltage values into μV. Remove backoff.
VC(1)=(VC(1)×10⁶/GN)+BO
VC(2)=(VC(2)×10⁶/GN)+BO
Calculate test current. ITEST.
Calculate zero load voltage offset, VØ
For I = 1 to NN
Remove BO and VØ. Convert into μV.
VA(I)=((VA(I)×10⁶/GN)÷BO-VØ)
VD(I)=((VD(I)×10⁶/GN)+BO-VØ)
Next I

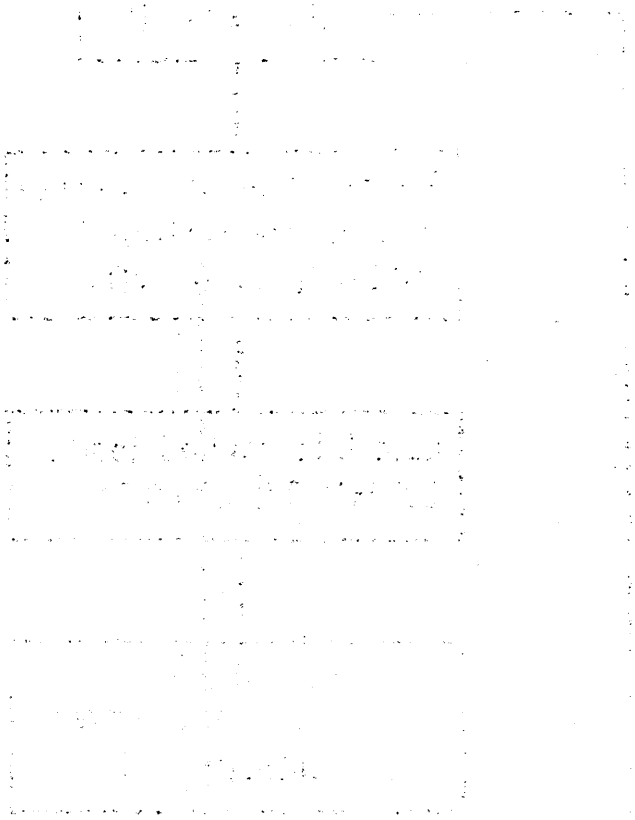

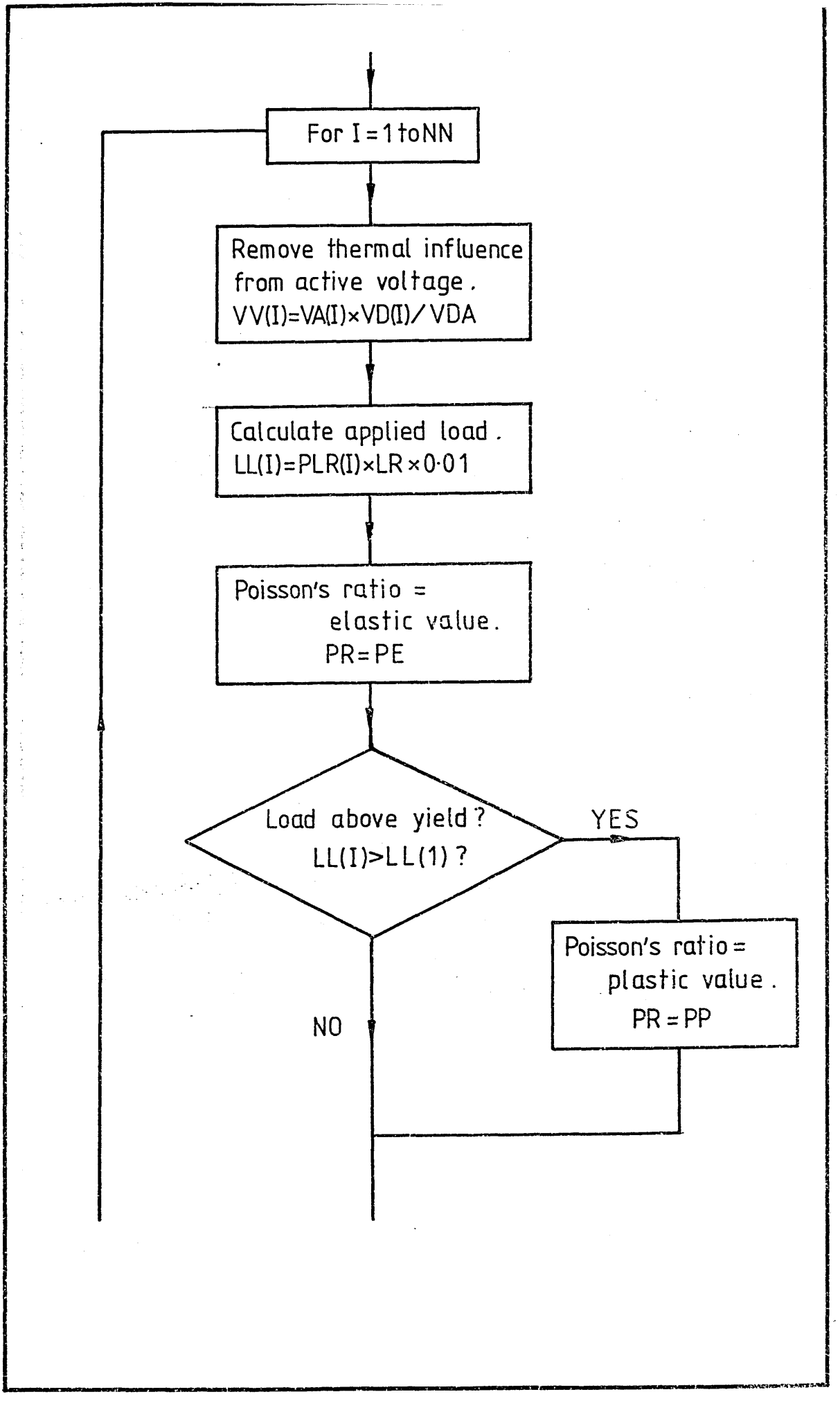
For I = 1 to NN
Remove thermal influence from active voltage.
VV(I)=VA(I)×VD(I)/VDA
Calculate applied load.
LL(I)=PLR(I)×LR×0·01
Poisson's ratio = elastic value.
PR=PE
Load above yield?
LL(I)>LL(1)?
YES
NO
Poisson's ratio = plastic value.
PR=PP

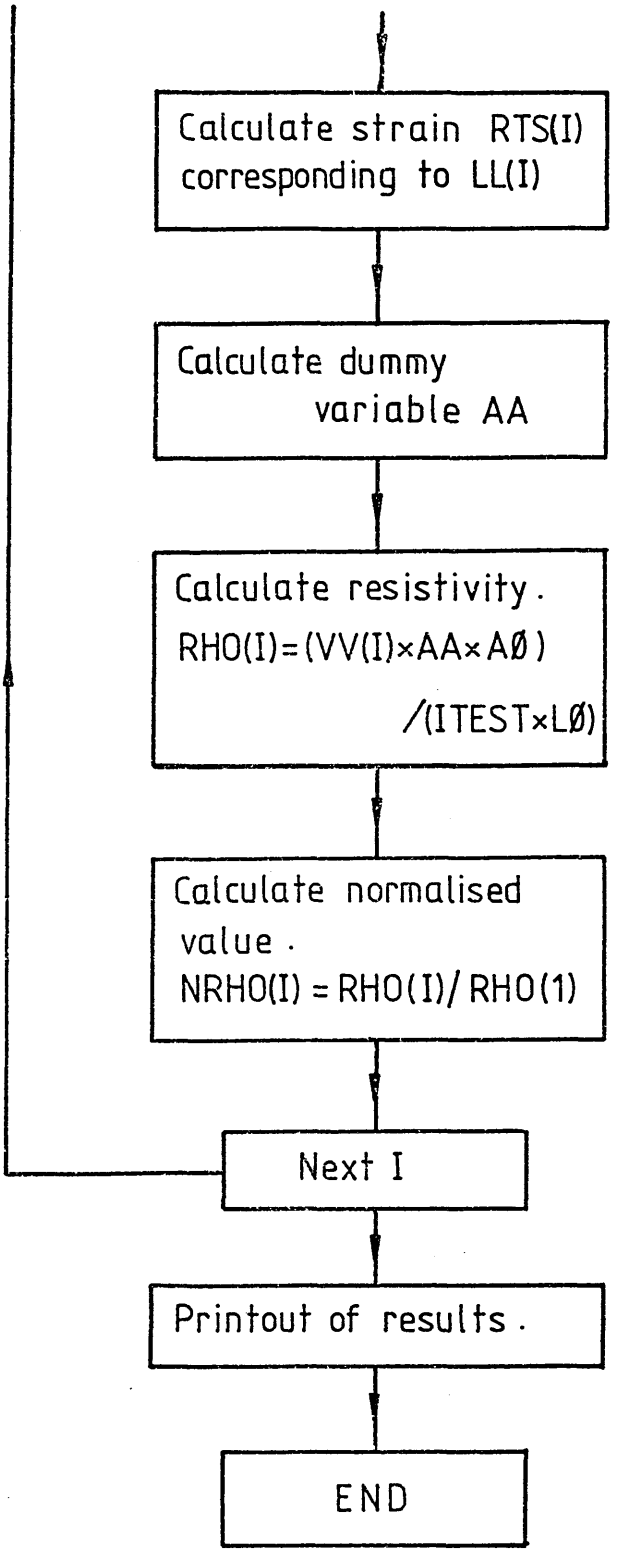
Calculate strain RTS(I) corresponding to LL(I)
Calculate dummy variable AA
Calculate resistivity.
RHO(I)=(VV(I)×AA×AØ)
/(ITEST×LØ)
Calculate normalised value.
NRHO(I) = RHO(I)/ RHO(1)
Next I
Printout of results.
END

```
100  REM
110  REM  PROGRAM "TESTWELL"
120  REM  RESISTIVITY VERSUS STRAIN EVALUATION
130  REM
140  REM  THIS PROGRAM EVALUATES THE VARIATION OF RESISITIVITY
150  REM  WITH INCREASING TENSILE STRAIN ALLOWING FOR
160  REM  CHANGES IN SPECIMEN DIMENSIONS DURING LOADING
170  REM
180  REM  CURRENT VERSION BY A.E.WALKER 20/12/86
190  REM
200  REM
210  REM  *** PROGRAM NOTATION ***
220  REM
230  REM  LD(100),STR(100) : COORDS DEFINING LOAD/STRAIN CURVE
240  REM                      OF THE MATERIAL
250  REM  IC(10),VC(10),BO(10) : CALIBRATION VALUES OF CURRENT ,
260  REM                 VOLTAGE AND BACKOFF
270  REM  VA(100)    : ACTIVE VOLTAGE
280  REM  VD(100)    : DUMMY VOLTAGE
290  REM  VV(100)    : ADJUSTED ACTIVE VOLTAGE
300  REM  PLR(100)   : % OF LOAD RANGE
310  REM  VTEST      : INITIAL ACTIVE VOLTAGE AT ZERO LOAD
320  REM  ITEST      : CURRENT APPLIED TO SPECIMENS DURING TEST
330  REM  RTS(100)   : ACTUAL STRAIN
340  REM  RHO(100)   : RESISTIVITY OF STRAINED MATERIAL
350  REM  NRHO(100)  : NORMALISED VALUE OF RESISTIVITY
360  REM  B$(50)     : ARRAY DEFINED TO AID FORMATTING OF OUTPUT
370  REM  DF$        : NAME OF DATAFILE TO BE READ
380  REM  AO         : INITIAL CROSS-SECTIONAL AREA OF SPECIMEN
390  REM  LO         : INITIAL SPAN BETWEEN VOLTAGE PICK-UPS
400  REM  PE         : ELASTIC VALUE OF POISSONS RATIO
410  REM  PP         : PLASTIC VALUE OF POISSONS RATIO
420  REM  LR         : LOAD RANGE
```

```
430  REM  BO          : BACKOFF VOLTAGE
440  REM  GN          : DC AMPLIFIER GAIN
450  REM  NP          : NUMBER OF COORD PAIRS DEFINING LOAD /STRAIN
460  REM                CURVE OF THE MATERIAL
470  REM  NN          : NUMBER OF DATA READINGS TAKEN DURING TEST
480  REM  VDA         : AVERAGE VALUE OF DUMMY VOLTAGE
490  REM  M           : GRADIENT OF CURRENT/VOLTAGE CALIBRATION
500  REM                CURVE
510  REM  VO          : ZERO LOAD VOLTAGE OFFSET
520  REM
530  REM
540  REM  ************************************
550  REM  *** EVALUATION OF RESISTIVITY ***
560  REM  ************************************
570  REM
580  REM
590  DIM LD(100),STR(100),IC(10),VC(10),BO(10)
600  DIM VA(100),VD(100),PLR(100),LL(100),RTS(100),RHO(100)
610  DIM VV(100),NRHO(100),B$(50)
620  DEF  FN ABV(X) = (((X * 1E6) / GN) + BO)
630  FOR I = 0 TO 49:B$(I + 1) = B$(I) + " ": NEXT
640  CLEAR
650  HOME : VTAB 10
660  HTAB 12: INVERSE : PRINT "PROGRAM TESTWELL": NORMAL : PRINT
670  PRINT "THIS PROGRAM CALCULATES THE ": PRINT : PRINT "SPECIFIC RESIST
     IVITY OF TENSILE": PRINT
680  PRINT "SPECIMENS WITH AUTOMATIC ALLOWANCE": PRINT
690  PRINT "FOR CHANGES IN DIMENSIONS": PRINT : PRINT : PRINT : PRINT
700  INPUT "PRESS RETURN TO CONTINUE ";G$
710  HOME : VTAB 10
720  PRINT "DO YOU WISH TO EITHER:": PRINT
730  PRINT ; TAB( 10);"(1) READ AN EXISTING FILE": PRINT : PRINT ; TAB( 1
     0);"(2) CREATE/MODIFY A FILE ": PRINT
```

```
740  INPUT "ENTER 1 OR 2 > ";ANS
750  IF ANS = 1 THEN  GOTO 780
760  IF ANS = 2 THEN  GOSUB 1690
770  GOTO 1680
780  HOME : VTAB 10: INPUT "ENTER FILE TO BE READ > ";DF$
790  HOME : VTAB 10: HTAB 5: INVERSE : PRINT "DATAFILE ";DF$;" NOW BEING
    READ": NORMAL
800  REM  READ DATAFILE
810  PRINT  CHR$ (4);"OPEN";DF$
820  PRINT  CHR$ (4);"READ";DF$
830  INPUT AO: INPUT LO: INPUT PE: INPUT PP: INPUT LR
840  INPUT NP: FOR I = 1 TO NP: INPUT STR(I): INPUT LD(I): NEXT
850  INPUT BO: INPUT GN
860 I = 0: FOR I = 1 TO 2: INPUT IC(I): INPUT VC(I): INPUT BO(I): NEXT I
870 I = 0:VDA = 0
880  INPUT NN
890  FOR I = 1 TO NN
900  INPUT PLR(I): INPUT VA(I): INPUT VD(I)
910 VDA = VDA + VD(I)
920  NEXT I
930  PRINT  CHR$ (4);"CLOSE";DF$
940  REM  MEAN DUMMY VOLTAGE
950 VDA = VDA / NN
960  REM   CALCULATE VOLTAGE OFFSET
970 VC(1) = (((VC(1) * 1E6) / GN) + BO(1)):VC(2) = (((VC(2) * 1E6) / GN) +
    BO(2))
980 M = (VC(2) - VC(1)) / (IC(2) - IC(1))
990 VO = ((VC(1) * IC(2)) - (VC(2) * IC(1))) / (IC(2) - IC(1))
1000 VTEST =  FN ABV(VA(1))
1010 ITEST = (VTEST - VO) / M
1020 VDA = ( FN ABV(VDA)) - VO
1030  PRINT : PRINT "AVGE VOLT="VDA":?
1040  REM  REMOVE ZERO OFFSET
```

```
1050 I = 0
1060  FOR I = 1 TO NN
1070 VA(I) =  FN ABV(VA(I))
1080 VD(I) =  FN ABV(VD(I))
1090 VA(I) = VA(I) - VO
1100 VD(I) = VD(I) - VO
1110  NEXT I
1120  REM  MAJOR CALCULATION
1130 I = 0:LD(0) = 0:STR(0) = 0
1140  FOR I = 1 TO NN
1150 VV(I) = (VA(I) * VDA) / VD(I)
1160 LL(I) = PLR(I) * LR * 0.01
1170 PR = PE
1180  IF LL(I) > LD(1) THEN PR = PP
1190 K = 0
1200 K = K + 1
1210  IF LD(K) > LL(I) THEN  GOTO 1230
1220  GOTO 1200
1230 KK = K - 1
1240 RTS(I) = STR(KK) + ((LL(I) - LD(KK)) * (STR(KK + 1) - STR(KK)) / (LD
    (KK + 1) - LD(KK)))
1250 AA = ((1 - (PR * RTS(I))) ^ 2) / (1 + RTS(I))
1260 RHO(I) = (VV(I) * AA * AO) / (ITEST * LO)
1270 NRHO(I) = RHO(I) / RHO(1)
1280  NEXT I
1290  REM  PRINTOUT OF RESULTS
1300 Z$ = "0000000000"
1310  HOME : PRINT "RESULTS WILL NOW BE REPRINTED": PRINT : PRINT "EITHER
    ONTO THE": PRINT
1320  HTAB 10: PRINT "(1) SCREEN": HTAB 10: PRINT "(2) PRINTER": PRINT
1330  INPUT "ENTER (1) OR (2) > ";QQ
1340  IF QQ = 1 THEN  GOTO 1370
1350  PRINT  CHR$ (4);"PR£1": POKE 1657,80
```

```
1360  PRINT  CHR$ (12): REM  CTRL-L;FORM FEED
1370  HOME
1380  PRINT "SPECIMEN ";DF$
1390  PRINT "RESISTANCE VS STRAIN RESULTS": PRINT
1400  PRINT "INTERPOLATED DC(A)= ";ITEST: PRINT
1410  PRINT "ZERO VOLTAGE OFFSET(MIC-V)= ";VO: PRINT
1420  PRINT : PRINT "VOLTAGE DRIFT (DUMMY)": PRINT
1430  PRINT  TAB( 3);"VARIANCE : ";VAR
1440  PRINT  TAB( 3);"STD.VAR. : ";SDE: PRINT : PRINT
1450  VTAB 3: PRINT "UNITS": PRINT
1460  PRINT "STRAIN          : - ": PRINT "VOLTAGE          : MICRO-VOLTS"
1470  PRINT "SPEC.RES.       : OHMMM": PRINT "NORM.SPEC.RES. : - ": PRINT
    : PRINT
1480  PRINT B$(3) + "STRAIN  *  ACTIVE      * SPEC.        *  NORMED."
1490  PRINT B$(11) + "*  VOLTAGE    * RESIST.      *"
1500 Z$ = " * ":L$ = "-----------"
1510  PRINT L$ + "-*" + L$ + "---*" + L$ + "---*" + L$ + "--"
1520  PRINT B$(11) + "*" + B$(13) + "*" + B$(13) + "*"
1530  FOR I = 1 TO NN
1540 RTS$ = "":VV$ = "":RHO$ = "":NRHO$ = ""
1550 RTS(I) = ( INT ((RTS(I) * 1E6) + 0.5)) / 1E6
1560 VV(I) = ( INT ((VV(I) * 1E4) + 0.5)) / 1E4
1570 RHO(I) = ( INT ((RHO(I) * 1E4) + 0.5)) / 1E4
1580 NRHO(I) = ( INT ((NRHO(I) * 1E6) + 0.5)) / 1E6
1590 RTS$ =  STR$ (RTS(I)):VV$ =  STR$ (VV(I))
1600 RHO$ =  STR$ (RHO(I)):NRHO$ =  STR$ (NRHO(I))
1610 RTS$ = B$(10 -  LEN (RTS$)) + RTS$ + Z$
1620 VV$ = B$(11 -  LEN (VV$)) + VV$ + Z$
1630 RHO$ = B$(11 -  LEN (RHO$)) + RHO$ + Z$
1640 NRHO$ = B$(10 -  LEN (NRHO$)) + NRHO$
1650  PRINT B$(0) + RTS$ + VV$ + RHO$ + NRHO$
1660  NEXT I
```

```
1670  PRINT : PRINT : PRINT : PRINT : PRINT "RESULTS PRINTOUT COMPLETED":
     PRINT : PRINT
1680  END
1690  REM  SUBROUTINE DATA CREATOR
1700  HOME : VTAB 10
1710  PRINT "****************************************"
1720  PRINT "*" + B$(33) + "*"
1730  PRINT "*" + B$(6) + "PROGRAM DATA CREATOR" + B$(7) + "*"
1740  PRINT "*" + B$(33) + "*"
1750  PRINT "* " + "PLEASE RUN TO CREATE DATA FILES *"
1760  PRINT "*" + B$(33) + "*"
1770  PRINT "****************************************"
1780  PRINT : PRINT : PRINT : PRINT : PRINT
1790  RETURN
```

APPENDIX IV

LISTING OF PROGRAM "CONVERSION"

In the following sectiona listing is given of the program "CONVERSION". The program processes the raw/strain voltage values from the magnetic permeability testing and outputs the corresponding values of the relative magnetic permeability, μ_r, and skin depth, δ.

```
100  REM
110  REM  PROGRAM "CONVERSION"
120  REM
130  REM  CURRENT VERSION BY A.E. WALKER 19/12/86
140  REM
150  REM
160  REM  *** PROGRAM NOTATION ***
170  REM
180  REM  RHO : ELECTRICAL RESISTIVITY
190  REM  MUO : RELATIVE MAGNETIC PERMEABILITY
200  REM  LO  : ORIGINAL SPAN BETWEEN PICK-UPS
210  REM  RO  : ORIGINAL RADIUS OF CONDUCTOR
220  REM  CU  : VALUE OF ENERGISING CURRENT
230  REM  FR  : FREQUENCY OF ENERGISING CURRENT
240  REM  OS  : OFFSET VOLTAGE
250  REM  GN  : SYSTEM GAIN
260  REM  PE  : ELASTIC VALUE OF POISSONS RATIO
270  REM  PP  : PLASTIC VALUE OF POISSONS RATIO
280  REM  YS  : YIELD STRAIN
290  REM  DTA : SKIN DEPTH
300  REM  STR : INPUT VALUE OF STRAIN
310  REM  PD  : INPUT VALUE OF POTENTIAL DROP
320  REM
330  REM
340  REM  ***************************************************
350  REM  *** EVALUATION OF RELATIVE MAGNETIC PERMEABILITY ***
360  REM  ***************************************************
370  REM
380  REM
390  CLEAR
400  HOME
410  VTAB 10: PRINT "PROGRAM CONSTANTS": PRINT
420 PI = 3.141592654
```

```
430  INPUT "RHO(MICRO-OHM MM) > ";RHO
440  INPUT "MUO(-) > ";MO
450  INPUT "LENGTH(MM) > ";LO
460  INPUT "RADIUS(MM) > ";RO
470  INPUT "FREQUENCY(HZ) > ";FR
480  INPUT "CURRENT(A) > ";CU
490  INPUT "OFFSET(V) > ";OS
500  INPUT "SYSTEM GAIN > ";GN
510  INPUT "PE,PP > ";PE,PP
520  INPUT "YIELD STRAIN (%) > ";YS:YS = YS * 0.01
530  INPUT "SET STRAIN(%) > ";PS
540  HOME : VTAB 10
550  PRINT "(1) LOAD INCREASING OR": PRINT "(2) LOAD DECREASING ?": PRINT
560  INPUT "ENTER (1) OR (2) > ";AN
570  HOME : VTAB 10
580  PRINT "ENTER VALUES OF STRAIN THEN PD"
590  PRINT "STRAIN : %STRAIN"
600  PRINT "PD     : VOLTS": PRINT
610  PRINT "TO END DATA INPUT ENTER 0,0": PRINT : PRINT
620 STR = 0:PD = 0:DTA = 0:MR = 0
630  INPUT "STR,PD > ";STR,PD
640  PRINT :STR = STR * 0.01
650 PD = (PD + OS) * 1E6 / GN
660  IF STR = 0 AND PD = 0 THEN  GOTO 790
670  IF AN = 2 THEN  GOSUB 800: GOTO 730
680  IF STR =  < YS THEN  GOTO 700
690 PR = PP: GOTO 710
700 PR = PE
710 R = (1 - (PR * STR)) * RO
720 L = (1 + STR) * LO
730  REM  DELTA IN MILLIMETRES
740 DTA = (RHO * L * CU) / (PD * 2 * PI * R)
750 MR = RHO / (PI * FR * DTA * DTA * MO)
```

```
760 MR = MR * 1E - 3
770  PRINT "PD(MICROV)= ";PD: PRINT "DELTA(MM)= ";DTA: PRINT "MUR(-)= ";MR
780  PRINT : PRINT : GOTO 620
790  END
800  REM  SUBROUTINE UNLOAD
810 RP = 0:LP = 0:R = 0:P = 0
820 RP = R0 * (1 - (0,5 * PS * 0,01))
830 LP = L0 * (1 + (PS * 0,01))
840 SR = STR - (PS * 0,01)
850 R = RP * (1 - (0,3 * SR)):L = LP * (1 + SR)
860  RETURN
```

APPENDIX V

LISTING OF PROGRAM "DRAGON"

In the following sectiona listing is given of the program "DRAGON". The program calculates the potential drop with increasing strain across a notch using a simple series impedance model based on the results from a finite element analysis.

```
100  REM
110  REM  PROGRAM "DRAGON"
120  REM  NOTCH FD/STRAIN EVALUATION
130  REM
140  REM  THIS PROGRAM EVALUATES THE VARIATION OF AC IMPEDANCE
150  REM  AND HENCE PREDICTS THE FD RESPONSE ACROSS
160  REM  A NOTCH WHEN USING THE COMPENSATION METHOD
170  REM  OF ACFD CRACK MONITORING
180  REM
190  REM  CURRENT VERSION BY A.E. WALKER 26/2/87
200  REM
210  REM
220  REM  *** PROGRAM NOTATION ***
230  REM
240  REM  EN(50)       : ELEMENT NUMBER
250  REM  SL(50)       : LENGTH ALONG SURFACE OF ELEMENT
260  REM  SA(50)       : AC IMPEDANCE OF ELEMENTS SPANNED BY ACTIVE PICK-UPS
270  REM               : AT EACH LOAD LEVEL
280  REM  SC(50)       : AC IMPEDANCE OF ELEMENTS SPANNED BY COMPENSATING
290  REM               : PICK-UPS AT EACH LOAD LEVEL
300  REM  STR(50,15)   : ELEMENT STRAIN AT EACH LOAD LEVEL
310  REM  MU(50,15)    : ELEMENT RELATIVE PERMEABILITY AT EACH LOAD LEVEL
320  REM  LMU(50,15)   : ELEMENT IMPEDANCE AT EACH LOAD LEVEL
330  REM  PE$(50)      : FLAGS INDICATING EITHER ELASTIC OR PLASTIC
340  REM               : BEHAVIOUR OF A PARTICULAR ELEMENT
350  REM  B$(50)       : ARRAY DEFINED TO AID FORMATTING OF OUTPUT
360  REM  ND           : NUMBER OF ELEMENTS DEFINED IN DATA STATEMENTS
370  REM  LA           : SURFACE LENGTH SPANNED BY ACTIVE PICK-UPS
380  REM  LC           : SURFACE LENGTH SPANNED BY COMPENSATING PICK-UPS
390  REM  CF           : MULTIPLICATIVE FACTOR FOR CONVERTING IMPEDANCE TO
400  REM               : POTENTIAL DROP IN MICRO-VOLTS
410  REM
```

```
420  REM
430  REM  ********************************
440  REM  *** EVALUATION OF IMPEDANCE ***
450  REM  ********************************
460  REM
470  REM
480  REM  LMU(50,15) : 2D ARRAY
490  HOME : CLEAR
500  DIM EN(50),SL(50),STR(50,15),MU(50,15),LMU(50,15),SA(50),SC(50)
510  DIM B$(40),PE$(50)
520  DATA    22,1,0,070296088,P,0,1026,,226,,3611,,5129,,6912,,9318,1,175,1,493
,1,879,2,0,070296088,P,,09311,,1824,,299,,4487
     ,,6063,,7954,1,0244,1,304,1,637
530  DATA  3,0,070296088,P,,07592,,1264,,188,,2745,,405,,5488,,7163,,9223,1,171
24,4,0,070296088,P,,05245,,088517,,10147,,1198
     6,,1847,,2498,,2892,,3541,,4458
540  DATA  17,,322101296,P,,02069,,036113,,04392,,04949,,05405,,06224,,06916,,0
6947,,06312,18,,322101296,P,,07575,,013407,,01
     6957,,01985,,02213,,02549,,03044,,03298,,02958
550  DATA  19,,322101296,E,0,00042,20,,322101296,E,,0001,21,,322101296,E,0,21,,
130125,E,0,26,,130125,E,0,31,,1951875,E,,001,3
     6,,1951875,E,,0017,61,,26875,E,,004
560  DATA  66,,5375,E,,0079,71,,80625,E,,0013,76,1,075,E,,00176,81,1,6125,P,,01
539,,02775,,03682,,04519,,05453,,06306,,07125,
     ,07899,,08663,98,2,16667,F,,01703,,03107,,041089,,05096,,06093,,07075,,080
33,,08949,,09823
570  DATA  103,2,16667,F,,01781,,03216,,04283,,05345,,06402,,0745,,08483,,09489
,,1046,108,2,16667,F,,01811,,03273,,043603,,05
     445,,06129,,07605,,08673,,09723,,1075
580  DATA  145,6,875,P,,01817,,03283,,04377,,05469,,06063,,0665,,08736,,09815,,
1088
```

```
590  REM  CONVERSION FACTOR TO MICRO-V
600  DATA    12.2123721
610  REM  PRODUCE SPACING ARRAY
620 B$(0) = ""
630  FOR I = 1 TO 20
640 B$(I) = B$(I - 1) + " "
650  NEXT
660 K = 0
670  REM  READ DATA STATEMENTS
680  VTAB 5
690  READ ND
700  FOR K = 1 TO ND
710 I = 0
720  PRINT  TAB( 5);"READING DATA POINT NO.";K
730  READ EN(K),SL(K),PE$(K)
740  IF PE$(K) = "E" THEN  GOTO 770
750  FOR I = 1 TO 9: READ STR(K,I): NEXT I
760  GOTO 800
770 STR = 0: READ STR
780 STR(K,1) = 8.3 * STR
790  FOR I = 2 TO 9:STR(K,I) = 5 * (I + 1) * STR: NEXT
800  PRINT
810  REM  CALCULATE ELEMENTAL PERMEABILITY
820  FOR I = 1 TO 9
830  IF STR(K,I) =  < 0.02 THEN MU(K,I) = 280
840  IF (STR(K,I) > 0.02) AND (STR(K,I) =  < 0.08) THEN MU(K,I) = 280 - (37 * (
STR(K,I) - 0.02) / 0.06)
850  IF (STR(K,I) > 0.08) AND (STR(K,I) =  < 0.12) THEN MU(K,I) = 243
860  IF (STR(K,I) > 0.12) THEN MU(K,I) = (243 - (45 * (STR(K,I) - 0.12) / 3.2))

870 LMU(K,I) = SL(K) *  SQR (MU(K,I))
880  NEXT I
890  NEXT K
```

```
900  REM  READ CONVERSION FACTOR
910  READ CF
920  REM  CALCULATE ZERO STRAIN IMPEDANCE
930  FOR I = 1 TO 17
940 LA = LA + SL(I)
950  NEXT
960  FOR I = 18 TO (ND - 1)
970 LC = LC + SL(I)
980  NEXT
990 LC = LC + (0.13 * SL(ND))
1000 SA(0) = LA *  SQR (280):SC(0) = LC *  SQR (280)
1010  FOR I = 1 TO 9
1020 SA(I) = 0:SC(I) = 0
1030  FOR K = 1 TO 17
1040 SA(I) = LMU(K,I) + SA(I)
1050  NEXT K
1060  FOR K = 18 TO (ND - 1)
1070 SC(I) = LMU(K,I) + SC(I)
1080  NEXT K
1090 SC(I) = (LMU(ND,I) * 0.13) + SC(I)
1100  NEXT I
1110  HOME : VTAB 5
1120  REM  PRINTOUT OF RESULTS
1130  HOME : PRINT "RESULTS WILL NOW BE REPRINTED": PRINT : PRINT "EITHER ONTO
THE": PRINT
1140  HTAB 10: PRINT "(1) SCREEN": HTAB 10: PRINT "(2) PRINTER": PRINT
1150  INPUT "ENTER (1) OR (2) > ";QQ
1160  IF QQ = 1 THEN  GOTO 1190
1170  PRINT  CHR$ (4);"PR#1": POKE 1657,80
1180  PRINT  CHR$ (12): REM  CTRL-L;FORM FEED
1190  HOME
```

```
1200  FOR K = 1 TO ND
1210  PRINT : PRINT : PRINT "ELEM NO ";EN(K)
1220  PRINT : PRINT "LOAD *  RELPERM    *    LMUR"
1230  PRINT "-------------------------------"
1240  FOR I = 1 TO 10
1250 A$ = "":B$ = "":C$ = ""
1260 A$ =  STR$ (I):B$ =  STR$ (MU(K,I)):C$ =  STR$ (LMU(K,I))
1270 A$ = B$(1) + A$ + B$(4 -  LEN (A$))
1280 B$ = B$(1) + B$ + B$(11 -  LEN (B$))
1290 C$ = B$(1) + C$ + B$(11 -  LEN (C$))
1300  PRINT A$ + "*" + B$ + "*" + C$
1310  NEXT I
1320  NEXT K
1330  PRINT : PRINT : PRINT "TABLE OF RESULTS": PRINT
1340  PRINT "CONVERSION FACTOR: "; STR$ (CF): PRINT
1350  PRINT "LOAD *   ACTIVE    *  COMPENS    *    DELTA     *     PD"
1360  FOR I = 1 TO 55:L$ = L$ + "-": NEXT
1370  PRINT L$
1380  FOR I = 0 TO 9
1390 D$ = "":E$ = "":F$ = "":G$ = "":H$ = ""
1400 D$ =  STR$ (1 + ((I > 1) * 4)):E$ =  STR$ (SA(I)):F$ =  STR$ (SC(I))
1410 G = (2 * SA(I)) - SC(I):G$ =  STR$ (G)
1420  REM  CONVERT IMPEDANCE TO POTENTIAL DROP
1430 H = CF * G:H$ =  STR$ (H)
1440 G$ =  STR$ ((2 * SA(I)) - SC(I))
1450 D$ = B$(1) + D$ + B$(4 -  LEN (D$))
1460 E$ = B$(1) + E$ + B$(11 -  LEN (E$))
1470 F$ = B$(1) + F$ + B$(11 -  LEN (F$))
1480 G$ = B$(1) + G$ + B$(11 -  LEN (G$))
1490 H$ = B$(1) + H$ + B$(11 -  LEN (H$))
1500  PRINT D$ + "*" + E$ + "*" + F$ + "*" + G$ + "*" + H$
1510  NEXT I
```

```
1520  PRINT : PRINT : PRINT : PRINT : PRINT "RESULTS PRINTOUT COMPLETED": PRINT
 : PRINT
1530  IF QQ = 1 THEN  GOTO 1550
1540  PRINT  CHR$ (4);"PR#0"
1550  END
1560  END
```